ACOUSTIC EMISSION

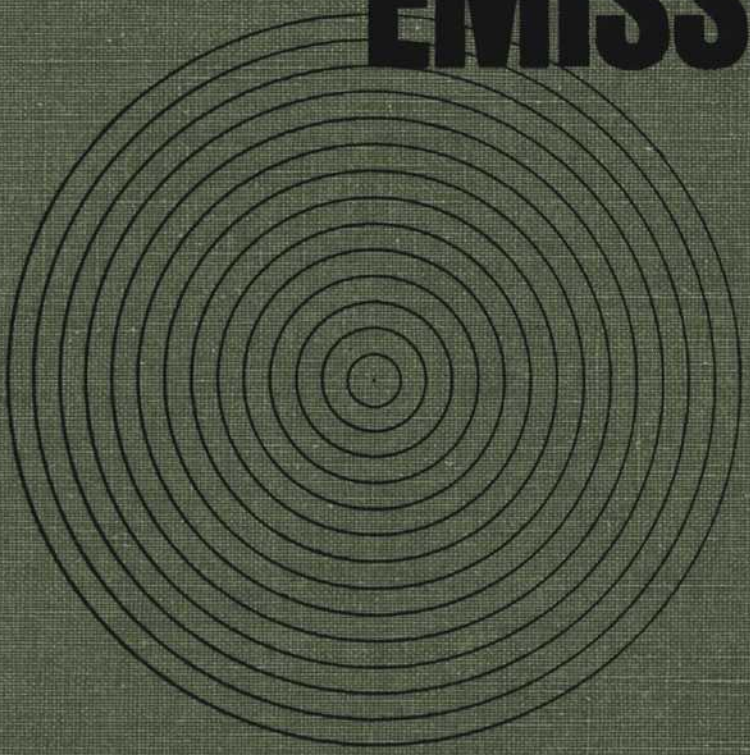

STP 505

75TH ANNIVERSARY
AMERICAN SOCIETY FOR TESTING AND MATERIALS

ACOUSTIC EMISSION

A symposium
presented at the
December Committee Week
AMERICAN SOCIETY FOR
TESTING AND MATERIALS
Bal Harbour, Florida, 7–8 December 1971

ASTM SPECIAL TECHNICAL PUBLICATION 505
R. G. Liptai, general chairman
D. O. Harris and C. A. Tatro, co-chairmen

List price $22.50
04-505000-22

75TH ANNIVERSARY
AMERICAN SOCIETY FOR TESTING AND MATERIALS
1916 Race Street, Philadelphia, Pa. 19103

Library of Congress Catalog Card Number: 72–75896

NOTE

The Society is not responsible, as a body,
for the statements and opinions
advanced in this publication.

Printed in Baltimore, Md.
May 1972

Foreword

The Symposium on Acoustic Emission was presented at the December Committee Week of ASTM held in Bal Harbour, Florida, 7-8 December 1971. The ASTM Publications Committee sponsored the symposium. R. G. Liptai, Lawrence Radiation Lab., presided as symposium chairman, and D. O. Harris and C. A. Tatro, also of Lawrence Radiation Lab., served as co-chairmen.

Related ASTM Publications

Effects of Environment and Complex Load History on Fatigue Life, STP 462 (1970), $22.00

Achievement of High Fatigue Resistance in Metals and Alloys, STP 467 (1970), $28.75

Fracture Toughness Testing at Cryogenic Temperatures, STP 496 (1970), $5.00

Contents

Introduction

The field of acoustic emission has grown tremendously in the past decade, as evidenced by the many new areas of application, the increasing number of workers, and the expanding literature on acoustic emission. To date, the literature has been scattered among many journals and reports. No comprehensive survey has existed. Many of the papers have presupposed advance knowledge of the technology and past developments, which works a hardship on newcomers to the field.

To remedy this situation and gather the relevant information in one place, ASTM has commissioned this Special Technical Publication, derived from the Symposium on Acoustic Emission at the ASTM Committee Meeting of December 7-8, 1971, in Bal Harbour, Florida. The papers cover a wide range of topics, from general reviews of the field to specific reports on research findings, technological advances, and applications in different industries. Their collective references, cited in the papers, include most of the published material on acoustic emission technology.

The first section is primarily introductory. It is intended for those who seek a general understanding of acoustic emission. Included here are the historical background and discussions of the relevant aspects of dislocation dynamics, microcracking processes, rock mechanics, materials studies, and structural evaluation studies.

The remaining sections comprise a state-of-the-art review of specific research and application areas. Much of this material is previously unpublished and at the forefront of present technology. Described here are applications in various industries and the results of research intended to advance the capabilities of acoustic emission. Experimental considerations and instrumentation are emphasized in several of the papers, ranging from direct application of commerical equipment to research efforts pushing the limits of instrument capabilities.

We hope this publication will prove interesting to a wide spectrum of readers,

to those who want a basic introduction to the field as well as research workers exploring the future directions for acoustic emission technology.

R. G. Liptai

Head, Mechanical Engineering Structural Test and Evaluation,
Lawrence Livermore Laboratory, Livermore, Calif.;
symposium general chairman

D. O. Harris

Director of Research
Dunegan Research Corp., Livermore, Calif.;
symposium co-chairman

C. A. Tatro

Head, Mechanical Engineering Materials Test and Evaluation,
Lawrence Livermore Laboratory, Livermore, Calif.;
symposium co-chairman

R. G. Liptai,[1] *D. O. Harris,*[2] *and C. A. Tatro*[3]

An Introduction to Acoustic Emission

REFERENCE: Liptai, R. G., Harris, D. O., and Tatro, C. A., "An Introduction to Acoustic Emission," *Acoustic Emission, ASTM STP 505,* American Society for Testing and Materials, 1972, pp. 3–10.

ABSTRACT: A brief introduction to the field of acoustic emission is presented. The basic mechanisms of acoustic emission and a brief historical survey of the technology, along with some of its application to materials research and structural evaluation programs, are discussed.

KEY WORDS: acoustics, emission, acoustic detection, stress waves, deformation, plastic deformation, failure, evaluation, cracking (fracturing), elastic waves, transient response

Acoustic emission may be defined as the stress or pressure waves generated during dynamic processes in materials. In its less conventional forms, acoustic emission can be so loud that it is audible to the unaided ear. A familiar example of this is the creaking of timber subjected to loads near failure; the sounds from timber are used as indicators of the impending failure of wooden structures. Another familiar example is the audible sound produced by the failure of rock; these sounds have been used to detect the impending failure of mine shafts[*1-3*] and the onset of land slides[*4,5*]. Emission analysis can also be used to model the fault movements that result in earthquakes; the use of seismometers to detect stress waves produced during an earthquake is familiar to nearly everyone.

In general, the use of sounds or acoustic emissions as a parameter to characterize the use, or abuse, of a material subjected to load has been largely neglected by the scientific and engineering communities. This situation has generally reversed during the last decade with the use of modern electronic

Work performed under the auspices of the U. S. Atomic Energy Commission.

The basic information in this paper appeared in *Materials Research and Standards,* MTRSA, Vol. 11, March 1971, No. 3, pp. 8-11.

[1] Head, Structural Test and Evaluation, University of California, Lawrence Livermore Laboratory, Livermore, Calif.

[2] Director of Research, Dunegan Research Corp., Livermore, Calif.

[3] Head, Materials Test and Evaluation, University of California, Lawrence Livermore Laboratory, Livermore, Calif.

instruments and transducers sensitive enough to detect dislocation phenomena in metals. Sounds and stress waves generated in materials systems have been noted in the literature for many years, including such descriptions as clicks, sounds, microseismic activity, rock noise, stress wave analysis technique (SWAT), stress wave emission, elastic shock, elastic radiation, seismo-acoustical activity, and acoustic emission. It appears that the term "acoustic emission" has been generally accepted around the world to describe low level sounds or pressure waves in materials.

Regardless of the phenomena studied, material used, or the application, one point becomes obvious: acoustic emission analysis is very sensitive to local transient instabilities. A material system will proceed towards its lowest energy state and in most situations will develop unstable conditions locally well before the whole mass becomes unstable. These conditions result in local dynamic movements, such as formation of a slipband or a platelet of martensite, propagation of a crack or a Lüders line, sudden reorientation of a grain boundary, bubble formation during boiling, or earth movement during an earthquake. In many material systems, local instabilities frequently cause catastrophic failures. For example, the stresses in a metallic system may be well below the elastic design limit; however, the region near a flaw or a crack may undergo plastic deformation from localized high stresses (stress intensity). In this situation, the flaw is the generator or source of acoustic emission activity.

Recent investigations into the sounds produced by metals have given rise to the modern work in acoustic emission. It has been found that most materials do indeed emit sounds or stress waves as they are deformed, and that these sounds provide information on the deformation characteristics and also warn of impending failure. However, acoustic emissions are generally of such a low level that sophisticated instrumentation is required for their detection.

This paper briefly reviews acoustic emission technology. It includes a brief historical survey and a discussion of materials research and characterization and the application of emission techniques to evaluation of structural integrity. Also, some discussion of future development in acoustic emission is presented.

Historical Review

Historically, the earliest use of acoustic emission analysis probably occurred in seismology. Elastic waves produced by an earthquake was analyzed to characterize fault movement in terms of energy released, location, and depth. Also, the possibility of detecting rock burst in coal mines was anticipated early in the studies.

Early observations of acoustic emission in metals were made by tin smiths who noted "tin cry," or twinning, during deformation of tin (twinning deformations in general are active generators of acoustic emissions). Audible sounds or clicks noted during heat treatment of steel were related to martensitic

transformations. In fact, later studies showed that martensitic transformations in general are prolific sources of acoustic emission. Joseph Kaiser and his coworkers[*6*] in Germany in the early 1950s are generally credited with initiating the present effort in acoustic emission. Kaiser was the first to use electronic instrumentation to detect audible sounds produced by metals during deformation. He reported that all metals examined, including zinc, steel, aluminum, copper, and lead, exhibited the emission phenomena. Kaiser also observed that acoustic emission activity was irreversible, that is, acoustic emissions were not generated during the reloading of a material until the stress level exceeded its previous high. The irreversible phenomenon has become known as the "Kaiser effect" and has proven to be very useful in acoustic emission studies.

Several years after Kaiser's work, investigators in the United States became interested in acoustic emission phenomena. Schofield[*7*] and Tatro[*8*] initiated research in the middle 1950s and did much to improve the instrumentation and to clarify the sources of acoustic emission. They found that emissions from metals were primarily due to dislocation motion accompanying plastic deformation[*9-12*] rather than being entirely due to grain boundary sliding as proposed by Kaiser.

In the decade of the 1960s, many engineers and scientists became interested in acoustic emission and utilized this technique in studies relating to materials research, materials characterization and evaluation, nondestructive testing, and structural evaluation. In addition, emission techniques have been found for such uses as detecting boiling and cavitation in fluid systems.

Extensive improvements in instrumentation in the early 1960s made possible many advances in acoustic emission technology. Early workers in the area were plagued by excessive background noises from the laboratory and surrounding areas. As a result, they often had to locate their laboratories in relatively isolated areas, design loading fixtures with extreme care, and work late at night to reduce background noise. They found that many of these problems could be eliminated, or at least minimized, by working with instrumentation whose frequency range was well above the audio range. This innovation[*13*] eliminated the need for sound isolated laboratories and was instrumental in leading to the present status of acoustic emission as a valuable scientific and engineering tool.

Present Areas of Application

Materials Research

Acoustic emission is well suited to studies of deformation in materials. In addition to the work on single crystals[*10,12*], considerable work has been conducted on polycrystalline tension specimens[*14-17*]. Acoustic emissions generated during phase transformations have also been studied[*18*], and

martensitic transformations were found to be particularly copious sources of acoustic emissions. Discussions of dislocation processes as possible sources of acoustic emission are presented in the following papers. Also, a review of emission studies from initially flawfree materials is presented in Ref *16*.

Studies have also been conducted on composite materials, such as fiberglass reinforced epoxy[*19*] and whisker reinforced materials[*20*]. Acoustic emission techniques are finding greater and greater applicability to characterization of materials, particularly composite materials. Because of the nature of composite materials, modes and criteria for deformation or fracture processes are very complex. Hence, acoustic emission techniques can be used advantageously to characterize the microfracturing characteristics during straining. This situation is true for all three classes of composite materials, namely dispersion strengthened composites, particle reinforced composites, and fiber reinforced composites.

Materials studies have included work in fracture mechanics on flawed specimens. Acoustic emission has been utilized in the detection of pop-in[*21, 22*] during rising load fracture toughness tests. In fact, the early studies of acoustic emission from flawed materials were concerned with the detection of this phenomenon[*23-25*], which requires insensitive equipment, since pop-in is usually composed of high amplitude acoustic emissions. Plastic deformation, which results in acoustic emission[*14,16*], occurs at crack tips and other highly stressed regions when a material is loaded; hence, acoustic techniques have been used advantageously for flaw detection. Acoustic emission has been used to study growing cracks, such as those occurring during hydrogen embrittlement[*26,27*], stress corrosion cracking[*27,28*], and low cycle fatigue[*29*]. Gerberich and Hartbower[*25,30,31*] have related the acoustic emission associated with pop-in to the newly developed crack area resulting from crack extension and have found quantitative relationships for a wide variety of materials.

Fatigue crack growth produced by fluctuating loads can be detected by continuous monitoring of acoustic emission. Hartbower et al[*32*] investigated the acoustic emission during low cycle fatigue from D6Ac steel with various heat treatments and reported that it was possible to detect the growth of fatigue cracks by continuous monitoring. Also, the amount of crack growth per cycle can be directly determined from acoustic emission data.

Acoustic emission techniques have been used to study deformation and fracture processes in geologic materials, whose mechanical properties are often complicated by anisotropic and inhomogeneous qualities. Because of the transient nature of the mechanistic processes involved in deformation and fracture, acoustic emission techniques can be used from the time of the propagation of cracks upon initial stress application to the time of final rupture. Each deformation and fracture process in rocks involves a transient phenomenon that is a known generator of acoustic emission activity. Names given to acoustic

emission from rocks include elastic shock, elastic radiation, rock noise, and microseismic activity, and scientists in Russia use the term "seismo-acoustical activity"[2]. All terms have been used to describe the transient vibrations or acoustic emissions generated during the straining of rocks. A later paper presents a more detailed description of acoustic emission from geologic materials[33].

Structural Integrity

The presence of cracks in structures alters the load at which plastic deformation begins, thus altering the acoustic emission pattern observed as the structure is loaded. Acoustic emissions have been used in assessing structural integrity[34-37] of machined parts by acoustic monitoring of the initial proof test. The acoustic emission record can determine if flaws are present and assess their severity. Triangulation techniques similar to those used to locate earthquakes can help to locate the flaws in the structure. Acoustic emissions for assessment of structural integrity have been applied to a wide variety of structures, including pressure vessels for nuclear and petroleum industries[35-37], rocket motor cases[34], and bridges, buildings, and wooden beams[38]. Techniques are also available to detect, during service, the degradation of structural integrity due to subcritical flaw growth. In some cases, this can be accomplished by continuous monitoring to detect the emissions produced as the crack extends under constant load; work on hydrogen embrittlement and stress corrosion cracking[26-29] has illustrated the feasibility of using acoustic emission for the detection of growing cracks. In some instances, excessive background noise would preclude the use of continuous monitoring. Periodical overload while monitoring for acoustic emission is another technique devised to assess growing cracks[28,39,40]. This technique shows great promise but has not yet been applied to complex structures.

Sonic signature analysis, a field largely undeveloped at present, is worth mentioning as one area of study related to acoustic emission. This technique applies primarily to rotating machinery such as generators, pumps, and turbines and is used to detect faulty components such as bearings. It is distinguished from acoustic emission in that the relative motion, not the material itself, is the source of the sounds or acoustic emission[41]. This subject is treated in greater detail in a later paper[42].

Future Developments

The application of acoustic emission to problems of interest to research and industry has only begun, and the future in these areas appears unlimited[43]. Studies of the sources of acoustic emission should lead to applications of acoustic emission techniques in dislocation dynamics and deformation of materials. It appears that acoustic emission will have a greater applicability in the

future as a material characterization parameter or technique. The application of acoustic emission to studies of the mechanical behavior of materials at high temperatures awaits the development of a transducer suitable for use at such temperatures (high temperature transducers are discussed in a later paper). Study in this area could lead to a greater understanding of the processes of creep and rupture, which presently limit the use of some materials at elevated temperatures.

The utilization of acoustic emission in the assessment of structural integrity is also in its infancy. Great progress has been made in the study of pressure vessels, primarily in initial evaluation before they are put into service. Proof testing and continuous monitoring of a wide variety of structures can be visualized: structures such as pressure vessels, pipelines, airplanes, buildings, and bridges. Certification of castings and in-process monitoring of welding, rolling, and other fabrication techniques is also conceivable. Basic studies in stress corrosion and hydrogen embrittlement as applied to structures are also in their initial stages and could be greatly extended for complex structures in service under various environmental conditions. Welding and joining in general, are areas where acoustic emission technology has only just been introduced. The list of possible future applications could be greatly extended, but it should be apparent that the application of acoustic emission to problems of practical importance has only begun and that this techniques has great potential.

It is anticipated that, as more people become aware of how acoustic emission techniques can be applied to their specific needs, this technology will grow rapidly. Already in 1971, four commercial companies produce and stock acoustic emission apparatus and instrumentation.

References

[1] Hodgson, E. A., "Dominion Observatory Rockburst Research 1938-1945," Dominion Observatories Report, Department of Mines and Technical Surveys, Canada, 1958.

[2] Antsyferov, M. S., Ed., *Seismo-Acoustic Methods in Mining*, S. E. Hall, Translation Consultant's Bureau, New York, 1966.

[3] Susuki, K., Sasaki, Z., Siohara, Z., and Hirota, T. in *Proceedings*, International Conference on Strata Control and Rock Mechanics, Columbia University, N. Y., 1965, p. 1.

[4] McCauky, M. L., *Engineering Geology*, ENGEA, Vol. 2, 1965, p. 1.

[5] Goodman, R. E. and Blake, W., *Rock Noise in Landslides and Slope Failures*, University of California Press, Berkeley, Calif., 1965.

[6] Kaiser, J., "Untersuchungen über das auftreten Geräuschen beim Zugversuch," Ph.D. thesis, Technische Hochschule, Munich, 1950; also, *Arkiv für das Eisenhuttenwesen*, AREIA, Vol. 24, No. 1/2, Jan./Feb. 1953, pp. 43-45.

[7] Schofield, B. H., Bareiss, R. A., and Kyrala, A. A., "Acoustic Emission Under Applied Stress," ASTIA Document AD 155674, WADC Technical Report. 58-194, 1958.

[8] Tatro, C. A., "Sonic Techniques in the Detection of Crystal Slip in Metals," Status report, Division of Engineering Research, College of Engineering, Michigan State University, East Lansing, Mich., 1959.

[9] Schofield, B. H., "Acoustic Emission Under Applied Stress," Report ARL-150, Aeronautical Research Laboratory, Office of Technical Services, U.S. Dept. of Commerce, Washington, D.C., 1961.

[10] Schofield, B. H., "Acoustic Emission Under Applied Stress," Final Report, Contract AF33(616)-5640, Project 7021, Task 70663, Aeronautical Research Laboratory, Wright-Patterson Air Force Base, Ohio, 1964.

[11] Tatro, C. A. and Liptai, R. G., in *Proceedings*, Symposium on Physics and Nondestructive Testing, Southwest Research Institute, San Antonio, Tex., 1962, pp. 145-158.

[12] Liptai, R. G. and Tatro, C. A. in *Proceedings*, Fourth Annual Symposium on Nondestructive Testing of Aircraft and Missile Components, Southwest Research Institute, San Antonio, Texas, 1963, pp. 287-341.

[13] Dunegan, H. L., Tatro, C. A., and Harris, D. O., "Acoustic Emission Research," Report UCID-4868, Revision 1, Lawrence Radiation Laboratory, Livermore, Calif., 1964.

[14] Dunegan, H. L., Harris, D. O., and Tatro, C. A., *Engineering Fracture Mechanics*, EFMEA, Vol. 1, No. 1, June 1968, pp. 105-122.

[15] Fisher, R. M. and Lally, J. S., *Canadian Journal of Physics*, CJPHA, Vol. 45, No. 2, Part 3, Feb. 1967, pp. 1147-1159.

[16] Dunegan, H. L. and Tatro, C. A. in *Techniques of Metals Research*, Vol. 5, Part 2, R. Bunshah, Ed., Wiley, New York, 1971, pp. 273-312.

[17] Dunegan, H. L. and Harris, D. O., *Ultrasonics*, ULTRA, Vol. 7, No. 3, July 1969, pp. 160-166.

[18] Liptai, R. G., Dunegan, H. L., and Tatro, C. A., *International Journal of Nondestructive Testing*, IJNTA, Vol. 1, No. 3, Aug. 1969, pp. 213-221.

[19] Liptai, R. G., in *Composite Materials: Testing and Design (Second Conference), ASTM STP 497*, American Society for Testing and Materials, 1972, p. 285.

[20] Tetelman, A. S., Harris, D. O., and Darwish, F. A. I. in *Acoustic Emission, ASTM STP 505*, American Society for Testing and Materials, 1972, pp. 238-249.

[21] Srawley, J. E. and Brown, W. F., Jr., in *Fracture Toughness Testing and Its Applications, ASTM STP 381*, American Society for Testing and Materials, 1965, pp. 133-198.

[22] Brown, W. F., Jr., and Srawley, J. E., *Plane Strain Crack Toughness Testing of High Strength Metallic Materials, ASTM STP 410*, American Society for Testing and Materials, 1967.

[23] Jones, M. H. and Brown, W. F., Jr., *Materials Research and Standards*, MTRSA, Vol. 4, 1964, p. 120.

[24] Romine, H. E., "Determination of the Driving Force for Crack Initiation from Acoustic Records of G_c Tests on High Strength Materials for Rocket Motor Cases," Report NWL 1779, Naval Weapons Laboratory, Washington, D.C., 1961.

[25] Gerberich, W. W. and Hartbower, C. E., *International Journal of Fracture Mechanics*, IJFMA, Vol. 3, No. 3, 1967, p. 185.

[26] Dunegan, H. L. and Tetelman, A. S., "Nondestructive Characterization of Hydrogen Embrittlement Cracking by Acoustic Emission Techniques," submitted for publication to *Engineering Fracture Mechanics*.

[27] Gerberich, W. W. and Hartbower, C. E., "Monitoring Crack Growth of Hydrogen Embrittlement and Stress Corrosion Cracking by Acoustic Emission," Proceedings Conference on Fundamental Aspects of Stress Corrosion Cracking, Ohio State University, Columbus, Ohio, 1967.

[28] Dunegan, H. L. and Harris, D. O., "Acoustic Emission Techniques," to be published in *Experimental Techniques in Fracture Mechanics*, A. S. Kobayashi, Ed., Society for Experimental Stress Analysis.

[29] Hartbower, C. E., Gerberich, W. W., and Crimmins, P. P., *The Welding Journal*, WEJUA, Vol. 47, No. 1, Jan. 1968, pp. 1s-18s.

[30] Gerberich, W. W. and Hartbower, C. E., "Monitoring Crack Growth of Hydrogen Embrittlement and Stress Corrosion Cracking by Acoustic Emission," Proceedings,

Conference on Fundamental Aspects of Stress Corrosion Cracking, Ohio State University, Columbus, Ohio, 1967.

[*31*] Hartbower, C. E., Gerberich, W. W., and Liebowitz, H., *Engineering Fracture Mechanics,* EFMEA, Vol. 1, No. 2, 1968, p. 291.

[*32*] Hartbower, C. E., Gerberich, W. W., and Crimmins, P. P., *The Welding Journal,* WEJUA, Vol. 47, No. 1, p. 1s.

[*33*] Hardy, H. R., in *Acoustic Emission, ASTM STP 505,* American Society for Testing and Materials, 1972, pp. 41-83.

[*34*] Green, A. T., Lockman, C. S., and Steele, R. K., *Modern Plastics,* MOPLA, Vol. 41, No. 11, July 1964, p. 137.

[*35*] P. H. Hutton, "Detection of Incipient Failure in Nuclear Reactor Pressure System Using Acoustic Emission," Report BNWL-997, Battelle-Northwest, Richland, Wash., 1969.

[*36*] Hutton, P. H., "Integrity Surveillance of Pressure Systems by Means of Acoustic Emission," Report BNWL-SA-2194, Battelle-Northwest, Richland, Wash., 1969.

[*37*] Parry, D. and Robinson, D., "Incipient Failure Detection by Acoustic Emission–Development and Status Report,", Report IN-1398, Idaho Nuclear Corp., Idaho Falls, Idaho, 1970.

[*38*] Muenow, R. A., "Uses of Acoustic Emission in Construction," presented at Symposium on Acoustic Emission, Bal Harbour, Fla., 7-8 Dec. 1971.

[*39*] Harris, D. O., Dunegan, H. L., and Tetelman, A. S. in Proceedings of the Air Force Conference on Fatigue and Fracture of Aircraft Structural Materials, Air Force Flight Dynamics Laboratory Report AFFDL TR 70-144, 1970, pp. 459-471.

[*40*] Harris, D. O. and Dunegan, H. L., in *Testing for Prediction of Material Performance in Structures and Components, ASTM STP 515,* American Society for Testing and Materials, 1972.

[*41*] Weichbrodt, B. and Smith, K. A. in *Proceedings* of Conference on Space Simulation held at National Bureau of Standards, Gaithersburg, Md., 14-16 Sept. 1970, pp. 407-448.

[*42*] Balderston, H. L., in *Acoustic Emission, ASTM STP 505,* American Society for Testing and Materials, 1972, pp. 297-317.

[*43*] Liptai, R. G., Harris, D. O., Engle, R. B., and Tatro, C. A., *International Journal of Nondestructive Testing,* IJNTA, Dec. 1971, and in *Proceedings,* Symposium on Advanced Experimental Techniques in the Mechanics of Materials, San Antonio, Texas, Sept. 1970.

B. H. Schofield[1]

Research on the Sources and Characteristics of Acoustic Emission

REFERENCE: Schofield, B. H., "Research on the Sources and Characteristics of Acoustic Emission," *Acoustic Emission, ASTM STP 505,* American Society for Testing and Materials, 1972, pp. 11-19.

ABSTRACT: A review of some of the less familiar acoustic emission characteristics and anomalies is presented with the objective of suggesting new or alternate approaches to better understand the phenomenon. Topical discussions include slip and twinning induced emission, acoustic responses during metal etching, residual stresses, and influence of grain size and fatigue. Specific shortcomings in acoustic emission research at present are noted as well as the need for additional research to keep up with the ever increasing and unusual practical applications.

KEY WORDS: acoustics, emission, grain boundaries, grain growth, twinning, yield strength, aluminum alloys, nondestructive tests, deformation, residual stress, corrosion mechanisms, dislocations (materials)

In the various experimental investigation in acoustic emission undertaken in the United States over the course of the past 17 years, the studies of practical applications far outstrip research concerning the source and nature of the phenomenon. Although significant strides have been made in improving our understanding of the fundamental aspects of the phenomenon, full realization of the potential and the limitations of acoustic emission will not be attained until we advance this basic understanding beyond the current state. This need for improved understanding takes on more urgent importance in view of some of the unusual practical applications currently being suggested and contemplated in various segments of industry.

In this paper a number of experimental anomalies observed in the course of emission studies are noted. For the most part these specific occurrences were secondary to the prime direction of the research effort and, consequently, were not pursued in great detail. Notation of these emission anomalies may suggest

[1] Section manager, Teledyne Materials Research, Waltham, Mass. 02154.

additional avenues of research concerning the sources of acoustic emission as well as applications of the phenomenon as a research and practical tool.

Experimental Cases and Observations

General

In the course of our research several experiments were designed to establish the nature of the source of acoustic emission and the relationship of the observed characteristics to the material behavior. In some instances direct measurements of a specific physical mechanism were made for correlation with the emission response; for example, slip line development on the surface. In other cases less direct techniques were employed. First, an *a priori* assumption of a relationship between acoustic emission and a specific deformation mechanism was made. The material was then subjected to a treatment or environment known to influence the assumed deformation mechanism in a given way and the emission response was then observed for similar correspondence of the influence.

Residual Stresses and Acoustic Emission

When acoustic emission was first encountered in 1954, the investigators at our laboratory [*1*] wanted to find out whether acoustic emission could be used to quantitatively and nondestructively measure the surface residual stresses in metals. The immediate application was related to surface residual stresses in aircraft propeller blades where such stresses can play a most significant role in the integrity of the blades.

Kaiser's thesis work [*2*] had indicated definite and consistent relationships between the occurrence of acoustic emission and certain physical and metallurgical characteristics of materials. His data exhibited results from which the quantitative state of stress in the material could be determined for a given physical and metallurgical material condition. Certain of those material conditions such as grain size and yield strength, which influenced the emission response, were peculiar to variations in surface residual stresses in metals.

The first experiments were performed on aluminum alloy specimens which were to be treated for variable and known states of residual stresses. The experiments on the first series of specimens, those without residual stresses for control purposes, exhibited variations in emission response which could not be adequately explained. Immediately it became apparent that preliminary experiments would be required to separate and identify the variables influencing the emission. This change in scope eventually led to the more basic studies of the emission sources, but no further effort was directed specifically to residual stress studies and, to my knowledge, no other investigation has been made since in this area.

With the ubiquitous acceptance of the jet engine, the interest in propeller blading has declined substantially. However, since residual stresses still play an important role in engineered items, a nondestructive tool to measure them would be of considerable value. Emission research reported by investigators over the years[*2,4*] has demonstrated that metallurgical and physical treatments do affect the emission response significantly. This information should be particularly valuable in developing nondestructive techniques for residual stresses.

Grain Boundary Distortion and Shear

Basic to Kaiser's original premise[*2*] concerning the significance of acoustic emission was that the primary or major source of the emission was the strain distortion and shear displacements occurring at grain boundaries. Because the results observed in the residual stress studies were ambiguous, efforts were concentrated on determining the quantitative aspect of the grain boundary deformations. The results of these efforts led to a further anomaly.

A series of pure aluminum test specimens were prepared; each set varied in grain size over a broad range, from extremely fine grains, which necessitated the microscope for resolution, to specimens containing grains of ¼ in. in diameter and ultimately specimens of a single crystal. All specimens, including the single crystal, were about ¼ by ¼ in. in cross section, and 4 to 6 in. long. (Such an emission source would necessitate volume control; hence, all specimens were accurately sized.) Deformation was induced by tensile loading at a constant overall load rate.

Based on Kaiser's premise[*2*] that grain boundary shear was the primary acoustic source, this group of specimens was designed to exhibit the quantitative relationship between acoustic emission and material deformation. The single crystals were designed to serve as the control group exhibiting a minimum, if not absence of, acoustic emission.

The major, and at the time, most startling result of these experiments was not the lack of noticeable decrease in emission energy, linear or otherwise, with increase in grain size, but the equally profuse occurrence of emission from the single crystal specimens. It became immediately clear that although grain size was an influential parameter in the emission behavior, it was not the primary contributor of acoustic emission.

The experiments had shown, nevertheless, some influence of the presence of grain boundaries; whether this presence was a source of some of the emission or merely an influence on the characteristics, was not determined. A number of investigators[*1,3,4*] have suggested and shown by data that differences in heat treatment and other metallurgical variations can be detected by acoustic emission characteristics. Inasmuch as grain size is most often a consequence of such treatment, it would appear fruitful to assess the quantitative influence and contribution of grain size on emission behavior. Certainly, if one expects to

utilize the emission as a practical tool in such areas as welding, the influence of grain boundary interactions may be a significant entry.

Surface Etching of Metals

A number of experiments were designed to isolate, identify, or eliminate certain physical parameters as sources of acoustic emission. One such experiment concerned the presence of the oxide layer on materials; that is, (1) in what way did the presence of this layer relate to deformation mechanics, and (2) was the oxide layer an independent contributor as an emission source.

These tests were conducted in two separate aspects: (1) one in which a material susceptible to natural development of an oxide layer (aluminum) was studied under conditions with and without the oxide layer present; and (2) one utilizing gold, which is not subject to surface oxidation.

The results of the experiments and their significance as to the influence of the surface film on the deformation induced emission have been presented elsewhere[*5-8*]. At the time that they were first observed they were not pursued to any great extent since they were not directly relevant to the research direction at the time, but they are discussed here since they may be of interest to the broad spectrum of emission application.

Preparatory to testing the aluminum single crystals, without the oxide layer, specimens were immersed in an etchant solution (methyl alcohol-nitric acid) through which various electrical current densities were applied to remove the oxide layer and a portion of the metal surface. It was observed that even prior to loading, a considerable amount of acoustic emission occurred. The amount of emission was generally high at the outset of etching, becoming relatively stable at lower emission rates after a period of time. Inducing deformation in the specimen tended to restore the high emission rate.

The obvious and immediate conclusion on observing the profuse bubble formation around the specimen, for the polarity producing material removal, was that the emission was related to bubble generation and collapse. However, in the reversal of polarity, material is no longer displaced from the specimen, although equally profuse bubble formation continues at both the anode and cathode. With the latter configuration; namely, no material removal, the distinct emission bursts were no longer observed, notwithstanding the active bubbling. The bubble formation and collapse were detected for both modes, but the energies and signal characteristics of the bubble activity were significantly different from the high energy acoustic bursts observed during the metal etchant mode.

This type of emission activity during material etching has been observed by others[*8*], in similar experiments. The technique has definite possibilities in relating acoustic emission to deformation mechanics such as dislocations. In addition, it would appear that this acoustic response could be extremely useful

in the study of the corrosion processes–not only in providing insight into the operative mechanisms and influence of various parameters, but also in the development of analytical studies of corrosion dynamics.

Emission Sources in Slip and Twin Development

In the early studies of emission, attempts were made to establish the relationships between the development of slip lines in the surface of a specimen and the occurrence of emission pulses. The results of this effort [9], which were limited in scope to aluminum single crystals, showed reasonable correlation for the simple slip (easy glide) mode. The presence of cross slip and other anomalous modes of slip deformation in some specimen tests greatly complicated interpretation, not to mention the increased difficulty of experimental observation, and reliable correlations diminished accordingly. In contrast with later twinning studies, the aluminum specimens were examined under static conditions [9]; that is, the deformation patterns were observed under a microscope after deforming the specimen and recording the emission.

In the case of twinning emission, a dynamic experimental method was used. Specimens of zinc single crystals were first thinly coated with Photostress, a birefringent material which exhibits unique color patterns when strained. The specimens were then loaded into a special device which permitted simultaneous microscopic observation of all four surfaces of the specimen. Output of the emission instrumentation was fed to earphones worn by the investigator controlling the loading and attending the microscope.

The development of twins was easily observed from the brilliant color patterns which suddenly appeared over the twinned region. Each twin occurrence was accompanied by a distinct acoustic burst heard by the investigator. An interesting feature of these studies was the occurrence, between twinning bursts, of lower energy pulses typical of slip line development. It was quite apparent that two separate and distinct mechanisms were operative in producing the acoustic emission. Although there did not appear to be a determinative or controlling role of either mechanism on the other, it was observed that the occurrence of large twins did tend to trigger a short duration avalanche of the emission associated with slip line development. Such experiments suggest that acoustic emission could be used to provide a better understanding of the deformation processes and their dynamic interactions. They further suggest the possibility of categorizing the deformation mechanism on the basis of a discrete acoustic characteristic which would be a marked advantage in the practical application of the emission phenomena.

The experimental observations of acoustic emission from martensitic transformations and during solidification of certain metals, also offer possibilities in relating emission to specific mechanisms. For the most part the significance of the emission has been related to the presence or absence of emission activity,

such as in recreating the equilibrium diagram from solidification emission, rather than to any distinguishing feature of the observed acoustic signal. The solidification of alloys involves a number of distinct transformations; hence, if unique signal features do exist, the emission would be immeasurably enhanced in its usefulness as a tool.

Evidence of being able to categorize deformation mechanisms from the acoustic characteristics has been obtained in the studies of composite structures where fiber fracture, matrix crazing and shear deformations can be distinguished to some degree from the acoustic chacteristics.

A further example of the insight that can be gained through acoustic emission was indicated in studies of gold single crystals. Except for thin film specimens, gold does not evidence mechanical twinning under load, but upon annealing a deformed gold specimen, fully developed twin structures, that is, the so-called thermal or annealing twins are apparent.

During our testing of virgin, gold single crystals, a rather substantial amount of the burst type signals was observed—signals very similar if not identical to those previously observed from twinning in zinc, cadmium, and tin. The emission behavior of the gold was unexpectedly different from that observed for the same fcc crystallographic structure of the aluminum.

Based on these results, it was speculated that the nucleus of a twin was formed by the sudden creation of faults, thereby generating an elastic emission pulse. The energy of the acoustic pulses suggested that a major portion of the twin mechanism had been accomplished and that the thermal treatment merely completed the surface ordering by which twins are normally observed optically. These experimental findings taken together with other observations over the years indicate that some predictability of the type of acoustic emission to be expected from a given material condition may be related to the stacking fault energy of the specimen. This hypothesis has not been developed by the writer and it is not known whether or not other work confirms such speculation.

Emission From Defects

One of the most significant assets of acoustic emission is the ability to detect the presence of active defects in structures and by the use of special techniques, to physically locate the defect in the structure. A major shortcoming in the practical application of this asset is the present inability to assess the severity of the defect with reasonable accuracy.

Experimental results[*9,10*] have shown that acoustic emission activity (emission rate) and emission energy are functions of the deformation rate, absolute stress level and volume of participating material, to name a few. Studies conducted on fatigue crack propagation in aluminum showed no qualitative emission characteristics which were indicative of crack severity. The fracture mechanics work of Dunegan et al[*11*], and recent work of others[*12*]

concerning emission response versus crack size are good beginnings to develop this potential, but much more effort is required in this specific area. Success in this effort would undoubtedly represent the greatest advancement in the nondestructive field.

Conclusion

Some of the less familiar characteristics of acoustic emission have been briefly outlined with the intent that they may suggest additional and alternate approaches to research in acoustic emission. For newcomers to the field the paper may serve to show some of the types of studies which have been made, but not widely reported, and duplication of effort may be avoided, depending on the reader's judgment of the technical expertise to be found in the original research reports.

Considering the current imbalance between research studies and the ever-increasing activity in practical applications of acoustic emission, the need for a broader understanding of the phenomenon becomes more urgent. Practical application necessitates data interpretation, the efficacy of which depends in turn on the depth and extent of knowledge of the tool, including its limitations. Until this is attained, we may answer a problem with more questions. For example, consider the hypothetical plight of the acoustic emission investigator at the current state of the art.

A large pressure vessel has been in service for several years and is to be tested for pressure integrity. Certain areas of the vessel are physically inaccessible for the more general ultrasonic and radiographic inspection methods because of structural configuration, insulation, concrete, radiation and other factors. Of course, a prime motive for employing acoustic emission is that immediate proximity to the area is not necessary, but also, more often than not these inaccessible areas contain discontinuity regions associated with relatively high local stresses.

The investigator begins to receive a number of distinct burst signals on his monitor. The rate that these signals occur provide important information on the defect propagation rate, while the time delays of the signals arriving at the transducers provide the data for computation of emission source location. How does the investigator distinguish between the rapid propagation of a large, critically growing crack, and the simultaneous emission from several smaller insignificant cracks, all in the near vicinity of each other? To date there have been no conclusive results reported from which the severity of the defect (size and propagation rate) can be determined. Presumably, distinguishing emission characteristics do exist and these need to be established in further research studies.

The situation outlined is not uncommon in many current designs; when ultrasonic and other techniques would not be available as confirmation or

backup to the acoustic emission, it is not only the emission investigator that may have a dilemma, but the user, fabricator, underwriter, and ultimate decision maker. Nevertheless, such present shortcomings do not justify avoidance of the dilemma by inaction. No other known tool even remotely affords the potential of acoustic emission. Without a doubt the solutions to the problems do not lie in research alone, but equally important, are the practical investigations accompanying the laboratory efforts. The reciprocal experience of the research and practical application will substantially enhance the development of the technique. The primary concern now is that research should be expanded in areas to accelerate realization of the full benefits of this method.

References

[1] Dunegan, H. L. and Green, A. T., *Materials Research and Standards*, MTRSA Vol. 11, No. 3, March 1971.

[2] Kaiser, J. "Untersuchungen über das Auftreten Gerauschen Beim Zugversuch," Ph. D. thesis, Technisch Hochschule, Munich, 1950.

[3] Liptai, R. G., Dunegan, H. L., and Tatro, C. A., *International Journal of Nondestructive Testing*, IJNTA, Vol. 1, No. 3, Aug. 1969.

[4] Borchers, H. and Kaiser, J., *Zeitschrift Für Metallkund*, ZEMTA, Vol. 49, 1958.

[5] Schofield, B. H., "Acoustic Emission From Metals–Its Detection, Characteristics and Source," Proceedings, Symposium on Physics and Nondestructive Testing, San Antonio, Tex. 1963.

[6] Schofield, B. H. "Acoustic Emission Under Applied Stress," AST-TDR-63-509, Part, I, USAF, Wright-Patterson air Force Base, Ohio, April 1963.

[7] Schofield, B. H., "Acoustic Emission Under Applied Stress," ASD-TDR-63-509, Part II, USAF, Wright-Patterson Air Force Base, Ohio, May 1964.

[8] Tatro, C. A. and Liptai, R. G., "Acoustic Emission from Crystalline Substances," Proceedings, Symposium on Physics and Nondestructive Testing, Southwest Research Institute, 1962.

[9] Schofield, B. H., "Acoustic Emission Under Applied Stress," ARL 150, USAF, Wright-Patterson Air Force Base, Ohio, Dec. 1961.

[10] Bareiss, R. A., Kyrala, A. A., and Schofield, B. H., "Acoustic Emission Under Applied Stress," ASTIA Document AD155674, WADC Technical Report 58-194, USAF, Wright-Patterson Air Force Base, Ohio, 30 April 1958.

[11] Dunegan, H. L., Harris, D. O., and Tatro, C. A., "Fracture Analysis by Use of Acoustic Emission," USAEC Report UCRL-70323 (CONF-670604-1), University of California, Lawrence Radiation Laboratory, Livermore, Calif., 6 Feb. 1967.

[12] Gerberich, W. W. and Hartbower, C. E., *International Journal of Fracture Mechanics*, IJFMA, Vol. 3, No. 3, Sept. 1967, pp. 185-192.

Related References

Books

Thewlis, J., et al., Eds., *Encyclopaedic Dictionary of Physics*, Supplementary Vol. 1, Pergamon Press, Inc., New York, 1967.

Journals, Proceedings, Transactions

Gillis, P. P., *Materials Research and Standards*, MTRSA, Vol. 11, No. 3, March 1971, p. 11.

Green, A. T., *Nuclear Safety*, NUSAA, Vol. 10, No. 1, Jan.-Feb. 1969, pp. 4-18.

Pollock, A. A., *Ultrasonics*, ULIQA, Vol. 6, No. 2, April 1968, pp. 88-92.

Tetelman, A. S., *Materials Research and Standards,* MTRSA, Vol. 11, No. 3, March 1971, p. 13.

Reports and Other Publications

Dunegan, H. L., "Acoustic Emission–A New Nondestructive Testing Tool," 1968 Symposium on Nondestructive Testing of Welds and Materials Joining, Los Angeles, Calif. 11-13 March 1968.

Green, A. T., "Stress-Wave Detection, Saturn S-II," Report NASA-CR-61161, Aerojet-General Corporation, Sacramento, Calif., Dec. 1966.

Hutton, P. H., *Materials Evaluation,* MAEVA, Vol. 26, No. 7, July 1968, pp. 125-129.

Parry, D. L., "Nondestructive Flaw Detection in Nuclear Power Installations in Incipient Failure Diagnosis for Assuring Safety and Availability of Nuclear Power Plants," USAEC Report CONF-671011, Jan. 1968, Conference Proceedings, Gatlinburg, Tenn., 30 Oct.-1 Nov. 1967.

Schofield, B. H., "Investigation of Applicability of Acoustic Emission," AFML-TR-65-106, USAF, Wright-Patterson Air Force Base, Ohio, May 1965.

Schofield, B. H., "A Study of the Applicability of Acoustic Emission to Pressure Vessel Testing," Report AFML-TR-66-92, Lessells and Associates, Inc., Waltham, Mass., March 1966.

P. P. Gillis[1]

Dislocation Motions and Acoustic Emissions

REFERENCE: Gillis, P. P., "Dislocation Motions and Acoustic Emissions," *Acoustic Emission, ASTM STP 505*, American Society for Testing and Materials, 1972, pp. 20-29.

ABSTRACT: The possible role of dislocations in producing acoustic emissions is discussed from a kinetic point of view. A general theory of the acoustic power of dislocation motions is developed. For deformations that tend towards homogeneity and are dependent on dislocation motions the implications of this theory are qualitatively described and shown to be corroborated by selected experimental results.

KEY WORDS: dislocations (materials), acoustics, emission, deformation, elastic waves, failure, phonons, kinetics, strain rate, plastic deformation

Acoustic emission is a phenomenon characterized by two principal features: in theory, there is no real definition of "acoustic emission"; and in practice the experimental data are largely dependent upon the equipment used and the settings selected by each individual observer. Thus, for example, we find in the literature count rates as low as a few events per deformation increment, and as high as 10^5 events per second under continous slow straining; estimated rise times of the pulses ranging from microseconds to nanoseconds; and substantially different results for tests in tension and compression.

Another notable feature of acoustic emission is that it is frequently attributed to dislocation motions although it is readily observed in noncrystalline materials in the deformation of which dislocations are generally assumed to be unimportant. It seems reasonable to conclude that acoustic emission is a term used to describe stress waves that arise from a variety of sources. The attempt made in this paper is to assess the kind of acoustic emissions that might be produced by dislocation motions.

For this purpose dislocation motions are broadly separated into two categories, homogeneous and nonhomogeneous. Only the first is treated here

[1] Associate professor, Department of Metallurgical Engineering and Materials Science, University of Kentucky, Lexington, Ky. 40506.

and is intended to include only such motions as tend to produce homogeneous deformation of the specimen under consideration. These motions need not be homogeneous in detail but they must be such as not to accentuate existing flaws or create new ones.

Propagation of a Lüders band front qualifies as a process tending to produce homogeneous deformation because the locally nonhomogeneous Lüders strain spreads throughout the specimen to finally produce a homogeneous strain condition. On the other hand, dislocation motions associated with crack initiation growth of the plastic zone at a crack front, void formation and coalescence, and other processes of localized necking or fracture are nonhomogeneous by the foregoing definition because they concentrate locally nonhomogeneous strains in highly localized regions. Most of these have been discussed by Tetelman[*1*]. It should be noted that nonhomogeneous processes have the greatest technological significance because they are indicative of impending failure. However, in many situations their signals differ mainly in degree from those of homogeneous processes so it seems worthwhile to treat the simpler case initially.

Some consideration was given in a previous paper[*2*] to the elastic energies of various static dislocation arrays and how these energies changed with changes of the dislocation configurations. Such energy changes were described as possible sources of acoustic emissions. However, it is well known that only a small fraction of the work of plastic deformation is stored in cyrstalline materials in the residual strain fields of dislocation arrays. The major portion of the work of plastic deformation is known to increase the temperature of the material. This heating is attributable to the traverse of dislocations through the crystal lattice which imparts added vibrational motion to the atoms as the dislocation passes. Thus in the present paper dislocation kinetics are treated in order to assess this major portion of the plastic work. This approach gives a more realistic insight to the possible role of dislocations in producing acoustic emissions, and it does not require the postulation of specific types of arrays.

Moving dislocations are the dominant mechanism of plastic deformation in most crystalline solids, especially metals. The total deformational energy is customarily divided into two portions, an elastic part that is recoverable upon unloading and the balance that is called the plastic work of deformation. This latter includes a small component, about ten percent of the total, associated with an increase in the number of dislocations (and other defects) in the crystal structure which can be recovered by annealing. The bulk of the plastic work, however, appears as thermal energy in the specimen. This thermal energy is the cumulative effect of the generation of a great number of phonons by dislocations as they pass through the crystal lattice.

A graphical discription of the phonon generation process is given by Hartl and Weiner[*3*]. Briefly it is based on the fact that there are periodic positions in the

lattice which provide a minimum energy configuration for a dislocation. As a dislocation moves from one of these to the next it must surmount the Peierls barrier before dropping into the next minimum energy position. (See, for example, Cottrell[*4*].) As the dislocation moves away from one minimum energy position the elastic lattice strain is increased until the "over-center" position is reached. After this the increment of elastic strain is suddenly released to produce a vibrational wave in the lattice. This process is considered here as the basic mechanism by which dislocations can cause acoustic emissions.

An enormous length of dislocation line is required for deformation even in the microplasticity range. However, it is speculated that the cooperative motion of all the dislocation line segments is such that each tends to move with a favorable position in the stress fields of its neighbors. In consequence, the vibrational waves produced by each tend to be in phase.

The total rate of plastic work in the specimen, called the plastic power, is the scalar product of each force with the nonelastic portion of its rate of displacement summed over all forces acting on the specimen. The equivalent result is expressible in terms of dislocation motions as the inner product of the stress tensor $\underset{\sim}{\sigma}$ and the plastic strain rate tensor $\underset{\sim}{\dot{\epsilon}}$ integrated over the specimen volume. The plastic strain rate tensor depends upon the dislocation motion in the following way.

Plastic Strain Rate

Consider an elementary segment of dislocation line within a specimen. As shown in Fig. 1, some glide plane can be assigned to the segment according to the following scheme. the crystallographic displacement associated with the dislocation is called its Burgers vector and is denoted by $\underset{\sim}{b}$. The unit vector $\underset{\sim}{t}$ is

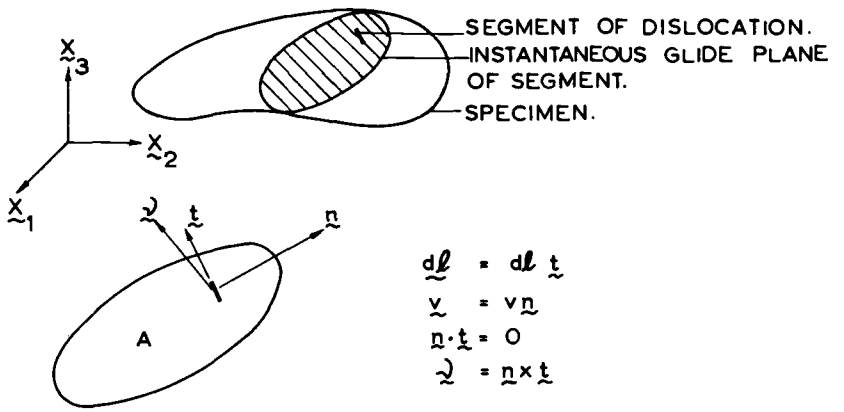

FIG. 1—*Geometry of a segment of dislocation and its glide plane.*

the local tangent to the segment of length dl. A velocity vector $\underset{\sim}{v} = v\underset{\sim}{n}$ where $\underset{\sim}{n}$ is a unit vector such that $\underset{\sim}{n} \cdot \underset{\sim}{t} = 0$ completes the description of the segment. The glide plane is then defined by means of its unit normal vector $\underset{\sim}{\nu} = \underset{\sim}{n} \times \underset{\sim}{t}$. If $v = 0$ there is no contribution to the plastic strain rate from the segment and so its glide plane is immaterial. Among all the dislocation segments in the crystal those characterized by the same $\underset{\sim}{b}$ and $\underset{\sim}{\nu}$ are classified as one family of dislocations.

Cottrell[4] shows that the average relative displacement of the two portions of the specimen separated by a glide plane of area A containing a dislocation loop of area α is $\underset{\sim}{u} = \underset{\sim}{b}\alpha/A$. In the present context, the average relative velocity of the two portions is:

$$d\dot{\underset{\sim}{u}} = \underset{\sim}{b}\, d\dot{\alpha}/A = \underset{\sim}{b} v\, dl/A \tag{1}$$

The consequent macroscopic plastic strain rate from a single family of dislocations is the velocity $\dot{\underset{\sim}{u}}$ of one end of the specimen relative to the other end divided by the appropriate separation. Obviously $\dot{\underset{\sim}{u}}$ is obtained by integration of $d\dot{\underset{\sim}{u}}$ over the total length of segments in the volume.

Calling the specimen volume V and introducing orthogonal unit vectors x_1, x_2, x_3 as a coordinate reference, characteristic specimen dimensions z_i can be defined by:

$$1/z_i = (A/V)\underset{\sim}{\nu} \cdot \underset{\sim}{x}_i = (A/V)\, \nu_i \tag{2}$$

This definition gives $A_i z_i = V$ where $A_i = A\nu_i$ is the projection of A onto the plane perpendicular to x_i. The plastic strain rate tensor components are $d\dot{\epsilon}_{ij} = (d\dot{u}_i/z_j + d\dot{u}_j/z_i)/2$. Substitution from Eqs 1 and 2 gives:

$$d\dot{\epsilon}_{ij} = (b_i\nu_j + b_j\nu_i)\,(v dl/2V) \tag{3}$$

Thus for a single dislocation family:

$$\dot{\epsilon}_{ij} = (b_i\nu_j + b_j\nu_i)/2V \int_L v dl \tag{4}$$

where the integration extends over the total length L of that family of dislocation lines in the crystal. For several different families several similar equations describe the contribution from each family to $\dot{\underset{\sim}{\epsilon}}$ and these are summed to obtain the total.

A familiar form of this relation is obtained by denoting the average dislocation velocity as $\bar{v}$; the average dislocation length per unit volume as dislocation density $\bar{\rho} = L/V$; and with the magnitude of $\underset{\sim}{b}$ denoted by b, $(b_i\nu_j + b_j\nu_i)/2b$ as an orientation factor Φ. Then for the i and j corresponding to Φ, $\dot{\epsilon} = \Phi b \bar{\rho} \bar{v}$.

The plastic strain rate specified by Eq 4 is macroscopic in the sense that it describes the behavior of one end of the specimen (or gage length) relative to the other. Because dislocation motions are seldom homogeneous except in an average sense it is more convenient to consider an equivalent local plastic strain rate based upon an elementary volume dV. To reasonably satisfy the conditions of Cottrell's analysis[4], dV must be considered as being reasonably large in comparison with the intense stress field at the dislocation core. Preceeding as above, the local dislocation density is defined as $\rho = dl/dV$ so that Eq 3 becomes:

$$d\dot{\epsilon}_{ij} = \tfrac{1}{2}(b_i\nu_j + b_j\nu_i)\mathrm{v}\rho dV \tag{5}$$

The equivalent of Eq 4 is then:

$$\dot{\epsilon}_{ij} = \tfrac{1}{2}(b_i\nu_j + b_j\nu_i)\int_V \rho \mathrm{v} dV \tag{6}$$

for a single family of dislocations, and a summation of such expressions when, as is usual, more than one family is involved in the deformation process.

Plastic Power

The corresponding plastic power is denoted by $d\dot{w}$ and equals the inner product of the stress and plastic strain rate tensors:

$$d\dot{w} = \sigma \circ d\dot{\epsilon} = \sigma_{ij} d\epsilon_{ij} \tag{7}$$

Introducing the expression for the plastic strain rate from Eq 5 the rate of plastic work per unit volume can most compactly be written using dyadic notation:

$$d\dot{w}/dV = \sum_{i=1}^{N} (\underset{\sim}{\sigma} \cdot \underset{\sim}{b}^i) \cdot \underset{\sim}{\nu}^i \mathrm{v}^i \rho^i \tag{8}$$

Here the superscript i is merely a family label for use in summation over the N families of dislocations.

Equation 8 represents the power per unit volume that is generated by moving dislocations. As previously discussed, most of this power is dissipated as heat in the crystal lattice and can be considered potentially as a power source for acoustic emissions. This power is proportional to the local stress in the region of dislocation motion and to the dislocation flux, that is, the product $\mathrm{v}\rho$.

Relation to Experiment

Whether the available power produces detectable acoustic emissions depends upon both the mode of dislocation motion and the signal detection equipment. For example, consider an ordinary uniform tension specimen being deformed

past the yield point at an approximately constant strain rate. For absolutely uniform dislocation motion within the specimen acoustic emissions are produced uniformly and continuously throughout the volume of the specimen and thus the plastic power will merely intensify the background noise level and no acoustic bursts will be observed. However, for spatially nonuniform or timewise discontinuous motion there will tend to be acoustic bursts whose frequency of occurrence (count rate) will depend directly on the frequency of the initiation of motion. The pulse shape of the bursts will depend on the details of the motion but will have an extremely rapid rise because of the quickness with which dislocations accelerate [5].

Experiments by Fisher and Lally [6] clearly demonstrate the applicability of the present analysis. They tested monocrystals of magnesium, copper, brass, copper-7 percent aluminum, and iron at various deformation rates under uniaxial tension. They observed count rates for each material directly proportional to the plastic strain rate.

To relate the macroscopic axial plastic strain rate, or deformation rate, to the count rate and the local plastic strain rate, the mode of deformation must be considered. Typically, monocrystalline deformation proceeds through the following stages. Some of the most readily moved dislocations are able to form a number of isolated slip bands. These are regions across the specimen but of limited axial extent which have local strains up to a few percent. They are characterized by having a much higher dislocation density than the adjacent material. These bands tend to spread axially increasing the dislocation density of the material into which they move. Then adjacent bands coalesce so that the entire specimen is covered. It then has a relatively uniform and high dislocation density and a fairly uniform strain of a few percent. The process is directly analogous to the propagation of Lüders bands in ordinary mild steel except that there are seldom more than two active band fronts in this latter process.

After the crystal has been filled by the growth of the initial deformation bands it is not clear microscopically how the further deformation proceeds because the dislocation density is too large to permit detailed further observations of behavior. From macroscopic observations the subsequent deformation usually appears to be somewhat homogeneous up to the onset of failure.

The process of band growth can be reasonably assumed to consist of screw dislocation segments in the band front moving off their primary glide planes into the virgin material adjacent the band and producing new dislocations there by the multiple cross glide mechanism. These new dislocations then move in the primary glide direction and multiply until an axial length ΔX has been strained an increment ϵ^* through the entire thickness of the specimen, in a time interval ΔT (Fig. 2). In the next interval ΔT this process is repeated at this or another of the band fronts.

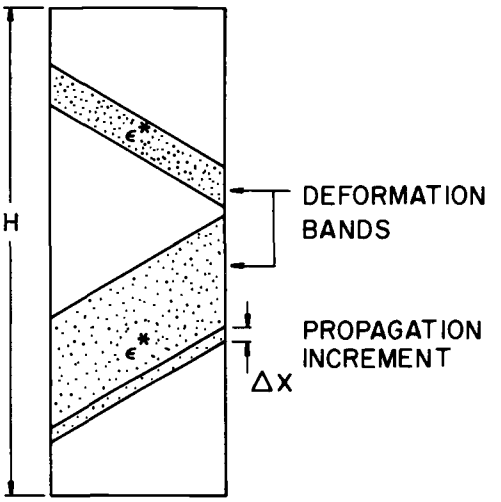

FIG. 2—*Propagation of deformation bands in a monocrystalline specimen.*

Associating each such event with an acoustic emission, the count rate is simply $\dot{N} = 1/\Delta T$. The local plastic strain rate is $\epsilon^*/\Delta T$ but the macroscopic plastic strain rate obtained by referring the incremental change of length $\epsilon^* \Delta X$ to the total specimen length H is $\dot{\epsilon} = (\epsilon^*/\Delta T)\,(\Delta X/H) = \epsilon^* \dot{N} \Delta X/H$. By assuming ϵ^* and ΔX to be constant the count rate $\dot{N} = \dot{\epsilon} H/\epsilon^* \Delta X$ is directly proportional to the plastic deformation rate as observed by Fisher and Lally [6].

Furthermore, in this model the count rate for specimens of different sizes deformed at the same macroscopic rate is proportional to specimen length but independent of cross sectional area. This is confirmed experimentally by Fisher and Lally.

With regard to this last point it is interesting to speculate on a corresponding result for polycrystalline specimens. In the absence of Lüders bands the individual grains tend to deform in much the same way as postulated for monocrystals. Associating an event then with the growth of a band within a single grain we denote the average number of grains in the cross section by G. With reference to Fig. 3 the macroscopic strain contribution from the deformation of G grains during an interval ΔT is again $\epsilon^* \Delta X/H$ where ϵ^* is an average, local plastic strain in the bands. If the grains deform individually the count rate is $\dot{N} = G/\Delta T$. The macroscopic deformation rate is now $\dot{\epsilon} = \epsilon^* \Delta X/H \Delta T = \epsilon^* \dot{N} \Delta X/HG$.

It is useful to denote the grain diameter by D and the cross sectional area by A so that the number G equals A/D^2. The deformation rate can then be written as $\dot{\epsilon} = \epsilon^* \dot{N} \Delta X D^2/AH$ or the count rate as $\dot{N} = \dot{\epsilon} AH/\epsilon^* \Delta X D^2$. If ϵ^* and ΔX are

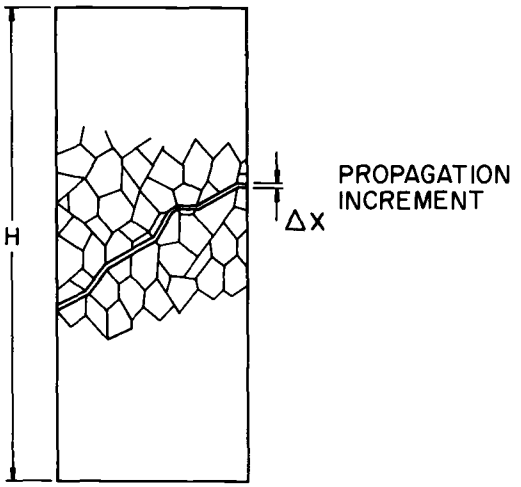

FIG. 3—*Propagation of deformation in a polycrystalline specimen.*

relatively insensitive to changes in other aspects of the deformation they can again be taken as approximately constant. Thus, the count rate at constant $\dot{\epsilon}$ and constant grain size becomes proportional to specimen volume. At constant $\dot{\epsilon}$ and specimen volume the count rate would increase with decreasing grain size although the energy of each burst would simultaneously decrease because of the smaller grain volumes involved in the events. There are presently no experiments within my ken which relate to the first two of these speculations. However, Dunegan and Green[7] substantiate that pulses are more difficult to discern in fine grained uranium than in the as-cast metal.

Other respects in which the experiments of Fisher and Lally were similar for all the materials tested were that count rates decreased gradually with strain but increased dramatically prior to failure. The first of these features is interpreted as an increasing tendency towards uniformity of straining. Once the dislocation density reaches the fairly high value associated with band saturation more and more of the subsequent straining is accommodated by diffuse motion of large numbers of the dislocations in a manner that does not generate observable emissions. Finally, however, deformation localizes at some defect and becomes extremely inhomogeneous as failure becomes imminent.

A principal respect in which the materials tested differed was the count rate at yield. Copper-7 percent aluminum the one material showing a drop of stress at this point also showed a simultaneous intense acoustic activity. As Fisher and Lally point out, this is caused by the very large increase in deformation rate that must occur to produce the stress drop. Materials with gradually rounded stress-strain curves had gradually increasing count rates up to the level associated

with band propagation. These differences reflect the dislocation motions associated with band formation. In the copper-aluminum the initial formation was much more precipitous than in the other materials, but nevertheless seemed to consist of a very large number of discrete events. Fisher and Lally obtained results from polycrystalline mild steel strikingly similar to those for copper-aluminum.

Experimental results published by Dunegan, Harris, and Tatro[8] can be interpreted as tending to confirm the foregoing analysis. Uniaxial tension tests of ordinary specimens of polycrystalline beryllium and aluminum produce approximately equal count rates under presumably identical testing conditions. Because of differences in their crystal structures the beryllium would be expected to deform much less uniformly than the aluminum and undoubtedly it does. However, the flow stress of the aluminum is more than double that of the beryllium and therefore the plastic power of smaller events in the aluminum can equal that of larger events in beryllium. This tends to produce a count rate for fairly uniform deformation in the former that is comparable so that for very nonuniform deformation in the latter.

Conclusion

It seems reasonably clear that acoustic emissions are detected in many deformation processes in which dislocations play no role. In homogeneous deformations which do involve dislocations, however, observed acoustic emissions can be correlated nicely with the apparent motion of the dislocations. A grey middle ground is occupied by the nonhomogeneous deformation processes accompanying crack propagation; certainly dislocation motion spreads the plastic zone at the crack tip and acoustic emissions are detected, but it is difficult to correlate the two.

Technologically, the nonhomogeneous deformations have the greatest significance because of their intimate connection with structural failures and so a substantial effort must be devoted to the detection and identification of their emissions. Theoretically, the most intriguing feature of the homogeneous deformation results, is their symmetry when plotted as count rate versus stress. Understanding of this pattern will undoubtedly lead to a substantially improved quantitative dislocation theory of post yield mechanical behavior.

Acknowledgments

This work was done at the Physics and Engineering Laboratory, Lower Hutt, during the course of a fellowship provided under the Fulbright-Hays Act by the New Zealand–United States Educational Foundation.

References

[1] Tetelman, A. S., *Materials Research and Standards,* MTRSA, Vol. 11, No. 3, March 1971, pp. 13-16.
[2] Gillis, P. P., *Materials Research and Standards,* MTRSA, Vol. 11, No. 3, March 1971, pp. 11-13.
[3] Hartl, W. F. and Weiner, J. H., *Physical Review,* PRVAA, Vol. 152, No. 2, Dec. 1966, pp. 634-644.
[4] Cottrell, A. H. in *Dislocations and Plastic Flow in Crystals,* The Clarendon Press, Oxford, 1953.
[5] Gillis, P. P. and Kratochvil, J., *Philosophical Magazine,* PHMAA, Vol. 21, No. 170, Feb. 1970, pp. 425-432.
[6] Fisher, R. M. and Lally, J. S., *Canadian Journal of Physics,* CJPHA, Vol. 45, No. 2, Part 3, Feb. 1967, pp. 1147-1159.
[7] Dunegan, H. L. and Green, A. T., *Materials Research and Standards,* MTRSA, Vol. 11, No. 3, March 1971, pp. 21-24.
[8] Dunegan, H. L., Harris, D. O., and Tatro, C. A., *Engineering Fracture Mechanics,* EFMEA, Vol. 1, No. 3, June 1968, pp. 105-122.

A. S. Tetelman[1] *and R. Chow*[1]

Acoustic Emission Testing and Microcracking Processes

REFERENCE: Tetelman, A. S. and Chow, R., "Acoustic Emission and Microcracking Processes," *Acoustic Emission, ASTM STP 505*, American Society for Testing and Materials, 1972, pp. 30-40.

ABSTRACT: The various stages of microcrack initiation, microcrack growth, and final fracture are reviewed and the relation between their processes and acoustic emission is discussed. A theoretical model relating acoustic emission to the microcrack density of low carbon steel is presented, based upon experimental results of the microcrack density in low carbon iron. The model predicts that the total number of acoustic emissions increases rapidly with applied stress, above a threshold value.

KEY WORDS: acoustics, emission, cracking (fracturing), crack propagation, crack initiation, fractures (materials), stresses, grain boundaries, shear stress, dislocations (materials), plastic deformation, failure

Microcrack Initiation

The initiation and micropropagation of cracks (microcracks) occur at stress levels that are well below the theoretical cohesive strength $\sigma_c = E/10$, where E is the elastic modulus. For fracture to occur, some form of internal stress concentration is required to raise the local stress level to the theoretical value and break atomic bonds. It is now generally agreed that piled up groups of edge dislocations (Fig. 1*a*) are responsible for crack initiation [*1*]. A tensile stress field is developed below the slip plane where a half plane of atoms is missing. If a sufficient number of adjacent half-planes are removed, then by definition the material is cracked and fracture has initiated.

A strong obstacle such as a grain boundary is required to hold the dislocation group and allow the applied shear stress τ to force the leading dislocations together. About a thousand dislocations are required to form a crack nucleus. The microplasticity of the material plays a large role in determining whether

[1] Materials Department, School of Engineering and Applied Science, University of California, Los Angeles, Calif. 90024.

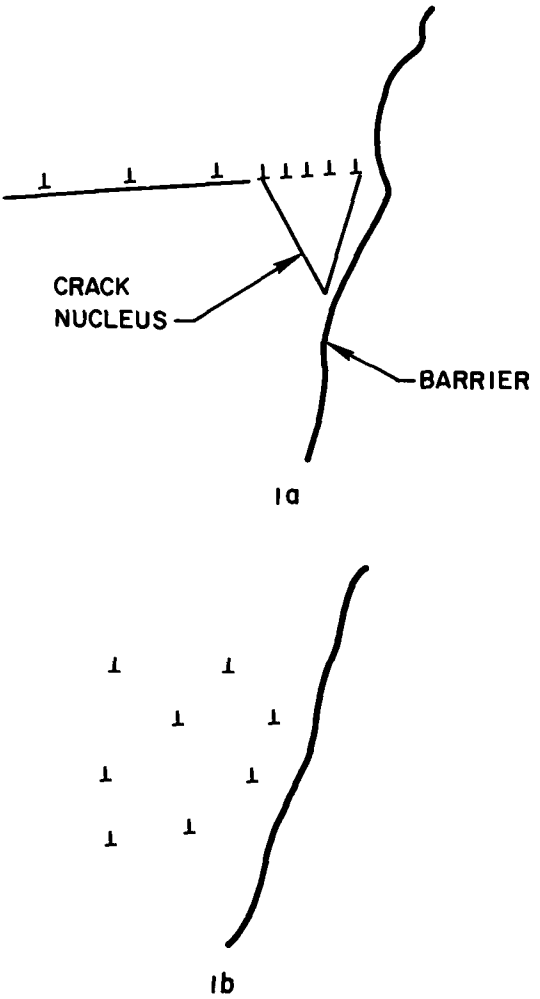

FIG. 1–(*a*) *Dislocation distributions associated with planar glide and microcracking and* (*b*) *homogeneous plastic flow.*

microcracking or large scale plastic deformation will occur. In soft materials such as pure copper and 2 oil caps aluminum, dislocations are able to cross slip from one plane to another and arrange themselves into a homogeneous array (Fig. 1*b*). At no point is there sufficient tensile displacement to cause the crack formation shown in Fig. 1*a*. However, bcc metals and ceramics deform by planar glide and twinning, and the dislocation pileup shown in Fig. 1*a* can form and lead to cracking at low temperature.

At higher temperatures, cross slip and activation of dislocation sources near

the pileup tip cause a relaxation of tensile stress and cracking does not occur. According to dislocation theory, the condition for crack initiation is

$$\tau_N nb = \tau_i nb + 2\gamma \tag{1}$$

where τ_N is the critical shear stress resolved on the slip plane, in the slip direction, τ_i is the frictional stress that opposes the motion of dislocations moving on their slip plane, n is the number of dislocations in the pileup, each having a Burger's vector b, and γ is the total elastic plus plastic work per unit area expended in making microcrack surface area. Materials that deform homogeneously have relatively few dislocations per slip plane (n small) so that crack initiation is more difficult (large τ_N), in comparison with those materials which deform inhomogeneously.

We expect that the instability associated with the movement of a packet of dislocations along a plane during planar glide would release more energy than the more stable deformation characterized by wavy glide. Acoustic emission signals results from rapid releases of energy. Thus, they record events while they are taking place and might be able to differentiate between these two forms of plastic flow. For example, it may be that the acoustic signals emitted by brittle materials during plastic flow appear in less frequent bursts of higher amplitude than those emitted by softer materials (Fig. 2). If this is the case, we may eventually be able to partially characterize brittle and ductile materials by their acoustic emission spectra. This opens the possibility of using acoustic emission testing to characterize progressive embrittlement of a material over a period of time (for example, due to strain aging or neutron irradiation embrittlement).

It is interesting to note that Eq 1 predicts that cracks can be initiated equally well under compressive or tensile loading, since it is the applied shear component

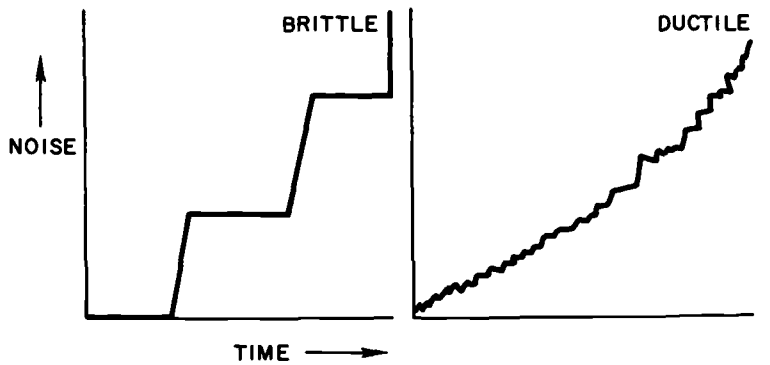

FIG. 2–*Schematic composition of possible acoustic emission patterns from brittle and ductile materials.*

of stress which is responsible for the cracking. This suggests that acoustic emission studies of the initiation process could best be conducted under compressive loading, to separate out the effects of propagation which release considerably more energy.

Microcrack Propagation

The microcracks that are initiated by dislocation pileups are quite small, on the order of 0.10 μm. These cracks will not grow unless sufficient energy is released during crack extension to overcome the energy required to create new crack surface. Consider (Fig. 3), a crack containing n dislocations of strength b that lie perpendicular to the tensile stress σ. The work done in opening up the crack of length a and unit thickness is

$$\sigma\, nba \tag{2}$$

while the total (elastic plus plastic) energy required to cause fracture is

$$2\,\gamma\, a \tag{3}$$

The condition for crack growth is thus

$$\sigma_G\, nb \geqslant 2\gamma \tag{4}$$

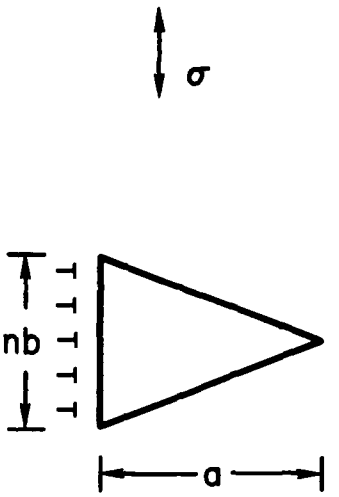

FIG. 3—*Dislocation representation of a growing crack.*

Again, we notice the importance of slip distribution (which determines n) in the cracking process. Once the crack has begun to spread, it will continue to propagate unstably because the driving force for propagation exceeds the resistance. The stress required for propagation drops below the stress σ_G at which the crack began to grow (Fig. 4*a*). Kinetic energy is thereby transmitted to surrounding materials and produces a sharp burst of acoustic emission.

In materials such as low carbon steel, cracks can begin to grow at low stress levels if brittle second phase particles such as carbides are present at grain boundaries. These particles restrict stress relaxation around the pileup and

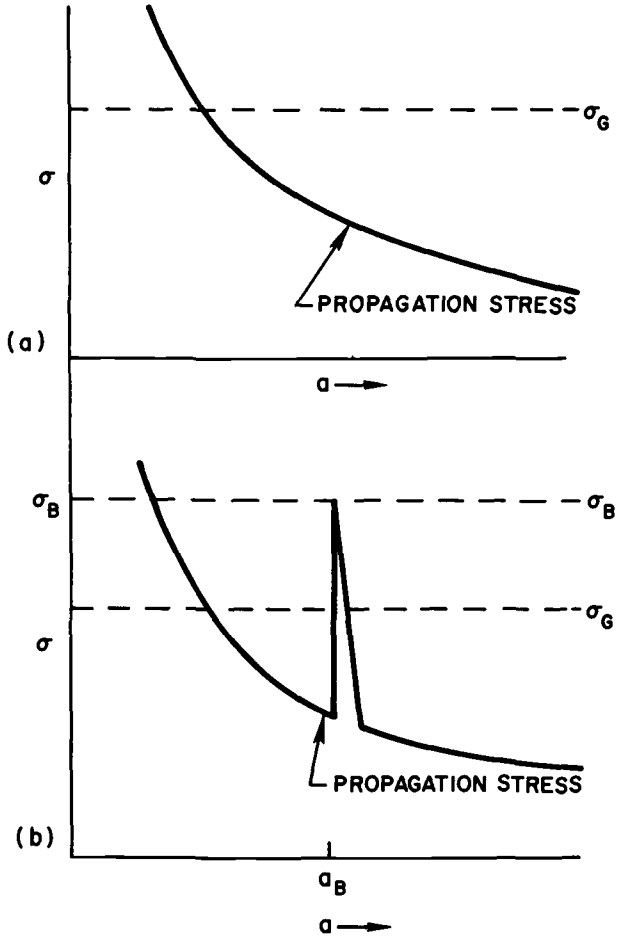

FIG. 4–(*a*) *Conditions for unstable fracture and* (*b*) *stable fracture. In* (*b*), *stress required for continued propagation is increased above applied stress at barrier.*

effectively keep γ to a minimum during pileup formation. In these cases, the stress σ_G at which cracks begin to grow will be less than the stress σ_B required to force the crack through a relatively strong barrier to its continued propagation (Fig. 4*b*). The cracks will then be arrested by the barrier and complete fracture will not occur until the applied stress is increased to σ_B. In low carbon steel, grain boundaries are able to serve as barriers to microcrack propagation and restrict the microcrack length to one or two grain diameters.

Numerous microcracks form prior to fracture as the applied stress is increased (Fig. 5)[*2,3*]. Each of these fracture events provides a source of acoustic emission, the energy released when a particular grain fractures. The energy stored in a grain stressed to a level σ is proportional to $\sigma^2/2E$. If we assume that

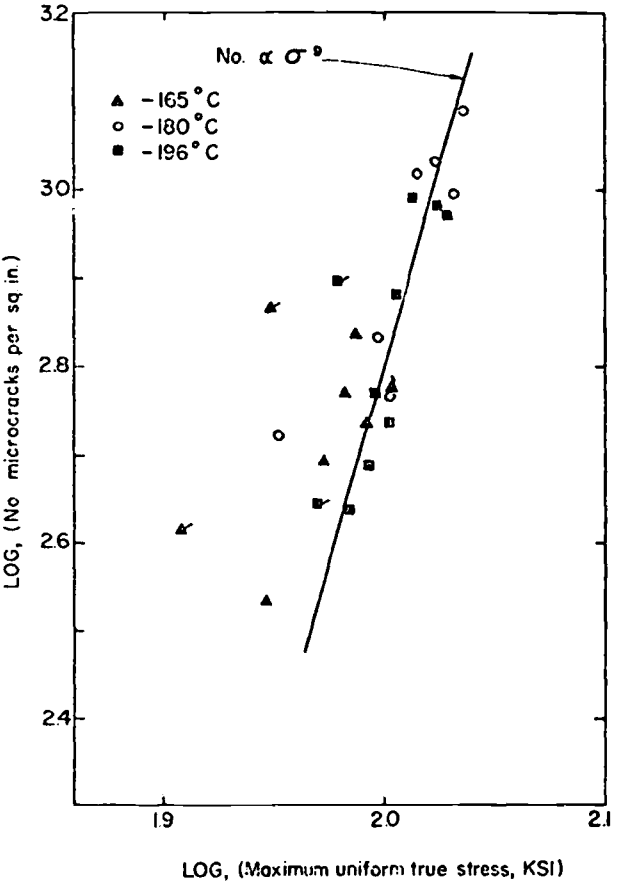

FIG. 5—*Stress dependence of microcrack formation in low carbon steel tension specimens* [*3*].

a grain is relaxed completely when a microcrack propagates across it, then the energy released during microcrack growth is

$$E_g = \alpha^2 \sigma^2 \tag{5}$$

where α is a constant that depends on grain size. Harris et al[*4*] have proposed that the initial voltage output from a transducer coupled to a deforming material, V_0, is proportional to the square root of the energy released during a given deformation process. For microcrack growth,

$$V_0 = \psi\sqrt{E_g} \tag{6}$$

Harris et al have also proposed that voltage V of the signal is an exponentially damped sinusoidal wave, according to the relation

$$V = V_0 e^{-\beta t} \cos\lambda t \tag{7}$$

where

β = damping constant,
λ = angular frequency = $2\pi f$
f = linear frequency.

The number of counts, N that is measured for a single event is the number of times that the signal exceeds the threshold voltage V_t at which the counter is set. If t' is the time for the signal to be damped down to V_t, then

$$V_t = V_0 e^{-\beta t'} \cos\lambda t' \tag{8}$$

Since (Fig. 6)

$$N = ft' = \frac{\lambda}{2\pi} t' \tag{9}$$

we have

$$V_t = V_0 e^{-\beta t'} \tag{10}$$

so that

$$\beta t' = \ln \frac{V_0}{V_t} \tag{11}$$

and then

$$N = \frac{f}{\beta} \ln \frac{V_0}{V_t} \tag{12}$$

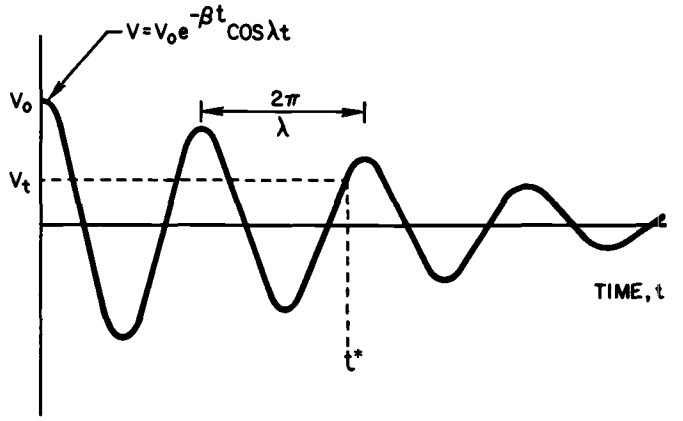

FIG. 6–*Excitation of transducer from acoustic signal [4].*

Substituting Eq 6 into Eq 12, we find a relation between the number of acoustic emission signals, N, and the energy of a given event

$$N = \frac{f}{\beta} ln \left(\frac{\psi \sqrt{E_g}}{V_t} \right) \tag{13}$$

If the energy released during an event is proportional to the square of the applied stress level (Eq 5), then

$$N = \frac{f}{\beta} ln \left(\frac{\psi \alpha \sigma}{V_t} \right) \tag{14}$$

Since $ln\ 1=0$, the limiting stress σ_0 is defined as

$$\sigma_0 = \left(\frac{\psi \alpha}{V_t} \right)^{-1} \tag{15}$$

so that

$$N = \frac{f}{\beta} ln(\sigma/\sigma_0)\ (\sigma > \sigma_0) \tag{16}$$

is the number of counts associated with one event that occurs at a stress level σ.

Figure 5 indicates that the microcrack density in low carbon steel obeys the relation

$$\rho = C\sigma^9 \tag{17}$$

so that the rate of microcrack formation, as measured in a tensile test under increasing stress is

$$\frac{d\rho}{d\sigma} = 9\, C\sigma^8 \tag{18}$$

The total number of acoustic emissions that are expected after a material has been stressed to a level σ, is therefore

$$N_{tot} = \int_{\sigma_0}^{\sigma} N(\sigma)\, d\rho = \int_{\sigma_0}^{\sigma} N(\sigma) \left(\frac{d\rho}{d\sigma}\right) d\sigma \tag{19}$$

From Eqs 16, 18, and 19 we have

$$N_{tot} = \left(\frac{f}{\beta}\right) 9C \int_{\sigma_0}^{\sigma} \ln(\sigma/\sigma_0)\sigma^8\, d\sigma \tag{20}$$

$$N_{tot} = \left(\frac{f}{\beta}\right) 9C \left[\frac{\sigma^9}{9}\left(\ln\frac{\sigma}{\sigma_0} - \frac{1}{9}\right) + \frac{{\sigma_0}^9}{81}\right] \tag{21}$$

We are presently in the process of determining experimentally whether the total acoustic emission count does, in fact, follow a 9th power law in low carbon steel. Preliminary data (Fig. 7) indicate a sharp rise in acoustic emission counts just prior to failure of a low carbon steel tension specimen at −321 F. Once a relation has been developed between the number of cracked grains and the failure stress, it may be possible to use acoustic emission testing to predict the impending failure of tensile specimens, or large structures containing preexisting flaws.

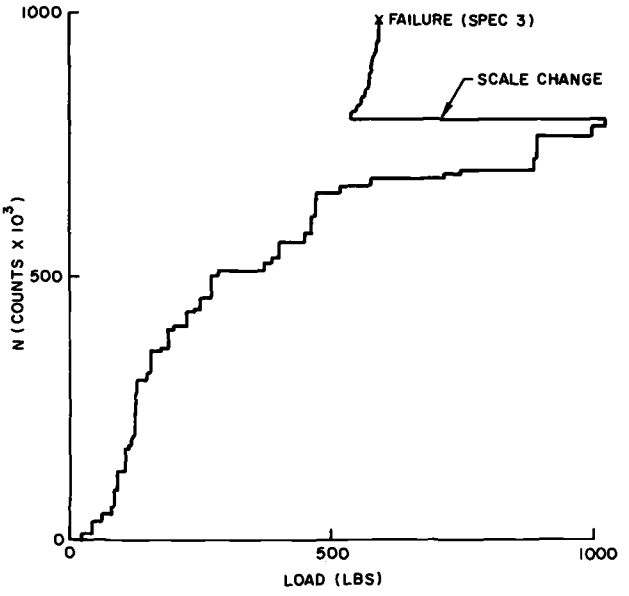

FIG. 7—*Acoustic signal rate observed during tensile testing of low carbon steel at −321 F.*

Fast Fracture

Final fracture of the entire specimen occurs when a microcrack is able to propagate through any barriers that restrict its growth or when a group of stopped cracks link together to form a sufficiently large macrocrack such that a macrocrack propagation will occur. The process of crack propagation in steel occurs discontinuously, with repeated microcrack initiation and growth taking place in the plastic zone ahead of the advancing macrocrack. These events, which occur rapidly across the entire crack front, produce large bursts of acoustic emission during final fracture.

In precracked specimens, the size of the plastic zone in the vicinity of the crack front increases with increasing stress intensity K, until $K = K_c$ and fast crack propagation occurs. Since the microcrack density increases with stress, it will also increase with plastic strain level in the zone, and hence it will increase with K. Although the experiments have not yet been conducted, we would expect that acoustic emission should increase as K approaches K_c, at temperatures just above the vicinity of the nondestructive test (NDT) where stable crack growth precedes fracture.

Environmental Fracture

Many fracture problems associated with high yield strength steel involve some form of environmental fracture, such as stress corrosion cracking or hydrogen embrittlement. Here too, acoustic emission has been extremely useful. For example, hydrogen cracking is sufficiently noisy that the acoustic emission rate dN/dt can be measured as a function of stress intensity factor K in cathodically charged 4340 steel. Since fast fracture occurs when K reaches a critical value, K_c, it is possible to accurately predict the onset of brittle fracture from a record of the acoustic signals emitted over a period of time. Figure 8 illustrates how this technique allowed failure prediction for 4340 bolts that had been cathodically charged and torqued to various loads.

By successively passing a variety of environments into a system containing a precracked specimen loaded to a constant K value, and measuring the amount of emission emitted by the crack in each environment, it should be possible to quickly determine what environments are harmful to a particular material. Acoustic emission testing may thus find an important role in materials selection for reactive environments.

Acknowledgments

We wish to acknowledge the United States Army Research Office, Durham, Massachusetts for its support under Contract DAH-04-68-6-0008 during this investigation.

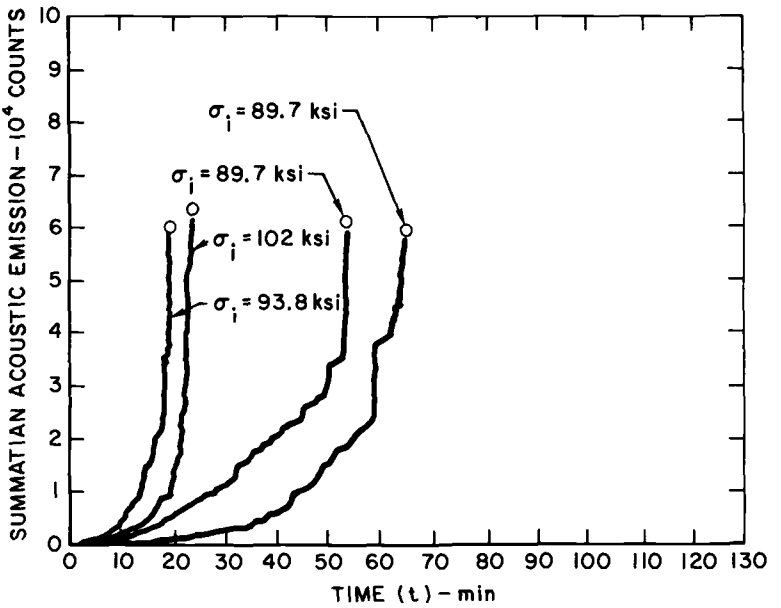

FIG. 8–*Summation of acoustic emission over a period of time* t, *for cathodically charged and torqued bolts of 4340 steel [5].*

References

[1] Tetelman, A. S. and McEvily, A. J. in *Fracture of Structural Materials,* Wiley, New York, 1967.

[2] McMahon, C. J. and Cohen, M., *Acta Metallurgica,* AMETA, Vol. 13, June 1965, pp. 591-604.

[3] Kaechele, L. and Tetelman, A. S., *Acta Metallurgica,* AMETA, Vol. 17, April 1969, pp. 463-475.

[4] Harris, D. O., Tetelman, A. S., and Darwish, F. A. in *Acoustic Emission, ASTM STP 505,* American Society for Testing and Materials, 1972, pp. 238-249.

[5] Dunegan, H. and Tetelman, A. S., "Non-Destructive Characterization of Hydrogen Embrittlement by Acoustic Emission Technique," to be published in *Engineering Fracture Mechanics.*

H. R. Hardy, Jr.[1]

Application of Acoustic Emission Techniques to Rock Mechanics Research

REFERENCE: Hardy, H. R., Jr., "Application of Acoustic Emission Techniques to Rock Mechanics Research," *Acoustic Emission, ASTM STP 505*, American Society for Testing and Materials, 1972, pp. 41-83.

ABSTRACT: Presented is a comprehensive review of the applications of acoustic emission in the field of rock mechanics. Acoustic emission experiments in rock mechanics were initiated in North America in the late 1930s as part of a study by the U. S. Bureau of Mines into problems associated with mine design and alleviation of rock bursts. More recently acoustic emission techniques had been employed to an increasing degree for the laboratory study of basic deformation and failure mechanisms in geologic materials. This paper outlines the major rock mechanics areas where acoustic emission techniques are being applied, and includes a brief description of a number of basic and applied studies.

KEY WORDS: acoustics, emission, sound transmission, microseisms, noise (sound), rock mechanics, geological structures, rocks, tests, field tests, acoustic detection, stability, instruments

Although the term acoustic emission is widely used in the materials science field to denote the phenomenon in which a material or structure emits transient vibrations when stressed, the term is not commonly used by workers concerned with mechanical behavior of geologic materials (rock mechanics). In this field a variety of other terms have been employed. These include: microseismic activity, rock noise, seismo-acoustic activity, and subaudible noise. The term microseismic activity is probably the one most commonly used in North American rock mechanics literature. Unfortunately the term microseismic activity has a completely different meaning to the seismologist, some of whom prefer to refer to acoustic emission as microearthquake activity. In reviewing the literature

[1] Professor of mining engineering and director, Rock Mechanics Laboratory, Dept. of Mineral Engineering, College of Earth and Mineral Sciences, The Pennsylvania State University, University Park, Pa.

referenced in this paper it is therefore necessary to remember that the various terms used are synonymous with acoustic emission.

In geologic materials the origin of acoustic emission is not well understood, but it appears to be related to processes of deformation and failure which are accompanied by a sudden release of strain energy. In geologic materials, which are basically polycrystalline in nature, acoustic emission may originate at the microlevel as a result of dislocations, or at the macrolevel by twinning, grain boundary movement, or initiation and propagation of fractures through and between mineral grains. It is assumed that the sudden release of stored elastic strain energy accompanying these processes generates an elastic stress wave which travels from the point of origin within the material, to a boundary where it is observed as an acoustic emission. Figure 1 illustrates a simplified experimental arrangement for studying acoustic emission and typical acoustic emission data for rock.

For the engineer and scientist concerned with the mechanical behavior of geologic materials the phenomenon of acoustic emission provides a unique method for the study of material deformation and failure. In the civil engineering and mining fields, this phenomenon has been employed to a limited extent to predict the impending failure of rock both on the surface and underground, to locate highly stressed regions, and to determine the effectiveness of the measures taken against the occurrence of rockbursts and outbursts of gas. Geophysicists concerned with the prediction and causes of earthquakes have become increasingly interested in the study of low-level acoustic emission.

To date, most laboratory studies related to acoustic emission in geologic materials have been carried out in an attempt to substantiate or clarify results obtained in the field. A few studies, however, have been conducted to investigate fundamental deformation and failure behavior of geologic materials loaded in tension, compression, and flexure. In these studies, the number, amplitude, and energy of the acoustic emission events as well as their frequency spectra have been investigated.

The majority of the laboratory studies have concentrated on the investigation of acoustic emission phenomena in rocks and minerals resulting from the application of mechanical stresses. Limited studies have been carried out on such geologic materials as soil by Cadman et al[*1*] and on ice by Gold[*2,3*]. Recently studies have been reported by Warren and Lathan[*4*] in which thermally induced microfracturing in a variety of geologic materials was investigated using acoustic emission techniques.

In North America, acoustic emission studies related to geologic materials were initiated in the late thirties and early forties by Obert[*5-7*], Obert and Duvall[*8-10*], Hodgson[*11,12*] and others as part of their research into the problems of mine design and rock burst prevention. Research in Europe and Asia appears to have been initiated somewhat later (late 1940's). A recent publication

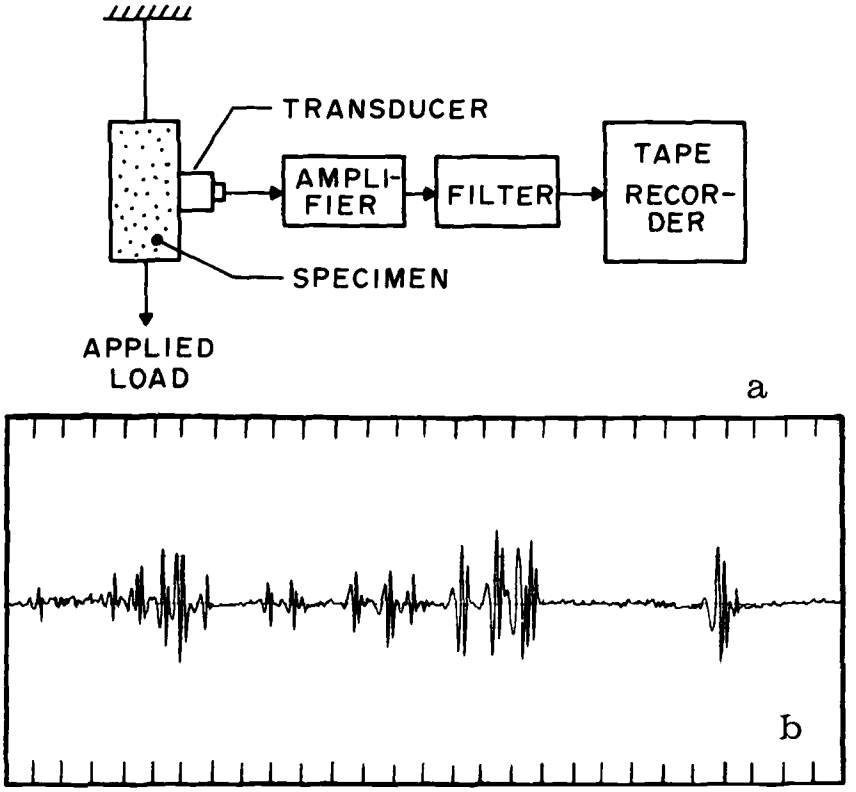

FIG. 1—*Simplified experimental arrangement* (a) *for studying acoustic emission in a laboratory test specimen and typical emission data for rock* (b). *(Horizontal divisions represent approximately 6 ms.)*

by Antsyferov[*13*] provides a review of a number of acoustic emission studies associated with mining undertaken in Russia.

During the last 30 years a considerable volume of literature related to the study of acoustic emission in geologic materials has been established. The purpose of the present paper is to provide a brief review of this literature and to acquaint those in the materials science and rock mechanics fields with the various applications of acoustic emission to the study of geologic materials. Throughout the paper a number of the more pertinent references will be designated. A brief bibliography containing a number of additional papers is also included.

General Considerations

Before proceeding to the detailed review of acoustic emission studies carried out on geologic materials, a number of general factors should be considered. The

first factor concerns the terminology used to describe acoustic emission in the rock mechanics field. Here acoustic emission is normally described in terms of parameters associated with the magnitude and rate of occurrence of acoustic emission events, and with the frequency spectra associated with a single event or a group of events. In the former case, the maximum amplitude of each event and its time of occurrence are the basic factors, and acoustic emission is most commonly described in terms of such parameters as the following:

(1) Accumulated Activity (N)—The total number of events observed during a specific period of time.
(2) Noise Rate (NR)—The number of events (ΔN) observed per unit time (Δt).
(3) Acoustic Emission Amplitude (A)—The maximum amplitude of each recorded event in arbitrary units.
(4) Acoustic Emission Energy (E)—The square of the event amplitude in arbitrary units.
(5) Accumulated Energy (ΣE)—The sum of the energy emitted for all events observed during a specific time period.
(6) Energy Rate (ER)—The sum of the energy emitted by all events observed per unit time (Δt).

It should be noted that accumulated activity (N) and noise rate (NR) are dependent on the sensitivity of the monitoring system and its signal to noise ratio. The parameters, amplitude (A), energy (E), accumulated energy (ΣE), and energy rate (ER) are similarly dependent on sensitivity and signal to noise ratio but are also dependent on the frequency response of the overall monitoring system.

Acoustic emission data obtained on geologic materials have also been described in terms of their frequency spectra. In general, any transient signal, such as a single acoustic emission event, may be considered as the superposition of a large number of steady-state components. The amplitude versus time form of any of the individual events shown in Fig. 1*B* may therefore be considered to be the superposition of a number of sinusoidal signals of specific frequency and amplitude. It is possible to represent such a signal in either the time or the frequency domain. Mathematically the conversion between these two domains may be carried out using the Fourier integral which has the general form

$$G(t) = \frac{1}{\pi} \int_0^\infty S(\omega) \cos\left[\omega t + \phi(\omega)\right] d\omega \tag{1}$$

$$\omega = 2\pi f \tag{2}$$

where $G(t)$ and $S(\omega)$ represent the amplitude of the signal in the time and frequency domain, respectively, f is frequency, t is time, and $\phi(\omega)$ is a phase

factor. Usually the function $G(t)$ is referred to as the "wave form" of the signal and $S(\omega)$ or alternately $S(f)$ is referred to as the "frequency spectrum" of the signal. A specific frequency present in the spectrum is known as a "frequency component." $S(\omega)$ or $S(f)$ is commonly obtained from $G(t)$ by computing the inverse transform of Eq 1 either by analog means using a frequency spectrum analyzer, or by digital means using a suitable computer program.

The second factor having considerable bearing on the acoustic emission data presently available in the rock mechanics field is that of instrumentation. The measurement of acoustic emission in geologic materials both in the laboratory and in the field presents many technical difficulties. In the laboratory, the design of suitable loading facilities is a major problem. First, the loading facilities themself must not generate mechanical noise which could be detected by the monitoring system and interpreted as acoustic emission; and second, if it is desired to evaluate the frequency spectra of the observed activity it is necessary that the loading facilities themselves have a generally flat mechanical frequency response (or exhibit a well defined spectrum) in the frequency range under study.

The study of acoustic emission in the field is complicated first by the presence of relatively low frequency (100 to 20,000 Hz) "cultural noise" from industrial or human sources, which must be selectively removed by filtering; second by the rapid frequency-dependent attenuation suffered by the stress waves associated with the acoustic emission as they propagate through low Q geologic materials; and third, by the difficulty in accurately determining microseismic source locations due to unknowns in propagation velocity and the complexities of the geologic structures involved.

In general, research related to geologic materials has been carried out by mining engineers, geologists, and geophysicists, the majority of whom are not highly specialized in the field of instrumentation. As a result, acoustic emission monitoring systems for the most part have been relatively simple. Furthermore, poor design in a number of the monitoring systems used has resulted in the publication of experimental data which are more a function of the characteristics of the monitoring system than of the actual acoustic emission character of the test material. Although the characteristics of the monitoring system are extremely important few authors have included a detailed description of the systems used. A recent paper by Knill et al[*14*], appears to provide the only extensive review of acoustic emission monitoring systems which have been developed specifically for research on geologic materials.

A third factor of considerable importance concerns the frequency range in which acoustic emission studies have been undertaken with respect to geologic materials. When considering studies on metallic materials and structures frequencies in the range of 100 kHz to 2 MHz are considered common. The majority of acoustic emission studies on geologic materials however have been

carried out at frequencies well below this range. Figure 2 illustrates the frequency range over which studies, generally termed acoustic emission, have been carried out. It is important also to note that attenuation of stress waves in solids and fluids are frequency dependent. This fact limits the distance over which acoustic emission signals of various frequencies may be monitored. Figure 3, prepared by Armstrong[*15*], illustrates the estimated range of such signals as a function of frequency (based on a 160 dB attenuation of the signal) for a number of substances. The importance of the Q factor (dissipation factor) in the case of rock is evident.

To date little is known in regard to the energy-frequency spectrum of acoustic emission events at their source location. However, since a number of successful acoustic emission studies have been carried out on small specimens of geologic materials over a number of frequency intervals in the range 300 Hz to 200-300 kHz it would appear that the energy-frequency spectra at the source location for such materials were relatively wide. Unfortunately since no wide band monitoring system covering the important frequency range (that is, 300 Hz to 300 kHz) has yet been utilized it is impossible to estimate the form of the overall energy-frequency spectrum, or the total energy released at the source location.

The fourth and final factor which should be considered is the types of acoustic emission studies which have been undertaken on geologic materials. Both basic and applied studies have been underway for some years, however the majority of these are of an applied nature. Basic studies are considered here as those studies specifically related to determining information regarding the source mechanism, effects during propagation, empirical relationships which associate observed activity to changes in physical character of the test material, etc. In

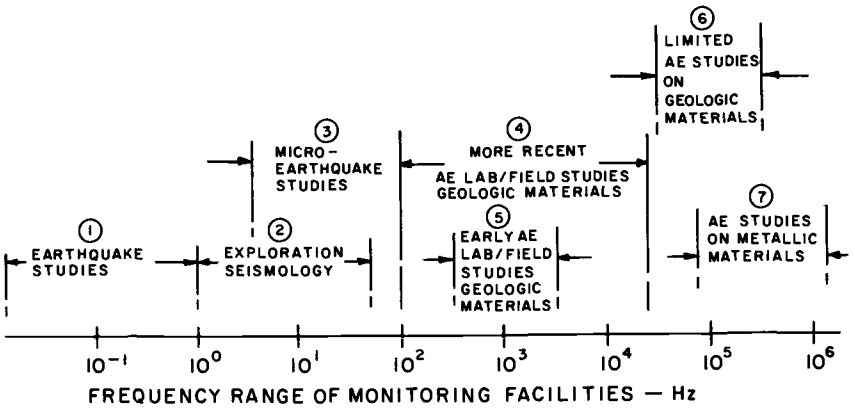

FIG. 2– *Frequency range of various types of acoustic emission studies. Circled numbers represent regions where studies were undertaken.*

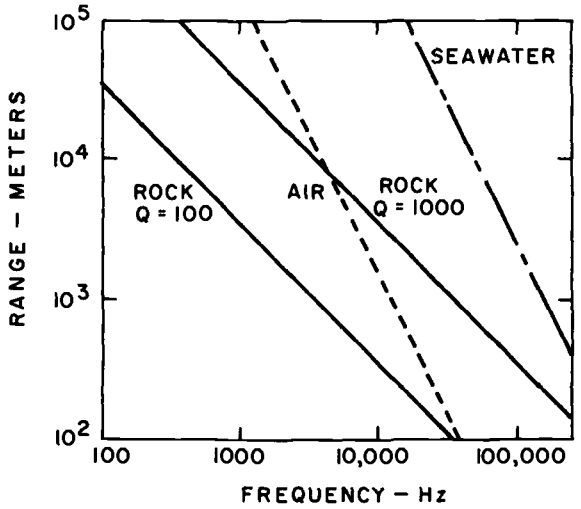

FIG. 3–*Range of acoustic signals as a function of frequency for various media*[15].

contrast however applied studies are concerned with the utilization of acoustic emission techniques for indirect monitoring of such phenomena as structural stability, and location of zones of failure. In rock mechanics a prime application of acoustic emission is that of monitoring the stability of natural or man-made geologic structures.

It is important to note that basic and applied studies are not necessarily synonomous with laboratory and field studies, since both basic and applied studies have been carried out under laboratory and field conditions. Since laboratory and field studies are characterized by the frequency range over which acoustic emission is monitored and in general by the sophistication of the instrumentation employed the literature will be reviewed in terms of these two major divisions.

Laboratory Studies

Basic Studies

Effect of Stress Level–Since the early studies of acoustic emission in geologic materials, workers have been attempting to establish reliable empirical relationships between observed acoustic emission and various other material properties. For example, Obert and Duvall[*8-10*] showed in the laboratory (as well as in the field) that under compressive load the acoustic emission noise rate increased greatly as a specimen or structure became more highly loaded. During these studies Obert and Duvall investigated the behavior of a number of rock types including greenstone, limestone, granite, hornstone, schist, sandstone, epidosite,

and dolomite. Figure 4 illustrates typical results for specimens of two different coarse grained granites. Field studies, carried out by Obert and Duvall[*8*] indicated that after a structural failure (for example, failure induced by blasting) that the noise rate decreased. In other words the noise rate appeared to be indicative of the degree of stability. More recent studies[*16-23*] indicate that under both uniaxial and triaxial compressive stress the acoustic emission noise rate increases rapidly as the compressive failure stress is reached. Typical results are shown for a granite under uniaxial compression in Fig. 5[*20*] and for a different granite (Westerly) under triaxial compression in Fig. 6[*21*]. A number of workers have reported disproportionately high noise rates at low stresses. This fact appears to be related to closure of pores and microfractures. Studies are presently underway by Mello Mendes[2] in which acoustic emission in rocks stressed under post-yield conditions are being investigated.

Goodman[*23*] has studied the effect of repeated compressive loading and unloading on acoustic emission. Typical results are shown in Fig. 7. Here the relative acoustic emission rate is indicated by the spacing of the horizontal lines.

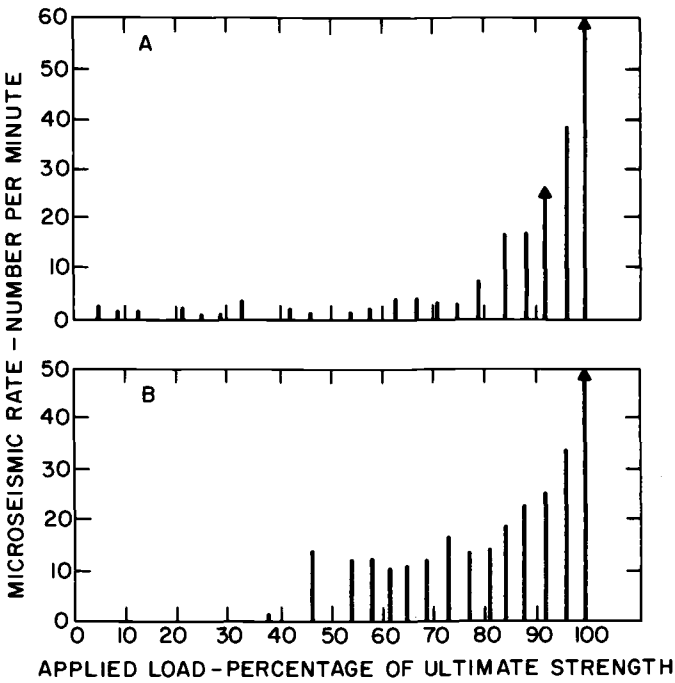

FIG. 4—*Variation of noise rate with applied load for 2 coarse grained granites*[10].

[2] Personal communication. F. Mello Mendes, University of Luanda, Angola, April 1971.

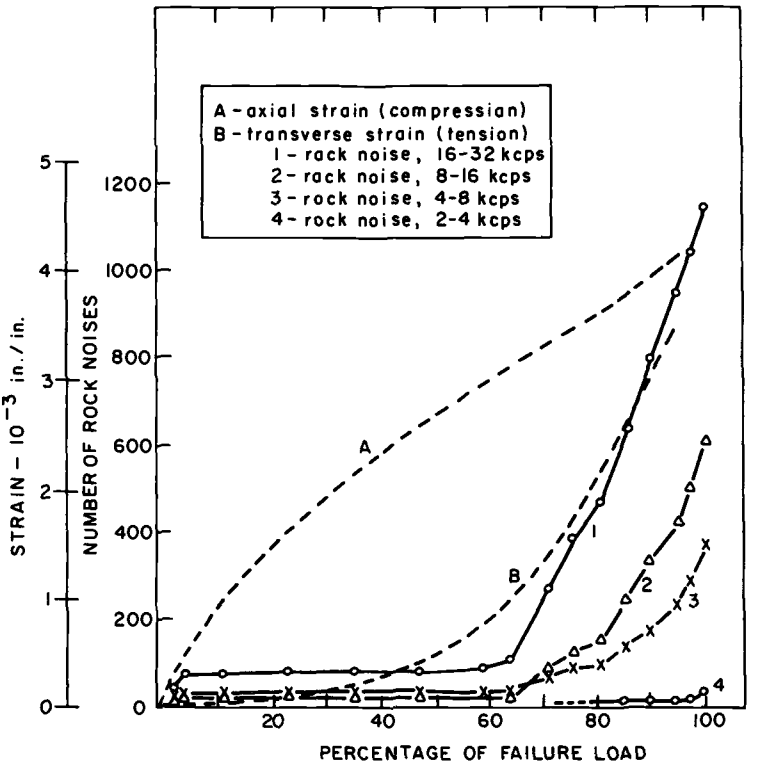

FIG. 5—*Relationship between acoustic emission, axial and transverse strain, and load for a granite* [20].

It was observed that if the load was not increased beyond a point *B*, referred to as the point of "accelerated rock noise activity," then fewer events were detected during the second and subsequent loading cycles. If higher loads were applied however, the rate of noise emission was found to increase in subsequent cycles. Goodman observed acoustic emission during unloading as well as loading. He classified the activity occurring during loading as follows:

(1) Acoustic emission events at low stress levels which disappear with numerous repetitions of load.
(2) Events at low stress levels which persist despite numerous load cycles.
(3) Events at high stress levels (above the point of accelerated activity) which occur more frequently when loading is repeated.

Goodman[*23*] also reported that although the first type of activity is lost temporarily by repeated cycles of loading, it reappears in tests conducted after the specimen remained unloaded for a period of time. This tendency for

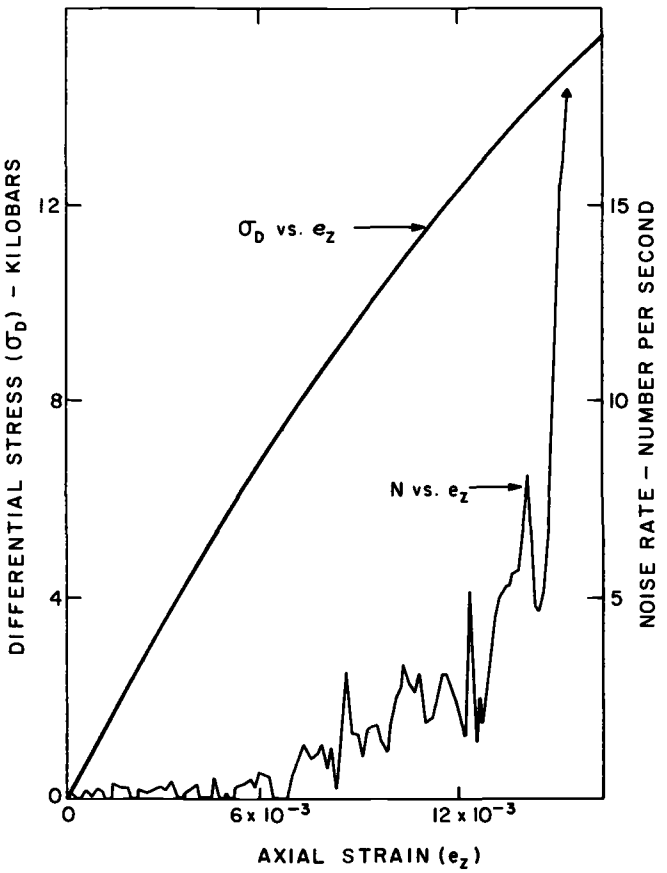

FIG. 6–*Microfracturing frequency and stress-strain data for Westerly granite under triaxial compression with a 4-kilobar confinement*[21].

specimens to recover acoustic emission generating capability after "resting" was found to occur for all rock types tested. Typical results for various rest periods are shown in Fig. 8. In all cases the maximum recovery was in the range of 40 to 60 percent of the number of events observed during the first load cycle. The major recovery of generating capability was found to occur during the first 12 hours of the rest period.

Under uniaxial tensile stress, acoustic emission is also observed. Brown[*24*] and Brown and Singh[*25*] have studied the behavior of Indiana limestone, Tennessee sandstone and Barre granite under incremental tensile stress. From the data obtained in these experiments the authors postulated that acoustic emission energy was the most suitable factor for describing the observed behavior. Figure 9 illustrates ΣE versus applied load (expressed as a percentage of the load at

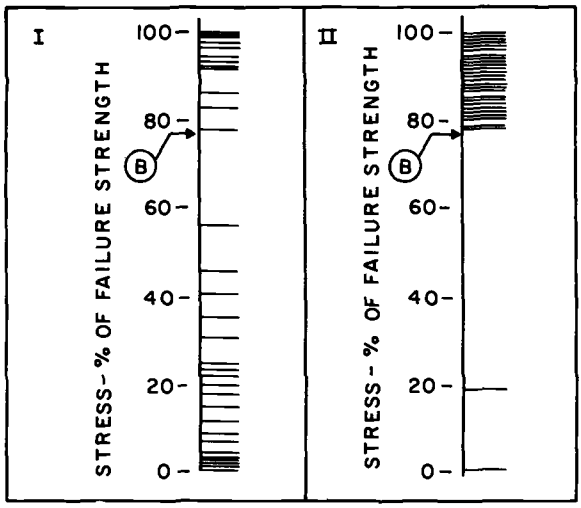

FIG. 7—*Acoustic emission patterns during loading*[23]: I —*first cycle and* II — *later cycle.*

failure) for the various materials tested in this study. The composite data in Fig. 9 indicates that in all cases ΣE increases with applied load, and in all but one case (Tennessee sandstone) the energy rate increases as the load approaches the failure point. Recent studies by Hardy et al[*26*] suggest that the energy data quoted by Brown and Singh[*25*] in these experiments should be utilized with caution since energy determinations in such experiments are highly sensitive to the characteristics of the monitoring facilities (for example, in the studies under consideration only microseismic energy in the region of 1000 Hz was taken into account).

Frequency Spectra—A number of workers have considered the frequency characteristics of individual acoustic emission events with the aim of determining

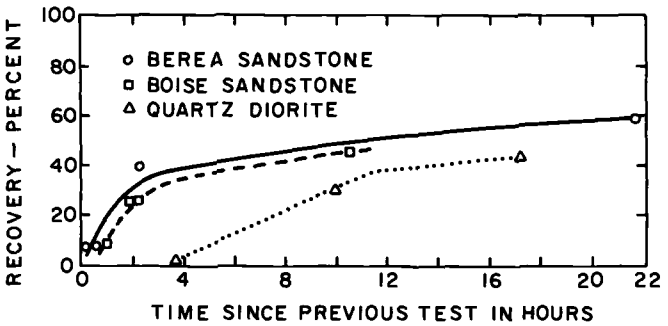

FIG. 8—*Recovery of acoustic emission generating capability*[23].

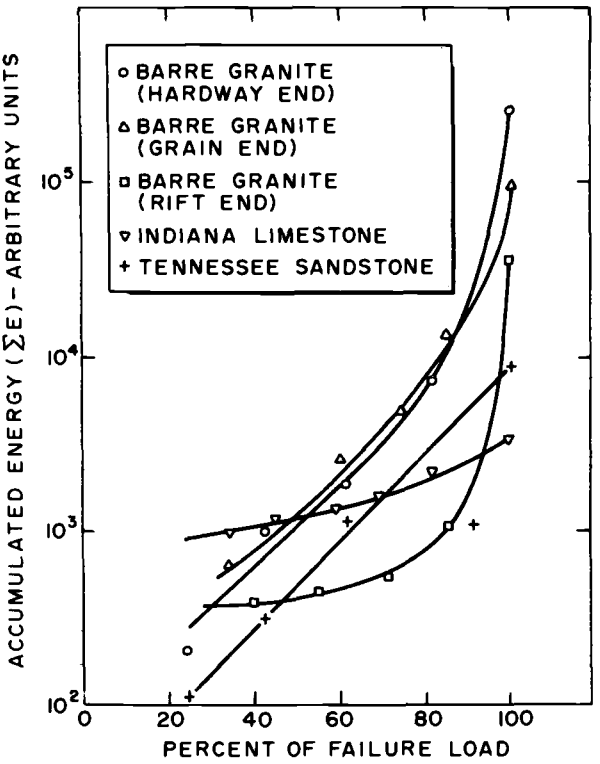

FIG. 9—*Accumulated acoustic emission energy versus applied load for several rock types*[25].

a relationship between frequency content and other physical properties. Results of studies by Suzuki et al[*20*], presented earlier in Fig. 5, illustrate a number of curves of accumulated activity versus applied stress obtained over a range of frequencies. It is apparent that the largest concentration of activity occurs for frequencies in the range of 16 to 32 kHz.

Chugh et al[*27*] have also carried out investigations on this subject, in this case under uniaxial tension. In these studies, specimens of three rock types (Tennessee sandstone, Indiana limestone, and Barre granite) were stressed under incremental tensile loading conditions and their acoustic emission monitored. Experiments were carried out on air-dried and wet specimens to evaluate the effect of moisture on activity. In these experiments acoustic emission was sensed by a commercial accelerometer cemented to the surface of the test specimen. The overall system was capable of monitoring acoustic emission at frequencies from 300 to 15,000 Hz with a flat frequency response in acceleration over this range. Figures 10 and 11 respectively show a block diagram and a photograph of

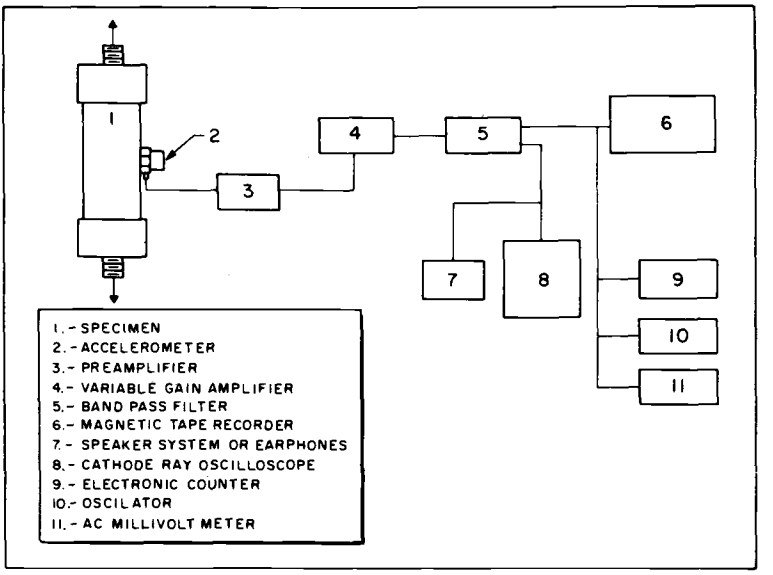

FIG. 10—*Block diagram of overall acoustic emission monitoring system for tension studies*[27].

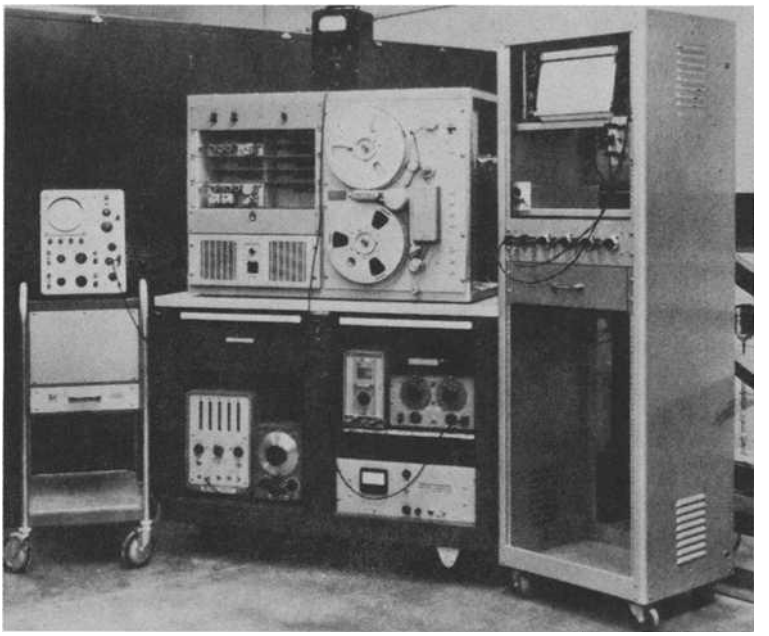

FIG. 11—*Typical acoustic emission monitoring system*[27].

the completed monitoring system used in these experiments. Specimen length and diameter were nominally 2.25 in. and 1.06 in. respectively.

Magnetic tape recordings of individual acoustic emission events were studied using an analog frequency analyzer, and the amplitude-frequency spectrum of each event obtained. For example, Fig. 12 illustrates a series of such spectra for acoustic emission observed in specimens of Tennessee sandstone at a number of stress levels. In these spectra it is interesting to note the presence of several dominant frequency bands (DFB) as well as regions in which very little activity is present. From Fig. 12 it is apparent that the observed amplitude-frequency spectra change as the stress level increases, with a general shift of the dominant bands to higher frequencies. An attempt has been made to utilize such data to predict structural instability, but results to date have not been encouraging.

Another approach in analyzing spectral data described by Chugh et al[*27*] has been more successful. This involved the use of a parameter known as the energy distribution ratio (EDR). This factor was defined as the ratio of the total acoustic emission energy observed in the range 500 to 5000 Hz, to that observed in the range 10,250 to 15,000 Hz for all events detected in a particular stress interval. Figure 13 illustrates graphically the variation of EDR with stress level for Tennessee sandstone in both the air-dried and wet state. Results for Barre granite and Indiana limestone were similar in form. In general, for the three rocks types tested, EDR values decreased with the increasing stress level. The results to date suggest that this parameter may be useful as a qualitative measure

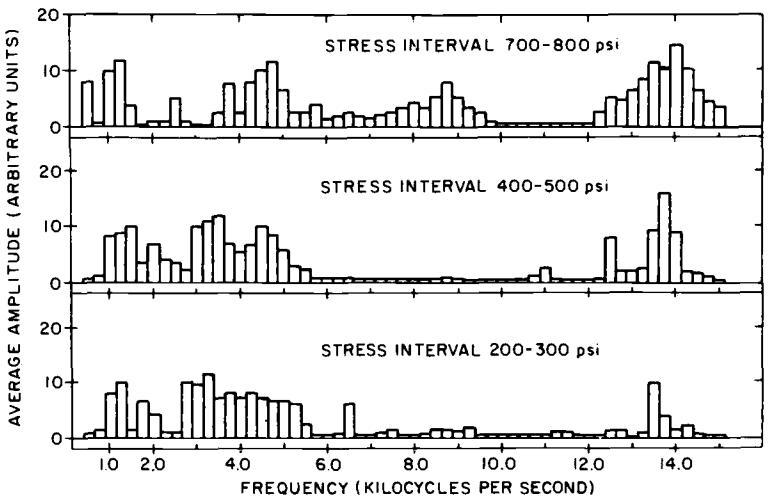

FIG. 12–*Average amplitude versus frequency at different stress intervals for Tennessee sandstone tested in air-dried state*[27].

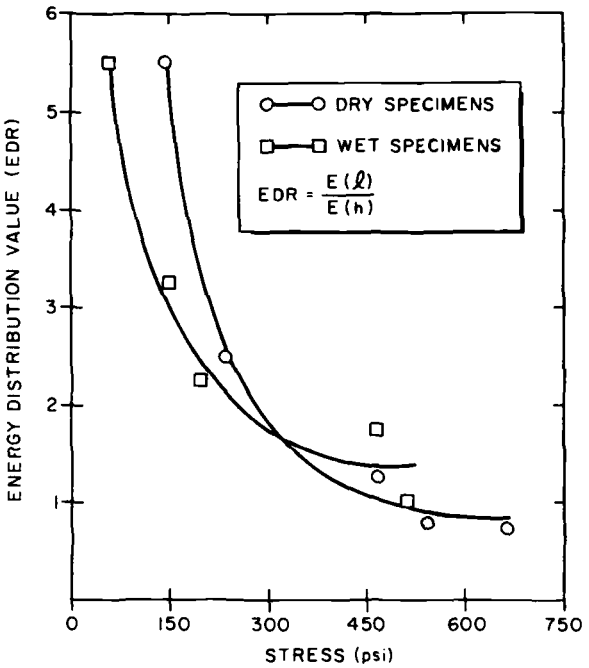

FIG. 13–*Energy distribution ratio values versus stress level for Tennessee sandstone*[27].

of the existing stress level in a particular region. Considerable study will be required to substantiate these initial conclusions.

As has been pointed out by a number of workers, many difficulties are involved in the study of acoustic emission frequency spectra. These include the effect of inherent resonant frequencies in the test specimen and loading system, the frequency dependent attenuation characteristics of the test material, and the necessity of insuring that the acoustic emission monitoring system itself has a flat frequency response in the region of interest. Many workers consider the measurement of meaningful frequency spectra as experimentally impractical.

Amplitude Distribution–The amplitude of acoustic emission events observed for geologic materials under stress have been found to vary over several orders of magnitude. In seismology the relationship between the cumulative number of events of magnitude M or greater in a given time interval $n(M)$, and their magnitude M,[3] has been found to obey the following relationship[*28*]:

$$\log n(M) = a + b(8 - M) \tag{3}$$

[3] It should be noted that in seismology the term magnitude is related to the logarithm of the observed amplitude of the recorded seismic event.

This relationship has been found to apply to small earthquakes as well as to acoustic emission data observed in stressed specimens of geologic materials[*14, 21,22,29-31*]. Rather than apply Eq 3 directly, Scholz[*21*] presents his experimental data in terms of the Ishimoto-Iida statistical relationship[*32*], namely:

$$N(A)dA = KA^{-m}dA \tag{4}$$

where $N(A)$ is the amplitude frequency, namely the number of events having amplitudes in the range A to $A + dA$, and K and m are constants. Scholz also notes that there is a relationship between the constants b and m in Eqs 3 and 4, namely:

$$b = m - 1 \tag{5}$$

Figure 14[*21*] illustrates the variation of $N(A)$ with amplitude for tests on Westerly granite at two different levels of uniaxial compressive stress. Two important features are indicated in this figure, namely the value of b varies with stress level, and the data deviate significantly from a straight line for large amplitude events. Scholz[*21*] observed that the factor b (Eq 3) varied inversely with the level of applied stress for a number of rock types investigated under uniaxial compression, as illustrated in Fig. 15. Such behavior indicates that with increasing stress level a higher percentage of the observed events have greater amplitude.

The reason for the deviation of the observed data from a straight line relationship for the high amplitude events may be due to a number of reasons. One possibility may be that different source mechanisms are responsible for the larger events. Experimental data presented in a recent paper by Mogi[*33*] may provide further insight into this problem.

Correlation with Inelastic Behavior—The relationship between acoustic emission and inelastic behavior has been under study for both uniaxial and triaxial loading conditions by a number of workers. Brown[*24*] and Brown and Singh[*25*] have carried out experiments under uniaxial tensile stress on specimens of Indiana limestone, Tennessee sandstone, and Barre granite. The loading procedure employed was incremental in form, that is, the load was increased or decreased in a series of steps and held constant at each level for a period of time during which acoustic emission was monitored. The resulting data were analyzed in terms of both the number and the energy of the emissions.

Figure 16 illustrates typical results for Tennessee sandstone. Energy values shown were computed as the square of the amplitude of the recorded activity. Energies quoted are therefore in arbitrary units. Data for two tests are presented. In one test the applied load was sufficiently high that the specimen failed during the test period; whereas in the other test the specimen remained relatively stable.

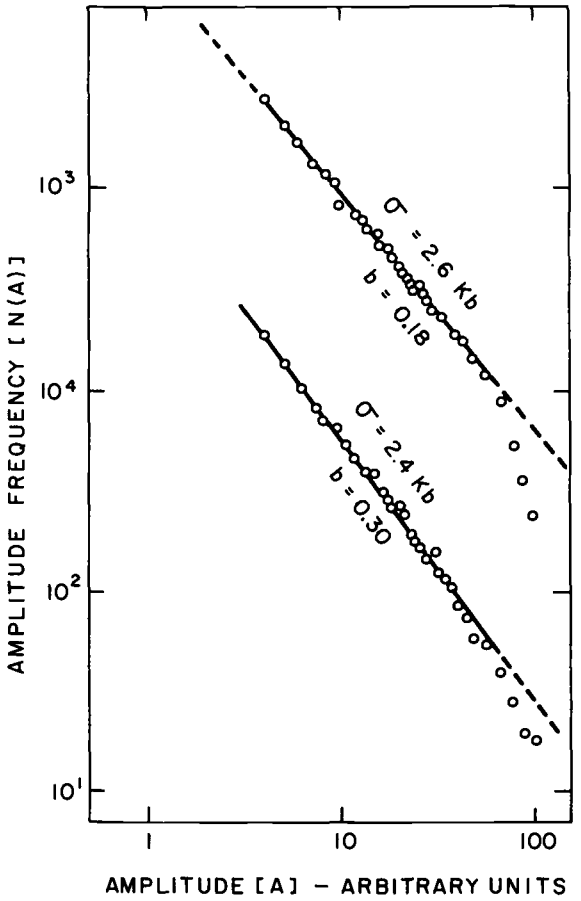

FIG. 14—*Amplitude frequency versus amplitude for acoustic emission events observed during 2 experiments on Westerly granite under uniaxial compression*[21].

It is interesting to note that the plots of both accumulated activity N and accumulated energy ΣE against time appear very similar to creep strain versus time curves normally obtained for geologic materials under similar loading conditions.

Incremental loading experiments under uniaxial compression have been carried out on a number of the geologic materials by Hardy et al[*26*]. The time dependent inelastic strain (creep) and acoustic emission occurring during these experiments were recorded. Special loading facilities developed for these experiments were capable of applying compressive specimen loads of up to 50,000 lbs and maintaining these constant for relatively long periods of time

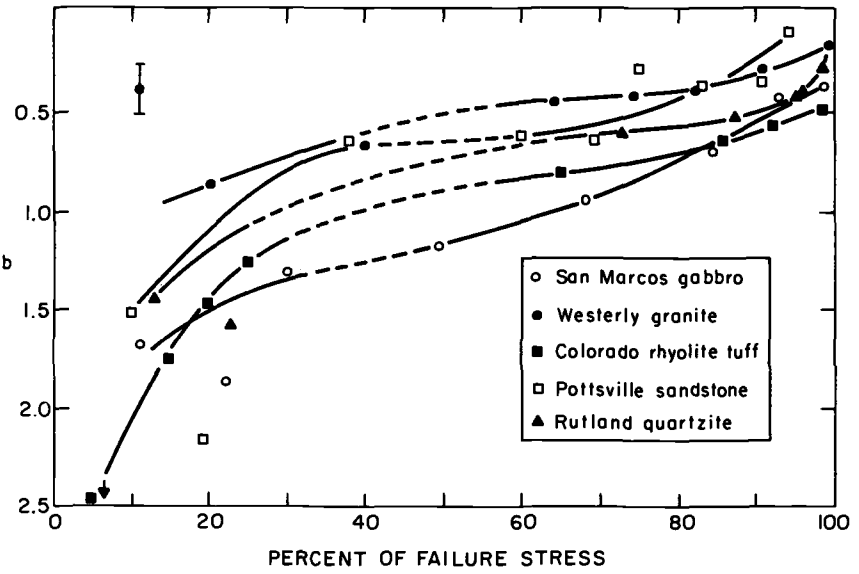

FIG. 15–*Variation of* b *with uniaxial compressive stress level for several rock types*[21].

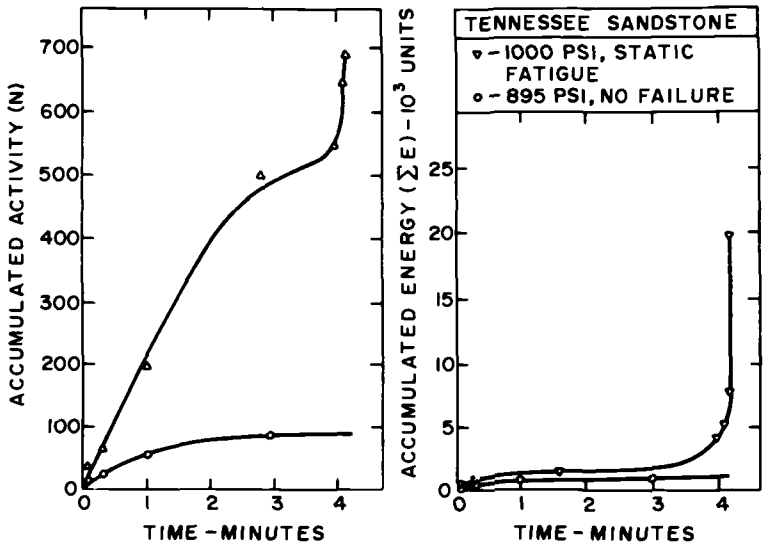

FIG. 16–*Results of study on Tennessee sandstone under tensile stress*[25].

(days). Figure 17 shows a block diagram of the overall monitoring and recording system utilized.

Axial creep strain versus time data from all experiments were fitted statistically to the generalized Burger mechanical model, as illustrated in Fig. 18, using a computer program developed for this purpose. The incremental creep form of the generalized Burgers model used was as follows:

$$e_I(t) = \frac{\Delta\sigma_m}{E_{n+1}} + \Delta\sigma_m \sum_{i=1}^{n} \frac{1}{E_i}\left[1 - \exp(-E_i\, t/N_i)\right] + \frac{\sigma_m t}{N_{n+1}} \qquad (6)$$

where $e_I(t)$ is the incremental strain due to a stress increment $\Delta\sigma_m$, σ_m is the resulting stress level, t is the time from when $\Delta\sigma_m$ was applied, and the E's and N's are the $2(n+1)$ inelastic parameters associated with the generalized Burgers model. The data in most cases was found to closely fit the model for $n = 2$. The improvement for $n = 3$ was not considered significant enough to merit the additional calculations required.

In this study Hardy et al[*26*] also observed that the accumulated acoustic emission activity versus time data could be expressed in a form similar to Eq 6. During the study, accumulated energy versus time data were also considered but preliminary investigation indicated that accumulated activity was a considerably

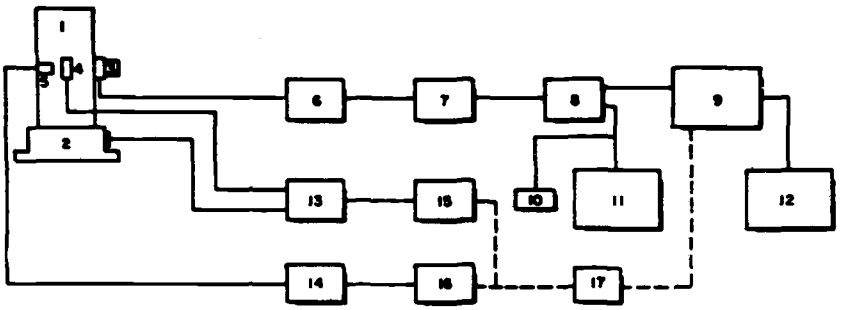

1. TEST SPECIMEN
2. LOAD CELL
3. ACCELEROMETER
4. AXIAL STRAIN GAGES
5. TRANSVERSE STRAIN GAGES
6. PREAMPLIFIER
7. MAIN AMPLIFIER
8. FILTER
9. MAGNETIC TAPE RECORDER
10. EARPHONES
11. OSCILLOSCOPE
12. VISICORDER
13, 14. STRAIN GAGE AND LOAD CELL SIGNAL CONDITIONING UNITS
15, 16. DUAL CHANNEL STRIP CHART RECORDERS
17. CHART EVENT MARKER UNIT

FIG. 17—*Block diagram of overall acoustic emission monitoring, and stress and strain recording facility for compression studies on rock*[26].

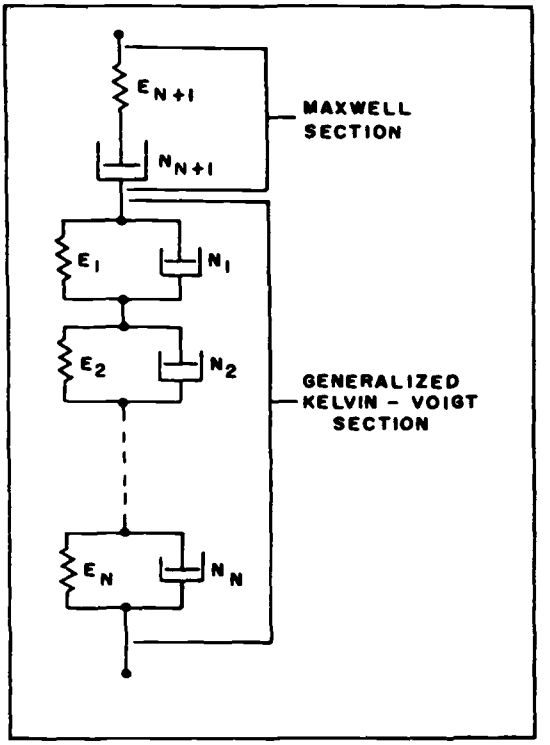

FIG. 18–*Generalized Burgers model*[26].

more consistent factor. Figures 19 and 20 illustrate typical data for Tennessee sandstone. In these figures axial creep strain and accumulated activity are plotted for a series of load increments (denoted by 10(5), 10(7), etc.) as functions of time. The solid lines represent a least squares computer fit of the experimental data to the Burgers model ($n = 2$).

The fact that the generalized Burgers model ($n = 2$) appears to fit both the axial creep strain and acoustic emission versus time data, strongly suggests a correlation between creep strain and acoustic emission. To investigate this further, the relationship between accumulated activity and axial creep strain was considered. For all three rocks, it was found that a nearly linear relationship existed between these two parameters. Figure 21 illustrates typical results for Tennessee sandstone.

Scholz[*21,34*] has studied the relationship between microcracking, as evidenced by observed acoustic emission and inelastic behavior for a number of rock types under both uniaxial and triaxial stress. Based on these studies Scholz developed a theoretical relationship between microcracking frequency and

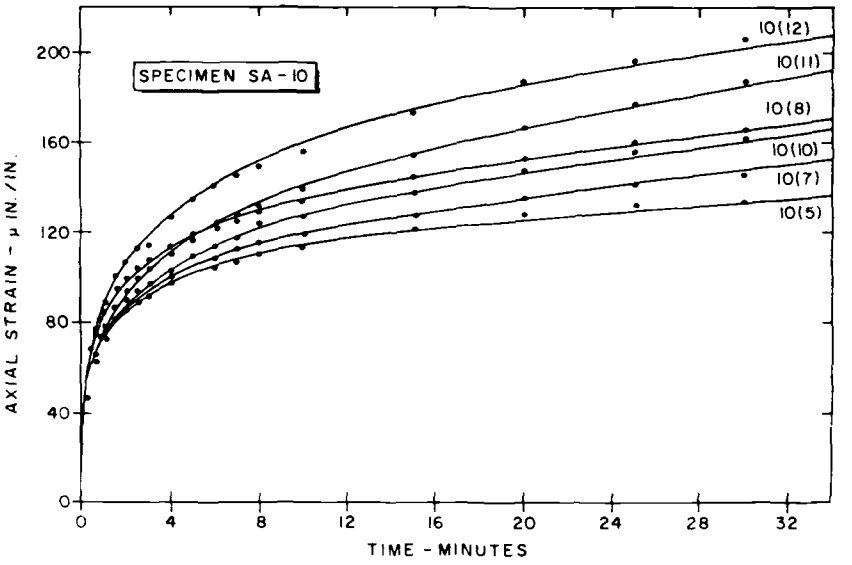

FIG. 19—*Typical axial creep strain versus time curves for Tennessee sandstone* [26].

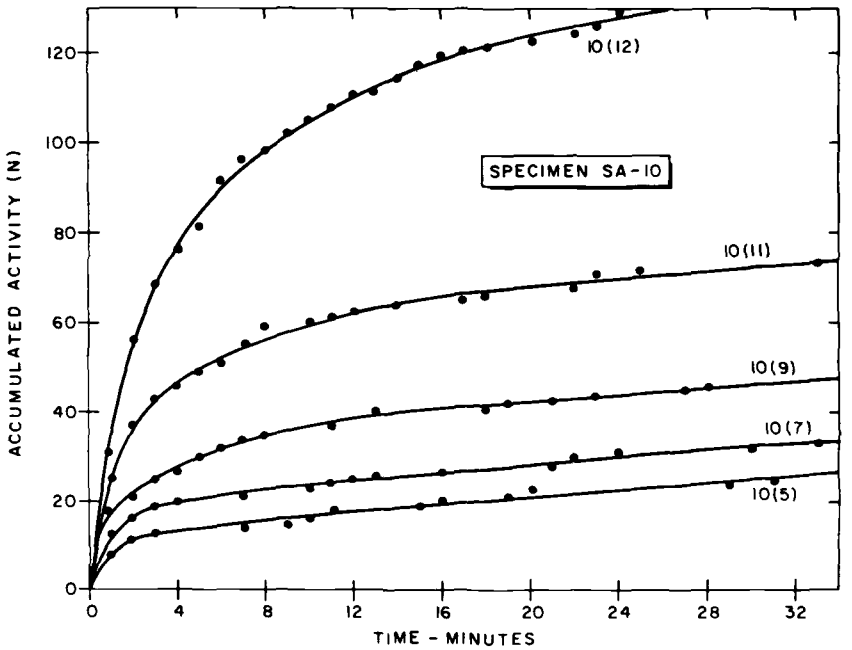

FIG. 20—*Typical accumulated activity versus time curves for Tennessee sandstone* [26].

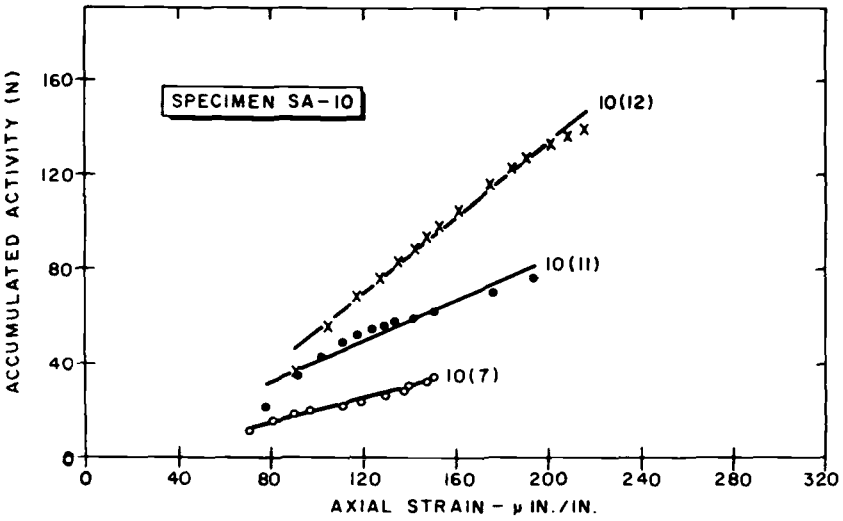

FIG. 21—*Typical curves showing variation of accumulated activity with axial creep strain for Tennessee sandstone*[26].

applied stress. In a later paper Scholz[*35*] develops a mathematical relationship between observed creep and microfracturing. Whether creep is due to microfracturing or vice versa[*36,37*] is debatable, at present, however it is certain that in geologic materials these two phenomenon are strongly related.

Source Location—Accurate location of the source of acoustic emission observed in a specimen or a structure is extremely important. First, from a fundamental point of view, unless the actual source location is accurately delineated it is impossible to estimate the true magnitude of an observed acoustic emission event, that is, a series of small observed events may be due to a weak source located close to the acoustic emission detector or due to a strong source located at a large distance from the detector. Secondly, in order to determine the mechanism responsible for the observed activity it is necessary that the location of the source be accurately known.

In general, source location techniques involve the use of a number of monitoring transducers located at various points over the body (specimen or structure) under study. Such a set of transducers are termed an array. Activity from a source of acoustic emission occurring within the body will be detected at each transducer at a different time depending on the distance between the particular transducer and the source. The difference in arrival time between the closest transducer and each of the others yields a set of arrival time differences (Δt_i) which, along with the geometry of the transducer array and the velocity of propagation in the material, may be used to determine the spatial coordinates of the emission source.

When considering geologic materials, source location is important both in laboratory and field studies. The experimental difficulties encountered in each case however are considerably different. In the present section only laboratory source location will be considered in detail. Field source location itself will be discussed later.

Relatively few workers have attempted to locate the source of acoustic emission in specimens of geologic material under laboratory conditions. In some respects the laboratory situation is considerably simpler than that of the field, since the geometry of the specimen is usually well defined, and it normally consists of a single type of material. However the relatively small size of the specimen necessitates very accurate location of the transducers in the monitoring array, and requires monitoring facilities capable of resolving very small arrival time differences.

Scholz[*21,34*] has carried out source location studies on cylindrical specimens of Westerly granite loaded under uniaxial compressive stress. Figure 22*a* illustrates the specimen and transducer array used. Scholz utilized 6 barium titanate transducers (6mm in diameter) attached to the specimen using a conductive epoxy cement. The electrical signals from each transducer were suitably amplified and recorded on a multichannel magnetic tape recorder having a flat frequency response over the range 200 Hz to 200 kHz. Following the experiment the six channels of recorded data were played out in pairs on a dual channel oscilloscope in order to obtain the necessary travel time difference data (ΔT_i). Scholz carried out a number of preliminary experiments in order to provide data for correction of any small magnetic tape misalignment which could contribute errors in determining the ΔT_i's. He estimated that ΔT_i could be determined to a "precision" of 0.5 μs. Utilizing a least squares form of the travel difference technique Scholz[*38*] determined the source location coordinates. He estimated that these could be evaluated to within approximately 0.11 in.

Figure 22*b* illustrates a number of source locations determined by Scholz[*21,34*] during a uniaxial compression test on Westerly granite at a constant rate of strain. The dashed line represents the location of a fracture plane which was observed when the specimen eventually failed. The circles represent the best estimate of the region in which various sources were located. The sources shown were determined at applied stress levels greater than 90 percent of the ultimate strength, denoted by Scholz as the "dynamic cracking region."

Although Scholz's studies represent a pioneering effort in laboratory scale acoustic emission source location in geologic materials, with the limited studies carried out, and the questionable location accuracy ($\Delta x_i \simeq 0.1$ in.) the results should be considered with caution. Recent comments by Harding[*39,40*], and Mogi[*41*] further reinforce this opinion.

Probably the most outstanding laboratory source location study carried out

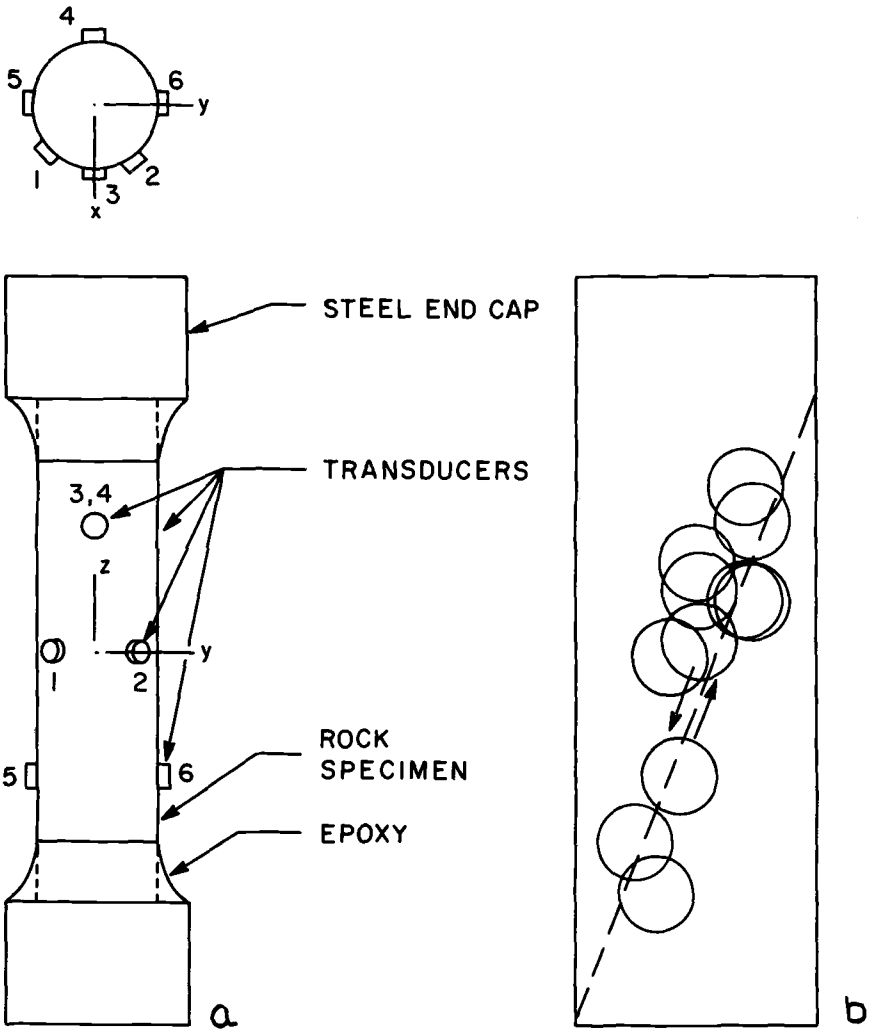

FIG. 22–*Source location technique and typical results for Westerly granite under uniaxial compressive stress*[21, 34]. (a) *specimen and transducer array,* (b) *source locations determined from events occurring at stresses greater than 90% of ultimate strength with respect to observed plane of failure.*

to date with respect to geologic materials is that by Mogi[*41*]. In order to provide a simple geometry, Mogi utilized beam shaped specimens deformed under four-point loading. During these studies Mogi investigated specimens of three marbles, three granites, a trachyte, and an andesite. Figure 23 illustrates the experimental arrangement used for one and two-dimensional source location.

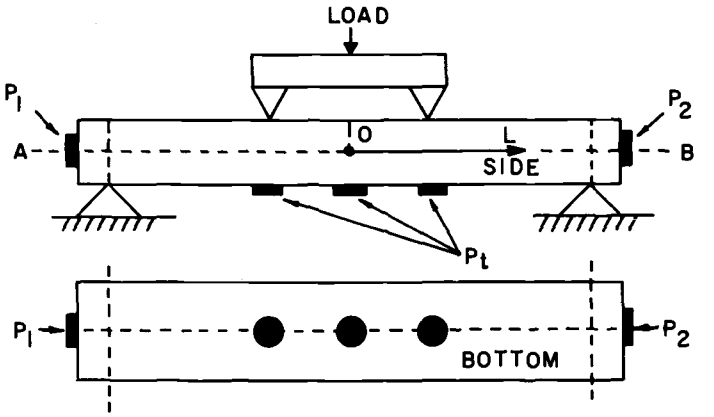

(A) SPECIMEN AND TRANSDUCER ARRAY USED FOR ONE-DIMENSIONAL SOURCE LOCATION.

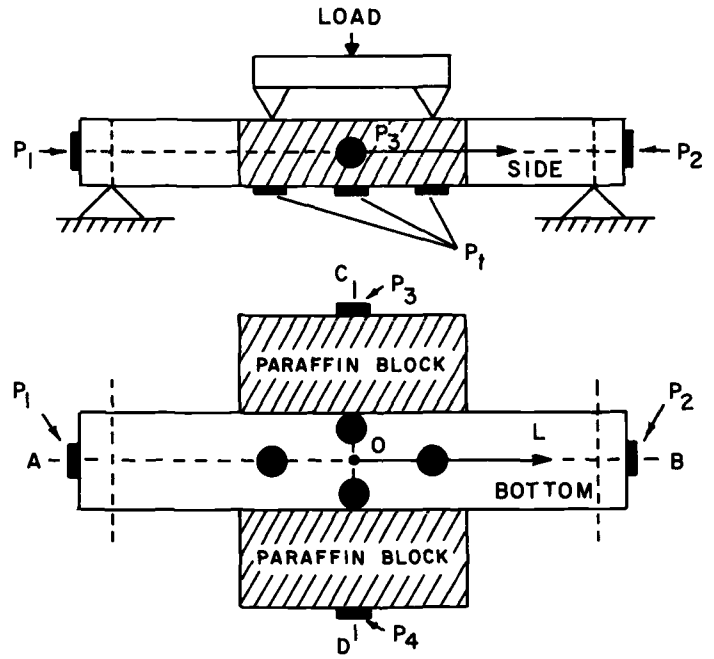

(B) SPECIMEN AND TRANSDUCER ARRAY USED FOR TWO-DIMENSIONAL SOURCE LOCATION.

FIG. 23—*Experimental arrangement for 1 and 2-dimensional source location*[41].

Mogi also suggests an extension of these arrangements for three-dimensional studies. In the one-dimensional case (Fig. 23*a*) P_1 and P_2 are the monitoring transducers and the three others transducers (P_t) are termed trigger transducers. The outputs of P_1 and P_2 were suitably amplified and applied to a dual channel oscilloscope. The three trigger transducers were connected together and provided a signal for triggering the oscilloscope sweep. A single frame movie camera was set up to photograph the oscilloscope screen and hence provide a permanent record of the signals from P_1 and P_2. The trigger signal was also used to advance the movie camera, and was also recorded on a strip chart recorder to provide a rough indication of the acoustic emission rate. If the acoustic emission source was located at the center point of the beam the acoustic emission signal would arrive at both P_1 and P_2 simultaneously, otherwise one or the other signal would be delayed. Knowing the degree of delay from the oscilloscope pictures, and the velocity of propagation for the test material, it was possible to determine the location of the source along the axis of the beam (AOB). Mogi states that the system was capable of resolving arrival time differences on the order of 1 μs. For a test material having a velocity of 10,000 ft/s the system was therefore capable of resolving source locations to within 0.12 in.

The two-dimension source location system described by Mogi[*41*] was basically an extension of that used for the one-dimensional studies, with two dual beam oscilloscopes and single frame movie cameras being utilized, along with four trigger transducers. One additional problem arises here however due to the relatively narrow width of the test beam and the resulting difficulty in triggering the sweep on the transverse oscilloscope sufficiently ahead of the arrival of the signal from P_3 or P_4. Mogi overcame this difficulty by mounting the transverse transducers (P_3 and P_4) on blocks of paraffin cemented to the central area of the beam (see Fig. 23*b*). Since the velocity of propagation in paraffin is relatively low the acoustic emission signal was effectively delayed allowing the trigger signal to activate the associated oscilloscope prior to the arrival of the signals from P_3 and P_4.

Figure 24 shows a typical set of data obtained by Mogi[*41*] from a test on Inada granite. The source locations determined under constant applied load during three time intervals (C_1, C_2, and C_3) prior to failure are presented, along with a composite figure showing all source locations observed during the three periods relative to the location of the final fracture. One important outcome of Mogi's studies was that at low stresses acoustic emission sources were scattered widely throughout the test specimen. As failure approached however this scatter decreased and the active source locations become more closely related to the location of the major plane of failure. Scholz[*21,34*] expressed a similar concept (using the terms static and dynamic fracturing region). However, Mogi after carrying out a considerable number of tests using his more refined experimental technique has firmly substantiated this observation.

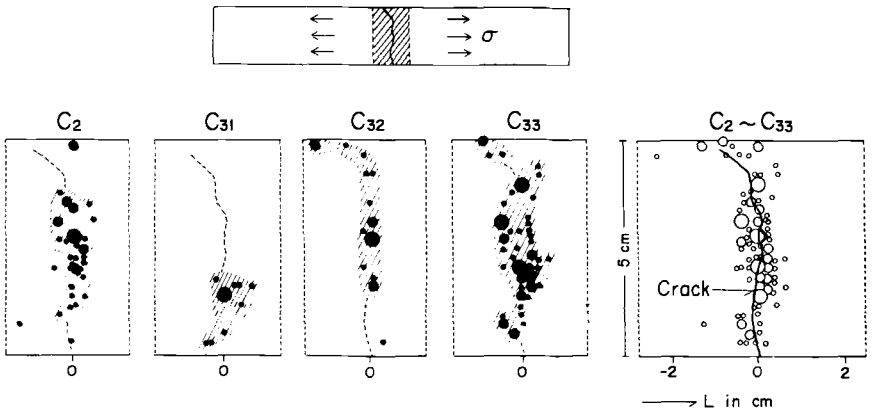

FIG. 24—*Successive development of acoustic emission sources during 4-point loading of a granite beam*[*41*].

Source Mechanisms—In considering basic acoustic emission phenomena two important and probably related problems require investigation, namely:

(1) What basic mechanisms are responsible for the observed acoustic emission in stressed rock, and

(2) Which factor, activity (N), or energy (E), is the most suitable for characterizing such phenomena.

Studies related to these two problems are presently under investigation by Harding and Hardy[*42*]. Here a number of tests under constant uniaxial compressive stress have been carried out on specimens of Barre granite. In the first series of experiments the specimens were loaded to approximately 80 percent of their ultimate compressive strength and held at this level until failure occurred through time dependent deformation. Test specimens were instrumented with three longitudinal and three transverse foil-type strain gages, and a solid-state transducer for monitoring acoustic emission.

Test data (stress, longitudinal and transverse strain, and acoustic emission rate) were continuously recorded during the experiments. The acoustic emission transducer used in these studies consisted of a solid-state strain gage mounted on a contoured brass plate cemented directly to the test specimen. This device has three distinct advantages over the piezoelectric transducers normally used in such studies. First, the gage measures acoustic emission energy in only one direction, namely parallel to the side of the specimen. Secondly, the solid-state strain gage element itself has a flat frequency response in strain up to at least 200 kHZ. Third, the device is relatively small ½ by ¼ by ⅛ in. thick) such that if desired a number of such devices could be mounted on a single specimen for such purposes as source location.

The major disadvantage of the solid-state transducers is that they are less sensitive than piezoelectric ones and the overall sensitivity of the monitoring system is probably reduced by a factor of 10 as a result. In this study therefore only the larger events were recorded.

As a result however of this originally undesirable reduction in sensitivity a number of interesting, previously unobserved features have been detected. Figure 25 illustrates typical data from a test on Barre granite. At the point *A* the applied stress was incremented from approximately 75 to 80 percent of the ultimate strength. The acoustic emission rate (*NR*) was found to rise and then fall slightly during incremental loading. With the exception of a number of peaks in the *NR* versus time curve (points *B* to *F*) the activity remained at a relatively low level until the specimen started deforming rapidly at the point *G* and failure occurred with a simultaneous dramatic increase in *NR*.

Examination of the strain versus time data between the points *A* and *G* in Fig. 25 indicates a number of sudden changes denoted as "strain jumps." These are found to correlate closely with the pronounced peaks in the *NR* data noted earlier. In the absence of acoustic emission data the observed strain jumps might simply be assumed to be due to instabilities in the strain monitoring system. Furthermore if only average strain were monitored it is possible that the strain jumps themselves would not be apparent. These experiments indicated however that the observed strain jumps are real features characteristic of the mechanical behavior of the material.

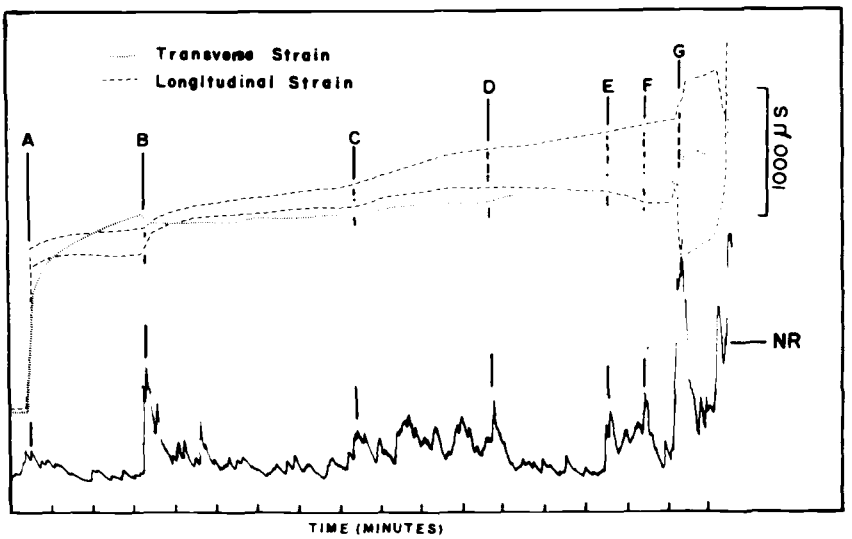

FIG. 25—*Typical curves showing relationship of "strain jumps" and acoustic emission rate during creep for Barre granite*[42].

Harding and Hardy are continuing the studies just described, as well as others involving fatigue behavior, however at this state it is interesting to speculate in regard to the meaning of the results obtained to date. Hardy et al[*42*] have shown that using a highly sensitive acoustic recording technique there appears to be a strong relationship between accumulated activity (N) and the associated creep strain. These workers also found that the correlation between accumulated energy (ΣE) was poor. In the present studies (using a less sensitive, acoustic emission monitoring technique) only the larger events were observed. These appear to be associated with instabilities within the rock mass (as evidenced by the observed strain jumps) and suggest a logical explanation for the energy discrepancies reported earlier by Hardy et al[*26*].

It would appear that acoustic emission records obtained using a high gain system contain a mixture of small and large events associated with micro level deformation and with strain jumps respectively. In evaluating the accumulative energy the sum of the squares of the microseismic amplitudes are utilized and it is obvious that relatively few, say 10, large events with relative amplitudes of the order of five would completely dominate any calculation of total energy, even if there were, for example, 150 small events of order one occurring during the same time period. Since the small events occur more or less continuously, curves of N or NR versus time would appear smooth and continuous even when one or two large events occurred during any time interval. On the other hand curves of E or ΣE versus time would not be expected to be as well behaved in such cases due to the presence of randomly occurring large events. These would result in exaggerated values of energy being calculated for those time intervals in which they occurred.

Early studies by Hardy[*43*] and later work by Harding and Hardy[*42*] strongly suggest that more than one mechanism is responsible for the acoustic emission observed in stressed geologic materials. In ice (a sedimentary rock) Gold[*2,3*] has actually observed time dependent crack formation during creep and has correlated this with observed acoustic emission. It would appear reasonable to assume that at least a portion of the acoustic emission observed in stressed rocks is due to the generation and propagation of inter and intragranular cracks. Recent studies by Byerlee and Preselnick[*44*] carried out on glass plates containing precut defects indicate that sudden crack growth in such a brittle material does give rise to acoustic emission. Their studies also indicate however that cracks may grow stably without generating acoustic emission (at least in the frequency range of the instrumentation utilized which appeared to have an upper limit of greater than 1 MHz). Their studies also indicate that acoustic emission is produced during unstable sliding between two surfaces of brittle materials and thus they suggest that unstable sliding between grain boundaries or crack surfaces, or both within specimens of geologic materials may be an important source of acoustic emission during compressive loading of such materials.

Applied Laboratory Studies

Acoustic emission phenomena provides a powerful method for investigating internal behavior in geologic materials. Even in the absence of a thorough knowledge of the mechanism involved, acoustic emission may be utilized as a tool. Barron[*17*], for example, has used acoustic emission to define the point of unstable fracture in specimens of geologic material under uniaxial and triaxial states of stress. Recently, Hardy[*45,46*] has employed acoustic emission to define initial failure in model gas storage reservoirs stressed under triaxial conditions.

These latter investigations are part of a continuing study associated with the optimization of pressures in underground gas storage reservoirs. Initial studies have been carried out on laboratory models (right-circular cylinders) containing spherical and ellipsoidal cavities. During testing the models were loaded under equivalent underground conditions and the reservoirs pressurized until failure occurred. In these studies it was necessary to determine the stress conditions for initial reservoir failure as well as the conditions for ultimate failure of the model. Acoustic emission techniques were utilized to monitor the stability of the model during pressurization. Instrumentation was developed for this purpose which makes use of semiconductor strain gage transducers bonded directly to the model, for monitoring acoustic emission during the test period. Figure 26*a* shows a typical reservoir model prior to testing. Figure 26*b* shows a magnified view of a pair of the semiconductor transducers used for acoustic emission detection.

Harding et al[*47*] at Penn State are presently utilizing acoustic emission to investigate tensile failure in Brazilian tests on geologic materials. In these tests, specimens in the form of disks are loaded in diametric compression in order to induce a tensile failure in the central region of the specimen. There appears to be considerable controversy as to the location of where initial failure occurs. The purpose of these tests was to verify the true location using acoustic emission techniques. Figure 27*a* illustrates a typical specimen disk instrumented with semiconductor acoustic emission transducers and foil-type strain gages, and mounted in a testing machine prior to loading. Figure 27*b* shows the associated acoustic emission monitoring facilities.

During the next few years the use of acoustic emission as a tool in the rock mechanics laboratory will increase many fold. Certainly the applications would appear to be limited only by the skill and ingenuity of the experimenter.

Field Studies

In the discipline of rock mechanics the major effort in relation to the application of acoustic emission techniques has been in the field. Unfortunately the field is an extremely difficult location in which to work and until very recently a great number of these field studies were most unrewarding.

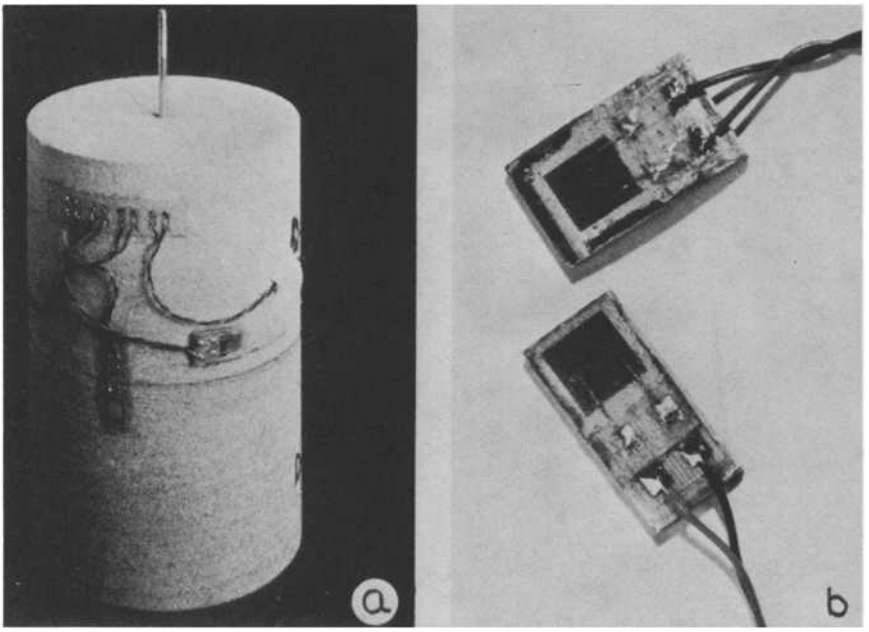

FIG. 26—*Gas storage reservoir model* (a) *and associated acoustic emission transducers* (b).

Historically, acoustic emission studies associated with geologic materials were initiated in order to study the stability of underground mining operations, and as a method for predicting the occurrence of violent underground disturbances such as rock and coal bursts. During the late 1930's and early 1940's Obert and Duvall [*8*], showed that in the laboratory as well as in the field, the acoustic emission noise rate increased greatly, as the specimen or structure became more highly loaded. Conversely, as equilibrium was reached after a major structural failure (for example, failure induced by blasting), the noise rate decreased. In other words, the noise rate appeared to be a factor indicative of the degree of instability of the structure. The early work of Obert and Duvall has provided the basis for the majority of acoustic emission field studies carried out in North America.

During the period 1940-1960 acoustic emission studies were carried out during numerous underground research programs but little real use of the resulting data appeared to have been made. In the early 1960's a renewed and more detailed interest in the field applications of acoustic emission occurred. The following section will be devoted to a brief description of various field studies which have been carried out, as well as a number of them presently

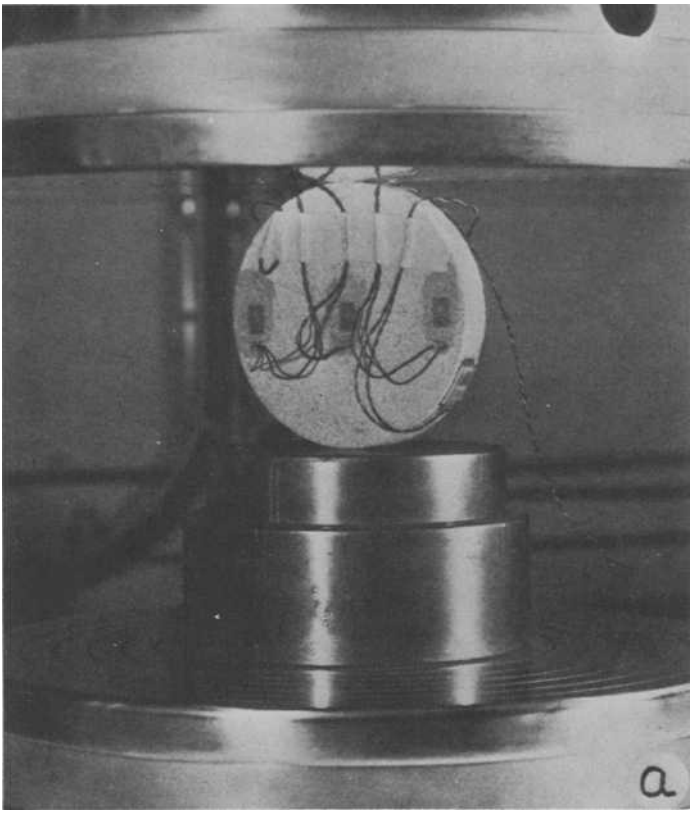

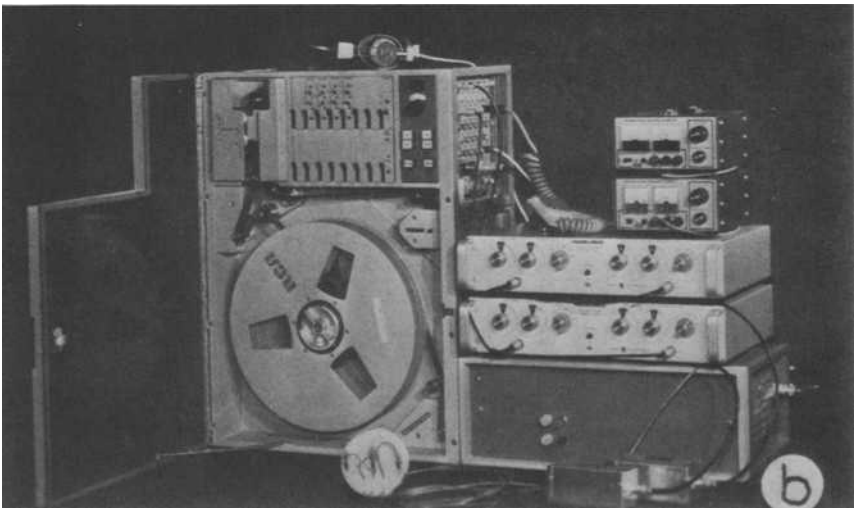

FIG. 27—*Instrumented disk test specimen* (a) *and monitoring facilities* (b) *for investigating crack initiation under diametric loading*[47].

underway, associated with mining, civil, and petroleum and natural gas engineering, and with seismology.

Typical Field Studies

Underground Mining–During the late 1930's and early 1940's government agencies both in the United States and Canada became involved in studies related to underground mining. These programs were initiated as a result of difficulties experienced in mining at increasing depths or in highly stressed zones; the most spectacular of these being the sudden violent failure of mine structures known as rock bursts[*11,12,38*].

In the late 1930's Obert[*5,6*] at the U. S. Bureau of Mines initiated studies to determine underground stresses. As part of this continuing program, facilities for monitoring acoustic emission underground were developed by Obert[*7*] and Obert and Duvall[*8-10*]. The original monitoring facilities[*7*] consisted of a "geophone" (containing a Rochell salt cantilever element enclosed in a moisture tight metal cylinder) the output of which was fed to a battery operated amplifier and then to a film-type recorder. A set of earphones was also included in the facility to provide an audible means of monitoring acoustic emission activity. In practice the geophone was located underground in a borehole. This monitoring system was sensitive to disturbances in the region of 1000 Hz due mainly to the design of the geophone itself. Using these facilities, Obert investigated the character and frequency of occurrence of acoustic emission events in rock burst prone mining areas. Field results indicated the acoustic emission rate increased prior to a rock burst.

After considerable refinement of the original monitoring facilities Obert and Duvall[*8*] undertook an extensive study of acoustic emission in a group of 9 mines including 2 deep mines in Canada. Figure 28 illustrates the monitoring facilities used. Similar facilities were employed in a number of U. S. Bureau of Mines' underground studies during the period 1940 to 1960[*48-50*].

Considerable application of acoustic emission techniques to underground mining was underway in Europe and Asia during the period 1940-1966. Antsyferov[*13*] lists a number of useful references, particularly in regard to the design of acoustic emission transducers for underground use, and statistical methods of analyzing acoustic emission data. A paper by Buchheim[*51*] describes a number of interesting field studies carried out in coal and potash mines.

During the early 1960's more sophisticated techniques for monitoring underground acoustic emission activity were investigated, and in particular techniques for accurate source location were developed. During this period Cook[*52*] developed a refined monitoring system for use in the Witwatersrand gold mining area. The system was capable of recording the outputs of up to 16 transducers on magnetic tape for a continuous period of 25 h. Normally 8

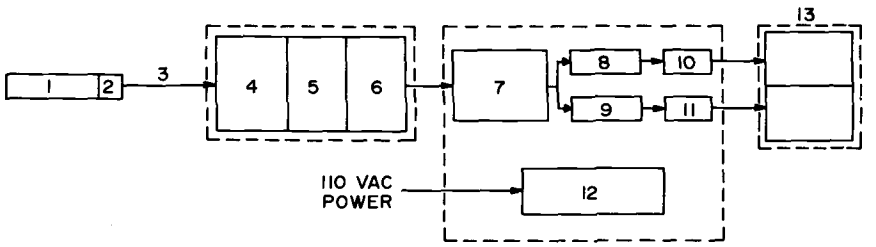

1 – GEOPHONE
2 – LINE TRANSFORMER
3 – COAXIAL CABLE
4 – HIGH GAIN AMPLIFIER
5 – ATTENUATOR
6 – BAND PASS FILTERS
7 – LOGARITHMIC AMPLIFIER
8 – FAST DISCRIMINATOR CIRCUIT
9 – SLOW DISCRIMINATOR CIRCUIT
10, 11 – POWER AMPLIFIERS
12 – SYSTEM POWER SUPPLY
13 – DUAL CHANNEL RECORDER

FIG. 28–*Monitoring facilities used in early underground mining studies*[8].

transducers were utilized each being connected into two channels of the recording system, the sensitivities of which differed by a factor of 30. In this way events having a wide range of energies could be recorded. As a preliminary investigation had indicated that a large proportion of the acoustic emission energy in the mining area under study occurred in the frequency range 20 to 50 Hz the frequency response of the overall monitoring system was restricted to approximately 15 to 300 Hz. Cook used electromagnetic type seismometers (having natural frequencies in the range 7.5 to 14 Hz) as acoustic emission transducers. As used underground, these units had an approximately flat velocity response in the range 15 to 300 Hz. Data recorded underground were played back through a 16-channel recording oscillograph to provide a permanent record. In terms of monitoring facilities developed more recently, such a system would be termed "narrow-band."

In order to determine source locations underground it is necessary to know the velocity of propagation in the associated material. Cook determined this by detonating two or three pounds of explosive at known locations and monitoring the arrival of the resulting stress waves at each of the transducers. Velocities determined in this manner were found to be accurate to within ± 5 percent and it was estimated that the detonation locations could be determined (using the recorded data) to an accuracy of ± 10 ft, and travel times could be determined to ± 1 ms. Rather than using an analytical method for determining source locations a mechanical analog in the form of a "string model" was employed.

In his conclusions, Cook states that it would appear from the underground studies that it is not possible to stop rockbursts but it may be possible to make them occur during normal blasting operations by relating the mining advance per

blast and the interval per blast to the local underground conditions. Cook also observed that there appeared to be no difference in energy or location between major failures which caused damage to the underground workings and those which do not. In other words the degree of damage appeared to be governed by local conditions.

Since 1963 a number of other field studies involving acoustic emission have been carried out. These include studies by Saski and Takata[*53*] in a number of coal and metal mines, Bollinger[*54*] on the surface over a coal mine, Hedley et al[*55*] in an iron ore mine, Stas et al[*56*] in a coal mine, and Blake and Leighton[*57*] in a number of metal mines. The monitoring facilities used by Saski and Takata, and Blake and Leighton are of particular interest since they are "wide band" compared to most earlier instrumentation.

The system developed by Blake and Leighton[*57*] was designed to have a flat frequency response in acceleration in the range of 20 to 10,000 Hz. It is interesting to note these authors state that "the frequencies generated by rock noise contain many high-frequency components." In contrast, Cook[*52*] indicated that the majority of the events occurred in the frequency range 20 to 50 Hz. This seeming disagreement is further evidence of our limited appreciation of the overall frequency spectrum involved in acoustic emission phenomena associated with geologic material. Until a better understanding of this frequency spectrum is obtained wide band systems should be employed exclusively.

Blake and Leighton[*57*] utilized commercially available piezoelectric accelerometers as acoustic emission transducers. In use these were cemented to the wall of bore holes drilled in various underground locations. The output of each transducer was connected to a preamplifier located in the bore hole itself, the signal from which was transmitted by cable to a post-amplifier and to one channel of a 7-channel FM magnetic tape recorder located at a central monitoring location. Using an array of at least five transducers, studies have been carried out in a number of hard rock mines. Data recorded on magnetic tape were processed by re-recording it on a multichannel oscillograph to determine a series of travel time differences. These data along with propagation velocity data obtained in the mine, in a manner similar to that described by Cook[*52*] earlier, were used to calculate source locations. In another paper Leighton and Blake[*58*] discuss the various methods for computing source locations from field data. They estimate the accuracy of such locations to be within ± 10 ft. Blake and Leighton conclude that broad-band monitoring provides much more quantitative information about the behavior of a rock structure than can be obtained using traditional narrow-band facilities. It is their opinion that "when used regularly by experienced personnel, it can become a valuable engineering tool in detecting, delineating and estimating the stability of potential failure zones in rock structures."

To date relatively few acoustic emission studies have been conducted in

North American coal mines. At present I am involved in one such study entitled Project–MACS (Microseismic Activity applied to Coal Mine Safety) under support provided by the U. S. Bureau of Mines. The object of this study is to investigate the feasibility of using acoustic emission techniques to locate potential zones of instability around coal mine workings. If such zones could be located sufficiently early there is strong evidence that remedial action could be taken to eliminate many of the roof control problems which create safety hazards and often result in production delays.

Basically this field study involves monitoring the acoustic emission generated by working mines during their normal operation. It is planned to monitor this activity from the surface using transducers located in shallow boreholes positioned over the working area of the mine. This study is unique in the fact that measurements will be made from the surface rather than underground. This approach provides several advantages, including the fact that there will be no electrical limitations on the monitoring system, and that the study will in no way interfere with normal mine operations. The monitoring facility being developed will be very broad-band (50 Hz to 200 KHz), and will be mounted in a small van along with its own battery and 110 VAC power supplies for complete mobility. Figure 29 presents a block diagram of the monitoring facility.

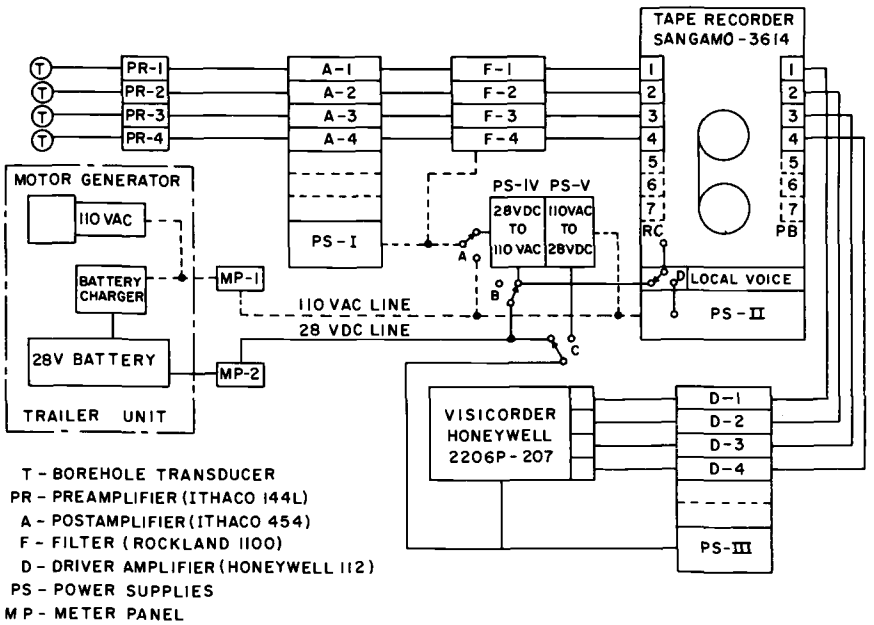

FIG. 29—*Block diagram for monitoring facility of Project–MACS research program.*

An important aspect of this project is the development of an accurate source location technique. In this regard studies have been underway by Harding[*40*] to develop a suitable computer program for calculation of source location coordinates.

Slope Stability–In the last few years research in the field of slope stability associated with both open pit mining and various civil engineering projects has increased rapidly. Acoustic emission techniques appear to provide a useful tool for monitoring slope stability. In such studies automatic long term monitoring systems are desirable and a number of special systems have been developed. For example, Cadman et al[*1*] describe an automated monitoring system for studying landslides; Broadbent and Armstrong[*59*] describe the design and application of various acoustic emission monitoring systems with particular application to slope stability studies.

Paulsen et al[*60*] have utilized acoustic emission techniques to study slope stability in an open pit mine at Boron, California. They sum up the situation by stating that a plot of the acoustic emission with time provides a graphic picture of what is going on in the Boron open pit. An increase in activity over and above the normal background probably indicates that a potential slope stability problem exists. A slow increase in activity indicates stabilization may be being achieved, whereas an accelerating activity rate indicates failure may be imminent.

During a recent study at Kennecott's Kimbley Pit in Nevada[*61*] extensive acoustic emission studies were undertaken as part of the routine monitoring of the pit slope stability during slope steepening.

The application of acoustic emission techniques to monitoring slopes associated with highway cuts, dam construction, and other civil engineering applications would appear to be extensive.

Petroleum and Natural Gas–Acoustic emission has wide field application in the petroleum and natural gas industry. The study of hydrofracturing being one application of considerable importance. Here fluids are injected under pressure into low permeability strata with the purpose of fracturing these strata, and increasing their permeability and porosity. Such techniques are commonly used to stimulate a poorly producing oil or gas well or to increase the storage capacity of an underground gas storage area. Aside from surface measurements of injection pressure and volume, little is really known in regard to the fracturing process that is going on perhaps 2000 to 10,000 ft below surface. Consideration is being given by a number of workers to the utilization of acoustic emission techniques to monitor the initiation and propagation of underground fractures associated with hydrofracturing. For example studies presently underway by Overbey and Pasini[4] are concerned with the development of techniques for

[4] Personal communication with W. K. Overbey and J. Pasini, III, U. S. Bureau of Mines, Morgantown, W. Va.

determining the location and orientation of underground fractures developed during hydrofracturing.

At present I am involved in a field program which utilizes acoustic emission techniques to study the stability of underground gas storage reservoirs. This program, entitled Project–SUR (Stability of Underground Gas Storage Reservoirs), is supported by the Pipeline Research Committee of the American Gas Association. Here it is planned to instrument selected gas storage reservoirs and study such factors as the degree of stability of the reservoir, the pressure at which the reservoir exhibits initial instability, the location of the point at which initial reservoir instability occurs, and the direction and rate of propagation of any resulting fractures in the reservoir rock, cap rock, or surrounding strata.

In the first phase of project–SUR a single transducer (A) will be located on the surface or embedded in a short hole above the reservoir, as shown in Fig. 30*a*. Associated with this transducer will be suitable monitoring and recording facilities. This type of installation will detect the overall acoustic emission occurring in the reservoir region, but will not supply sufficient data to locate the source of any instability. Such an installation will however make it possible to determine how the general activity is influenced by various stages of the gas storage injection-withdrawal cycle.

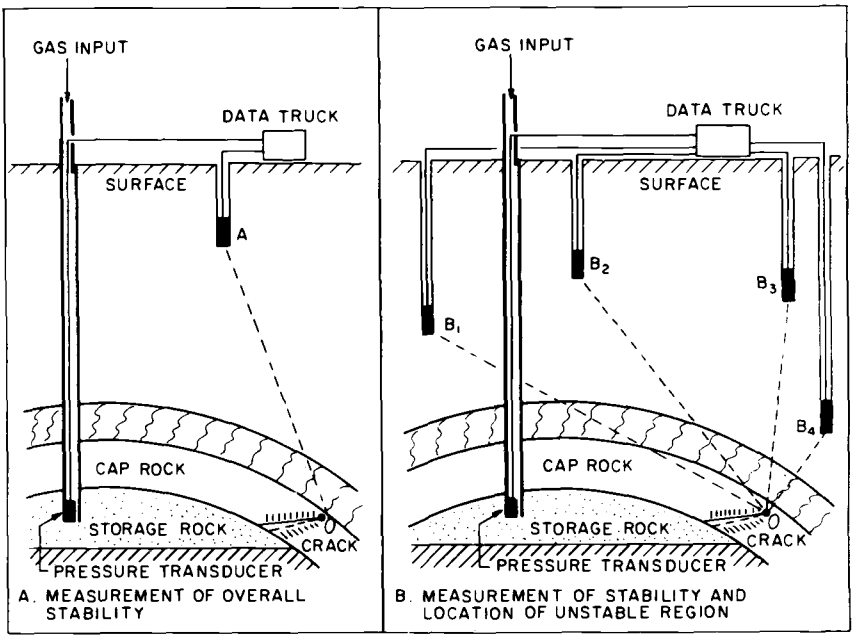

FIG. 30– *Application of acoustic emission techniques to 2 field studies associated with underground storage of natural gas.*

In the second phase of the project, efforts will be made to locate the source of the instability. Here an array of at least four transducers (B_1–B_4), as shown in Fig. 30*b*, will be required. Each transducer requires its own monitoring system with the output from all monitoring systems being recorded on a multichannel magnetic tape recorder. The acoustic emission associated with an unstable region, (for example, a crack located at the point 0 in Fig. 30*b*) will be detected at each of the transducers at a time which is dependent on the relative distance of each transducer from the source location. Knowing the position of each transducer and the difference in arrival times, it should be possible to locate the position of the instability.

The instrumentation to be used on project–SUR is similar to that described earlier for use in studying acoustic emission associated with longwall mining (project–MACS).

Other Studies–Acoustic emission techniques appear to be gaining increased attention in a variety of field oriented projects. For example one of the earlier applications of this technique was that of Crandell[*62*] who employed it as a safety monitor for use in tunneling projects. More recently Beard[*63*] lists a number of tunneling projects where simple acoustic emission monitoring devices have been used with great success.

In recent years geophysicists concerned with the prediction and causes of earthquakes have become increasingly interested in the study of low-level acoustic emission[*15,64,65*] since it is felt that the background pattern of such activity may provide important information relative to the future earthquakes.

Discussion

In the present paper, I have attempted to provide a state-of-the-art review of acoustic emission techniques as they apply to the field of rock mechanics. There is little doubt that such techniques are already widely applied in both laboratory and field studies associated with geologic materials, and it is predicted that they will be utilized to an increasing degree in the future. Our understanding of acoustic emission phenomena in geologic materials is at present relatively limited; however, acoustic emission represents perhaps the most important tool available in the rock mechanics field today.

Acknowledgments

I would like to acknowledge the financial support provided for acoustic emission research on geologic materials at the Pennsylvania State University by the National Science Foundation (Grants GK-151 and GK-1598), the American Gas Association (Pipeline Research Committee Project PR-12-43) and the U. S. Bureau of Mines (Project G0101743[MIN-451]) during the period 1965-1971.

References

[1] Cadman, J. D., Goodman, R.E., and Van Alstine, C., "Research on Subaudible Noise in Landslides", Geotechnical Engineering Report of Investigation (NSF Grant GK 109), 27 June 1967, Department of Civil Engineering, University of California, Berkeley.

[2] Gold, L. W., *Canadian Journal of Physics*, CJPHA, Vol. 38, No. 9, 1960, pp. 1137-1148.

[3] Gold, L. W., "Time to Formation of First Cracks in Ice", Proceedings International Conference on Low Temperature Science (Sapporo Japan 1966), NRC 10226, National Research Council, Ottawa, 1968.

[4] Warren, N. W. and Latham, G. V., *Journal of Geophysical Research*, JGREA, Vol. 75, No. 23, 1970, pp. 4455-4464.

[5] Obert, L., "Measurement of Pressures on Rock Pillars in Underground Mines – Part I," U.S. Bureau of Mines RI 3444, 1939.

[6] Obert, L., "Measurement of Pressures on Rock Pillars in Underground Mines – Part II," U.S. Bureau of Mines RI 3521, 1940.

[7] Obert, L., "Use of Subaudible Noise for Prediction of Rock Bursts," U.S. Bureau of Mines RI 3555, 1941.

[8] Obert, L. and Duvall, W. I., "Use of Subaudible Noise for Prediction of Rock Bursts – Part II," U.S. Bureau of Mines RI 3654, 1942.

[9] Obert, L. and Duvall, W. I., "Microseismic Method of Predicting Rock Failure in Underground Mining – Part I. General Method," U.S. Bureau of Mines RI 3797, 1945.

[10] Obert, L. and Duvall, W. I., "Microseismic Method of Predicting Rock Failure in Underground Mining – Part II. Laboratory Experiments", U.S. Bureau of Mines RI 3803, 1945.

[11] Hodgson, E. A., *Canadian Institute of Mining and Metallurgy Transactions*, TCIMA, Vol. 46, 1943, pp. 313-324.

[12] Hodgson, E. A. and Gibbs, Z. E., "Seismic Research Program, Rock Burst Problem – Lakeshore Mines", Department Mines, Resources, and Surveys, Engineering Branch Report 14, Ottawa, Canada, 1945.

[13] Antsyferov, M. S., Ed., *Seismo-Acoustic Methods in Mining*, Consultants Bureau, New York, 1966.

[14] Knill, J. L., Franklin, J. A. and Malone, A. W., *International Journal of Rock Mechanics and Mining Sciences*, IJRMA, Vol. 5, 1967, pp. 87-121.

[15] Armstrong, B. H., *Bulletin of the Seismological Society of America*, BSSAA, Vol. 59, No. 3, 1969, pp. 1259-1279.

[16] Barron, K., "The Fracture of Brittle Rocks Around Mine Excavations", Internal Report MR 69/25 LD, Mining Research Center, Department of Energy, Mines and Resources, Ottawa, 1969, pp. 10.6-10.7, 10.48-10.58.

[17] Barron, K., *International Journal of Rock Mechanics and Mining Sciences*, IJRMA, Vol. 8, 1970, pp. 55-59.

[18] Pérami, R. and Thénoz, B., *Revue De L'Industrie Minerale*, RINMB, July 1969, pp. 50-62.

[19] Mogi, K., *Bulletin of the Earthquake Research Institute*, TDJKA, Vol. 40, 1962, pp. 125-173.

[20] Suzuki, T. et al, "A New Approach to the Prediction of Failure by Rock Noise", Fourth International Conference on Strata Control and Rock Mechanics, Columbia University, N. Y., 1964.

[21] Scholz, C. H., *Bulletin of the Seismological Society of America*, BSSAA, Vol. 58, 1968, pp. 399-415.

[22] Mae, I. and Nakao, K., *Journal of the Society of Materials Science*, ZARYA, Vol. 17, No. 181, 1968, pp. 62-67.

[23] Goodman, R. E., *Geological Society of America Bulletin*, BUGMA, Vol. 74, 1963, pp. 487-490.

[24] Brown, J. W., "An Investigation of Microseismic Activity in Rock Under Tension", M.S. thesis, Mining Department, The Pennsylvania State University, 1965.

[25] Brown, J. W. and Singh, M. M., *Transactions of the Society of Mining Engineers*, TMENA, Vol. 233, 1966, pp. 255-265.

[26] Hardy, H. R., Jr., Kim, R. Y., Stefanko, R., and Wang, Y. J., *Rock Mechanics – Theory and Practice*, Proceedings of the Eleventh Symposium on Rock Mechanics (Berkeley 1969), AIME, New York, 1970, pp. 377-413.

[27] Chugh, Y. P., Hardy, H. R., Jr., and Stefanko, R., "An Investigation of the Frequency Spectra of Microseismic Activity in Rock Under Tension", presented at the Tenth Rock Mechanics Symposium, Austin, Texas, May 1968, proceedings in press.

[28] Gutenberg, B. and Richter, C. R. in *Seismicity of the Earth*, Princeton University Press, 1949.

[29] Suzuki, Z., "A Statistical Study on the Occurrence of Small Earthquakes – I", Science Reports Tohoku University, Fifth Series Geophysics, 5, 1953, pp. 177-182.

[30] Suzuki, Z., "A Statistical Study on the Occurrence of Small Earthquakes – II", Science Reports Tohoku University, Fifth Series Geophysics, 6, 1954, pp. 105-118.

[31] Mogi, K., *Bulletin of the Earthquake Research Institute*, TDJKA, Vol. 40, 1962, pp. 831-853.

[32] Ishimoto, M., and Iida, K., *Bulletin of the Earthquake Research Institute*, TDJKA, Vol. 17, 1939, pp. 443-478.

[33] Mogi, K., *Tectonophysics*, TCTOA, Vol. 5, No. 1, 1967, pp. 35-55.

[34] Scholz, C. H., *Journal of Geophysical Research*, JGREA, Vol. 73, 1968, pp. 1447.

[35] Scholz, C. H., *Journal of Geophysical Research*, JGREA, Vol. 73, 1968, p. 1417.

[36] Savage, J. C. and Mohanty, B. B., *Journal of Geophysical Research*, JGREA, Vol. 74, No. 17, 1969, pp. 4329-4332.

[37] Scholz, C. H., *Journal of Geophysical Research*, JGREA, Vol. 75, No. 11, 1970, pp. 2148-2149.

[38] Obert, L., and Duvall, W. I. in *Rock Mechanics and the Design of Structures in Rock*, Wiley, New York, 1967.

[39] Harding, S. T., "A Critical Evaluation of Microseismic Studies". Internal Report RML–IR/70-24, Department of Mineral Engineering, The Pennsylvania State University, 1970.

[40] Harding, S. T., "A Least Squares Seismic Location Technique and Error Analysis", Internal Report RML–IR/71-8, Department of Mineral Engineering, The Pennsylvania State University, 1970.

[41] Mogi, K., *Bulletin of the Earthquake Research Institute*, TDJKA, Vol. 46, 1968, pp. 1103-1125.

[42] Harding, S. T., and Hardy, H. R., Jr., "Acoustic Emission During Transient and Secondary Creep, and During Creep Recovery", presented at the Joint Annual Meeting of the Seismological Society and Geological Society of America, Milwaukee, Wis., Oct. 1970.

[43] Hardy, H. R., Jr., in *Proceedings of the Third Symposium on Rock Mechanics*, 54, Quarterly Colorado School of Mines, 1959, pp. 134-175.

[44] Byerlee, J. D., and Peselnick, L., *Naturwissenschaften*, NATWA, Vol. 57, 1970, pp. 82-85.

[45] Hardy, H. R., Jr., "Stability Studies on Gas Storage Reservoir Models", paper prepared for presentation at the Underground Storage Session, American Gas Association Transmission Conference, Denver, Colorado, April 1970, published in conference proceedings, AGA Catalogue No. X59970, Fall 1970, pp. T132-T139.

[46] Hardy, H. R., Jr., in *Proceedings of the 2nd Congress-International Society Rock Mechanics*, Belgrade, Jugoslavia, September 1970, Vol. II, paper 4-42.

[47] Harding, et al, "Investigation of Crack Initiation in Rock Discs Loaded in Diametric Compression Using Acoustic Emission Techniques", Internal Report, RML–IR/71-14, Department of Mineral Engineering, The Pennsylvania State University, 1971.

[48] Merrill, R. H., "Design of Underground Mine Openings, Oil Shale Mine, Rifle, Colorado", U. S. Bureau of Mines, RI 5089, 1954.

[49] Merrill, R. H., "Roof-Span Studies in Limestone," U. S. Bureau of Mines RI 5940, 1957.

[50] Merrill, R. H., and Morgan, T. A., "Method of Determining the Strength of a Mine Roof," U. S. Bureau of Mines RI 5406, 1958.
[51] Buchheim, W., "Geophysical Methods for the Study of Rock Pressure in Coal and Potash – Salt Mining", International Strata Control Congress, Leipzig, 1958, pp. 222-233.
[52] Cook, N. G. W. in *Rock Mechanics,* Proceedings Fifth Symposium on Rock Mechanics (Minneapolis 1962), Pergamon Press, New York, 1963, pp. 493-516.
[53] Sasaki, K., and Takata, A., *Rock Mechanics in Japan,* 1, Japan Society of Civil Engineers, Tokyo, 1970, pp. 167-169.
[54] Bollinger, G. A., *Earthquake Notes,* EAQNA, Vol. 41, No. 4, Eastern Section Seismological Society of America, 1970, pp. 26-27.
[55] Hedley, D. G. F., et al in *Proceedings Fifth Canadian Rock Mechanics Symposium* (Toronto 1968), published by Department Energy, Mines, and Resources, Ottawa, 1969, pp. 105-125.
[56] Stas, B., et al, *Dynamic Rock Mechanics,* Proceedings Twelfth Symposium on Rock Mechanics (Rolla, 1970), AIME, New York, 1971, pp. 109-119.
[57] Blake, W., and Leighton, F., *Rock Mechanics–Theory and Practice,* Proceedings Eleventh Symposium on Rock Mechanics (Berkeley 1969), AIME, New York 1970, pp. 429-443.
[58] Leighton, F. and Blake, W., "Rock Noise Source Location Techniques", U. S. Bureau of Mines RI 7432, 1970.
[59] Broadbent, C. D., and Armstrong, C. W., *Proceedings Fifth Canadian Rock Mechanics Symposium* (Toronto 1968), Published Department of Energy, Mines and Resources, Ottawa, 1969, pp. 91-103.
[60] Paulsen, J. C., Kistler, R. B., and Thomas, L. L., *Mining Congress Journal,* MCJOA, Vol. 53, 1967, p. 28.
[61] Wisecarver, D. W., "Changes in Stress, Strain, and Displacement with Changes in Slope Angle at the Kimbley Pit, Ely, Nevada", Preprint 68-AM-84, 1968 Annual AIME Meeting, New York.
[62] Crandell, F. J., *Journal of the Boston Society of Civil Engineers,* JBOSA, Jan. 1955, pp. 39-59.
[63] Beard, F. D., *Civil Engineering,* CVEGA, Vol. 32, No 5; 1962, pp. 50-51.
[64] Oliver, J., Ryall, A., Brune, J. N., and Slemmons, D. B., *Bulletin of the Seismological Society of America,* BSSAA, Vol. 56, 1966, p. 899.
[65] Watanabe, M., "The Occurrence of Elastic Shocks During Destruction of Rocks and Its Relation to the Sequence of Earthquakes", geophysical papers dedicated to Professor Kenzo Sassa, Kyoto University, Kyoto, Japan, 1963.

Related References

Chugh, Y. P. and Hardy, H. R., Jr., "Application of Microseismic Techniques in Mining", presented at Mine Mechanization Symposium, Varanasi, India, 8-9 March, 1969.
Duvall, W. I., and Stephenson, D. E., *Transactions,* AIME, TAIMA, Vol. 232, No. 3, 1965. pp. 235-240.
Franklin, J. A., *"Some Effects of Loading Technique on the Acoustic Emissions from Stressed Rock",* M.S. thesis, Geology Department, Imperial College, London University, 1965.
Goodman, R. E., and Blake, W., "Microseismic Detection of Potential Earth Slumps and Rock Slides", Report MT-64-6, Inst. of Engineering Research, University of California, Berkeley, 1964.
Goodman, R. E. and Blake, W., *Felsmechanik and Ingenieurgeologie,* RMFMA, Supplement II, 1965.
Goodman, R. E., and Blake, W., "Rock Noise in Landslides and Slope Failures", Highway Research Board, 44th annual meeting, No. 119, Washington, D. C., 1966.
Hall, A., "Microseismic Measurements," M. H. No. 30, Akademic fur Eng. Wissensch FKO, Stockholm, 1959.

Hardy, H. R., Jr., "Microseismic Activity and its Application in the Natural Gas Industry", *Transmission Conference Proceedings,* American Gas Association, Catologue No. X59969, 1969, pp. T-147 to T-156.

Helfrich, H. K., *Rock Mechanics and Engineering Geology,* RMEGB, Vol. 4, No. 1, 1966.

Herron, T. J., *"The Detection and Delineation of Subsurface Subsidence by Seismic Methods,"* thesis, Geophysics Department, Michigan College of Mines and Technology, 1956.

Hodgson, K. and Joughin, N. C. in *Failure and Breakage of Rock,* Proceedings Eighth Symposium on Rock Mechanics, Minneapolis 1966, AIME, New York, pp. 194-203.

Kundorf, W. and Rotter, D., *Freiberger Forschungschefte, FFRCA, No. 120, 1961.*

Malone, A. W., *"An Experimental System for the Laboratory Study of Acoustic Emission from Stressed Rock",* M.Sc. thesis, Geology Department, Imperial College, London University, 1965.

McCauley, M. S., *Accociation of Engineering Geologists* AEGBB, 1965, p. 1.

Obert, L., and Duvall, W. I. "Micro-seismic Method of Determining the Stability of Underground Openings," *Bulletin of the U.S. Bureau of Mines,* XMBUA, Vol. 573, 1957.

Obert, L., and Duvall, W. I. "Seismic Methods of Detecting and Delineating Sub-surface Subsidence," U. S. Bureau of Mines RI 5882, 1961.

Perami, R., Rarran, J., and Capdecomme, L., *Proceedings of the 1st Congress International Society of Rock Mechanics,* Lisbon, 1, 1966, p. 621 (in French).

Persson, T. and Hall, B., "Microseismic Measurements for Predicting the Risk of Rock Failures and the Need for Reinforcement in Underground Cavities," Royal Institute of Technology, Stockholm, 1958.

Rummel, F. and Angenheister, G., "Investigation on the Occurrence of Noise Effects in a Landslide at Kaunertal," Institute of Applied Geophysics, University of Munich, 1964.

Simane, J., *Freiberger Forschungshefte,* FFRCA, No. 126, 1962.

Simane, J., "The Use of the Seismoacoustic Method in Investigations into Rockbursts," 15th Mining and Metallurgy Day at Berkakademie Freiberg, 1963.

Simane, J., *Freiberger Forschungshefte,* FFRCA, Series C, 1964.

Stateham, R. M., and Vanderpool, J. S., "Microseismic and Displacement Investigations in an Unstable Slope", U. S. Bureau of Mines RI 7470, 1971.

C. A. Tatro[1]

Design Criteria for Acoustic Emission Experimentation

REFERENCE: Tatro, C. A., Design Criteria for Acoustic Emission Experimentation," *Acoustic Emission, ASTM STP 505*, American Society for Testing and Materials, 1972, pp. 84-99.

ABSTRACT: Acoustic emission experiments that can be performed in the laboratory using a single transducer and involving specimens or simple components are discussed. The emphasis is on experimental design rather than on single experiments or results produced. The experiments described are restricted to those where application of mechanical load is used to condition the material, and where commercially available equipment is adequate for instrumentation.

The magnitudes and characteristics of the acoustic emission response are described. The compromises in signal detection and data acquisition methods follow from this description. Those aspects of experimental design which are most likely to be foreign to the new user of acoustic emission techniques are pointed out, as are ways to assure that a proper design has been achieved. Results of an experiment which reveals the unique power of acoustic emission technology to reveal subtle changes in material are given as an example.

KEY WORDS: acoustics, emission, acoustic properties, sonic tests, mechanical tests, nondestructive tests, fabrication, quality control, piezoelectric transducers, yield, yield strength, dislocations (materials), loads (forces), noise (sound)

Acoustic emission technology in its present state is ready for application to a variety of problems facing materials engineers and scientists. Equipment necessary to support this work is avilable in either a prepackaged or component selectable form. Much meaningful work can and should be done without breakthroughs in either instrumentation or technology. The innovative insight of scientists and engineers knowledgeable about materials and materials testing needs is most needed.

This work was performed under the auspices of the U. S. Atomic Energy Commission.

[1] Head, Materials Test and Evaluation Section, Materials Engineering Division, University of California, Lawrence Radiation Laboratory, Livermore, Calif. 94550.

For many trained as materials scientists or engineers, reorientation is required to understand and appreciate acoustic emission technology, which deals with changes, not with absolute values. The changes are extremely small, with dimensional changes of 10^{-12} in. being an easily realizable threshold. Such changes are six orders of magnitude below the sensitivity threshold of a resistance strain gage. Pertinent, measurable microdynamical processes take place in materials during slow loading of the material. If you can ignore these processes and their implications for the load bearing integrity of the material under study, then you do not need acoustic emission testing. Instrumentation for acoustic emission testing is operated at frequencies in the low ultrasonic range, so that some rudimentary knowledge of the behavior of ultrasound in matter is necessary. The detector is a piezoelectric element, so the peculiarities of this selfgenerating transducer must also be understood.

Material Conditioning

In the usual laboratory test, the material under test is conditioned to emit acoustic emission pulses by applying a load at normal testing machine rates. Through the application of such a load, strain energy is stored in the specimen where most of it remains until the specimen is unloaded, if the load is confined to the elastic range. If the specimen is taken to the plastic range, part of the energy is stored as plastic strain energy and part is converted to heat. Energy partition into plastic strain, heat, sound, and energy to create new surface occurs if the specimen fractures. In both the so-called elastic range and in the plastic range, however, a small fraction of the energy is lost in the form of high frequency bursts of sound. These bursts are the acoustic emissions. In the elastic range, it is assumed that these sounds are emitted from local volumes where plastic processes are occurring. The fact that the acoustic emission process is an irreversible process supports the contention that plastic processes are involved although one notable reversible process has been observed in materials testing[*1*].

Sources and Responses

A wide variety of micromechanical events are known or suspected of serving as acoustic emission sources. A partial list would include mechanical twinning, breakaway of dislocations from pileups, cracking of crystal grains, crack extension and arrest, fine slip formation, Lüder's band formation, and vacancy coalescence. It is doubtful whether a single dislocation can be detected, with the possible exception of those moving at very high velocity that are subsequently stopped abruptly. An interesting speculation on a further source of acoustic emissions has been given by Fitzgerald[*2*].

In composite materials, easily recognizable sources of practical importance are fiber fracture, matrix crazing, and matrix-fiber disbonding. Analogous events

exist for particulate composites. Metal composites should have sources of this gross variety in addition to those listed in the preceding paragraph.

The events described are all abrupt, discontinuous events. It is reasonable to expect a high frequency, transient, acoustic event to accompany each of them. One can argue from fairly sound first principles that the acoustic event is detectable with properly designed equipment.

The fact of detectability has been firmly established in many laboratories. However, the fidelity of the detected signals leaves much to be desired. An accurate description of the source event from a study of the detected event may be forever impossible. Reasons for this are many, but principally the micromechanical structure of the test material, the size and shape of the test specimen, and the size, shape, and response characteristics of the detecting device all act to modify the source signal before it can be rendered observable by any known set of instruments.

By fixing the size and shape of the test specimen and by carefully choosing a transducer and an instrumentation system, some information concerning the signal source might be inferred from amplitude and frequency analysis of the detected event. However, the fact of detectability and the fact that acoustic emission occurrences can be correlated with one or more macroscopic engineering parameters leads to immediate practical results. The details of experimental design and associated data acquisition, data processing, and display systems will be emphasized here.

Elements of the Experiment

The most important elements of an acoustic emission experiment are the transducer, the loader, electronics for signal amplification and conditioning, and the data collection and display system.

The Transducer

The most popular transducer for acoustic emission experiments is a piezoelectric ceramic element. Perhaps the most used of these elements is a variety of lead zirconate-titanate (PZT-5). There are several reasons for this choice. Its low impedance at resonance makes satisfactory coupling on the electronic side simple. Its characteristics leave open to the experimenter a choice of either a voltage or a charge amplifier as a first stage amplifier in most cases. It is readily available, mechanically rugged, and matches most metals acoustically.

For usual acoustic emission work, the crystal mounting is comparatively simple. The crystal is electrostatically shielded by a metal case; it is electrically isolated from the part being tested by a thin plastic shoe, which may be contoured to the surface of the test part. It is acoustically isolated from the case, and is essentially unbacked. Such a transducer will respond to an impulse (acoustic emission) with a sharp rise and slower decay of voltage amplitude, with

a frequency inside this envelope determined by the most easily excited resonance of the transducer crystal. No detailed information about the shape or duration of the acoustic emission as it originated can be obtained with this transducer. One simply gets an electrical impulse from the transducer for each acoustic impulse originating in the specimen.

This transducer will produce a detectable response to a quick displacement change of 10^{-12} in. By performing the experiment sketched in Fig. 1, one may show this. In the experiment, a small steel ball is dropped on a straight rod

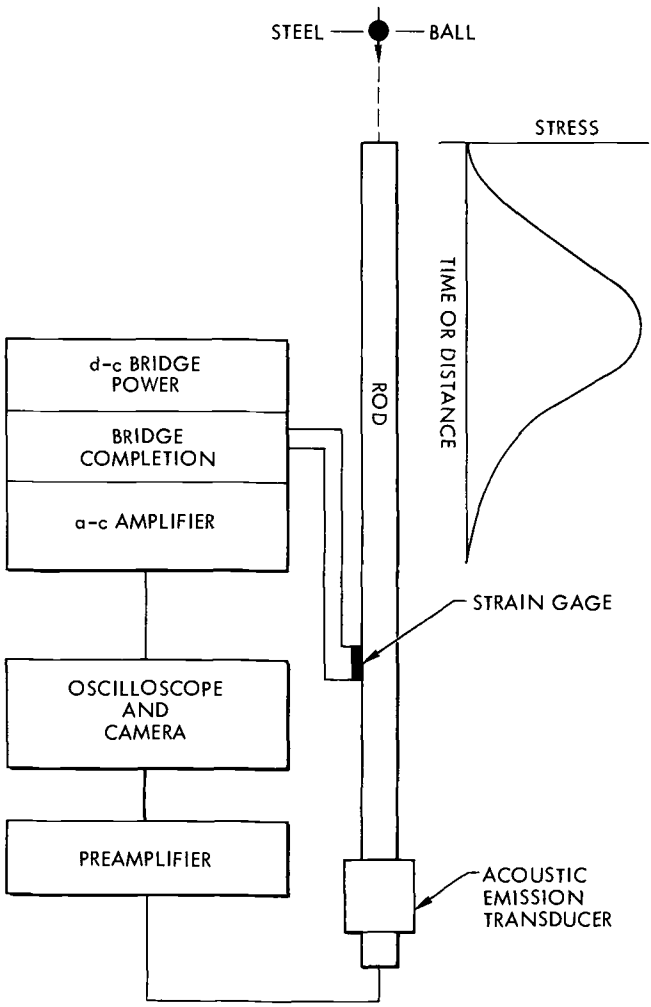

FIG. 1.—*Ball drop sensitivity comparison test.*

instrumented with a short gage length strain gage near its midsection and with the acoustic emission transducer at its opposite end. The ball produces a stress pulse with a rise time of less than 10μs. The results of measurements from each of the transducers is shown in Fig. 2. Only the leading pulses are used in the analysis. With knowledge of the strain gage parameters and instrumentation, and with knowledge that the electronic noise figure referred to system input is 10μV, the displacement deduction can be made.

Again referring to Fig. 2, a penalty for operating the transducer in its resonance mode can be clearly seen. Although the trailing pulse is not as complicated or persistent for lower excitations of the transducer, it does occur.

For reasons discussed elsewhere[*3*], the specific frequency at which the crystal is resonant is not a primary consideration. It is necessary to make a compromise in frequency selection so that extraneous excitations of the crystal are discriminated against while the efficiency for detecting an acoustic emission is not seriously impaired. (The extraneous excitations come from mechanical vibrations, audible acoustic noises, and electrical noise impulses internal and external to the instrumentaion.) Experience indicates that the frequency range between 70 and 170 kHz is a satisfactory compromise, especially in a laboratory not exclusively devoted to acoustic emission tests. The frequency response of an acoustic emission transducer used at Lawrence Livermore Laboratory is shown in Fig. 3. It shows the filter pass band used when tape recordings are taken of the acoustic emission acitivity.

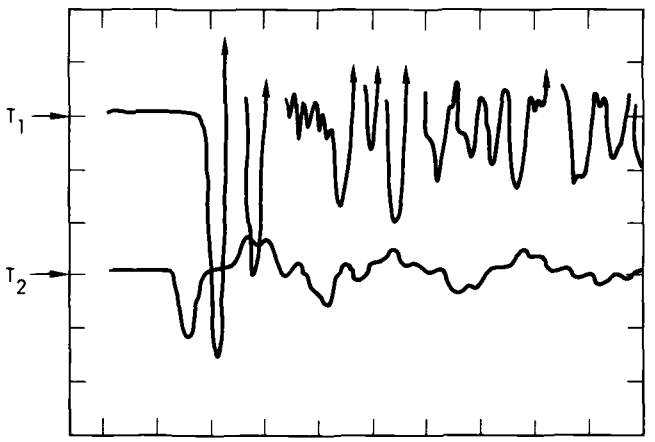

T_1: 20 psi/div, 50 μs/div -- transducer

T_2: 5 με/div, 50 μs/div -- strain gage

FIG. 2.–*Signal traces of strain gage and acoustic emission transducer.*

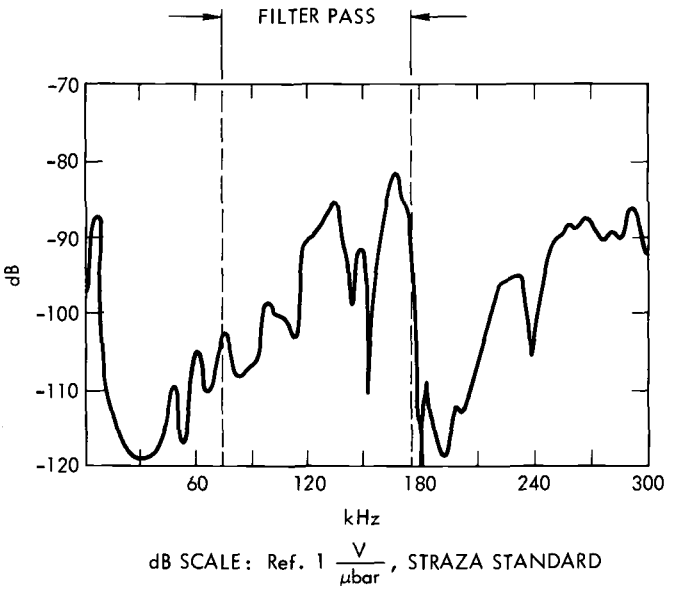

FIG. 3.—*Frequency response of an acoustic emission transducer.*

Further principles involved in acoustic emission transducer design have been given elsewhere[*4*]. Included in the referenced report is a description of a differentially connected transducer, which permits acoustic emission testing in high stray electrical fields.

Other crystal and transducer types have been used by various experimenters. These include Rochelle salt, contact microphones, ADP stacks, and other ceramic piezoelectric elements. Shock accelerometers have also been used extensively[*5-7*].

Comparison of the accelerometer with the acoustic emission transducer is complicated by the differences in the way sensitivites are quoted. One accelerometer that has been used has a quoted sensitivity of 50 m V/g and system input noise of 50μV. Evaluating the wave equation using results of an experiment like that sketched in Fig. 1, it is possible to estimate 3×10^{-11} in. as the minimum detection sensitivity of this transducer to a quick change in displacement. Thus, its sensitivity is less by a factor of 30 than the acoustic emission transducer. High frequency shock accelerometers are even less sensitive.

The location of the transducer on test parts normally encountered in laboratory work is usually not critical. An acoustic emission event tends to fill the test part with sound over a broad spectrum of frequencies. However, thin shell or filament sections, abrupt changes of cross section, and composite parts with large changes in acoustic impedance between materials could all serve as

severe attenuators of sound if they occur between the acoustic emission source and the transducer.

In addition to forming the transducer shoe to the part, a coupling medium must be used to encourage efficient sound coupling between the test part and transducer. Two specific suggestions are offered for this couplant. Dow Chemical V-9 polyester resin is a highly viscous resin with the consistency of cold honey. It is an efficient couplant, but permits the transducer to creep unless light clamping is used. General Electric RTV-116 is strong enough to support the weight of a transducer, but must be allowed to cure. With either couplant, removal and reuse of the transducer is possible.

The Loader

If one is interested in testing representative specimens or small parts of components, the most desirable loader is the universal testing machine. Such machines are used routinely as loaders in acoustic emission tests. The basic machine is usually not a significant sonic noise generator if an acoustic emission test is properly designed. However, the method of gripping a specimen is quite important. There are two precautions that must be followed: the first is that the gripping should not produce sound in the detection range of the acoustic emission system; the second is that sound paths through solid material from the machine to the specimen must be eliminated if the testing machine produces sound in the detection range of the transducer.

File grips have been found generally unsatisfactory because they tend to produce growing zones of plasticity in the specimen ends during the test. One case of successful use of file grips has been reported[8], however, the grip loading was low.

The most successful tension specimen is a flat bar with pin connections to the testing machine load line[9]. The pin area is preloaded before the test begins, and advantage is taken of the irreversibility of acoustic emission with loading.

A good gripping system is difficult to design. One plausible design that failed is shown in Fig. 4. The specimen is a small round specimen with threaded ends which is threaded into an open steel box at either end. The open space allows placement of the transducer on the flattened top of the specimen. The signals, injected into the specimen midway in the critical section, were short bursts with 100 kHz frequency. The bar graph shows the relative signal strength detected at transducer T_1 located on the specimen compared to transducer T_2 on the open frame. For a good design, the ratio would have been large and independent of load. Thus, the results indicate poor design.

In addition, a good gripping design should provide favorable discrimination of the signals originating in the critical section from those being led to the specimen via the load line. As shown in Fig. 5, signals were injected at each of the points indicated, and the response of transducer T_1 was noted. The bar graphs indicate

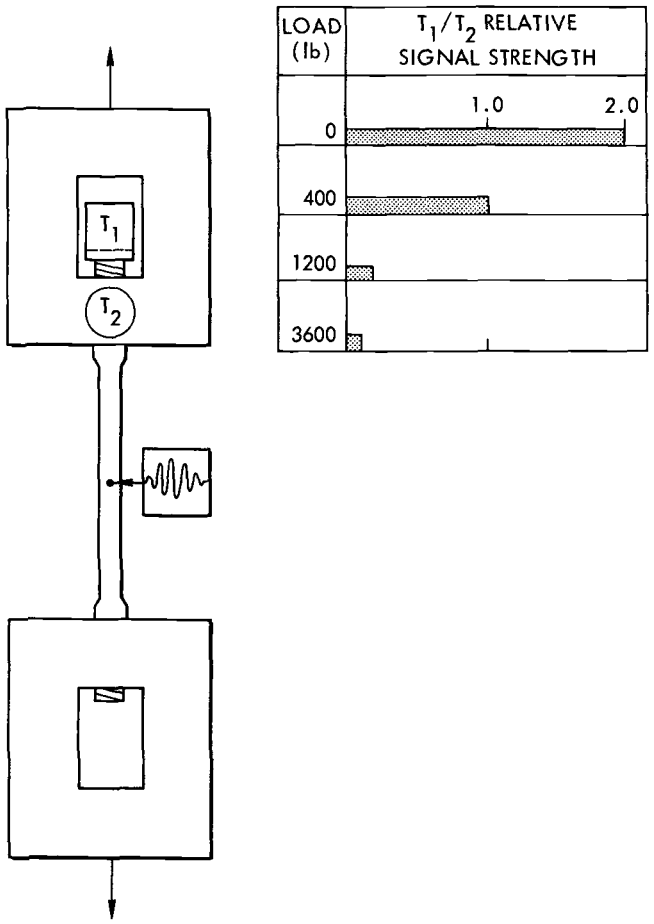

FIG. 4.–*Poor grip design showing reduction of signal reception with load.*

the response of the transducer to signals from each injection point relative to signals injected at position 4. Ideally, the bars should be zero for all loads. That the reception was good from the extraneous points and tended to improve with increasing load again indicates failure of the design.

The results discussed above are dependent upon the nature of the injected pulses, which were tacitly assumed to be mock acoustic emissions. The wavelength of sound used in the experiment corresponded roughly to the lateral dimensions of the open boxes, or of the specimen length. Injection of higher frequency pulses would probably have led to more favorable results. This case has been discussed elsewhere [*10*].

The precautions described must be observed in all acoustic emission tests. The

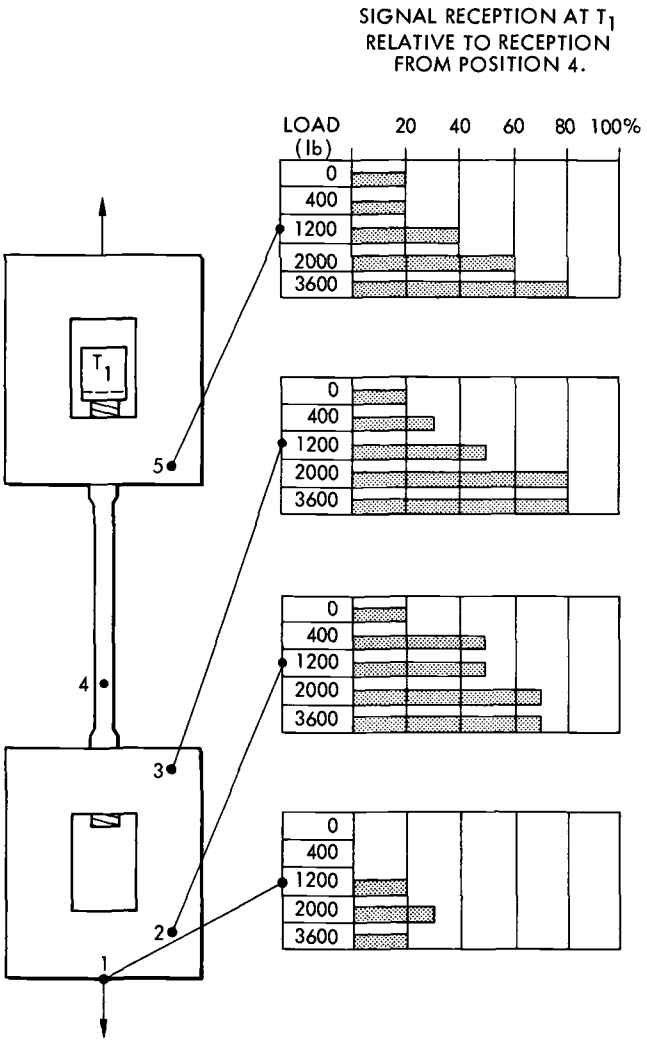

FIG. 5.—*Poor grip design showing low discrimination against extraneous signals.*

desired signals are usually quite small, far below the threshold of hearing. Thus, one must always be suspicious that extraneous noises of many sorts are modifying the desired data.

Electronics

Perhaps the only electronic component in the instrumentation chain that needs detailed discussion is the preamplifier. The signal one must detect is low,

perhaps 10 μV, yet it is easy to obtain a signal output from a crystal transducer of 100 V (for example, by dropping it on a testing machine platen). Thus, the preamplifier input should be protected against burnout from signals of 100-V magnitude. The preamplifier should also be capable of quick recovery from overload. A secondary consideration is that the preamplifier should not be sensitive to wide changes in the impedance across its input terminals. The preamplifier should be separable in space from the rest of the instrumentation. It should act as a line driver at low impedance for the line connected to the remaining instrumentation. A voltage gain of 100 to 1000 is desirable so that signals beyond this stage can be handled without the special precautions necessitated by small signals. Control of gain at this stage is convenient for establishing calibration procedures.

A charge amplifier could be substituted for the voltage amplifier. The charge amplifier could be a practical necessity if some of the piezoelectric elements mentioned were used, although there is little advantage so long as the high capacitance PZT-5 element is used.

A fast cutoff active filter is an invaluable aid in establishing a system passband reasonably well optimized to receive acoustic emission pulses and suppress the small extraneous impulses that could be confused with them. An attenuation rate of at least 24 dB/octave is desirable. Passive filters built into the preamplifier are usually not adequate, since they tend to be of the 6-dB/octave variety.

An electronic counter is typically used to count the acoustic emissions per unit of time, load, strain, or other correlated engineering parameter. The trigger is the critical feature of the counter from an acoustic emission viewpoint. It must have both good stability and good resolution. The trigger level is usually set at twice the electronic noise level of the instrumentation system which immediately precedes it. Every electrical pulse reaching the counter with amplitude above the preset trigger level is registered as one acoustic emission. Thus, a small drift from the preset level can cause an unacceptable amount of electronic noise to be spuriously recorded. Careful checks should be made to ensure that the counter registers only one count for each input voltage excursion above the present level.

Because the number of acoustic emissions per unit of correlated engineering parameter can vary from 0 to perhaps 100,000, an alternative to the electronic counter is a logarithmic amplifier with selectable time constant. Such a device, with perhaps a four-decade span, can produce a satisfactory record.

Data Collection and Display

An almost indispensable tool for acoustic emission work is the cathode ray oscilloscope. It serves as a monitoring tool and displays the amplified signal that is to be presented to the more permanent recording system. A few minutes of

observation of acoustic emission signals on an oscilloscope screen are of more value to a new experimenter in the field than any amount of verbal description of those signals.

A useful tool for displaying the results of an acoustic emission test is an X-Y-Y recorder. This recorder permits plotting of a conventional load-deflection curve, for instance, and superposition of the acoustic emission record by utilizing the second y axis. Such a recording requires an electronic BCD output of the counter, plus a digital-to-analog converter to permit plotting the output of the counter as a voltage. Alternatively, satisfactory records can be made with a multipen time drive recorder if one of the engineering parameters can be correlated with time. Frequently such a chart, drawn while the experiment is in progress, furnishes all the information required to make a useful acoustic emission record.

Experience with the material under test, drawn from acoustic emission records of several specimens of the same material, provides the basis for judging behavior of a material from its acoustic emission characteristics. The quantity of acoustic emission, its onset as a function of stress or strain, the point at which its maximum occurs, or the broadness of the acoustic emission peak are quick measures of the material behavior which can be read immediately from such a chart. An otherwise undetected flaw or crack, subtle changes in metallurgy, handling or processing damage, and sensitivity to special environments can all be detected quickly by properly designed acoustic emission experiments. In addition, specimen testing by acoustic emission can serve to characterize a material so that testing in more complicated geometries can be more precisely interpreted. In many such cases, the x-y-y plot can serve as the final form of test record. It has the advantage that it is simple and economical to acquire.

The acoustic emission data, with conventional engineering data, can be recorded on magnetic tape both for postprocessing and as assurance against recorder breakdown or maladjustment. To record the acoustic emission pulses directly, an instrumentation quality tape recorder equipped with direct record/reproduce electronics is required. It is convenient to include FM electronics to simultaneously record selected conventional engineering parameters. Alternatively, an incremental magnetic tape recorder may be used, and all channels may be digitized, with the acoustic emission information retained from an electronic counter reocrd as described above. This is a convenient means of storing data for post processing by a central computer.

A further step in sophistication can be achieved by replacing the electronic counter with a differential pulse-height analyzer, although there is a difference of opinion as to whether additional test information can be gained by this method [*11,12*]. The usefulness of such records may well depend on the specific material being studied. Other alternatives include utilization of an on-line computer.

At the rate new signal processing and display equipment is being produced, the list of useful techniques cannot be exhaustive. Those mentioned above have all been used successfully in acoustic emission systems, and are therefore of proven utility.

Experimental Configurations

In this section a few experimental configurations will be described with the experiments grouped according to general type. A system diagram will be given that should serve as a generic guide to system configuration and component selection.

All Signal Experiments–Standard Method

The primary goal in the standard experiment is to record all of the acoustic emissions emanating from the test part in such a way that their numbers distribution can be correlated with one or more conventional test parameters.

A schematic diagram of a typical experimental setup, showing the appearance of typical signals at key points in the system, is presented in Fig. 6. The cutins marked (*a*) and (*b*) indicate the appearance of a single event as it might be viewed on an oscilloscope. In addition, (*b*) shows a typical bias level to which the electronic counter might be set. Note that this acoustic emission would register two counts. The system described here weights the higher amplitude acoustic emissions by the bias method. An economical way of assuring one count per acoustic emission has been reported[*13*], although electronic circuitry can be designed for that specific purpose.

A survey instrumentation system can be constructed by replacing all the components beyond the bandpass filter by a cathode ray oscilloscope. While the bandpass filter is not absolutely necessary, it is very convenient, because it can be used to suppress the multitude of low frequency noises that occur in the test laboratory.

A permanent record can be extracted by tape recording the output of the main amplifier. With only FM electronics available, the record could be extracted at the inputs to the X-Y-Y recorder, which could either be retained for a quick look device or be eliminated.

By disabling the reset mechanism on the electronic counter, one can record the summation of all the acoustic emissions during a test. The summation curve is occasionally easier to interpret than the rate curve. Alternatively, a second counter can be added to the instrumentation chain in parallel with the first. It would then be possible to display the summation and rate as functions of a single engineering parameter.

Dunegan[*9*] has shown that the acoustic emission rate curve is nearly symmetrical when plotted against stress rather than strain. In this configuration, predictions of stress at failure can be made most reliably.

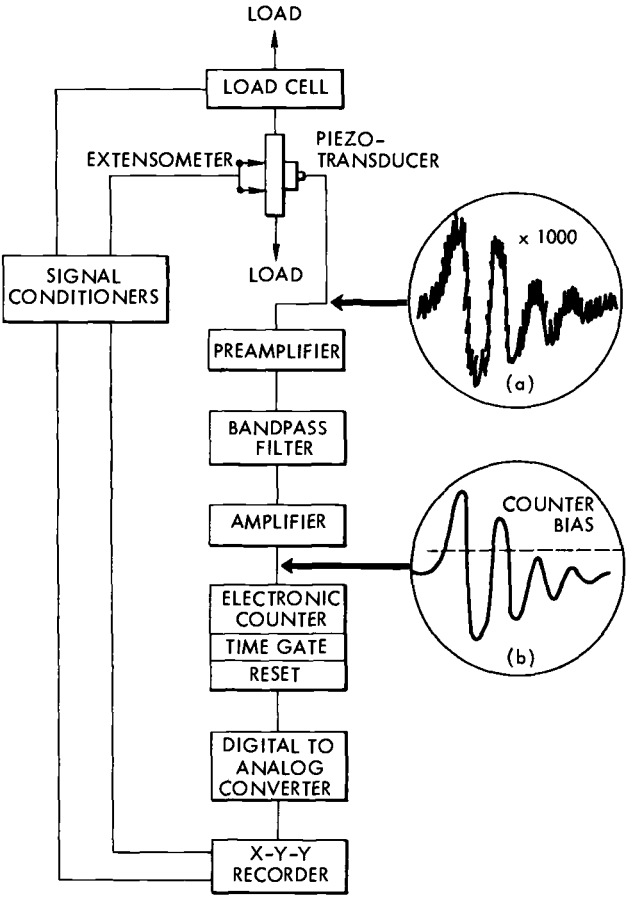

FIG. 6.—*Schematic diagram of an acoustic emission system.*

High Signal Experiments

Acoustic emission techniques may be modified slightly to study crack or flaw growth. That is, they can be used to establish that a specimen is either sound or unsound. (A high signal experiment might also be performed to characterize a material by acoustic emission if a test of a complicated structure made of the test material is to follow.) Under these circumstances, the acoustic emissions emitted by the microstructure (as distinguished from those emitted by a gross flaw) could confuse the record without making a compensating contribution.

Using the equipment in Fig. 6, one may have only to raise the bias on the counter trigger (excluding the weaker microstructure emissions) to achieve a

satisfactory record. Recording either the square of the pulse amplitudes or the integral of the rectified pulse are other techniques that have possible merit.

An Example of Results

The results of a series of test performed with a system similar to that described above are shown in Fig. 7. In this series, six identical tension specimens were fabricated from a single plate of 7075-T6 aluminum. The long axis of each specimen was parallel to the rolling direction of the plate. All specimens were tested under carefully controlled identical conditions. The shaded band in the figure is the full scatter band of all acoustic emission results from five of these specimens. The single curve is the result for the sixth of this set of specimens, and shows highly anomalous results. Visual inspection of the sixth specimen revealed only one unique feature. There was a region of fine slip, covering approximately ¼ in. of the 2-in. cross section. Since this feature was not observed upon inspection of the other specimens, it is probably that a significant material variation was included in the critical section of the subject specimen.

This example shows the ability of the acoustic emission test to reveal in a

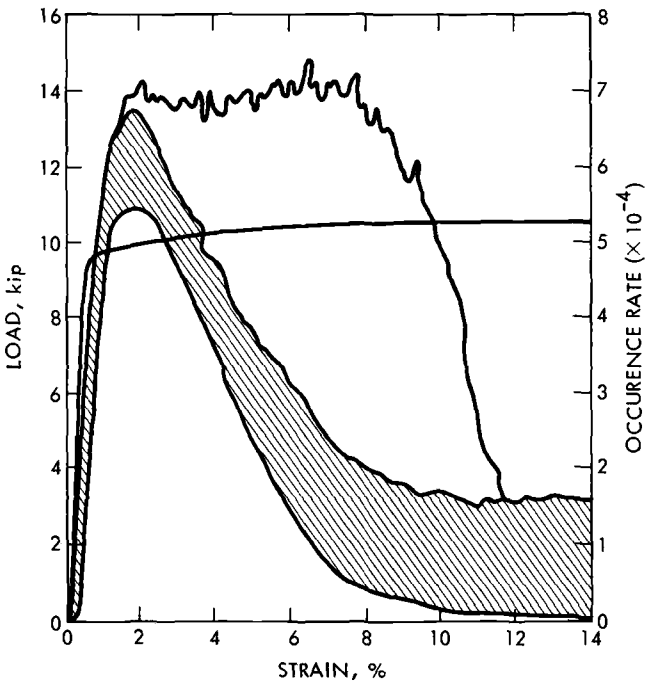

FIG. 7.–*Composite results of a series of acoustic emission tests.*

dramatic manner subtle changes in the microstructure, heat treatment, or composition of a test specimen. It could be a valuable addition to the other tools used in quality assurance testing of materials. The acoustic emission response is intimately connected with the specific microstructure of materials and their intentional or unintentional variations. It could well be a more reliable way of determining quality uniformity than chemical analysis, for instance.

Summary and Conclusions

Acoustic emission testing as it would be performed in a typical laboratory situation has been described. Design of experiments has been discussed with emphasis placed on those aspects that would be most likely to be foreign to those without prior experience with this type of test. An attempt has been made to supply the rationale for the choice of those components and procedures that are most likely to raise controversy. The transient, high frequency nature of acoustic emission sources has been qualitatively discussed and the minimum signal amplitude of such sources has been quantitatively established.

Problems connected with display of the large number of acoustic emission signals encountered in a single test have been discussed as have methods of compacting this information in a way that permits a meaningful interpretation of test results.

While it was not the primary purpose to show large amounts of test data, results of one such test are presented as an example. This example illustrates in a striking way the ability of the acoustic emission test to reveal subtle differences in materials being tested.

Acknowledgments

Thanks are due to A. E. Brown, B. A. Kuhn, and H. A. Appleton for performance of the laboratory work that led to the results reported.

References

[1] Liptai, R. G., Dunegan, H. L., and Tatro, C. A., *International Journal of Non-destructive Testing*, IJNTA, Vol. 1, No. 3, Aug. 1969, p. 213.

[2] Fitzgerald, E. R. in *Particle Waves and Deformation in Crystalline Solids*, Interscience Publishers, New York, 1966.

[3] Liptai, R. G., Harris, D. O., Engle, R. B., and Tatro, C. A., "Acoustic Emission Techniques in Materials Research," Report UCRL-72582, Lawrence Radiation Laboratory, Livermore, Calif., 1970.

[4] Dunegan, H. L., Brown, A. E., and Knauss, P. L., "Piezoelectric Transducers for Acoustic Emission Measurements," Report UCRL-50553, Lawrence Radiation Laboratory, Livermore, Calif., 1968.

[5] Green, A. T., Hartbower, C. E., and Lockman, C. S., "Feasibility Study of Acoustic Depressurization System," Report NAS7-310, Aerojet-General Corp., Sacramento, Calif., 1965.

[6] Mehan, R. L. and Mullin, J. V., *Journal of Composite Materials*, JCOMB, Vol. 5, 1971, p. 266.

[7] Rathbun, D. K., Beattie, A. G., and Hiles, L. A., "Filament Wound Materials Evaluation with Acoustic Emission," Report SCL-DC-70-260, Sandia Laboratories, Livermore, Calif., 1971.

[8] Pollock, A. A., "Acoustic Emission from Solids Undergoing Deformation," Ph.D. thesis, University of London, 1970.

[9] Dunegan, H. L., Harris, D. O., and Tatro, C. A., *Engineering Fracture Mechanics*, EFMEA, Vol. 1, No. 3, 1968, pp. 105-122.

[10] Kroll, R. J. and Tatro, C. A., *Experimental Mechanics*, EXMCA, Vol. 4, No. 5, 1964, pp. 129-134.

[11] Engle, R. B. and Dunegan, H. L. in *Proceedings of Eighth Symposium on Physics and Nondestructive Testing*, Schiller Park, Ill., 1968.

[12] Fisher, R. M. and Lolly, J. S. in *Proceedings of Conference on Deformation of Crystalline Solids*, Ottawa, Canada, 1966.

[13] Tatro, C. A. and Liptai, R. G. in *Proceedings of the Symposium on Physics and Nondestructive Testing*, Southwest Research Institute, San Antonio, Tex., 1962, pp. 145-158.

H. L. Dunegan[1] *and A. T. Green*[1]

Factors Affecting Acoustic Emission Response From Materials

REFERENCE: Dunegan, H. L. and Green, A. T., "Factors Affecting Acoustic Emission Response from Materials," *Acoustic Emission, ASTM STP 505*, American Society for Testing and Materials, 1972, pp. 100-113.

ABSTRACT: This paper presents selected examples of the acoustic emission response from widely differing materials with varied mechanical history, heat treatment, and state of stress. It presents the case that there is a need for characterization of the acoustic emission response of materials prior to application of the techniques for determining structural integrity so that all parameters are represented under similar conditions.

KEY WORDS: acoustic detection, acoustic properties, sound transmission, tension tests, mechanical properties, heat treatment, toughness, cracking (fracturing), stresses, composite materials, strains

There is great variety in the acoustics emissions produced by materials. Some materials produce acoustic emissions copiously when stressed, while others are quiet by comparison. The characteristic response of a material when tested in the form of a smooth tension specimen can differ markedly from that observed from a tension specimen containing a sharp crack. The acoustic emission response from a precracked specimen of low alloy steel tested in thin sections is quite different from the same material tested in thick sections. The basic crystalline structure of a material plays a major role in its acoustic emission response, with signal amplitude level differences of an order of magnitude in some cases. The past history of a material, say, whether or not it has been previously stressed, whether it is in the cast or wrought condition, whether it has a duplex structure or is a composite mixture of different materials, and many other factors will determine the sensitivity of the instrumentation to be used, the optimum strain rate for testing, and the proper interpretation of the data obtained. Selected examples of the acoustic emission response from widely

[1] President and vice-president, respectively, Dunegan Research, Livermore, Calif. 94550.

differing materials with varied mechanical history, heat treatment, and state of stress are presented in this paper.

General Factors

Other papers in this series have discussed the two major types of acoustic emission, continuous and burst type. The continuous designation is normally applied to the low level, high signal density emission observed during tension tests of unflawed specimens. In this type of test a peak in the acoustic emission rate occurs near the yield stress of the material. The data shown in Fig. 1 were obtained from a mild steel specimen and show the peak acoustic emission rate occurring at the yield stress of the material. This continuous emission is strain rate sensitive and under conditions of slow strain rates can disappear completely in some materials. A 533 pressure vessel steel is one material that exhibits this strain rate effect. Recent tests[*1*] on this material at low crosshead rates resulted in no continuous emission at yield. Burst-type emission was observed prior to yield, but during the early stages of yielding these signals disappeared.

Fracture specimens of the same material containing fatigue cracks were tested and yielded primarily burst-type emissions as the plastic zone formed at the

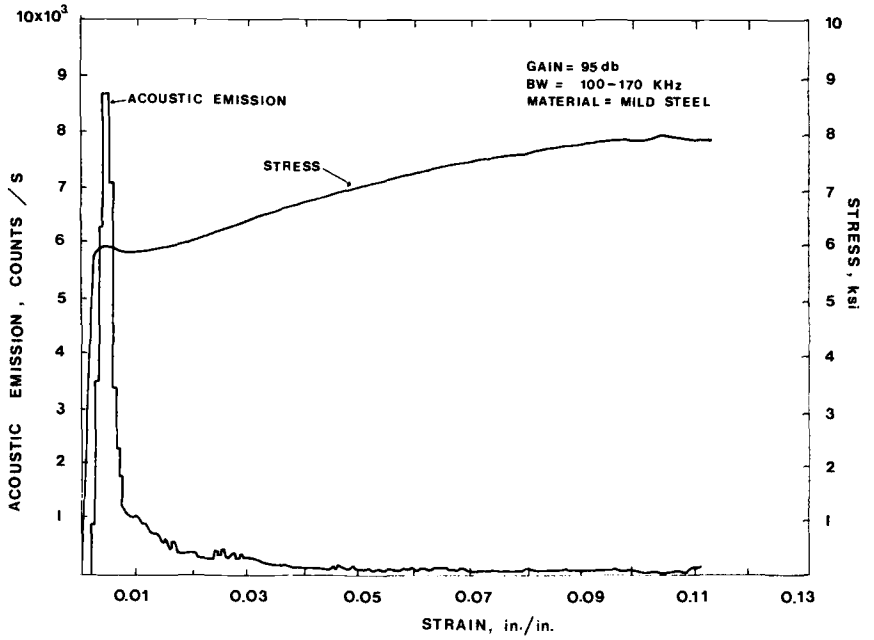

FIG. 1—*Acoustic emission and stress as a function of strain for a mild steel tension specimen.*

fatigue crack tip. No continuous-type emission was observed. The presence of burst-type emissions, due to the growth of a plastic zone at the crack tip, may be explained by the higher effective strain rate in the region near the crack tip and the large stress gradients that occur in this region. In many cases in which high strength materials exhibit sharp fatigue cracks, it is difficult to distinguish between the signals due to growth of the plastic zone and those due to small increments of crack extension since both appear to grow in jumps and steps.

Thickness effects also influence the amplitude of the burst-type emissions from specimens containing sharp cracks. No extensive study has been made yet on the exact nature of the primary causes of this effect, but in recent experiments some noticeable differences were observed between the amplitude of the signals received from 1-in.-thick and 1½-in.-thick through crack, compact tension specimens of A 533 pressure vessel steel. Higher amplitude acoustic emission signals were obtained from the thicker specimen. Some possible causes for the different behavior are (1) the crack front in the thicker specimen was exposed to more material simply because of its greater thickness, thus the probability of exposure to nonmetallic inclusions near the crack front was much higher; (2) the triaxial stresses in the vicinity of the crack front also were higher in the thicker specimen, which could lead to a greater likelihood of cleavage-type failure and plane strain instabilities near the center of the specimen. The second is the more logical explanation for the higher amplitude signals as a thicker specimen is pulled to failure.

A much more extensive investigation is required before the full scientific description of this effect can be determined. The primary purpose in presenting these preliminary data is to point out that extrapolation of thin section acoustic emission data to determine thick section response is probably no more accurate than extrapolation of thin section (plane stress) fracture toughness data to thick section (plane strain) toughness.

Another factor that can strongly influence the amplitude of acoustic emission from materials is the basic crystalline structure of the material. One can usually estimate whether the material will be "noisy" or "quiet" from its crystalline structure. In general, the more anisotropic the crystalline structure, the higher the amplitude of the acoustic emission signals. Thus, materials such as tin, uranium, and beryllium usually result in higher amplitude signals in comparison to face centered cubic (fcc) materials which are more isotropic and do not twin and body centered cubic (bcc) structures above temperatures at which twinning will occur.

Figure 2 shows acoustic emission as a function of strain for a cast uranium smooth tension specimen. Note that the instrumentation gain required for recording these data was only 60 dB, compared to 95 dB required for obtaining equivalent acoustic emission rates on the mild steel specimen previously shown in Fig. 1. These two examples illustrate the extremes in sensitivity required for

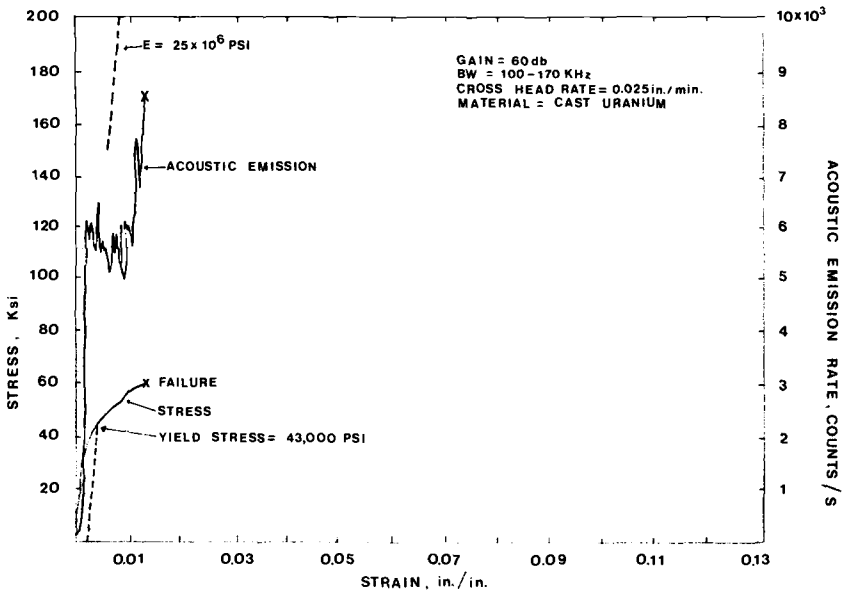

FIG. 2—*Acoustic emission rate and stress as a function of strain for a cast uranium tension specimen.*

acoustic emission detection, with most other materials falling somewhere in between these amplification values.

Specific Factors

Homogeneity

The presence or lack of homogeneity can dramatically affect the acoustic emission response of a material. The presence of inclusions, a second phase, or combinations of different material which make up a composite structure will result in an entirely different response from that of the major component alone.

Concrete is an example of a widely used composite material containing a brittle matrix and comparatively ductile and high modulus reinforcing members. The permanent deformation mode of this material is primarily cracking of the matrix material, which gives rise to acoustic emission signals of higher amplitude[*2*] than are found in most metals. Another example of a comparatively new material which contains a ductile, low ductile material is the graphite/epoxy composite. An example of the acoustic emission response obtained from a tension specimen of this material is shown in Fig. 3. Note that the instrumentation gain used to record these data is lower by more than one order of magnitude than that used on the mild steel specimen shown previously.

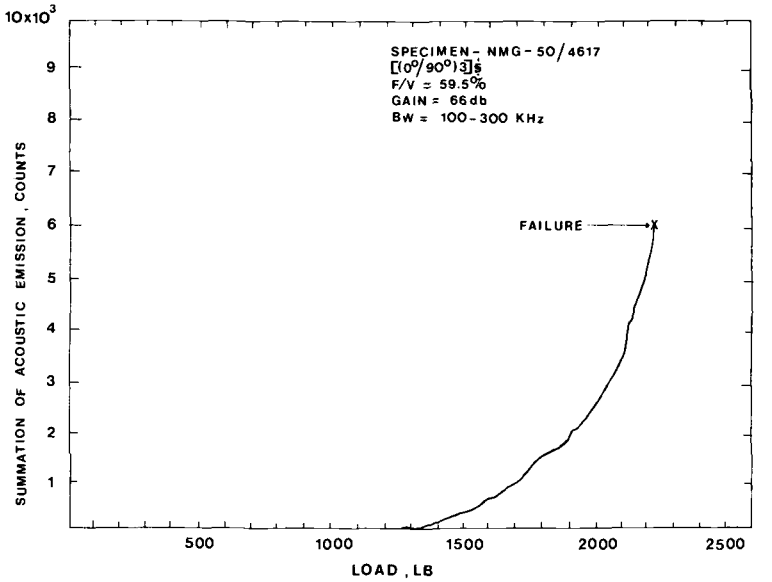

FIG. 3—*Summation of acoustic emission as a function of load for graphite/epoxy specimen pulled in tension.*

The discrimination level on the counter used to record these data was set to record only the higher amplitude signals caused primarily by filament fracture. Lower level signals due to matrix shear were present at loads below the values shown and could have been recorded easily. It has been observed in many different combinations of composite materials with a lower modulus matrix that acoustic emission due to filament fracture begins at approximately 50 percent of the failure load; a peak in the emission rate occurs at some point in the stress history (this point can be affected by material composition and filament orientation), and a rising rate of emission occurs prior to failure. The data previously shown in Fig. 3 show a small peak in the count rate occurring at 1800 lb of load (inflection point in the summation of acoustic emission counts) and an increase in counts per unit load (increasing slope) prior to failure.

There are three primary features of the deformation of composites that can be distinguished by acoustic emission techniques[3]: (1) matrix-filament shear deformation and crazing, (2) filament fracture, and (3) delamination between layers of the filaments. These are deformations which are difficult if not impossible to distinguish in any other way.

Composites have acoustic emission characteristics similar in some ways to those of metals. For one, they exhibit irreversibility in the same manner as metals and, thus, lend themselves to techniques for detecting degradation due to

cyclic loading or environmental effects based on a periodic overstress [4,5], second, the summation acoustic emission as a function of stress follows a form of

$$\Sigma N = AK^m \tag{1}$$

where

ΣN = total cumulative acoustic emission measured during test,
A = proportionality constant,
K = applied stress intensity, and
m = empirically derived exponent,

similar to that exhibited by metals containing flaws; and, third, many of these materials exhibit creep type time dependent effects, which make them excellent candidates for nondestructive acoustic emission techniques based on periodically tuning in on these structures while they are under load to determine if degradation is occurring.

Material History

The history of the material can play an important role in variation in acoustic emission response. Aside from the Kaiser effect described in another section, mechanical working, stress relief, heat treatment, and other processes in the material's history should be considered in any thorough investigation. As-cast materials, for example, usually have large grain size, low dislocation density, and random orientation of the crystalline structure. These conditions are the most conducive for promotion of large amplitude acoustic emission signals when the material is stressed. If along with these conditions a high crystalline anisotropy exists, slight instrumentation amplification is needed for recording these signals. This condition was present in the tests conducted on the cast uranium; the data are shown in Fig. 2.

If the material conditions are changed in any way, for instance by radiation damage, heat treatment, or mechanical processing, the acoustic emission response also changes, in many cases drastically. Figure 4 shows the acoustic emission rate as a function of strain on a depleted uranium tension specimen that has been subjected to cross rolling and then annealed. In comparison to the cast material (Fig. 2), we see that an increase of better than one order of magnitude in instrumentation gain was required with this specimen to achieve similar rates. The combination of texture, grain refinement, and other factors due to the cross rolling and heat treatment led to different mechanical and acoustic emission characteristics.

Thus, an important factor to consider when applying acoustic emission techniques to welded structures is that the acoustic emission properties of the

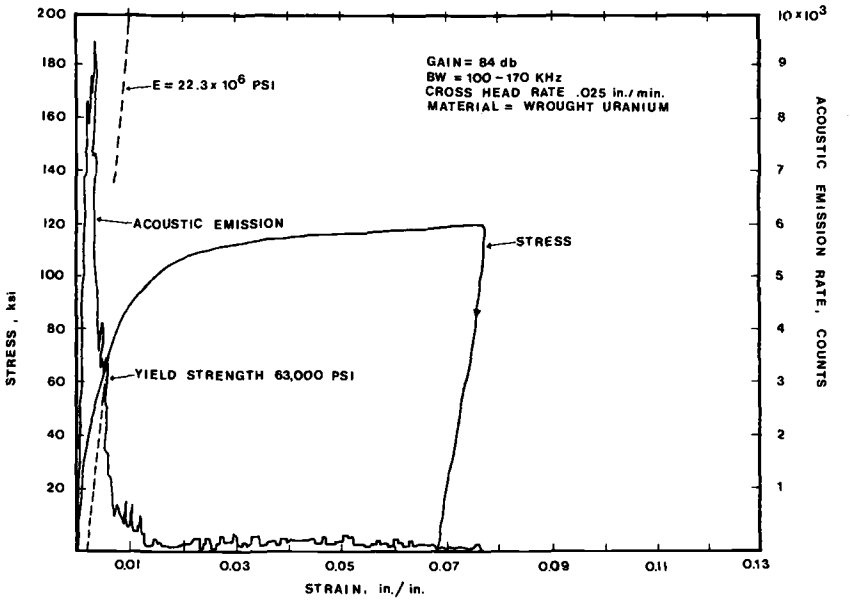

FIG. 4—*Acoustic emission rate and stress as a function of strain for a wrought uranium tension specimen that has been subjected to cross rolling and then annealed.*

weld metal and heat effected zone should be studied in the laboatory prior to testing of the structure. In most cases the base material is wrought and therefore will have different acoustic emission characteristics than the weld material.

Yield Strength

The effect of yield strength on acoustic emission response has been shown by Green et al[*6*], to vary considerably when based upon acoustic emission data recorded from 6A1-4V-Ti of standard and extra low interstitial (ELI) grade and from different heat treatment conditions of D6aC steel (both materials of 0.1-in. thickness). The data are shown in Fig. 5, with the higher strength material showing a marked increase in signal amplitude. These specimens were tested at a constant stress rate and instrumentation gain.

Although a thorough study has not been made, a few other acoustic emission researchers have also reported differences in the acoustic emission response of materials as their yield strength is varied. For example, Parry[*7*] reported that a significant increase in the acoustic emission amplitude occurred when a pressure vessel material was irradiated. Recent work by Ireland et al[*1*] on A 533 pressure vessel steel tested at cryogenic and ambient temperatures in the irradiated and unirradiated conditions also confirmed that the amplitude of the acoustic emission signals increased at the lower temperatures over that at room

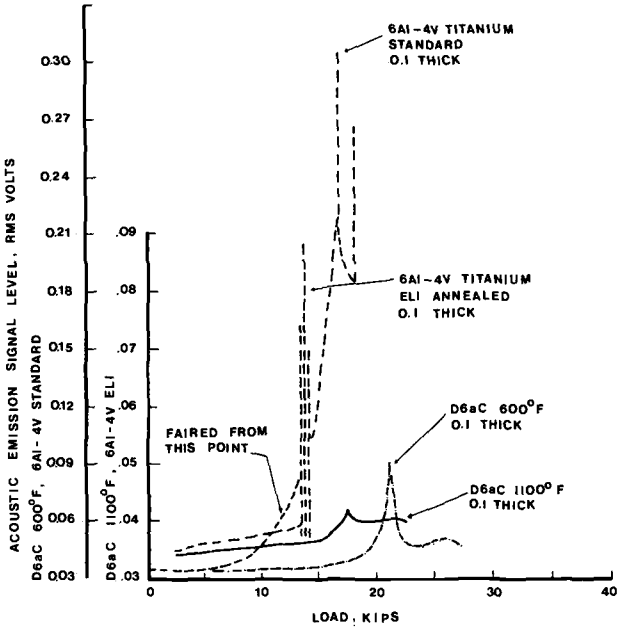

FIG. 5—*Acoustic emission signal level for 0.1-in.-thick smooth tension specimens.*

temperature while the irradiated material was noisier at all temperatures than the unirradiated material. Both irradiation and cryogenic temperatures will increase the yield strength of mild steel. Nevertheless, it is plausible that it is not the increase in yield strength, but some other effect such as a change from ductile to cleavage fracture that is causing the increase in the amplitude of the signals at cryogenic temperatures.

A series of tension specimens of 4340 steel were tested under different heat treatment conditions to clarify this effect further. These data are shown in Fig. 6. The summation of acoustic emission is shown as a function of stress. The inflection point in the curves corresponds to the peak acoustic emission rate and occurs at the yield stress of the material. Note that the highest yield strength material produced a larger number of total counts. These specimens were identical in size and all were tested at the same crosshead rate and instrumentation gain. Precracked fracture sprecimens of this material also will give larger amplitude signals in the higher yield strength condition.

Strain Rate

Continuous acoustic emission associated with plastic deformation of materials is strain rate sensitive. This was mentioned previously in connection with experimental data obtained from A 533 pressure vessel steel. Normally materials

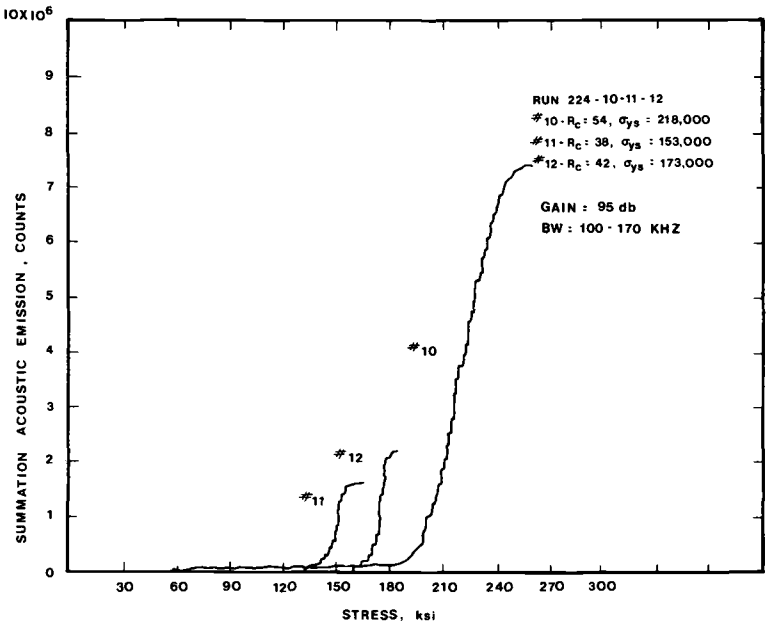

FIG. 6– *Summation of acoustic emission as a function of stress for three 4340 steel tension specimens heat treated to varying yield strengths.*

of this type also show strain rate sensitivity in their stress-strain properties. Therefore, it was difficult to directly evaluate the acoustic emission effects independent of the change in material properties. Type 7075-T6 aluminum was chosen as a material to continue these studies because this aluminum alloy has been shown to have material properties, namely, yield strength and ultimate strength, which are independent of the strain rate over a wide range. Tension specimens were prepared and, while being pulled to failure over three different crosshead rates (0.02, 0.05, and 0.10 in./min), the acoustic emission rate was recorded and a summation made of acoustic emission counts as a function of strain.

Figure 7 shows the acoustic emission rate from three specimens at the different crosshead velocities. Some of the large signals below 1 percent strain in Fig. 7 are due to noise from the pin loaded area. Normally specimens of this type are preloaded in the pin region to a value above the ultimate load in the gage section to eliminate the acoustic emission from the pin area. This was not done in this series of experiments because the primary information sought was the acoustic emission response in the plastic region where no pin noise is observed. Figure 8 shows the same data on a four-decade log plot obtained from a digital logarithmic converter which compresses the curves. The tail on the

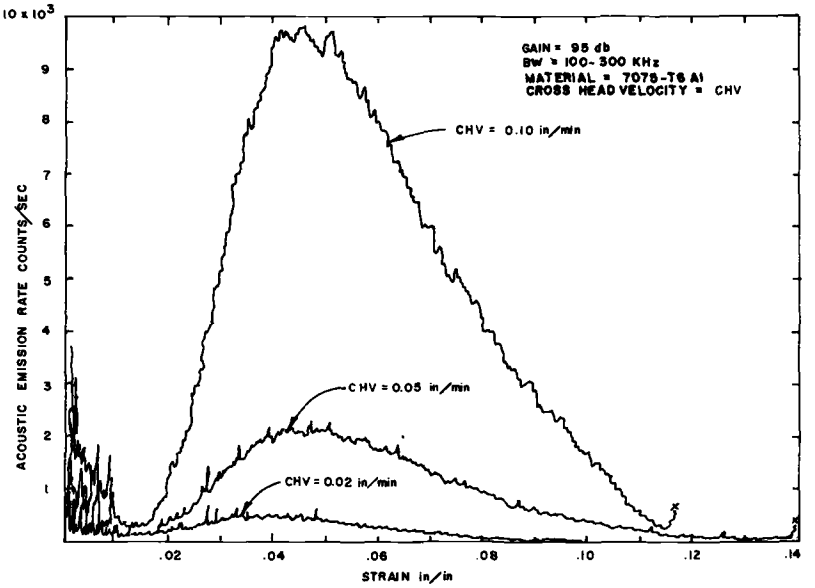

FIG. 7—*Acoustic emission rate from 7075-T6 aluminum tension specimens as a function of strain for three different crosshead velocities.*

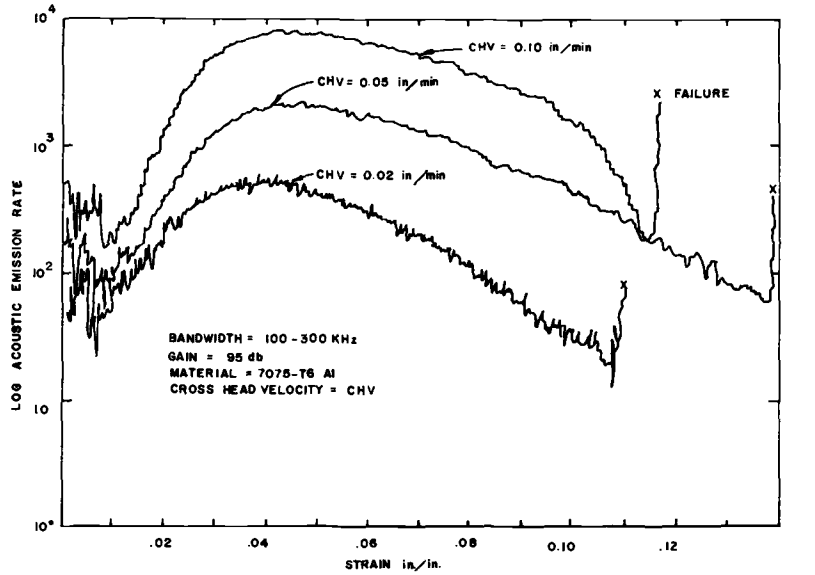

FIG. 8—*Log of the acoustic emission rate from 7075-T6 aluminum tension specimens as a function of strain for three different crosshead velocities.*

curves prior to failure is due to the formation of microcracks in the reduced section. A test can easily be terminated just prior to failure by observing when this increased rate begins. Note that these precursor signals are much more pronounced on the log plot than on the linear plot in Fig. 7.

Figure 9 shows the summation of acoustic emission signals as a function of strain for the same three specimens. A previous report[8] presented a model for the acoustic emission associated with the formation of a plastic zone at a crack tip. The relationship developed is expressed by

$$V_p = B \sum N \tag{2}$$

where

V_p = volume of plastically deformed material,
B = proportionality constant, and
ΣN = total cumulative acoustic emission measured during test.

This model was developed on the basis of constant strain rate test data that showed a direct correlation of the plastic volume with the total number of counts. Therefore, the derivative with respect to time would show a direct correlation between strain rate and acoustic emission rate. From this one would expect to see the changes in the peak rate in Figs. 7 and 8 at different crosshead

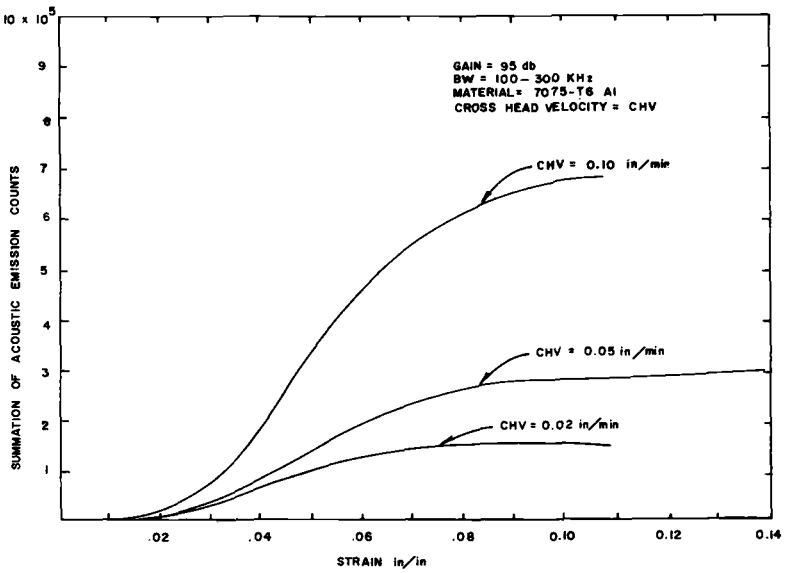

FIG. 9—*Summation of acoustic emission from 7075-T6 aluminum tension specimens as a function of strain at three different crosshead rates.*

velocities, and the total number of counts in Fig. 9 should be identical if no rate effects are present because all of the specimens are identical. It is obvious from the data in Fig. 9 that the curves are not identical but are strongly influenced by the strain rate.

This behavior due to strain rate helps to explain the differences in the exponent m relating the total number of counts to the stress intensity factor at a crack tip (Eq 1, $\Sigma N = AK^m$). The strain rate in the plastic zone of a cracked specimen will be strongly influenced by the geometry, size of the crack, and the loading rate. Further investigations are continuing on determining rate effects from specimens containing cracks. This information is necessary before proper interpretation of continuous acoustic emission monitoring of long term tests can be made.

Phase Transformations

Martensitic phase transformations have been found to be particularly active sources of acoustic emission[9], also some transformations due to temperature changes have been studied. Strain induced martensitic transformations are copious emitters, and acoustic emission techniques appear promising for the study of such transformations. Figure 10 presents the results of two tension tests performed on a wrought copper alloy in which minor composition adjustments result in varying amounts of martensitic transformations at varying strain

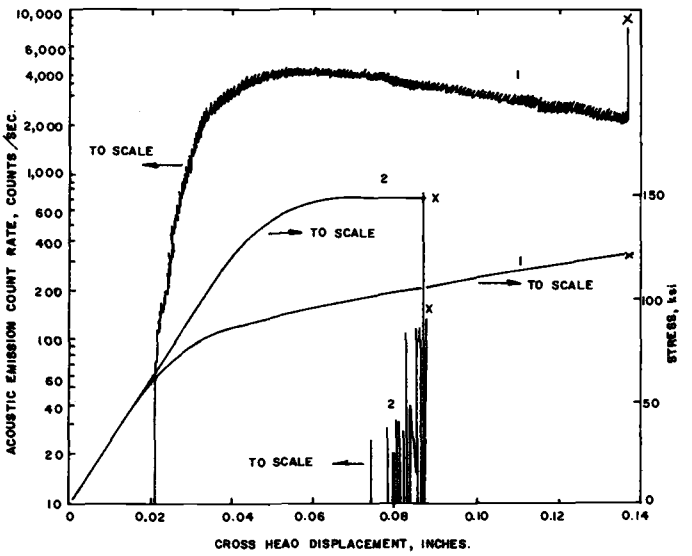

FIG. 10—*Acoustic emission rate and stress versus crosshead displacement for tension tests performed on a wrought copper alloy exhibiting various amounts of a strain induced martensite phase transformation.*

levels[*10*]. These tests were performed on specimens with a 1-in. gage length, at a gain of 80 dB and bandpass of 100-300 kHz.

Specimen 1 is observed to be a very active emitter, with the emission beginning at about the proportional limit, and continuing until final failure. Subsequent metallographic observation of the specimen showed that the martensitic transformation had occurred throughout the gage length of the specimen. Specimen 2 is observed to be a sporadic emitter, with acoustic emission being observed only just before final failure. Subsequent metallographic observation of this specimen revealed that the transformation was restricted to the locale of the fracture surface of the specimen. Thus, it is seen that the extent of the strain induced transformation correlates very well with the observed emission patterns. The relatively low gain (80 dB) used in these tests precludes the possibility of monitoring the emission due to plastic deformation, thus only the activity due to the "noisy" phase transformation was detected in these tests.

Summary

Table 1 presents a summary of the factors which can influence the detectability of the acoustic emission signals. This paper has not attempted to present data discussing each of these but only to alert the reader to the variety of factors which can cause considerable variation in acoustic emission data gathered from supposedly similar tests. Knowledgeable use of acoustic emission data towards practical nondestructive testing for structural integrity surveillance requires acoustic emission characterization.

For example, the very high amplification required to detect plastic deformation during smooth tension specimen tests under laboratory conditions may completely preclude accomplishing this same objective under in-field

TABLE 1–*Factors that influence acoustic emission detectability.*

Factors Resulting in Higher Amplitude Signals	Factors Resulting in Lower Amplitude Signals
High strength	Low strength
High strain rate	Low strain rate
Anisotropy	Isotropy
Nonhomogeneity	Homogeneity
Thick section	Thin section
Twinning materials	Nontwinning materials
Cleavage fracture	Shear deformation
Low temperatures	High temperatures
Flawed material	Unflawed material
Martensitic phase transformations	Diffusion controlled transformations
Crack propagation	Plastic deformation
Cast structure	Wrought structure
Large grain size	Small grain size

conditions. Similarly, acoustic emission systems for in-field structural monitoring in which sensor spacing has been based upon typical acoustic emission amplitudes from low strength material at room temperature might be uneconomical, whereas if the structure is to be used, or tested, at a low temperature the higher amplitude emissions will allow greater sensor spacing and more economy of application.

The claim that acoustic emission data can be used to avert catastrophic failure of any structure must be made with many reservations unless the acoustic emission data are taken and analyzed under conditions similar to those to which the structure would be exposed, and the relationship between acoustic emissions and the failure process has been clearly established.

References

[1] Ireland, D. R., Wullert, R. A., and Scotti, V. G., "Connecticut Yankee Reactor Vessel Radiation Surveillance Program," Battelle-Columbus Laboratory, to be published.

[2] Green, A. T., "Stress Wave Emission and Fracture of Pre-Stressed Concrete Reactor Vessel Materials," report for Oak Ridge National Laboratory, Sub-Contract 3118, Contract W-7405-eng-26, June 1969.

[3] Green, A. T. and Lockman, C. S., "Accelerometer Techniques as Applied on Polaris First Stage A3 Production Chamber Hydrotests," Aerojet General Corporation Report 75-466, July 1964.

[4] Dunegan, H. L., Harris, D. O., and Tetelman, A. S., *Materials Evaluation Journal*, MAEVA, Vol. 28, No. 10, Oct. 1970, pp. 221-227.

[5] Harris, D. O., Dunegan, H. L., and Tetelman, A. S., "Detection of Fatigue Lifetime by Combined Fracture Mechanics and Acoustic Emission Techniques," Air Force Conference on Fatigue and Fracture of Aircraft Structures and Material, Miami Beach, Fla., 15-18 Dec. 1969.

[6] Green, A. T. and Hartbower, C. E., "Development of a Nondestructive Testing Technique to Determine Flaw Criticality," Advanced Research Projects Agency Order 1244, Program Code 8D10, Contract K33615-68-C-1705, May 1970.

[7] Parry, D. L., "Nondestructive Flaw Detection in Nuclear Power Installations," USAEC Report, Conference Proceedings, Incipient Failure Diagnosis for Assuring Safety and Availability of Nuclear Power Plants, Gatlinburg, Tenn., Nov. 1967.

[8] Dunegan, H. L., Harris, D. O., Tatro, C. A., *Journal of Engineering Fracture Mechanics*, EFMEA, Vol. 1, No. 1, June 1968.

[9] Liptai, R. G., Dunegan, H. L., Tatro, C. A., *International Journal of Nondestructive Testing*, IJNTA, Vol. 1, No. 3, Oct. 1969.

[0] Private communication with D. Weinstein, Stanford Research Institute, Menlo Park, Calif.

P. H. Hutton[1]

Acoustic Emission Applied Outside of the Laboratory

REFERENCE: Hutton, P. H., "Acoustic Emission Applied Outside of the Laboratory," *Acoustic Emission, ASTM STP 505,* American Society for Testing and Materials, 1972, pp. 114-128.

ABSTRACT: The paper presents a cross section of beneficial applications which illustrate the wide variety of present day uses of acoustic emission surveillance. These uses range from detection of flaws in pressure vessels during hydrostatic testing to inspection of building floors for detecting weak points, detection of impending failure in localized segments of rock structure in mining, and process control in metal forming work. While these examples are not all inclusive, they do show that acoustic emission is not just a laboratory novelty and that beneficial use of the phenomenon is beginning to be realized.

KEY WORDS: acoustics, emission, nondestructive tests, construction, hydrostatic tests, triangulation, acoustic detection, weld defects, laminated wood, prestressing, ceramics, mines (excavations), gas caps, metal drawing

Acoustic emission has received considerable attention in recent years as a potential tool for integrity monitoring. The phenomenon involves elastic waves propagated through a solid by energy released when the solid plastically deforms or fractures. It was first recognized in this context in the late 1940s and the early 1950s and, since then, has been the focal point of increasing investigation world wide for potential application as a nondestructive test (NDT) technique for evaluating structural integrity. One major question being asked by practical minded scientists is will it ever progress beyond the point of being an interesting laboratory toy? The answer to this question is, Yes, it already has.

Acoustic emission analysis is a new nondestructive test tool with the phenomenon of propagating elastic waves, which are generated by energy released during deformation and fracture in a solid. Motivation for developing acoustic emission technology came from its unique surveillance features and the

[1]Senior development engineer, Nondestructive Testing Section, Battelle-Northwest, Richland, Wash.

acknowledged fact that the standard nondestructive test techniques utilized in industry today are costly, time consuming, and sometimes inapplicable or incomplete. Efficient and sophisticated use of structural materials requires more discerning and reliable techniques for assessing structural integrity.

The technique of detecting the deformation and fracture of solids by monitoring the attendant acoustic emission is still relatively in its infancy; however, it has already achieved a variety of applications dealing with structural integrity determination. These applications range from detecting flaws in pressure vessels during hydrostatic testing to surveillance of buildings and earth structures to detect incipient structural failure.

System Principles and Concepts

To be fully useful as a nondestructive test tool, an acoustic emission monitor system should have the capability to

(1) Detect and locate the origin of acoustic signals from any point in the structure under test

(2) Exclude typical field and inplant electrical and mechanical noise interference

(3) Distinguish between insignificant and significant flaws, and other pertinent sources of acoustic information such as leaks

(4) Function on structures with complicating features such as vessels with nozzles and other penetrating fixtures, stainless steel cladding, internal structures, large wall thickness, and inaccessibility to some parts of the structure

(5) Produce continuous records suitable for comparison with records from future inspections

(6) Display and reduce data for timely interpretation

Although all of the above desired functions have not been realized yet, particularly item 3, flaw evaluation, there are many useful systems available now. These systems consist mainly of a detection section, a parametric analyzer, and a source location analyzer. The detection section is made up of high sensitivity piezoelectric sensors, low noise amplifiers capable of providing gains up to 10^5 to 10^6, and sharp rolloff filters to eliminate unwanted noise. The parametric analyzer provides a measure of the acoustic emission signal density in terms of rate of emission per unit time, or a running total of the number of signals or both. An approximation of the area under the signal envelope is also used as a measurement parameter in some cases. This information is usually printed out on a strip chart recorder, and provides an indication of flaw severity or rate of flaw growth. As the name implies, the source location analyzer produces information on the location of the emission source(s) and, hence, the flaw. Basically, this is accomplished with an analyzer which measures the difference in time of signal arrival at two to four sensors in the vicinity of maximum emission

activity. This information goes to a small computer which determines the source coordinates corresponding to the relative signal travel times. The resulting information is usually presented on a printer tape or a visual display or both.

Thirty or more detection channels may be required to monitor a structure such as a large pressure vessel. Parametric information concerning, for example, emission rate is used to select significant channels for source location analysis. Figure 1 shows in schematic form one type of monitor system currently in use for activities such as monitoring hydrostatic testing of pressure vessels and pipe lines. A somewhat different system, shown in Fig. 2, is presently used for laboratory study work with structural materials, weld quality monitoring, fatigue test surveillance, etc.

Since the acoustic emission signal is basically pulse transient in nature, a wide range of selected monitoring frequencies is available for acoustic emission detection. In practice, this range extends from about 50 kHz to 2 MHz. Choice of monitoring frequency for a given application resolves itself to a trade-off between minimizing lower frequency noise interference and minimizing emission signal attenuation which becomes more pronounced with increasing frequency.

Application Examples

The brief background given above will enable discussion of some of the applications of acoustic emission technology to the study and investigation of

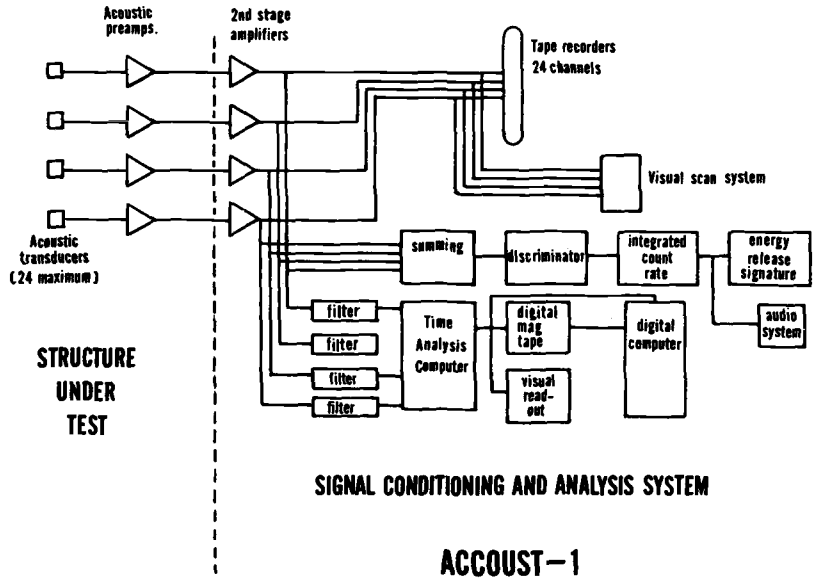

FIG. 1—*Block diagram, Acoust-I acoustic analysis system.*

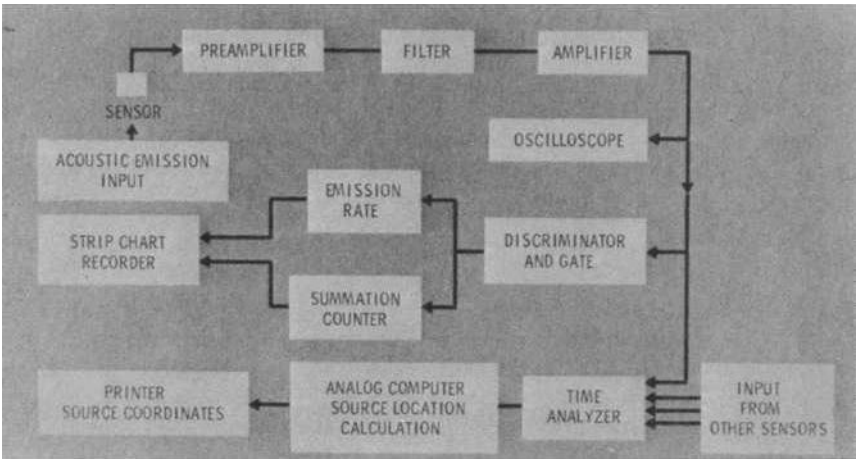

FIG. 2—*Block diagram, acoustic emission monitor system.*

structures. The discussion will not attempt to present a complete account of all applications but, rather, a representative cross section. The applications cited involve work done with a variety of monitoring systems including the ones described earlier.

One of the earliest engineering applications of acoustic emission occurred in 1963[*1*], namely, monitoring the integrity of fiberglass rocket chambers during hydrotest. Analysis of the emission recordings made while hydrotesting these chambers indicated that acoustic energy is released in a random manner. Furthermore, by using amplitude and frequency analysis, it was possible to distinguish the mode of structural failure, that is, filament breakage or bond and interlaminar shear failures. It was concluded that a summation of the acoustic energy released could be related to the strength of the chamber after the proof hydrotest. This relationship was established on the basis of emission data from the first 50 percent of the proof hydrotest pressure cycle and offered the possibility of reducing the peak hydrotest pressure, while still verifying the structural integrity of a motor case.

The use of triangulation techniques to locate the source of the acoustic emission and, hence, the flaw area was also employed. Triangulation is a method used in seismic studies to locate the origin of earthquakes. Three or more sensors are located at different distances and angles from the source; analysis of signal arrival times allows calculation of the source location if the wave propagation velocity is known. For most acoustic emission applications, the accuracy of determining source location by this method is limited by the resolution of time difference measurements and by the definition of propagation velocity.

Nondestructive testing of metallic structures is, however, the most predominant field for acoustic analysis at this time mainly because of the disastrous potential consequences associated with the failure of pressure vessels and piping, specifically in the chemical, oil, and nuclear power industries. Field application has shown that acoustic analysis techniques can detect and accurately locate flaws in a structure that may cause eventual failure of the structure and also assess the degree of embrittlement of metal structures[2]. Figure 3 shows the

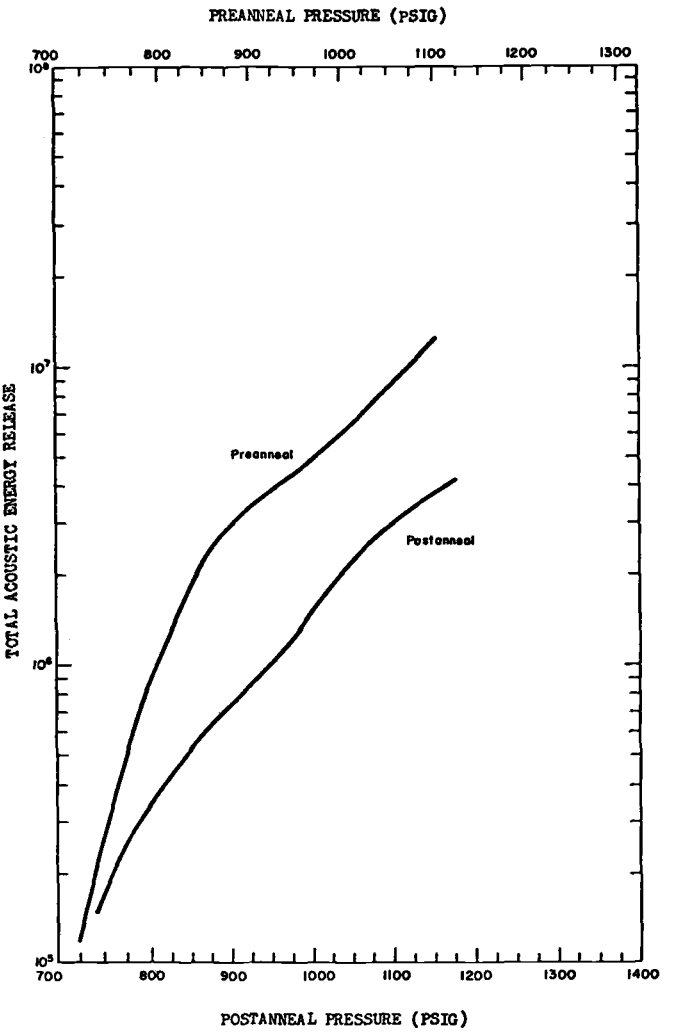

FIG. 3–*Acoustic energy related to pressure vessel annealing.*

results of two acoustic signatures taken on a large vessel which had become embrittled[2]. The signatures were obtained during vessel stressing before and after annealing. They indicated that the vessel embrittlement shifted by a factor of 4.2 during annealing. This shift in acoustic energy release due to a decrease in embrittlement corresponded to within less than 10 percent with the reduction in embrittlement value obtained by metallurgical analysis.

Table 1 is a partial listing of the flaws acoustically identified during testing of a large chemical pressure vessel[2] similar to that shown in Fig. 4. Even though all flaws shown in this table proved to be insignificant to the integrity of the vessel, during the test, they were mapped and confirmed by independent NDT technology. The types of flaws mapped during this test (insignificant to the structural integrity) generally produced a constant energy release signature as shown in Fig 5. Significant flaws, or those that will effect structural integrity, generally produce acoustic energy release signatures similar to that shown in Fig. 6. These signatures, coupled with the rate of accumulation of triangulation coordinate data, allow some interpretation of the significance of detected structural flaws. The accuracy of flaw location in this test was within one wall thickness of the structure undergoing test.

Surveillance of welds to detect flaw formation is an application of acoustic

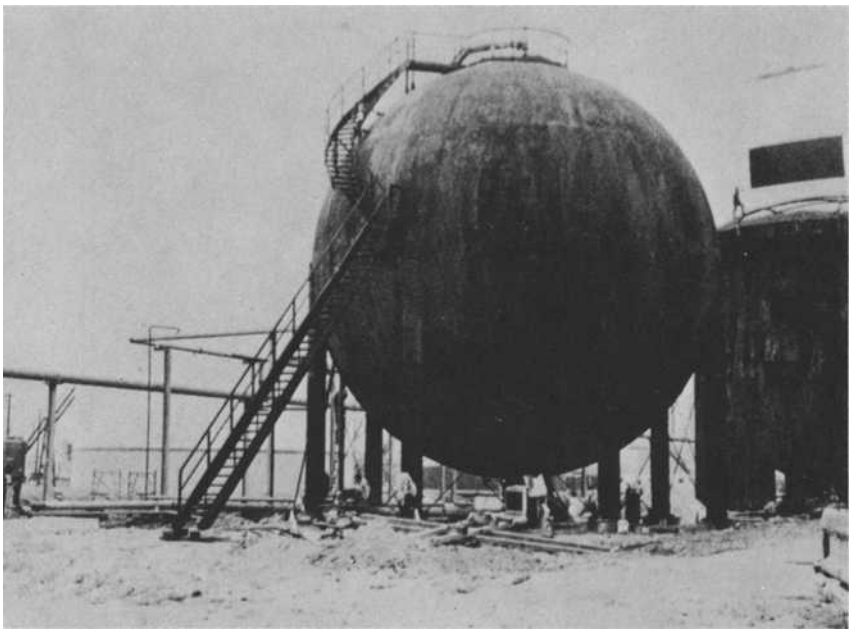

FIG. 4—*Typical pressure vessel monitored for acoustic emission during hydrostatic testing.*

TABLE 1—*Data Summation For Acoustic Source Locations on Industrial Pressure Vessel (16 ft–diameter, 120 ft long).*

Acoustic Emission Source	Verification by Conventional NDT Methods								
	Ultrasonic Check								
	Longitudinal		Transversal		X-ray Check				
	Check	Sensitivity	Check	Sensitivity	Plate Number	Check	Size, mm	Visual and Dye Check	Description
1	Yes	ASME + 10 dB ASME + 16 dB	Yes	ASME + 10 dB 40% ASME + 10 dB	19–20 20–21	Yes	1	No	Weld seam porosity void
2	Yes	20% ASME + 10 dB	Yes	50% ASME + 4 dB	18–19 19–20	Yes	1	No	Weld seam porosity void
3	Yes	100%	Yes	40%	20–21	Yes	1	No	Weld seam porosity void
4	No		No			No	25.4	Yes	Internal structure weld crack
5	No		No			No	25.4	Yes	Internal structure weld crack
6	No		No		33–34 34–35	No		No	Weld seam, but no confirmation
7	Not checked with other nondestructive test techniques								
8	Yes		Yes	ASME + 10 dB 50%	2–3 4–5	Yes	1	No	Weld seam porosity void
9	Yes		Yes	ASME 60%	1–2, 2–3 3–4	Yes	1 to 2	No	Weld seam porosity void

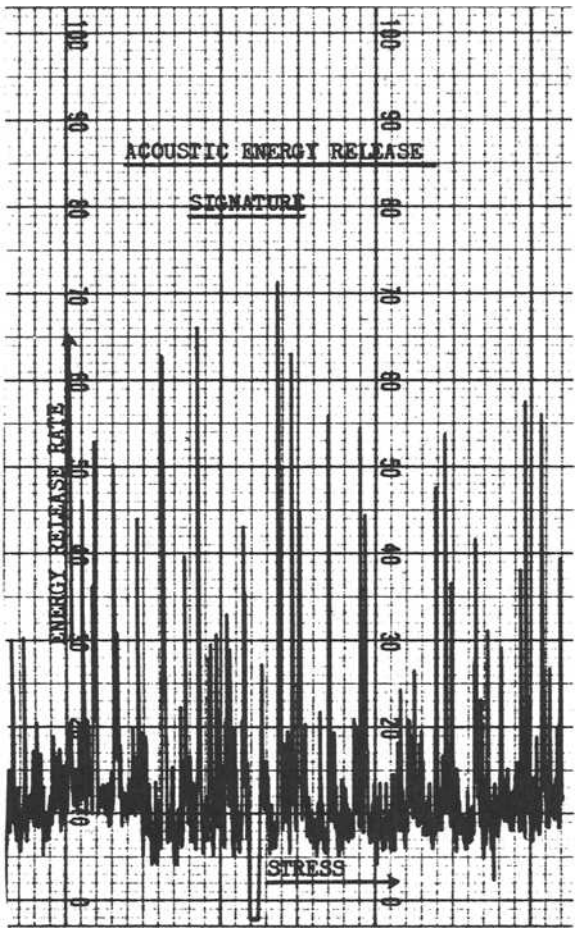

FIG. 5—*Energy release signature for minor flaws.*

emission that is particularly significant for fabrications using heavy section steel requiring multipass welds. It has been demonstrated[*3*] that the acoustic emission technique can be used to detect crack initiation and growth by monitoring the acoustic activity while welding is actually in progress. This method has been explored as a means of monitoring the multipass, submerged arc welding process which is employed during the fabrication of heavy section pressure vessels[*4*]. It has been found that acoustic emission techniques can successfully detect conditions leading to the formation of slag inclusions, one of the more troublesome defects encountered with this type of welding. Figure 7

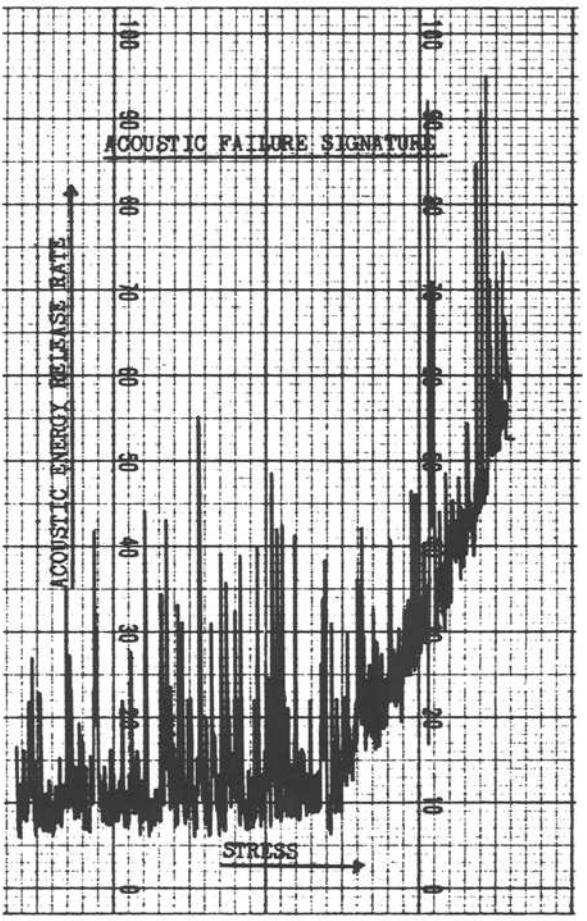

FIG. 6–*Energy release signature for a significant flaw.*

shows the acoustic emission response obtained from various bead configurations, as indicated above the emission traces. Note that the rope bead, which can trap slag on the next pass and produce an inclusion, provided a characteristic emission response pattern. This large emission response was attributed to fracture of the glassy cover which becomes partially trapped in a poorly formed weld bead. This ability to detect variations in the bead quality could possibly lead to reductions in rework time since defects are actually being located before they occur.

The acoustic emission method has been used to continuously monitor TIG welds in HY-80 steel for several days after welding[5]. An acoustic emission

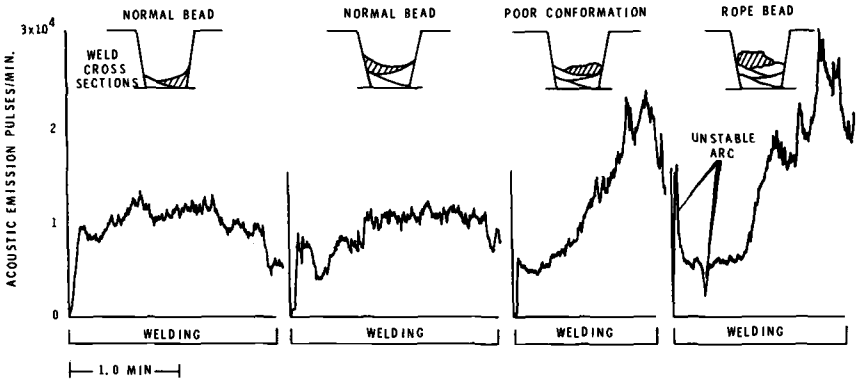

FIG. 7—*Acoustic emission response during the submerged arc welding process.*

sensor was placed near the weldment after the temperature had decreased to approximately 225 F, or about 1 h after the last weld pass. Square butt joints in 0.7-in.-thick plate specimens were used during these tests to promote incomplete penetration, hence weld cracking. The first emission bursts were recorded about 9 min after sensor attachment, and during the next four days some 7100 emissions were recorded. Almost 90 percent of these had occurred within the first 7 h. For all practical purposes, all of the delayed cracking occurred during the first 24 h after welding. The practical utility of monitoring these welds arises from the fact that nondestructive inspection of critical structures is often delayed several days after welding to assure completion of the delayed cracking processes. Thus, acoustic emission monitoring may reduce the weld hold time prior to nondestructive testing, or at least provide a quantitative basis for selecting an appropriate hold time.

The acoustic emission response from elevated temperature burst tests on reactor piping materials has been utilized as an indicator of the start time for short term recording devices such as high speed movie cameras[6]. Twelve-foot-long sections of 24-in.-diameter, 1.64-in.-wall, Type A106-B carbon steel pipe, containing large milled notches, were pressurized to failure at typical power reactor operating temperatures. In one such test, an 18-in.-long notch was milled completely through the pipe wall and a patch placed on the inside to hold the pressure. Figure 8 illustrates the acoustic emission rate versus pressure data obtained in the 10 min prior to catastrophic pipe failure. It is apparent that the acoustic emission rate provided ample warning of impending failure. Posttest data analysis indicated that crack growth was detected with acoustic emission about 10 min before it was visually evident and 3 to 4 min before strain gages near the notch ends indicated crack growth. To repeat, the rapidly rising emission rate is an indicator of the onset of a significant flaw condition. These

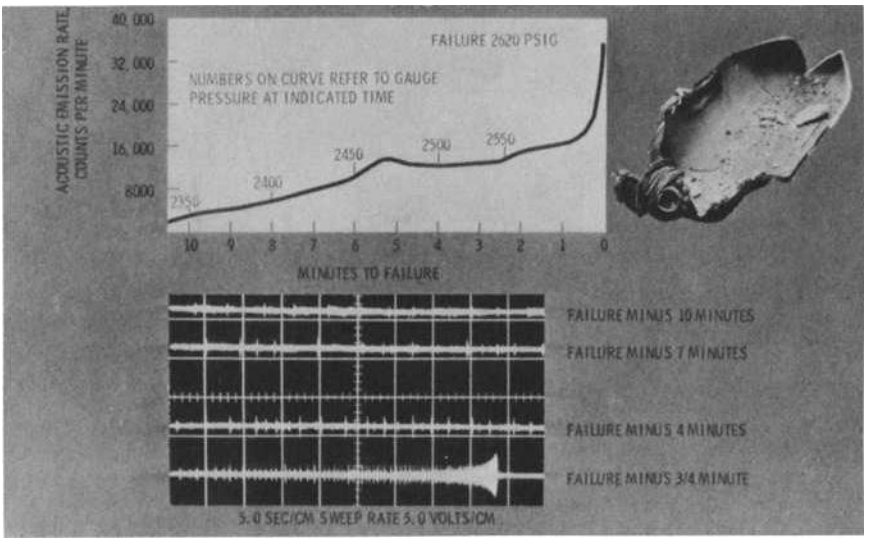

FIG. 8—*Acoustic emission response from a pressure vessel burst test.*

tests were representative of reactor monitoring conditions in that all instrumentation except the sensors and preamplifiers were located some 300 ft from the specimen and the sensors were exposed to temperatures to 700 F. The acoustic emission system included PZT-5 sensors, 0.3 MHz band-pass filters centered at 0.6 MHz, and a total operating gain of approximately 10^4.

Determination of the approximate location of regions of nonbond in large laminated wood beams is another unique application of acoustic emission [8]. Suspect areas thus identified are examined radiographically or with low frequency untrasonics to ascertain the size of the nonbond area. This technique eliminates the need for complete examination by radiographic or ultrasonic techniques, so that there are significant cost savings.

Acoustic emission is also being applied to a variety of civil engineering problems [8]. To perform safety inspections on buildings, the building is water loaded and acoustic emission sensors are placed under the load and on a circle with its center on the load line. Weld problems in structural steel, deterioration in concrete, and areas of soft wood have been located in this manner and, in one case, an area damaged by an unreported fire was located. Standards specify safety inspections of large cranes by complete radiography or ultrasonics on a monthly basis. Acoustic emission transducers attached to critical welds and pin bolts provide adequate warning of incipient failure at much reduced cost. The release of prestressing strands in concrete has also been monitored to determine if the prestressing is adequate for critical applications. Several major bridges over

the Ohio and Mississippi Rivers are being monitored with acoustic emission equipment to detect any indication of structural weakening.

In the area of non metals, acoustic emission has proven to be applicable to ceramics[9]. Ceramic tubes submerged in liquid sodium as part of a system to measure oxygen content were prone to failure from thermal shock. Acoustic emission was applied as part of the investigation of the problem in hopes that it would show crack formation and growth. Figure 9 shows the lack of emission produced by subcritical shock. Formation of a crack and subsequent crack growth induced by critical shock is shown in Fig. 10 and total failure from

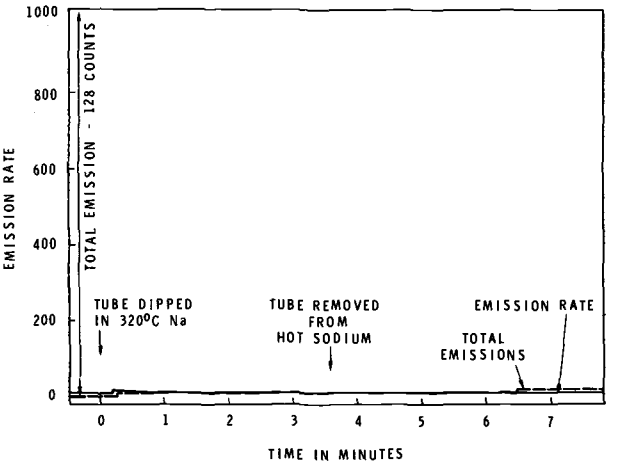

FIG. 9—*Acoustic emission from subcritical heat shock of ceramic tube.*

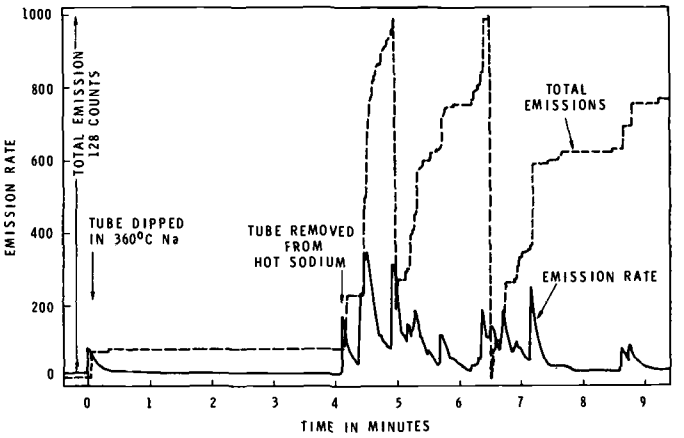

FIG. 10—*Acoustic emission from critical heat shock of ceramic tube.*

continued shock is shown in Fig. 11. The total data from this work provided new insight to the process of thermally induced cracking in ceramic materials.

Another very large area where acoustic emission techniques are being applied is that of geological studies. It is being used to study phenomena such as rockbursts in underground excavations. Russian investigators have been active in this area[*10*] promoting the use of acoustic emission techniques to detect impending structural failure in mines.

The Pennsylvania State University has also been active in this area[*11*]. One of their applications is to determine optimum pressures for underground storage of natural gas in a porous rock structure known as "reservoir rock." Due to the permeable nature of the reservoir rock, great quantities of natural gas can be pumped into it from the surface. Usable reservoir rocks are surrounded by an adjacent strata of less porous rock which acts as a pressure vessel and is known as "cap rock." As the reservoir rock is filled to capacity, the pressure develops stresses in the cap rock which can ultimately crack the "pressure vessel." Acoustic emission in the form of microseismic activity, offer a promising means of detecting incipient failure of the cap rock.

One final example of an application of acoustic emission concerns using the data to provide process control information for metal drawing operations. One specific case involves the formation of metal jackets for small arms ammunition bullets[*12*]. Initial work in this area has shown that it is possible to detect clean acoustic emission from the jacket drawing process at the outer surface of the die. As shown in Fig. 12, the pattern of the emission information is sensitive to process variations effecting the quality of the product. The intent here is to use a visual display of the emission pattern to indicate process abnormalities.

As stated earlier, these examples of applications of the acoustic emission

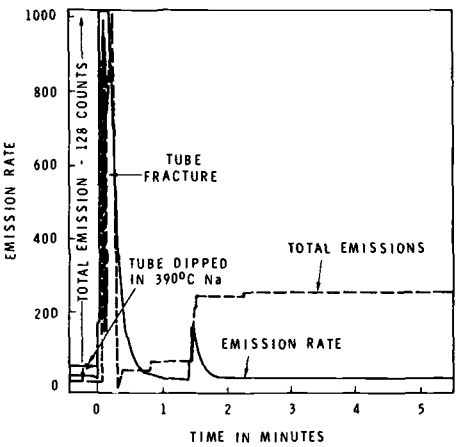

FIG. 11–*Acoustic emission from total failure of ceramic tube by heat shock.*

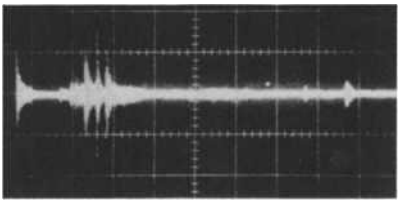

TEST No. 4
GOOD PRODUCT

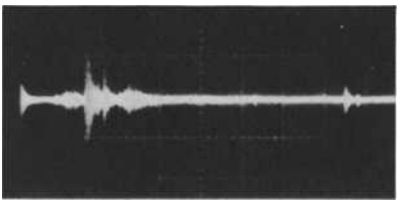

TEST No. 6
BLUNT - 0.025" SHORT

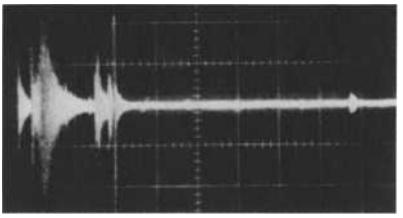

TEST No. 7
CHIPPED PUNCH - 0.015" LONG

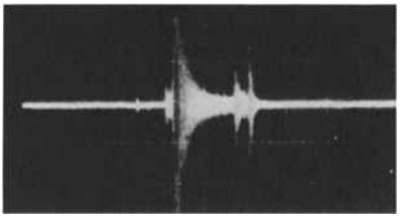

TEST No. 9
CHIPPED PUNCH - 0.032" LONG

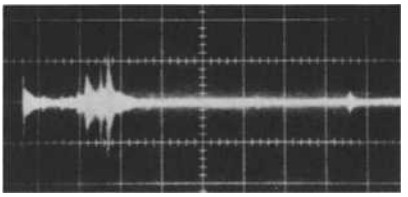

TEST No. 10
GOOD PRODUCT
ALL PHOTOS: HORIZONTAL SCALE - 0.010 SEC./CM.
VERTICAL SCALE - 1.0 VOLTS/CM.

FIG. 12–*Sample acoustic signal patterns from bullet jacket drawing operaton.*

surveillance technique are only representative. They do serve, however, to illustrate that acoustic emission has now taken a place in the real world as a beneficial means of assessing structural integrity and product quality.

References

[*1*] Green, A. T., Lockman, C. S., and Steele, R. K., *Modern Plastics,* MOPLA, Vol. 41, July 1964, pp. 137-139.

[2] Parry, D. L. and Robinson, D. L., *"Incipient Failure Detection by Acoustic Emission, A Development and Status Report,"* IN-1398, Idaho Nuclear Corp., Idaho Falls, Idaho, Aug. 1970.
[3] Jolly, W. D., *The Welding Journal*, WEJOA, Vol. 48, No. 1, Jan. 1969, pp. 21-29.
[4] Jolly, W. D., "The Application of Acoustic Emission to In-Process Weld Inspection," BNWL-SA-2212, Battelle-Northwest, Richland, Wash., March 1969.
[5] Hartbower, C. E., "Application of SWAT to the Nondestructive Inspection of Welds," Technical Note, Aerojet-General Corp., Sacramento, Calif., Sept. 1969.
[6] Hutton, P. H., *Materials Evaluation*, MAEVA, Vol. 26, pp. 125-129, July 1968.
[7] Hutton, P. H., "Integrity Surveillance of Pressure Systems by Means of Acoustic Emission," BNWL-SA-2194, Battelle-Northwest, Richland, Wash., Oct. 1969.
[8] Private communication with R. A. Meunow, Law Engineering Testing Co., Atlanta, Ga., 1970.
[9] Romrell, D. M., Bunnell, R. A., "Acoustic Emission Monitors Crack Growth in Ceramics," BNWL-SA-3064, Battelle-Northwest, Richland, Wash., March 1970.
[10] Antsyferov, M. S., Ed., *Seismo-Acoustic Methods in Mining*, S. E. Hall, translator, Consultant Bureau, New York, 1966.
[11] Hardy, H. R., Jr., "Applications of Acoustic Emissions in Rock Mechanics," presented at the Acoustic Emission Working Group Meeting, Philadelphia Pa. Oct. 1969.
[12] Hutton, P. H., "Identification of Worn Bullet Forming Dies by Acoustic Signature In Process," BNWL-SA-3813, presented at the Eighth Symposium on Nondestructive Evaluation in Aerospace, Weapons Systems, and Nuclear Applications, April 1971.

J. R. Frederick[1] *and D. K. Felbeck*[1]

Dislocation Motion As a Source of Acoustic Emission

REFERENCE: Frederick, J. R., and Felbeck, D. K., "Dislocation Motion as a Source of Acoustic Emission," *Acoustic Emission, ASTM STP 505,* American Society for Testing and Materials, 1972, pp. 129-139.

ABSTRACT: The sudden strain increment that results from the unpinning of dislocations or from the activation of dislocation sources can result in observable acoustic emission. A model has been developed that relates the amount of acoustic emission to the size of a dislocation source, the distance the dislocations slip, and to the grain size. The model is able to explain the effect of the microstructure of the metal on the amount of observed acoustic emission. Data obtained on the acoustic emission from various metals support the model. In general, the greatest amount of emission occurs during the application of stress to a test specimen and particularly during yielding. However it is also possible to obtain acoustic emission during removal of a stress in those materials that show a Bauschinger effect.

KEY WORDS: strains, dislocations (materials), acoustics, emission, grain size, grain boundaries, stresses, yield, crack initiation, crack propagation, plastic deformation, cracking (fracturing), elastic properties, Bauschinger effect

If there is an abrupt relaxation of either localized or long range stresses within a solid material, strain waves are produced in the material that can be detected by means of a sensitive piezoelectric transducer attached to it. The noise that is produced is referred to as "acoustic emission." Most solid materials produce acoustic emission when they are loaded in tension and the following mechanisms have been suggested as sources of emission: the slip of dislocations, twinning, crack initiation, and crack propagation.

This paper is concerned with acoustic emission that originates from dislocation motion. As might be expected, the amount of dislocation related emission produced at any given stress level depends on the microstructure of the material. Parameters such as grain size, dislocation density, and the size and distribution of second phase particles have been found to be important.

[1] College of Engineering, University of Michigan, Ann Arbor, Mich. 48104.

The acoustic emission also depends on whether or not a specimen had been previously loaded. Generally, a specimen will not give off acoustic emission until it has been stressed to a level that exceeds the previously applied stress. This characteristic is known as the "Kaiser" effect.

In some circumstances it is possible to observe acoustic emission when an applied stress is removed from a test specimen. This phenomenon has been observed in magenesium, a copper – 7.9 percent aluminum alloy, 70–30 brass, and several other materials. The effect appears to correlate with the magnitude of the Bauschinger effect in these materials.

Since acoustic emission of dislocation origin is a microstructure dependent phenomenon it has potential use in monitoring those processes in which the microstructure changes during a manufacturing process. Such changes occur, for example, during metal forming, welding, and casting.

Fracture phenomena involve plastic deformation, that is, dislocation motion, prior to and during crack propagation. Hence it may be possible for acoustic emission to provide some useful information about the fracture properties of the material in which cracks are propagating or might have a tendency to propagate.

A Model for Dislocation Related Acoustic Emission

In order to explain the sensitivity of dislocation related acoustic emission to microstructure a model[*1*] is proposed that is based on the activation of dislocation sources and the subsequent shutting off of the sources by the back stress of piled up dislocations[*2*]. The model is based on the assumption that below certain limits of free dislocation line length and dislocation glide distance there will be no detectable emission. These limits are determined by the strain sensitivity of the detection system, that is, the minimum displacement δ_{min} at the surface of a test piece that can be detected by a piezoelectric transducer. This can be calculated from the following equation,

$$\delta_{min} = \frac{V_{min}}{g_{33} E_x} \tag{1}$$

where V_{min} is the voltage corresponding to the background noise level of the system, g_{33} is the piezoelectric stress constant of the transducer material and E_x is the elastic modulus of the transducer material.

The shear stress σ required to activate a dislocation source of initial length f if given[*3*] as

$$\sigma \simeq \frac{\mu b}{f} \tag{2}$$

where μ is the shear modulus of elasticity and b is the Burgers vector. Equation 2

represents an average value for a combined edge and screw dislocation and is considered representative of those dislocations that can act as sources.

The number n of dislocations in the double pile up that would be expected from a source that has been shut off by the back stress of the piled up dislocations has been shown to be[4]

$$n = \frac{(1-\nu) L\sigma}{\mu b} \tag{3}$$

where ν is Poisson's ratio and L is the total width of the pile up. If the average glide distance of the dislocations in the pile up is $3/4(L/2)$, the total area A_s swept out by n dislocations will be more than $n\ \pi\ (3L/8)^2$ but less than $n\ \pi\ (L/2)^2$; the latter value will be used in the calculations that follow. Thus if

$$A_s = n\ \pi \left(\frac{L}{2}\right)^2$$

then by the use of Eqs 2 and 3,

$$A_s = \frac{\pi (1-\nu) L^3}{4f} \tag{4}$$

Assume that a tensile stress is applied axially to a simple cylindrical specimen of cross sectional area A. Consider a slip system whose normal to the slip plane makes an angle, ϕ, with the applied tensile stress and whose slip direction lies at an angle, λ, to the applied tensile stress. The shear displacement δ_s at the end of the specimen that results from slip over an area A_s is

$$\delta_s = \frac{b A_s}{A/\cos \phi}$$

The axial displacement δ_a is therefore

$$\delta_a = \delta_s \cos \lambda$$

If $\nu = 1/3$, and the value of $\cos \phi \cos \lambda$ in the case of $\{111\}$ $<110>$ slip in aluminum is assumed to be 1/3, then by the use of Eq 4 the axial displacement at the end of an aluminum cylinder that results from the activation of a dislocation source is

$$\delta_a = \frac{\pi}{18} \frac{bL^3}{Af} \tag{5}$$

where b is Burgers vector for aluminum, L is the slip area diameter, f is the dislocation source length, and A is the cross sectional area of the specimen. If Eq

5 is combined with Eq 1 for the minimum detectable strain, the following relationship between the slip region diameter L and source length f, both in meters, is obtained.

$$L^3 = (1.78 \times 10^{-9}) f \tag{6}$$

The constant in Eq 6 is based on a specimen area A of 31.7 mm^2, 2.86 × 10^{-10}m for the Burgers vector of aluminum, threshold voltage V_m of 4 μV, piezoelectric stress constant g_{33} of 24.4 × 10^{-3} V–m/N and elastic modulus E_x of 58.5 GN/m^2. Figure 1 defines the minimum slip region diameter L that will give detectable emission for a source of length f in an aluminum specimen whose area is 31.7 mm^2. Any values of L and f below the solid line will not be detected in the system that has been postulated.

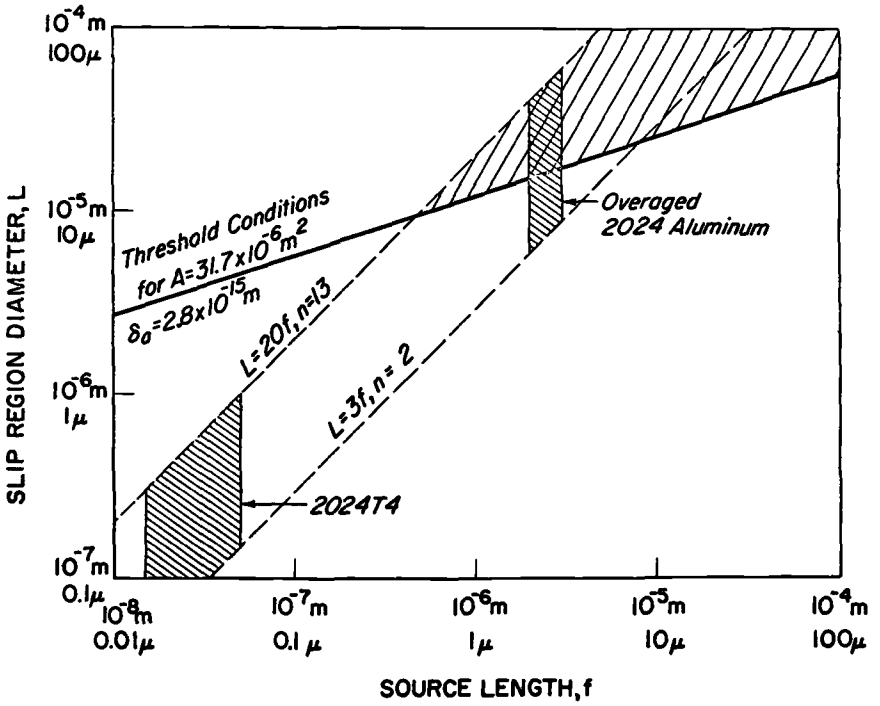

FIG. 1—*The plot of Eq 6 on log-log coordinate graph. Acoustic emission which results from the activation of a dislocation source can be detected if the slip region diameter,* L, *exceeds a minimum value which depends on the dislocation source length,* f. *Pinning mechanisms may also limit the possible values of* L *and* f *to values lying between the dashed lines. The region in which slip can be detected is shown by the coarse shading. The limits on* L *and* f *for fully aged (T4 condition) and overaged 2024 aluminum alloy are shown by the fine shading. For the model that is described it should be possible to detect acoustic emission from overaged 2024 aluminum alloy[1].*

There are certain limitations on the ratio L/f. The length of a dislocation line that is free to move is limited because of pinning either at the nodes of the dislocation network or because of local defects such as hard particles. The maximum possible glide distance for dislocations that are expanding out from a source is also limited. If fine particles limit the glide distance to the order of $10f$, then $L/f = 20$. If the Frank network limits the glide distance, then L/f will probably be closer to unity. A reasonable maximum value of L/f would be 20 for the strains considered here. These strains are well below those corresponding to the engineering yield stress. The solid line in Fig. 1 provides a lower boundary for detectable emission and the line $L = 20f$ provides an upper boundary for plausible slip systems that may operate in the microstrain region at stress levels less than macroscopic yielding. The area bounded by these lines in Fig. 1 is therefore the region where slip can be detected by acoustic emission with the specimen size and transducer sensitivity that have been used in developing the model. The graph indicates that no acoustic emission should be detected from sources having a length of less than about 5×10^{-7} m (0.5 μm).

Application of the Model to Various Materials

Annealed Aluminum (99.99 percent)

High values of acoustic emission[5] are observed in this material which indicates the presence of dislocation sources that are greater than 0.5 μm in length, in fact probably of the order of 10-100 μm. This falls in the range of grain sizes normally encountered in annealed specimens of this material. The region of detectable emission shown in Fig. 1 shows that a wide range of values for L/f can be expected to give measurable emission. Both air cooled and furnace cooled specimens of this material give detectable emission and this suggests that even if the impurities have some pinning effect, the source lengths that are encountered are still large enough to be detected. (A parallel series of tests on 2024 aluminum shows that water quenching from 975 F (524 C) results in large load emission but air and furnace cooling from the same temperature allow enough precipitation of impurities to prevent detectable load emission from occurring[5].)

Cold Worked Aluminum (99.99 percent)

If it is assumed, for purposes of rough calculation, that the increase in dislocation density as a result of cold work produces a uniform simple cubic dislocation network of progressively smaller unit size, it is possible to make an estimate of the highest dislocation density for which acoustic emission can be detected in these tests. A reasonable value of L/f for such a network may be taken as 2. Figure 1 gives the minimum detectable source length as about 8 μm. For a cubic cell side dimension d in this assumed network, a $\{100\}$ intersection

will give a dislocation density of $\rho_1 = 1/d^2$. For a $\{110\}$ intersection, the density will be

$$\rho_2 = \frac{2}{d^2}\Big/\sqrt{2} = \frac{\sqrt{2}}{d^2}$$

And for a $\{111\}$ intersection, the density will be

$$\rho_3 = \frac{3}{2d^2}\Big/\frac{\sqrt{3}}{2} = \frac{\sqrt{3}}{d^2}$$

This can be approximated as $\rho = 1.5/d^2$. Then if $d = 8\ \mu m$,

$$\rho = 1.5/(8 \times 10^{-4}\ cm)^2 = 2.34 \times 10^6\ cm^2$$

This value is not much larger than the dislocation density in the annealed material and suggests that very little cold work will eliminate detectable load emission. This has been observed in all tests conducted to date, even when the test loading is not in the same orientation as the cold work deformation loading.

Naturally Aged 2024 Aluminum

As the precipitates form with time following solution heat treating, the maximum value of f decreases until it is less than 0.25 μm. Alloys of this composition are known to have an average particle spacing in the range 0.015-0.050 μm. If f is of the same order of magnitude as the particle spacing, then Fig. 1 indicates that no emission should be detectable from a fully aged 2024 aluminum alloy. The fine cross-hatched region for 2024-T4 does in fact fall well below the threshold curve. Partially aged 2024 should give a limited amount of detectable emission because the particles would be expected to have average spacing in the μm range. This agrees with the experimental results[5] shown in Fig. 2.

Overaged 2024 Aluminum

Aging A1-4 percent Cu at 572 F (300 C) for 1 h or A1-4.6 percent Cu at 482 F (250 C) for 48 h gives an average $CuA1_2$ particle spacing in the range 1.0–2.5 μm. The aging treatment in these experiments, namely, 600 F (316 C) for 100 h, may therefore result in slightly higher spacing, probably in the range of 2 to 3 μm. Figure 1 shows that part of this region falls within the detectable range and part below the threshold. Experimental results that have been obtained do show a small amount of emission for this condition[5].

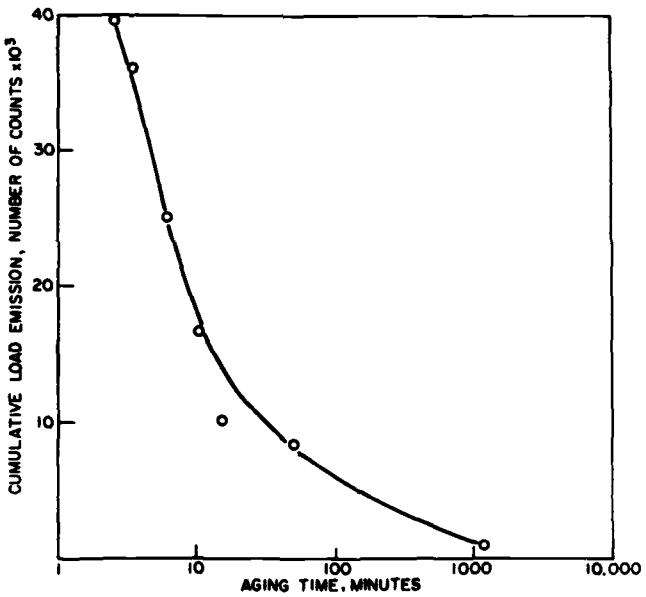

FIG. 2– *Dependence of the cumulative load emission from 2024 aluminum on aging time*[5].

Effect of Grain Size

The cumulative acoustic emission that is obtained for a given applied stress depends on the grain size of the aluminum as shown in Fig. 3[6]. For small or large grain sizes the emission is low, but at an intermediate size there is a maximum total acoustic emission. The bandwidth for the data shown in Fig. 3 is 80 to 200 kHz. The same shape of curve is also observed in a frequency band of 6 to 20 kHz.

The increase and subsequent decrease in the amount of acoustic emission with increasing grain size can be explained on the basis of the dislocation source model described above. An average grain size of 10 μm in the 99.99 percent aluminum is sufficient to allow enough dislocations to be generated and glide away from the source so that a detectable strain pulse, or acoustic emission pulse, is produced. As the grain size is increased the dislocation glide distance increases and a larger strain pulse is produced. However, as the grain size increases the grain boundary area decreases. This means that there are fewer grain boundary sources of dislocations. Hence a reduction in the emission is to be expected. The maximum emission occurs at a grain size of about 350 μm for the data shown in Fig. 3.

It can be seen in Fig. 3 that the acoustic emission activity declines at a rate inversely proportional to the grain size as the grain size increases beyond a

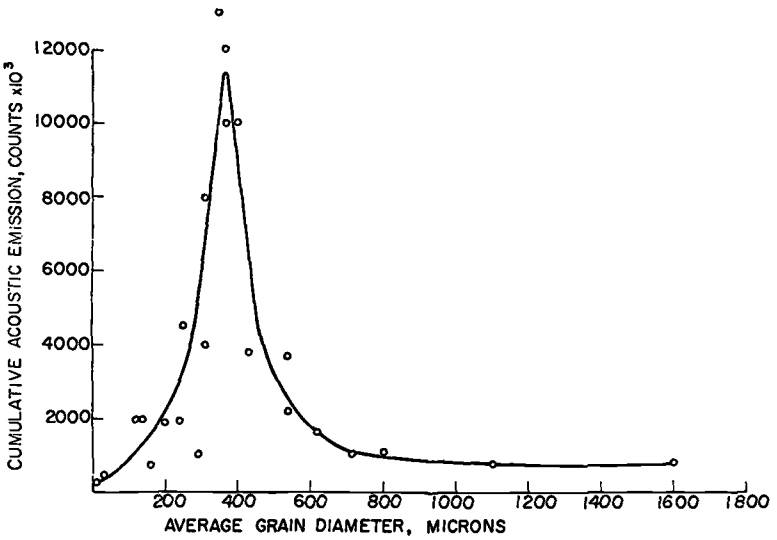

FIG. 3—*The cumulative acoustic emission from 99.99 percent aluminum depends on grain size. All specimens were loaded to a maximum stress level of 1500 psi[6].*

certain value. Hence, since the grain boundary surface area in a specimen is inversely proportional to the grain size, the acoustic emission activity is proportional to the grain boundary surface area. From this it can be concluded that the grain boundaries act as unstable sources of dislocations when slip progresses from one grain to an adjacent grain. This is the case during the plastic deformation of metals.

Acoustic Emission from Metals During Removal of Stress

Several cases have been reported in which acoustic emission has been observed when a tensile load is removed from a test specimen prior to fracture of the specimen[*7-9*]. This "unload" emission is reversible, that is, it occurs on repeated loading and unloading cycles. Furthermore, materials that show an unload emission effect do not show a Kaiser effect[*10*]. In other words, they produce acoustic emission during reloading instead of not emitting until the value of the previously applied load has been exceeded. The unload acoustic emission is generally an order of magnitude or more smaller than the load emission.

Another characteristic of the emission that is of interest is that it occurs under test conditions in which the specimen is normally considered to be behaving elastically, such as during the removal of an applied load.

A typical plot of the load and unload emission and the corresponding plastic strain is shown in Fig. 4 for a copper – 7.9 percent aluminum alloy. The

frequency bandwidth for these data was from 6 to 12 kHz. A PZT-5 transducer was used. The peak value of the background noise level was 4.0 μV.

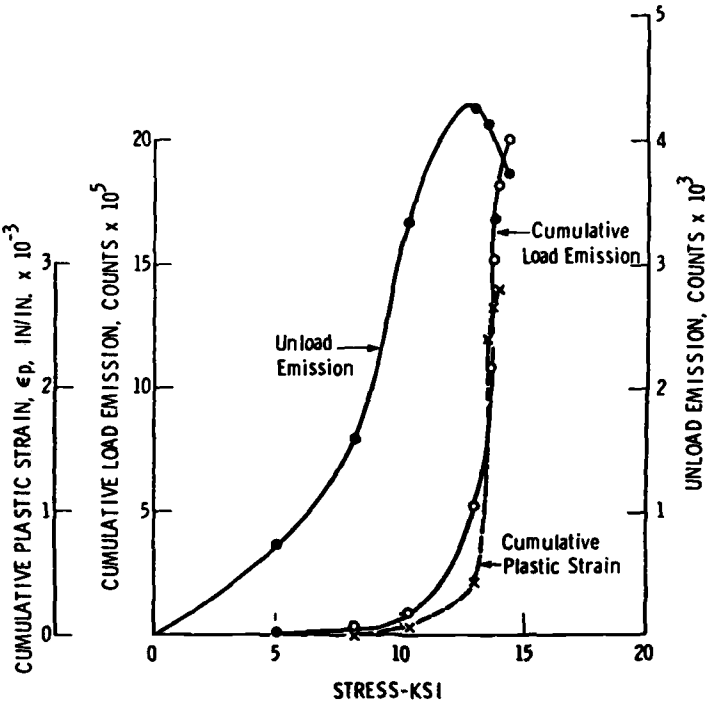

FIG. 4– *Stress versus cumulative load emission, unload emission, and cumulative plastic strain in a copper-7.9 percent aluminum alloy, annealed at 568 C (1022 F) for 24 h. Average grain size 40 μm, hardness 67* R_E. *The unload emission was determined by applying successively larger loads to the specimen and noting the emission when the load was removed* [10].

Data on the unload emission behavior for several other materials are shown in Table 1, along with their crystal structure, stacking fault energy, and Bauschinger strain. The acoustic emission data were observed under the same conditions as that shown in Fig. 4.

It can be seen from the table that a correlation appears to exist between the magnitude of the Bauschinger strain and the unload emission. A large unload emission is associated with a large Bauschinger strain in a particular material.

The Bauschinger effect can be attributed to the back stress of dislocations that have piled up against grain boundaries or other obstacles. It therefore is possible that the observed unload acoustic emission is due to the reverse movement of dislocations caused by the back stress of the pile ups.

The low value of unload emission obtained for the aluminum and the

TABLE 1– *Stacking fault energy, Bauschinger effect, and unload emission in several annealed materials* [10].

Material	Crystal Structure	Stacking Fault Energy, erg/cm^2	Bauschinger Strain,[a] 10^{-6}	Unload Emission, Counts[b]
99.99% Al	fcc	200	100	340
6061 Al alloy	fcc	117	480	610
2024 Al alloy	fcc	...	510	580
70–30 brass	fcc	10 to 12	1150	2 300
Cu-7.9% Al alloy	fcc	4	1210	3 600
99.95% Mg	hcp	...	3000	12 400

[a] Bauschinger strain was measured on a separate set of specimens at a compression stress which was 50 percent of the tension stress needed to produce a strain of 0.005.

[b] Unload emission counts were recorded for a cumulative plastic strain of 0.0001.

aluminum alloys may be due to the fact that cross slip of the dislocations is relatively easy in these materials because of their high stacking fault energy. Any dislocations that cross slip out of the original slip plane will not contribute to reverse plastic flow when the stress is removed. The Cu - 7.9 percent Al alloy and brass show a larger unload emission because they have less tendency to cross slip and exhibit a characteristic known as planar glide[*11*].

Conclusions

Acoustic emission resulting from the motion of dislocations can be explained by the use of a model based on the activation of sources of dislocations by an applied stress. Whether or not acoustic emission will be detected depends on the source length and on the dislocation glide distance. The model is useful in explaining the changes in the acoustic emission that result from cold work, age hardening, or changes in microstructure.

Acoustic emission is also observed in some materials when an applied stress is being removed from a test specimen. This effect occurs in materials that show an appreciable Bauschinger effect, and is attributable to the reverse movement caused by the back stress of piled up dislocations.

Acknowledgments

We would like to acknowledge the contributions of A.B. Agarwal, N. G. Sankar, and R. C. Bill to the work that is being reported here. The work has been supported in part by the National Science Foundation (Grant GK 697) and the Advanced Research Projects Agency.

References

[*1*] Agarwal, A. B. L., Frederick, J. R., and Felbeck, D. K., *Metallurgical Transactions*, MTGTB, Vol. 1, 1970, p. 1069.

[*2*] Eshelby, J. D., Frank, F. C., and Nabarro, F. R. N., *Philosophical Magazine*, PMJTA, Vol. 42, 1951, p. 351.

[3] Hirth, J. P. and Lothe, J. in *Theory of Dislocations*, McGraw-Hill, New York, 1968, p. 683.
[4] Hirth, J. P. and Lothe, J. in *Theory of Dislocations*, McGraw-Hill, New York, 1968, p. 700.
[5] Agarwal, A. B. L., "An Investigation of the Behavior of the Acoustic Emission from Metals and a Proposed Mechanism for its Generation," Ph.D. thesis, University of Michigan, 1968.
[6] Bill, R. C., "An Acoustic Emission Study of the Deformation Mechanisms of Polycrystalline Aluminum and Copper," Ph.D. thesis, University of Michigan, 1970.
[7] Sankar, N. G., Frederick, J. R., and Felbeck, D. K., *Metallurgical Transactions*, MTGTB, Vol. 1, 1970, p. 2979.
[8] Schofield, B. H., "Acoustic Emission Under Applied Stress," Technical Report ASD-TDR-63-509 Part II, Air Force Materials Laboratory, Wright-Patterson Air Force Base, Ohio, 1964.
[9] Kerawalla, J. N., "An Investigation of the Acoustic Emission from Commercial Ferrous Materials Subjected to Cyclic Tensile Loading," Ph.D. thesis, University of Michigan, 1965.
[10] Sankar, N. G., "Unload Emission Behavior of Materials and its Relation to the Bauschinger Effect," Ph.D. thesis, University of Michigan, 1969.
[11] Feltner, C. E. and Laird, C., "Cyclic Stress-Strain Response of FCC Metals and Alloys – I. Phenomenological Experiments," *Acta Metallurgica*, AMETA, Vol. 15, 1967, p. 1621.

G. R. Speich[1] *and R. M. Fisher*[1]

Acoustic Emission During Martensite Formation

REFERENCE: Speich, G. R. and Fisher, R. M., "Acoustic Emission During Martensite Formation," *Acoustic Emission, ASTM STP 505*, American Society for Testing and Materials, 1972, pp. 140-151.

ABSTRACT: Martensite formation in an Fe-28Ni-0.11C alloy has been studied using acoustic emission, electrical resistivity, and quantitative metallography techniques. Comparison of these three techniques indicates that about 15 martensite plates are involved in each acoustic emission and that the volume of martensite formed per acoustic emission decreases with increasing volume fraction. The first observation is consistent with the autocatalytic effect and the second with the geometric partitioning effect which are both present in martensitic transformations. Because acoustic emission gives an almost plate by plate record of the martensitic transformation, more detailed studies of the transformation kinetics can be made with this technique than by other techniques such as dilatometry or electrical resistivity.

Key Words: alloys, iron containing alloys, nickel alloys, acoustics, emission, martensite

Although it has been known for at least 40 years that acoustic emission in the form of "clicks" may be heard during the formation of martensite[*1,2*], little effort has been put forth to utilize this phenomenon to study the transformation. Recently, advances in electronic instrumentation developed for the study of acoustic emission during plastic deformation[*3,4*] permit these clicks to be studied in greater detail[*3,5*]. Liptai et al[*5*] have studied acoustic emission during martensite formation in Au-Cd, In-Tl, and cobalt both on heating and cooling. They have also studied the eutectoid transformation in Sn-10 atomic percent Cd and showed that this "nucleation and growth" transformation did not produce acoustic emission. This is not unexpected since such transformations involve low, diffusion-controlled growth rates where there is sufficient time

[1] U. S. Steel Corporation Research Laboratory, Monroeville, Pa. 15146.

for strains to be relaxed by creep. Martensite formation on the other hand is a diffusionless shear transformation involving the cooperative movement of large numbers of atoms and produces high-amplitude acoustic emission. The individual plates form in 10^{-6} to 10^{-8} s [6] and the transformation is known to be autocatalytic in nature with each plate triggering the nucleation of other plates in adjoining regions[7]. In the present work we have studied acoustic emission during martensite formation in a coarse grained specimen of an Fe-28Ni-0.11C alloy. Simultaneous measurement of the electrical resistance permitted the volume of martensite formed per acoustic emission to be determined. Quantitative metallography was used to ascertain the number of plates involved in each acoustic emission.

Compared to plastic deformation and crack propagation, martensite formation is a clearly defined acoustic emission source[8]. Mechanical twinning is another well defined source, but this requires application of a carefully controlled stress which is not as convenient experimentally as simply changing the temperature of the specimen. In addition, martensite formation is reversible and the source can be reused many times. Thus, an important additional goal of these studies is to establish a quantitative relationship between acoustic emission amplitude, rise time, and frequency, and the local stress pulses generated by a standard martensite acoustic emission source. Knowledge of these parameters should be useful when interpreting acoustic emission in more complex situations involving dislocation avalanches[4] and crack growth[3].

Experimental Procedure

The Fe-28Ni-0.11C alloy[2] was a vacuum melted 20-lb ingot, hot rolled to ½-in. plate at 1100 C. Specimens cut from the plate were centerless ground to ⅛-in.-diameter and then cut into 3-in. lengths. These were austenitized 1 h at 1200 C in evacuated quartz capsules and water quenched.

The acoustic emission equipment arrangement is shown schematically in Fig. 1. The specimen was welded to a nickel rod ⅛ in. in diameter and 3½ in. long which served as a wave guide. A machined ¾-in.-diameter plate at the end of the nickel rod permitted a lead zirconate split transducer to be attached. Stopcock grease was used to bond the transducer to the plate. Current and potential leads for electrical resistance measurements and a copper-constantan thermocouple were spot welded to the specimen. The specimen was lowered into a Freon 11 bath and liquid nitrogen added to the space between the two steel dewars (see Fig. 1). Conduction of heat through the internal dewar which contained helium gas gave a constant controlled cooling rate. A stirrer motor and propeller gave enough agitation to insure a constant temperature throughout the bath.

[2] Chemical analysis in weight percent: 28.4 Ni, 0.11 C, 0.01 Mn, 0.001 P, 0.0026 S.

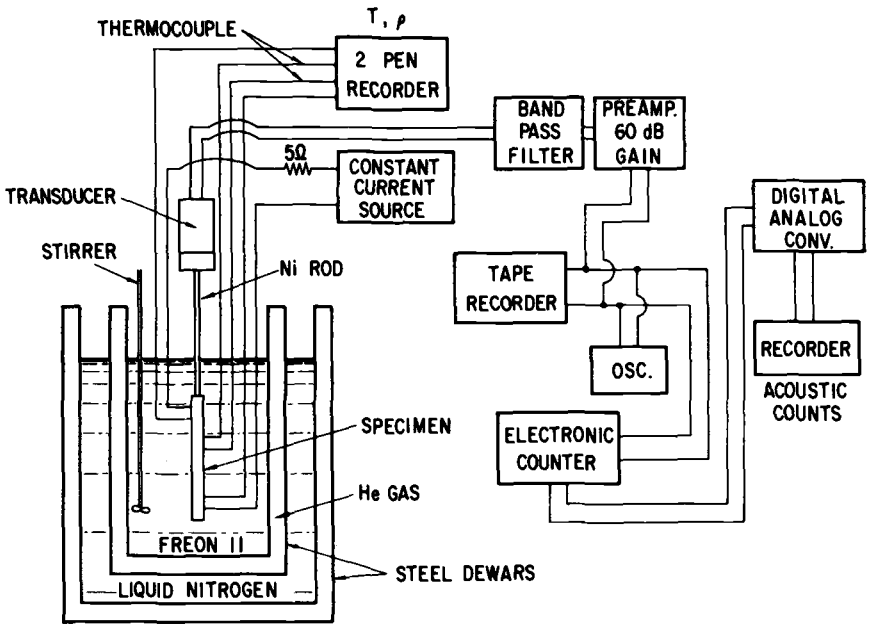

FIG. 1–*Block diagram of acoustic emission equipment.*

The acoustic signals recived by the transducer were passed through a 60-dB low noise preamplifier which also contained a band-pass filter to filter out low frequency noise. The signals were sufficiently large so that no secondary amplifier was needed. The signals from the preamplifier were then fed to an audio tape recorder, an electronic counter, an oscilloscope, and a digital to analog converter. The acoustic emission was monitored by displaying the analog output on a standard mV recorder. In later work, it was found convenient to replay the magnetic tape, rectify the pulse with a full wave rectifier circuit, and shape the pulse with an r-c circuit before counting pulses. This eliminated most of the multiple counting caused by reflection of elastic waves within the specimen. In addition use of an audio tape recorder rather than a high frequency tape recorder has a heterodyning effecting because it reponds only to lower frequencies (6-10 kHz) and cannot resolve the multiple reflections. When the counting rate was low enough to permit a direct determination of it on the oscilloscope, good agreement with the counting rate obtained by the above procedure was observed.

The electrical resistivity and temperature were monitored by displaying the mV output from the thermocouple and the mV drop across the specimen on a 2-pen mV recorder. The current passing though the specimen was maintained constant by use of a constant current regulator. With a constant current, the mV drop across the specimen is directly proportional to the electrical resistivity.

With the cooling source shown in Fig. 1, no background noise was obtained from liquid nitrogen bubbling or from the stirrer motor. However, during the initial filling of the space between the dewars with liquid nitrogen, considerable acoustical noise developed because of thermal contraction of the steel dewars. Fortunately, this problem ceased once the dewar had cooled sufficiently, and did not interfere with subsequent measurements.

A number of specimens were cooled in a stepwise manner to different temperatures to form various amounts of martensite. These were then metallographically polished, etched, and the volume fraction and number of plates per unit volume determined by quantitative metallography [9].

Results

Figure 2 shows the electrical resistivity, total acoustic emission, acoustic emission rate, and temperature of the specimen during continuous cooling. The martensite start temperature (M_S) of this alloy is 0 C and acoustic emission is observed in a sporodic manner in the form of bursts (labelled 1 and 2) below this temperature. Such bursts are known to occur during martensite formation in Fe-Ni alloys [10]. Little or no acoustic emission is observed between bursts. Accompanying these bursts are sudden drops in the electrical resistivity and a

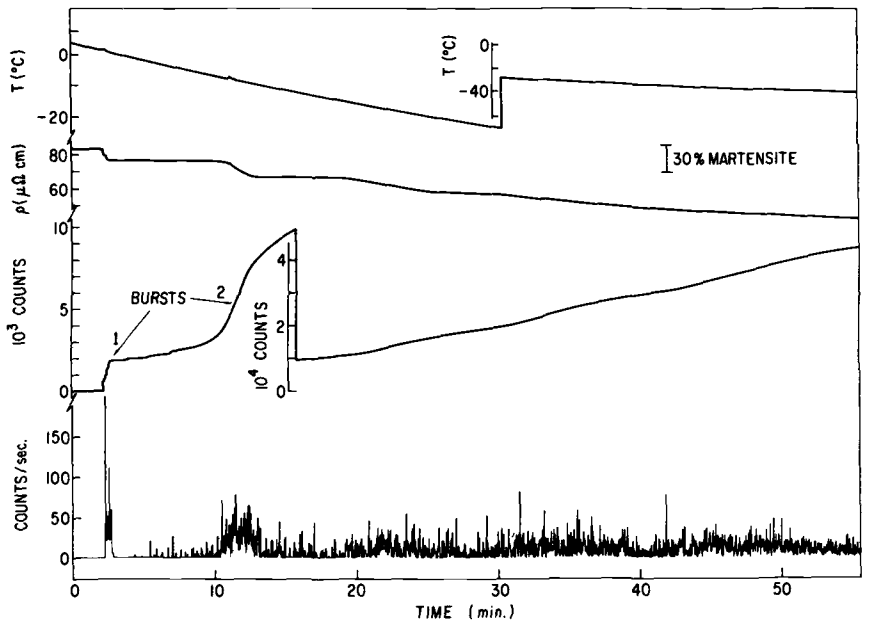

FIG. 2—*Acoustic emission pulse rate and total counts, electrical resistance, and temperature during martensite formation.*

release of heat due to the enthalpy difference between martensite and austenite (650 cal/mol)[*11*]. This is manifested in an increase in the temperature of the specimen. After these bursts, the acoustic emission rate becomes rather steady, with the total number of counts steadily increasing and the electrical resistivity steadily decreasing with decreasing temperature.

The volume fraction of the martensite formed during cooling may be estimated from the electrical resistivity change:

$$f_v = \frac{\rho_A - \rho_S}{\rho_A - \rho_M} \tag{1}$$

where f_v = volume fraction martensite,
ρ_A = electrical resistivity of austenite,
ρ_S = electrical resistivity of specimen,
ρ_M = electrical resistivity of martensite.

The values of f_v thus calculated are shown in Fig. 3. Since the total number of acoustic emissions, N, and the specimen volume are known, it is possible to

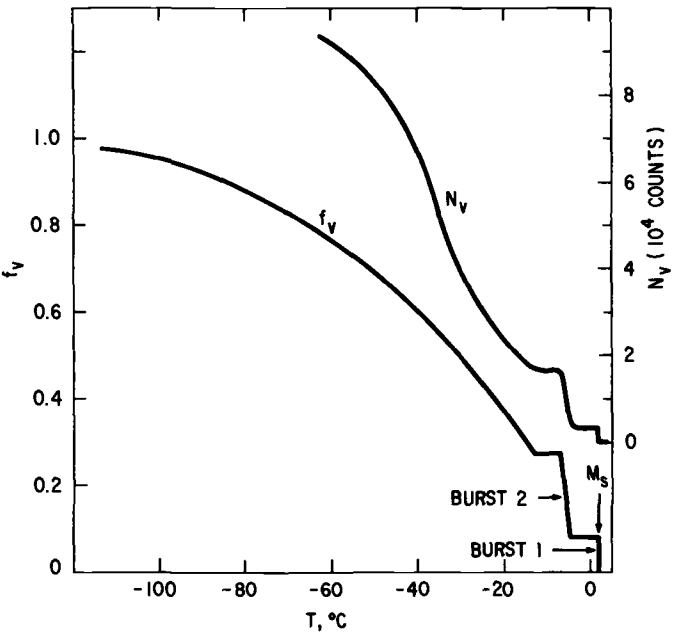

FIG. 3—*Total volume fraction of martensite* (f_v) *and total counts per unit volume* (N_v) *generated during transformation.*

calculate the mean volume of martensite formed per acoustic emission from the expression

$$\bar{V}_e = \frac{df_v}{dN_v} \tag{2}$$

where $\bar{V}_e$ = mean volume of martensite formed per acoustic emission and N_v = total number of acoustic emissions per cm^3 of specimen. The values of N_v and f_v are given in Fig. 4 and the value of $\bar{V}_e$ is given in Fig. 5. The values of $\bar{V}_e$ are labelled $\bar{V}_e$ (resistance) in Fig. 5 since the values of f_v used in their determination were obtained from electrical resistance measurements. This is done also to differentiate them from $\bar{V}_e$ obtained from the transducer voltage which is discussed later. As the volume fraction increases, $\bar{V}_e$ decreases.

Quantitative metallography of specimens transformed at different temperatures permits the mean volume per plate of martensite to be established from the expression [9]:

$$N_V{}^p = \frac{8}{\pi^2} N_A \bar{Z} \tag{3}$$

and

$$\bar{V}_p = \frac{f_v}{N_V{}^p} \tag{4}$$

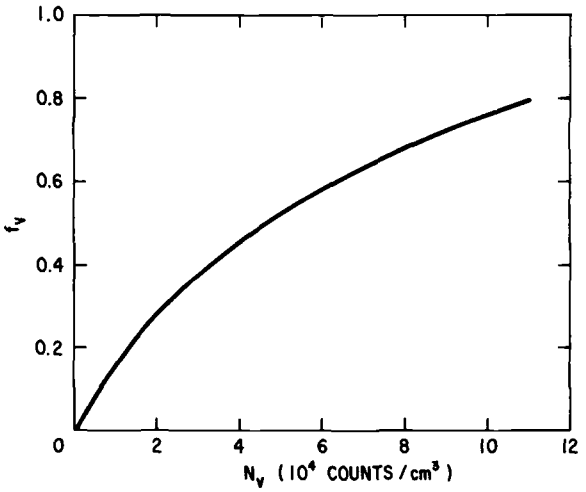

FIG. 4—*Total counts per unit volume* (N_V) *compared with increasing volume fraction* (f_V) *during transformation.*

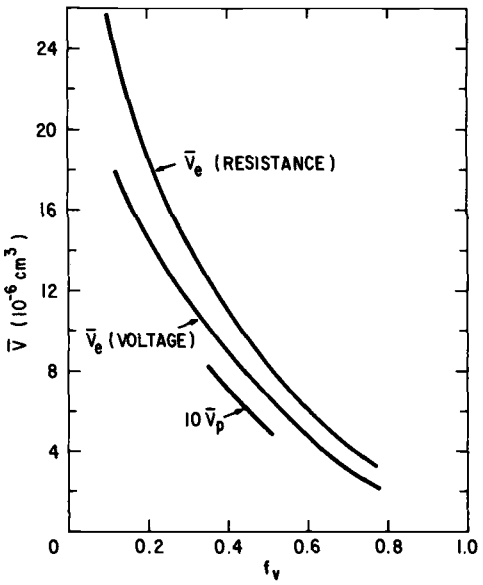

FIG. 5—*Mean volume of martensite formed per acoustic emission* ($\bar{V}_e$) *and mean volume of martensite plate* (V_p) *decrease with increasing volume fraction* (f_v).

where N_V^p = number of martensite plates per cm^3,

N_A = number of martensite plates per unit area of polished surface,

$\bar{Z}$ = mean of the reciprocal of martensite plate intersections with polished surface, and

$\bar{V}_p$ = mean volume of martensite plate.

The values of $\bar{V}_p$ shown in Fig. 5 are considerably smaller than the values of $\bar{V}_e$. Thus, one concludes that a large number of plates must be involved in each acoustic emission. The number of plates per emission is simply given by $\bar{V}_e/\bar{V}_p$. Its value is equal to about 15 and is nearly independent of volume fraction.

It is also possible to estimate the volume per acoustic emission from the voltage of the acoustic pulse if some simplifying assumptions are made. Thus, if we take 4 percent to be the volume change accompanying complete transformation to martensite, the final specimen elongation is $\frac{\Delta l}{l} = \frac{1}{3}\frac{\Delta V}{V} = 0.0133$. We shall assume this is the elongation sensed by the transducer. This is an underestimate since the specimen length actually "rings-down" to this final value during the multiple reflections of the elastic waves as shown in Fig. 6. The voltage generated at the transducer is

$$E = g_{33}\, Y_{33}\, \Delta l \tag{5}$$

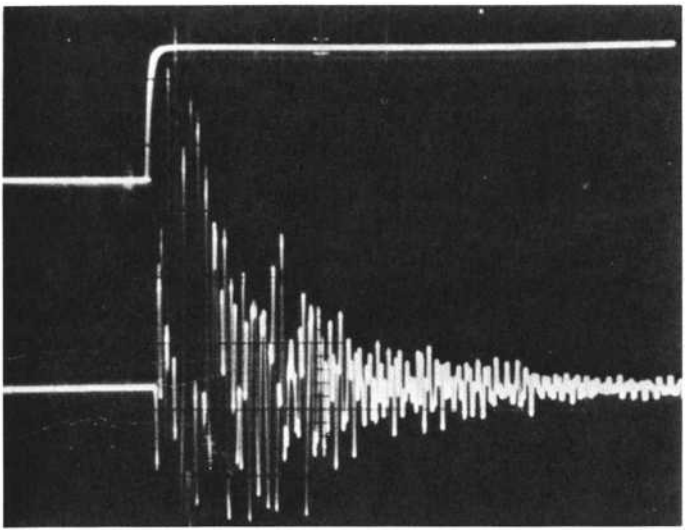

FIG. 6—*Oscilloscope trace illustrating specimen resonance after single test pulse.*

where E = voltage,
g_{33} = piezoelectric constant,
Y_{33} = Young's modulus in thickness direction,
Δl = change in specimen length.

Taking $g_{33} = 24.8 \times 10^{-3}$ $\frac{\text{Vm}}{\text{N}}$ and $Y_{33} = 5.3 \times 10^{10}$ N/m^2, values typical of lead zirconate we find

$$\bar{V}_e = \frac{E V_s}{1.66 \times 10^5 l} \tag{6}$$

where V_s is the specimen volume. If the transducer area, A_t, is larger than the specimen area, A_s, the value of E must be multiplied by A_t/A_s since the length shape sensed by the transducer is proportionably smaller. For $l = 7.57$ cm, $A_t = \frac{\pi}{4}$ (¾ in.)^2, $A_s = \frac{\pi}{4}$ (⅛ in.)^2, and $V_s = 0.618$ cm^3, we obtain $\bar{V}_e = 1.78 \times 10^{-5}$ E (cm^3 V^{-1}). At $f_v = 0.1$, a mean voltage observed on the oscilloscope was 10V. For a 60-dB amplifier and a 10-V signal, $E = 10 \times 10^{-3}$ V, and $\bar{V}_e = 17.8 \times 10^{-6}$ cm^3. This value should be compared with the $\bar{V}_e = 24 \times 10^{-6}$ cm^3 calculated from the resistance change, at $f_v = 0.1$. The

values of $\bar{V}_e$ calculated from the mean transducer voltage at various volume fractions of martensite are labelled $\bar{V}_e$ (voltage) in Fig. 5. They decrease with increasing volume fraction as was observed for values of $\bar{V}_e$ (resistance). Typical voltage observed on the oscilloscope before preamplification and the accompanying martensite microstructures are shown in Fig. 7 for two different volume fractions.

Discussion

Acoustic emission during martensite formation arises from the sudden shearing of a volume of austenite ($\approx 6 \times 10^{-7}$ cm^3) into martensite. The shearing process can be resolved into a macroscopic dilation (≈ 0.04) and a simple shear strain (≈ 0.20). These strains are large enough so that the local yield stress of the

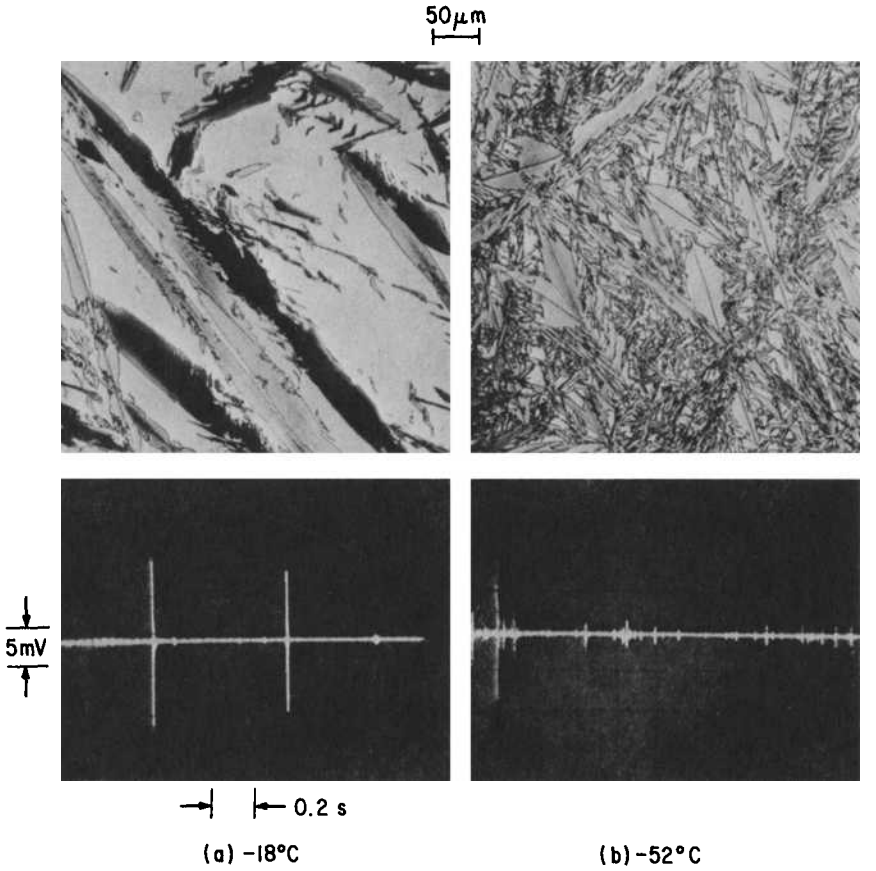

FIG. 7—*Typical martensite microstructure and acoustic emission pulses at −18 and −52 C.*

austenite is exceeded and dislocation generation occurs. In addition the martensite plates are twinned on an exceedingly fine scale[*12,13*]. Thus, the initial stress waves responsible for the observed acoustic emission accompanying the transformation are complicated. However, since the plastic deformation is extremely localized and because the dislocations and twins occur on such a fine scale, the major source of the acoustic emission is undoubtedly the large macroscopic shear and dilatational strains accompanying this transformation similar to the phenomenon of mechanical twinning.

Sudden generation of a large shear or dilatational strain (10^{-6} to 10^{-8} s) results in the generation of elastic waves which are detected and counted as acoustic emission pulses. Comparison of the observed values of $\bar{V}_e$ and $\bar{V}_p$ (Fig. 5) indicate that about 15 plates are involved in each emission event. This appears reasonable because of the autocatalytic nature of the martensitic transformation[*7*]. The plastic deformation and kinetic energy associated with each plate triggers the formation of other martensite plates in the same or adjoining grains. These plates, however, form in 10^{-6} to 10^{-8} s[*6*] so that their individual formation is not resolved. The formation of these 15 plates is seen as one acoustic emission event. Whether this autocatalytic behavior also is characteristic of lath martensite found in low alloy steels[*14,15*], in contrast to the plate martensite studied here is not yet known and will require further study.

The observation that initially the transformation occurs in very large bursts where several thousand emissions occur in a closely spaced time interval is of considerable interest. These large bursts result in a temperature rise in the specimens which may be detected easily. Generally two bursts are found in each specimen, the second being considerably larger than the first. The specimen remains quiet between bursts but after the second burst a steady rate of transformation ensues. Although the autocatalytic nature of the transformation is understood to result from the activation of nucleation centers by the plastic deformation of the surrounding austenite, the formation of these large bursts is not clearly understood. They are not characteristic of all martensitic transformations[*7*]. Also, isothermal martensite forms in some composition ranges[*7*] and it would be of interest to study this form of the transformation by acoustic emission techniques.

The gradual decrease in $\bar{V}_e$ with increasing volume fraction indicated by electrical resistivity, quantitative metallography, and the voltage signals is consistent with a geometric partitioning effect first discussed by Fisher[*16*] and more recently by Raghaven and Cohen[*17*] and Entwistle[*18*]. This results from the restriction of plates to individual austenite grains. Subsequent plates must then form in the partitioned volume formed by the first plate. The autocatalytic factor, $\bar{V}_e/\bar{V}_p$, appears to remain constant as f_v varies although it was possible only to obtain information on $\bar{V}_p$ over a limited range of f_v values (Fig. 5). Thus, the argument by Magee[*7*] that the volume fraction versus

temperature curve for martensite may be derived using a constant mean volume for the newly formed martensite plates is unjustified. However, the reduction in $\overline{V}_e$ or $\overline{V}_p$ seems less sensitive to volume fraction than suggested by the partitioning model of Fisher[*16*], a conclusion also reached by Ragavan and Cohen[*17*].

It is clear that detection and analysis of acoustic emission will play an important role in furthering our understanding of the martensite transformation. It will be particularly useful in obtaining information on the detailed kinetics of the transformation such as nucleation rates, burst phenomenon, and characterization of the volume fraction curve. In contrast to other techniques such as electrical resistivity or dilatometry, acoustic emission gives an almost plate by plate record of the transformation.

Acknowledgments

The skillful assistance of A. J. Schwoeble with the experimental phase of the work and helpful discussions with J. S. Lally, both of this laboratory, are gratefully acknowledged.

References

[*1*] Scheil, E., *Zeitschrift für Anorganische Allgemeine Chemie*, ZAACA, Vol. 183, 1929, p. 98.
[*2*] Forster, F. and Scheil, E., *Zeitschrift Für Metallkunde*, ZEMTA, Vol. 9, 1936, p. 245.
[*3*] Dunegan, H. L. and Tatro, C. A., in *Measurement of Mechanical Properties*, Vol. 5, Part 2, Interscience, New York, 1971, p. 273.
[*4*] Fisher, R. M. and Lally, J. S., *Canadian Journal of Physics*, CJPHA, Vol. 45, 1967, p. 1147.
[*5*] Liptai, R. G., Dunegan, H. L., and Tatro, C. A., *International Journal of Non-Destructive Testing*, IJNTA, Vol. 1, 1969, pp. 213-21.
[*6*] Bunshah, R. F. and Mehl, R. F., *Transactions of the American Institute of Mining, Metallurgical and Petroleum Engineers*, TAIMA, Vol. 197, 1953, p. 1393.
[*7*] Magee, C. L., in *Phase Transformations*, American Society for Metals, Cleveland, 1970, p. 115.
[*8*] Liptai, R. G., "Round-Robin Testing of Acoustic Emission Source, *Acoustic Emission*, ASTM STP 505, American Society for Testing and Materials, 1972, pp. 318-331.
[*9*] DeHoff, R. T. and Rhines, F. N., *Quantitative Metallography*, McGraw-Hill, New York, 1968.
[*10*] Machlin, E. S. and Cohen, M., *Transactions of the American Institute of Mining, Metallurgical and Petroleum Engineers*, TAIMA, Vol. 191, 1951, pp. 346-54.
[*11*] Scheil, E. and Norman, W., cited by L. Kaufmann and M. Cohen in *Progress in Metal Physics*, Vol. 7, Pergamon, New York, 1958.
[*12*] Speich, G. R. and Swann, P. R., *Journal of the Iron and Steel Institute*, JISIA, Vol. 203, 1965, pp. 480-5.
[*13*] Wayman, M., in *Advances in Materials Research*, Vol. 3, Interscience, New York, 1968, pp. 147-301.
[*14*] Speich, G. R. and Warlimont, H., *Journal of the Iron and Steel Institute*, JISIA, Vol. 206, 1968, pp. 385-92.
[*15*] Krauss, G. and Marder, A. R., *Metallurgical Transactions*, MTGTB, Vol. 2, 1971, pp. 2343-58.

[16] Fisher, J. C., Hollomon, J. H., and Turnbull, D., *Transactions of the American Institute of Mining, Metallurgical and Petroleum Engineers,* TAIMA, Vol. 185, 1949, pp. 691-700.

[17] Raghaven, V. and Cohen, M., *Metallurgical Transactions,* MTGTB, Vol. 2, 1971, pp. 2409-18.

[18] Entwistle, A. R., *Metallurgical Transactions,* MTGTB, Vol. 2, 1971, pp. 2395-07.

Kanji Ono,[1] *Richard Stern,*[1] *and Marshall Long, Jr.*[1]

Application of Correlation Analysis to Acoustic Emission

REFERENCE: Ono, Kanji, Stern, Richard, and Long, Marshall, Jr., "Application of Correlation Analysis to Acoustic Emission," *Acoustic Emission, ASTM STP 505,* American Society for Testing and Materials, 1972, pp. 152-163.

ABSTRACT: Correlation analysis techniques have been used to characterize acoustic emission pulses from metals. A brief description of correlation functions and the method of their determination is presented. The time varying spectra of a magnesium sample have been obtained using the present techniques, and then compared with the more common methods of measuring acoustic emission. Other uses of correlation analysis in acoustic emission studies are included.

KEY WORDS: acoustics, emission, correlation, nondestructive test, dynamic structural analysis, spectrum analyzers, plastic deformation, strains, stresses, waveforms, magnesium alloys, tension tests

In the past ten years, acoustic emission (AE) from materials and structures has been studied extensively and has emerged as a useful nondestructive testing (NDT) technique. The total numbers and rates of AE have been correlated with such factors as the applied stress, total strain, stress intensity at a crack tip, for a variety of materials. Initially, frequencies in the tens of kHz were detected but now it has become more common to extend the frequency ranges to one or two orders of magnitude higher. While basic knowledge of AE and practical usages of AE technique are expanding, discrimination of AE signals from interfering background noise is still a major obstacle to a wider use of AE in NDT.

A limited number of studies have been made on the characteristics of AE signals[*1-5*]. Hutton[*1*] used visual analysis of oscilloscope traces of AE signals and reported that AE during plastic deformation of a steel has an average

Work was supported by the Office of Naval Research Acoustics Program.

[1] Materials Department, and Mechanics and Structures Department, respectively, School of Engineering and Applied Science, University of California, Los Angeles, Calif. 90024.

frequency of 5 kHz for the continuous emission and 20 kHz for the burst emission. On the other hand, AE during ductile fracture has a frequency content in the 40 to 50 kHz range. Brittle fracture produces a burst signal and its frequency content extends from 200 kHz to megahertz ranges. Since AE is a nonstationary random signal, lasting a few hundred ms, quantitative analysis of AE signals is difficult with conventional spectrum analyzers. Typically, a frequency spectrum analyzer is in essence a narrow bandpass filter with a sweeping center frequency. The fastest sweep speeds are on the order of ms so that only a limited segment of AE signals are sampled to represent any given frequency range. Results can hardly be regarded as the frequency spectrum of an AE signal. Simultaneous passage of an AE signal through many narrow band filters can overcome this difficulty[*6*]. However, a set of sampling frequencies cannot be changed easily and the number of channels is limited because of cost.

The aims of the present study are: (a) to utilize correlation analysis methods in order to obtain the frequency content of AE signals; (b) to explore the potential of this method as a new NDT technique; and (c) to investigate the physical processes of AE from various materials. The correlation analysis method has been developed in modern information theory and in dynamic structural analysis[*7,8*]. It is extremely useful in the analysis of random phenomenon, especially when the total input may contain very low level signals within some particular frequency region, plus much larger noise at other frequencies. This paper presents a brief summary of pertinent correlation analysis methods, both theoretical and experimental, and describes their application to frequency spectrum analysis of AE signals. Results as well as potentials of this method will be discussed.

Random Signal Analysis

Like many natural phenomena, AE from a material is a random process. An AE signal is nonperiodic, contains many frequencies, and cannot be described by an explicit mathematical relationship. Even when specific voltage time data have been determined, future values cannot be predicted. Random AE signals can be characterized, however, by their statistical or average properties, which include mean square values, probability-density functions, autocorrelation functions, and power density functions. The mean square value is the average of the squared values of the time history and describes the intensity of the signals. The probability-density function describes the probability that the signals will assume a value within some defined range at any instant of time. The last two functions, autocorrelation and power density functions, are most important for our discussions.

The autocorrelation function describes the general dependence of the values of the signals at one time on the values at another time. It involves the comparison of a signal waveform (or a sample time history), $x(t)$, against a

delayed version of the same waveform. Particularly, a value $C_x(\tau)$ of the autocorrelation function of $x(t)$ can be obtained by averaging the product of the values of $x(t)$ and those of $x(t + \tau)$ over the observation time from $t = 0$ to $t = T$. To be exact, T must approach infinity. In equation form, the autocorrelation function at a given delay time τ is given by

$$C_x(\tau) = \lim_{T \to \infty} \frac{1}{T} \int_0^T x(t)\, x(t + \tau)\, dt \tag{1}$$

The values of $C_x(\tau)$ are always real, but can be positive or negative. C_x is even and always has a maximum at $\tau = 0$, but may also have additional maxima. $C_x(0)$ is equal to the mean square value of $x(t)$, and $C_x(\infty)$ gives the mean value of $x(t)$.

The power density function (or power per cycle) of the signal $x(t)$ indicates the contribution of each frequency component to the total power. For a small frequency interval Δf, the power density function, $D_x(f)$ can be defined such that $D_x(f) \cdot \Delta f$ is equal to one-half the mean square value of $x(t)$ in a frequency range between f and $f + \Delta f$. Such mean square values can be obtained by filtering $x(t)$ by a band pass filter and computing the average of the squared output from the filter. Strictly, Δf must approach zero, in order to define $D_x(f)$.

The two functions, $C_x(\tau)$ and $D_x(f)$, for a stationary signal $x(t)$, are related by a Fourier transform and its inverse as follows:

$$D_x(f) = \int_{-\infty}^{\infty} C_x(\tau) \exp(-i \cdot 2\pi f \tau)\, d\tau \tag{2}$$

$$C_x(\tau) = \int_{-\infty}^{\infty} D_x(f) \exp(i \cdot 2\pi f \tau)\, df \tag{3}$$

It can be seen that they contain the same information and that if one is known, the other can be calculated. It is important to note that $D_x(f)$ is given over both positive and negative frequencies, while an experimentally determined power density spectrum covers only positive frequencies. Thus, the former has values twice those of $D_x(f)$ for $f \geqslant 0$ and its integral over positive frequencies gives the mean square value of $x(t)$, that is,

$$\langle x^2 \rangle \equiv \lim_{T \to \infty} \frac{1}{2T} \int_{-T}^{T} x^2(t)\, dt = \int_0^{\infty} 2\, D_x(f)\, df \tag{4}$$

In our attempt to characterize AE signals, the autocorrelation functions will be determined and subsequently the power density spectra of various types of

AE will be deduced. By nature, AE is usually associated with irreversible processes such as plastic deformation and fracture in solids and is dependent on prior deformation, applied stress, etc. Consequently AE signals from a single specimen are nonstationary and their statistical properties vary with time, loading history etc. On the other hand, when a large number of tension tests are performed using metallurgically identical specimens (allowing for statistical variations in the compositions, microstructures and heat treatment), the AE signals emitted from one of the specimens at a given stress level may be considered as a sample record. It is reasonable to assume that the collection of all such sample records at the stress level form a set and can be regarded as a stationary random process. Until this is proven experimentally by performing a large number of tests or shown to be false, it forms the basic assumption in our approach to AE signal analysis. AE signals from a single specimen can be considered as a series of sample records that vary as a function of stress or strain. Where the sample records vary slowly with deformation and when a sufficient averaging time is allowed, reasonably good approximations of the statistical functions may be determined in a single test.

The determination of $C_x(\tau)$ is often a cumbersome procedure and is very difficult in the frequency range of interest to AE techniques. This is mainly due to the requirement that one treat a large number of digitized data points. For example, consider the analysis of a typical signal in the range of 50 to 250 kHz. According to the Nyquist theorem, the sampling rate must be at least 500 kHz and a data record 1 s long consists of 5×10^5 points. To evaluate 100 values of $C_x(\tau)$ on line requires 5×10^7 multiplications per second, a rate of data processing yet impractical. It should be noted that direct digital Fourier transform of the data record would utilize the whole core storage space of a large general purpose computer and the processing time is on the order of 100 s. This method cannot be practically used for AE signal analyses at the present time. Recently, several correlation analyzers have been developed commercially utilizing either analog or digital circuitry or both. Typically 100 values of C_x are computed simultaneously and the resolution of delay time, $\Delta\tau$, ranges from 100 ns to 1 μs and greater. When repeated processing of input data is possible or when a respectively), and a larger number of C_x values provide naturally a better be adopted to obtain 1000 to 10,000 values of C_x. A smaller delay time increment will allow the analysis of higher frequency signals (for example, maximum frequency is 5 MHz and 500 kHz for $\Delta\tau$ of 100 ns and 1 μs, respectively), and a larger number of C_x values provide naturally a better definition of the correlation and power density functions. The averaging time, T in Eq 1, is another important parameter. Theoretically, T should approach infinity. In practical measurements of C_x, T must be reasonably short so that possible changes in C_x as a function of other parameters can be detected. However, T should be long enough so as to define statistically meaningful values

of C_x. In a digitally averaged instrument, the selection of different values of T can be done easily over a wide range (for example, 36 ms to 10^7 s), but is limited or is very difficult in an instrument that utilizes RC averaging. In AE signal analysis, a useful range of T appears to be on the order of tenths of a second. In order to obtain power density spectra, Fourier transforms must be performed on C_x. Either a hard wired Fourier analyzer or a properly interfaced digital computer can be employed for this task. While the former is simple to operate, the latter can be programmed to store the results and to perform various postcomputational analyses.

Experimental Procedures

In this study, AE signals emitted during deformation of a commercial magnesium alloy were analyzed. The alloy contains 3 percent Al and 1 percent Zn and is designated as AZ31B. Half-sized ASTM standard sheet tension specimens were machined using a Tensilkut cutter. The reduced section was 1.2 in. long and the cross section was 0.23 by 0.068 in. The alloy was in an annealed (–0) condition. The average yield strength (0.2 percent offset) of 10 specimens was 21 ksi and the average tensile strength was 36.5 ksi. The average uniform elongation was 21 percent. All the tension tests were performed using an Instron at room temperature and a nominal strain rate of 2.8×10^{-4}/s.

Two AE test systems were used. One of them was made by Dunegan Research Corporation (DRC) and consists of a piezoelectric transducer (S140B), a preamplifier (S/D-60), a combined amplifier totalizer and an X-Y recorder. The use of the DRC system provides base AE data that can be compared to conventional AE testing elsewhere. The other system consists of the same transducer, a low noise preamplifier (AD-YU Electronics, A102E), amplifiers and a high pass filter. The output of this broad band (BB) system was fed directly to a correlation analyzer-Fourier analyzer combination (Progress Electronics of Oregon, 810A and 825A). The time constant of the averaging of correlation function output was 0.5 s. This implies that an observed power density spectrum represents the averaged spectrum covering the period of approximately 1.0 s prior to the measurement. The voltage gain of the two systems, DRC and BB, was in the range of 80 to 120 dB. The nominal bandwidth of the DRC system was 100 to 300 kHz and that of the BB system was 50 to 500 kHz at 3 dB down. The high frequency limit of the latter is due to the limitation of two input amplifiers of the correlation analyzer.

Results and Discussion

System Characterization

The transfer function or system response of an electrical circuit can be determined by taking the Fourier transform of the autocorrelation function of

the output, when white noise is introduced to the circuit input. The overall electrical system response, including the input amplifier of the correlation analyzer, but excluding the piezoelectric transducer, is shown in Fig. 1. A random noise generator (General Radio 1390B) provided white noise with a flat frequency spectrum between 1 kHz and 5 MHz. The results indicate that the electrical system responses of the two systems are essentially flat within their respective nominal bandwidth. While other methods of measuring a frequency response are readily available, correlation analysis provides a rapid and simple

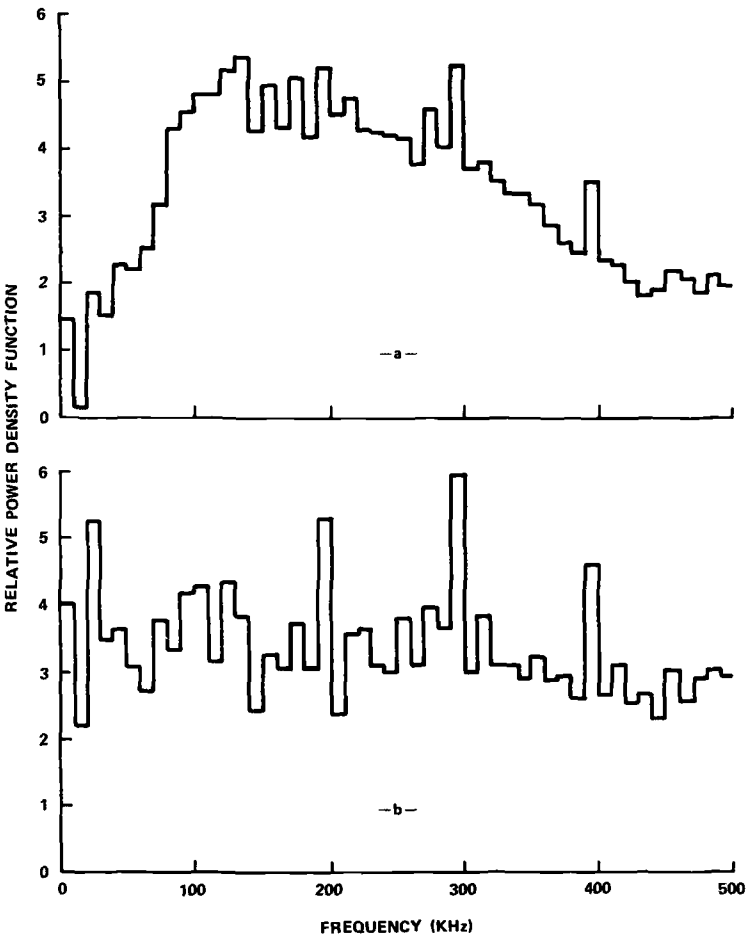

FIG. 1—*Electrical system response of two systems (peaks appearing at multiples of 100 kHz are switching errors in the correlator and should be ignored):* (a) *DRC system;* (b) *broad band system.*

means of assuring the proper working condition of an electrical system. The peaks that appear at multiples of 100 kHz are due to switching pulses between each group of 10 correlation points in the correlator. However, they are not inherent in the system, and can be eliminated. (These peaks also appear in Figs. 2 and 4).

Characterizing a transducer is a more difficult task, since a calibrated source of acoustical white noise is not readily available in the frequency range of interest. Chambers' silicon carbide noise source [9] appears to fulfill this need and will be examined. Uncalibrated white noise was generated by scratching a transducer or a specimen with a fine emery paper in the present study. Figure 2*a* shows the power density spectrum as detected by a free transducer (DRC-S140B) and amplified by the BB system. The resonance peak at 140 kHz is very prominent and another peak at 80 kHz is clearly shown. The slightly negative values of the power density function appear to arise from the baseline noise of the analyzer combination and are negligible when a high signal to noise ratio is provided. Figure 2*b* illustrates the effects of loading the transducer. In this case, the transducer is bonded to a magnesium tension specimen by a viscous liquid supplied by DRC. A drastic decrease in the resonance peak height and a frequency shift from 140 to 160 kHz are observed. The peak at 80 kHz is

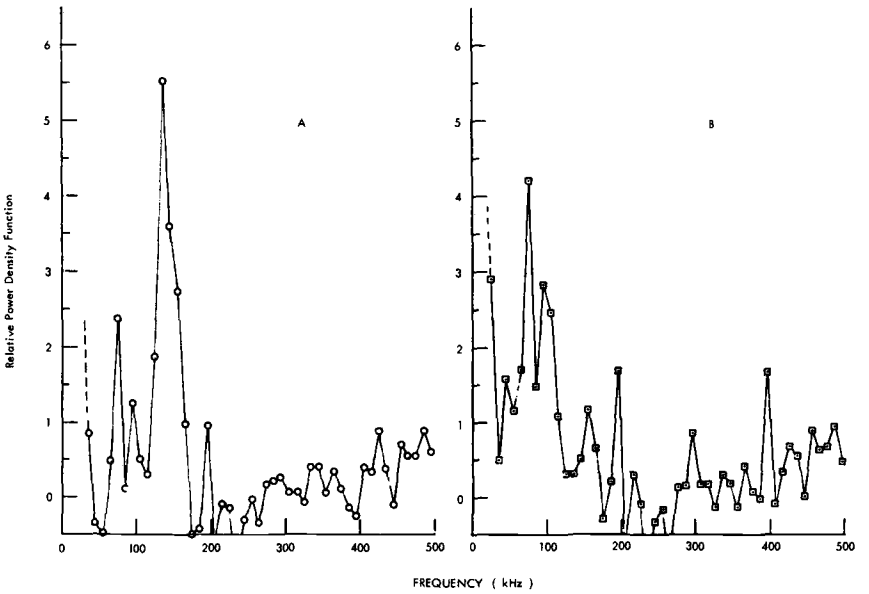

FIG. 2—*Transducer response to wideband acoustical noise (disregard peaks appearing at multiples of 100 kHz);* (a) *a free transducer;* (b) *identical transducer bonded to a magnesium alloy tension specimen.*

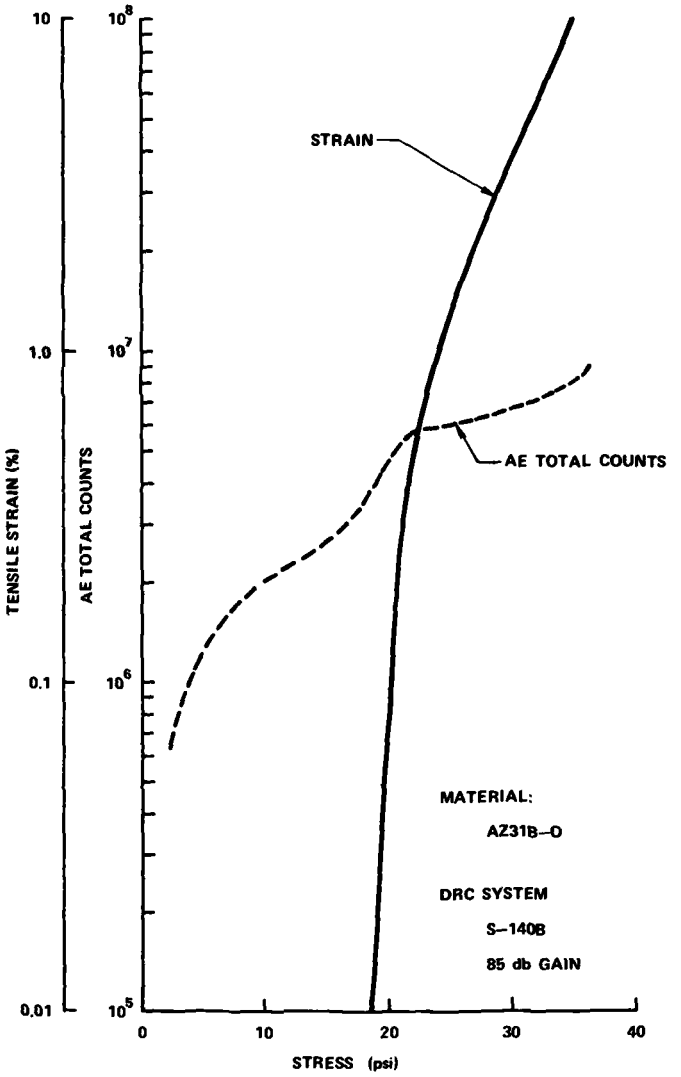

FIG. 3—*Tensile strain and AE total counts versus tensile stress. The DRC system set at 85 dB gain was used to obtain the AE data.*

relatively unaffected by the loading, suggesting that this peak is due to a different vibration mode of the transducer.

These observations indicate that the correlation method is suitable for characterizing a transducer as well as the quality of bonding. Thus, a calibrated white noise source together with the correlation analysis method provides a rapid evaluation of the total system. Reproducible (but not necessarily

calibrated) noise sources and a correlation analyzer can be employed for periodic on-site inspection of bonded transducers.

Acoustic Emission Analysis

Magnesium and its dilute alloys twin profusely during plastic deformation, and consequently produce a large number of AE signals. For reference, Fig. 3 shows the stress-strain relation of a typical magnesium alloy specimen, and the total count of AE as determined by the complete DRC system. The AE activity was the highest just below the yielding.

The power density spectra of AE signals at six different stress levels during plastic deformation of another magnesium specimen are shown in Fig. 4. (It must be pointed out that the representation of power density functions in Fig. 1 is accurate and preferable to that in Fig. 4, since a value of power density function covers a finite frequency range, Δf. In these cases, Δf = 10 kHz.) It is most evident that the power density spectra of the AE signals are quite similar to that shown in Fig. 2*b*. In all cases, the main transducer resonance peak at 160 kHz is always the highest. As the applied stress is increased, the other peak at 80 kHz starts to become stronger. At the applied stress of 18.7 ksi, the height of 80 kHz peak reaches 60 percent that of the main peak. At higher stress levels, the dominance of the 160 kHz peak is again the main characteristic. The relative changes in heights of two resonance peaks are shown in Fig. 5. It should be

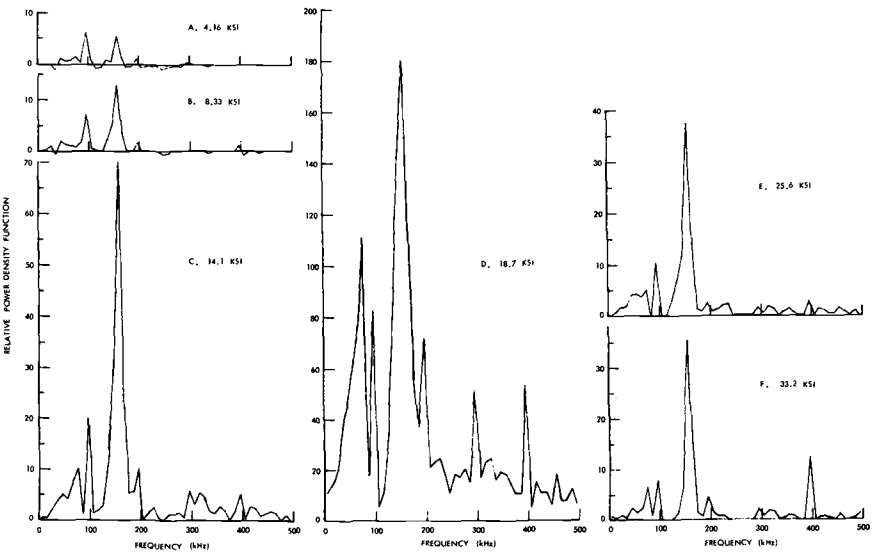

FIG. 4—*Power density spectra of AE from a magnesium allow specimen at different stress levels (disregard peaks appearing at multiples of 100 kHz.)*

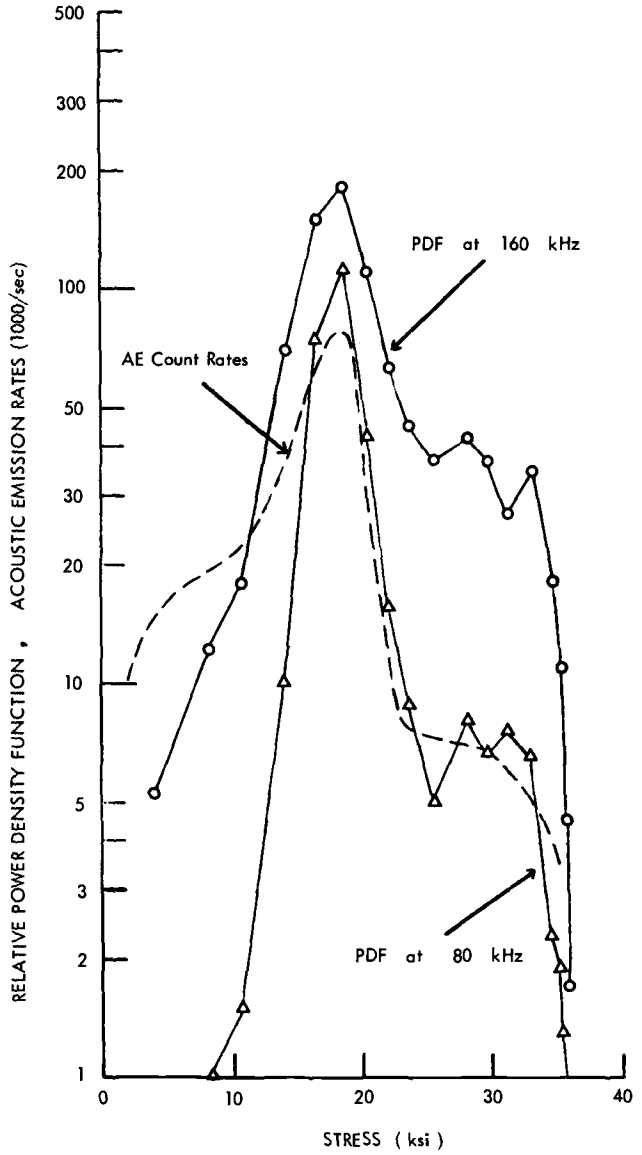

FIG. 5—*Power density functions at 80 and 160 kHz against applied stress. The dashed line represents AE count rate data.*

noted that the DRC amplifiers are bandlimited from 100 to 300 kHz, and the activity at 80 kHz would not be added to the total count as registered on the "totalizer." Indeed, frequency shifting of the AE within the bandwidth would produce false readings. The values of the power density function at 160 and 80 kHz reach a maximum just before reaching the yield stress. In the work hardening stage (22 to 33 ksi), they remain relatively unchanged. Upon reaching the tensile strength (36 ksi), the AE activity subsides almost completely as indicated by a sharp drop in the power density function at both frequencies. Figure 5 indicates clearly that the lower frequency components of the AE signals increase near yielding. It is quite plausible that the PDF stress curves are composed of two parts, one of which corresponds to AE near yielding and contains stronger low frequency components. The other part contains a stronger high frequency component and increases gradually with stress, producing a maximum in the power density function at stress levels of 25 to 30 ksi.

The AE count rates were determined from the AE count data presented in Fig. 3. The count rates are plotted against stress by a dashed line in Fig. 5. Although the count rate and power density function data were obtained from different specimens, the general stress dependence of the AE count rates is similar to that of the power density functions. At low stress levels, however, the ratios of the AE count rate to the peak rate are high in comparison to the corresponding ratios of the power density functions.

The experiments reported here will have to be repeated with a wide band transducer in order to gain knowledge of true power density spectrum of AE signals, and subsequently to understand mechanisms of AE. However, the above results have amply demonstrated that the correlation analysis approach is a valuable tool in revealing the nature of AE from various sources. Currently, many aspects of AE such as the effects of resonant frequency and quality factor of transducers, modes of vibration, coupling and external damping of both tension specimens and transducers, are being evaluated. Attempts will be made to establish the origins and mechanisms of several types of AE, including those due to plastic deformation and fracture processes of low and high strength steels, precipitation and solution hardened alloys and composites.

References

[1] Hutton, P. H., *Materials Evaluation*, MAEVA, Vol. 26, 1968, pp. 125-129.
[2] Dunegan, H. L. and Tatro, C. A. in *Techniques of Metals Research*, Vol. 5, Part 2, R. F. Bunshah, Ed., Wiley, New York, 1971, pp. 273-312.
[3] Fisher, R. M. and Lally, J. S., *Canadian Journal of Physics*, CJPHA, Vol. 45, 1967, p. 1147.
[4] Engle, D. M. and Tatro, C. A., *Journal of The Acoustical Society of America*, JASMA, Vol. 41, 1967, p. 321.
[5] Chambers, R. H., ARPA Semiannual Report, Sept. 1969-April 1970, University of Arizona, Tucson, Ariz., 1970.

[6] Chambers, R. H., Symposium on Advanced Nondestructive Techniques, Army Materials and Mechanics Research Center, Watertown, Mass., June 1971.
[7] Bendat, J. S., Crandall, S. H., Mark, W. D., in *Principles and Applications of Random Noise Theory*, Wiley, New York, 1958.
[8] Bendat, J. S., Crandall, S. H. and Mark, W. D. in *Random Vibration in Mechanical Systems*, Academic Press, New York, 1963.
[9] Chambers, R. H., ARPA Semiannual Report, March 1968-Aug. 1969, University of Arizona, Tucson, Ariz., 1969.

Yosio Nakamura,[1] *C. L. Veach,*[1] *and B. O. McCauley*[1]

Amplitude Distribution of Acoustic Emission Signals

REFERENCE: Nakamura, Yosio, Veach, C. L., and McCauley, B. O., **"Amplitude Distribution of Acoustic Emission Signals,"** *Acoustic Emission, ASTM STP 505,* American Society for Testing and Materials, 1972, pp. 164-186.

ABSTRACT: Acoustic emission signals from slowly growing cracks have been studied experimentally using precracked compact tension specimens of D6ac steel heat treated to several different fracture toughness values but with the same yield strength. The observed signal amplitude is distributed over a range of more than 60 dB, reflecting the statistical nature of the fracture process in a microscopically heterogeneous medium. A clear correlation between the crack growth behavior and the emission amplitude distribution is found. A shift in the amplitude distribution with stress intensity level at a crack tip and a definite difference between the amplitude distribution of emission signals and that of rubbing noise may have direct bearing on the application of the acoustic emission technique as a nondestructive inspection method for materials as well as structural tests.

KEY WORDS: high strength steels, low alloy steels, fracture properties, cracking (fracturing), crack propagation, stress waves, toughness, elastic waves, ultrasonic frequencies, amplitude, emission, energy, fractures (materials), distribution functions, nondestructive tests

In recent years, the acoustic emission technique has been used increasingly for detecting cracks in materials either under test or in service. When one attempts to apply this technique for nondestructively inspecting such complex structures as aircrafts, however, he encounters several problems. The first problem we faced when we started our effort was that of detecting acoustic emission signals buried in an enormous acoustic noise background. To overcome this problem we[*1,2*] developed a series of spatial filtration techniques to eliminate background noise. With these techniques, extremely low level acoustic

[1] Applied Research Laboratory, Convair Aerospace Division, General Dynamics Corp., Fort Worth, Tex. 76116.

emission signals can be detected in a heavy noise environment of aircraft structural tests.

After this first task was accomplished, we realized that we were facing other, more difficult problems. Ironically, the intrinsically high sensitivity of the technique for detecting flaws was the source of one of the problems. Because of the extremely high sensitivity of this flaw detection method, compared with other nondestructive inspection techniques, too many emission signals were being detected, some of which might not be important to monitoring the integrity of the structure. To avoid this problem it would be necessary to provide ways to assess the criticality of cracks emitting these acoustic signals.

The other problem occurred when a noise source such as a bolt rubbing in a bolt hole existed in very close proximity to an acoustic emission source of interest. In this case, the spatial filtration technique could not work effectively, and some other method of discriminating between the two types of signals was needed. When observed individually, the rubbing noise was found to have very similar signal characteristics to those of an acoustic emission signal from a growing crack; thus, it could not be distinguished from the latter in real structural tests.

A clear understanding of both the emission signal characteristics and the mechanism of acoustic emission is mandatory to solution of these problems. Consequently, the primary objective of the present study was to seek emission characteristics which might be useful both to determining the criticality of the crack which emits the signals and to gaining an understanding of the emission mechanisms.

In the present study, compact tension fracture toughness specimens of D6ac steel, heat treated to give various fracture toughness values, were tested, and emission signals were observed and analyzed. Particular emphasis was placed on obtaining amplitude distributions of emission signals. This emphasis was important because the growth of a crack is a nearly stochastic process in which the amount of each growth increment is determined by the balance between the amount of energy required to produce additional crack surface areas and the amount of energy available, both of which have their own statistical distributions along a crack tip in a heterogeneous medium. Since the balance should be influenced by the stress level at the crack tip, some variation of emission amplitude distribution with stress level is expected. The amplitude distribution is also related to the way a crack propagates and for this reason can be expected to supply important data for understanding fracture mechanisms.

After the present study was well under way, reports by Pollock and Radon[*3,4*] came to our attention. These authors studied the amplitude distribution of acoustic emission signals from fractures of mild steels and aluminum alloys. The main difference between their study and ours is that they are concerned with emissions associated with critical crack growths, in amounts

of a few centimeters at a time, occurring when the critical stress intensity level is reached; whereas we are investigating subcritical crack growths of microscopic order, in amounts of a few micrometers to a small fraction of a millimeter, occurring prior to a critical crack growth.

Experimental Setup and Procedures

Specimens

The specimens used for the present experiments were precracked compact tension fracture toughness specimens of D6ac steel plates and forgings. The nominal dimensions of the specimens are given in Fig. 1. The orientation of all the plate specimens was in the RW direction; that is, the crack surfaces were perpendicular to the rolling direction, with the crack front advancing along the width direction of the plate.

The specimens were heat treated in several different ways to give various fracture toughness values and a uniform yield strength in the 1.52 to 1.65 GN/m^2 range. Pertinent data are given in Table 1. All the specimens were fatigue cracked in three consecutively smaller loading levels. The loading range of the

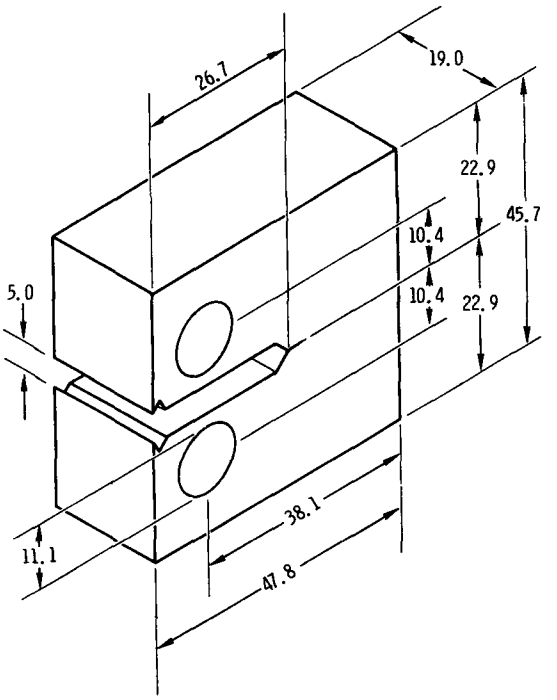

FIG. 1—*Configuration and nominal dimensions, in millimeters, of the specimen.*

TABLE 1—*Heat treat methods for test specimens.*

Specimen	Source Material	Austenitizing Temperature, deg C	Quench Media	Relative Circulation Rate	K_{Ic}, $MN/m^{3/2}$ Target	K_{Ic}, $MN/m^{3/2}$ Measured
34C17	Forging	930	60 C oil	Good	88–110	108.6
7H35	Plate	930	60 C oil	Good	88–110	98.1
3M8	Plate	900	163 C salt	Fair	56–77	86.4
25A33	Forging	900	204 C salt	Fair	56–77	77.7
6L49	Plate	900	204 C salt	Poor	38–55	52.3
30B3	Forging	900	191 C salt	Fair	38–55	39.9

final fatigue cycles was 0.60 to 6.68 kN, corresponding to a range of approximately 1.6 to 17.6 $MN/m^{3/2}$ in the stress intensity factor.

Data Acquisition

The experiments were conducted in two steps: (1) data acquisition and (2) data playback and analysis. Figure 2 is a block diagram of a typical experimental setup for data acquisition. Some minor changes were made from time to time during the course of the study to improve the accuracy of the measurements.

The receiving transducers, lead zirconate titanate plates 1.27 mm thick, polarized in the thickness direction and cut to 5 by 5 mm pieces, were attached

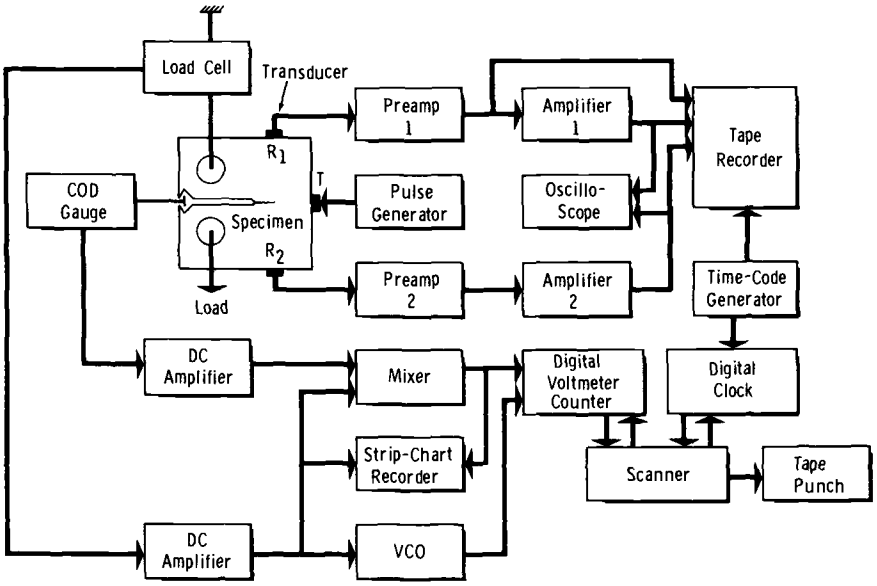

FIG. 2—*A block diagram of experimental setup for data acquisition.*

to the specimen, one directly above and the other directly below the crack front as shown in Fig. 2. High vacuum grease was used to achieve a good coupling to the specimen, and the transducers were fixed in place with adhesive. The specimen was then placed in a tension testing machine having a maximum capacity of 53.4 kN (12,000 lb). The loading pins were wrapped with pipe thread sealant tapes in some cases to reduce friction noise. Small lumps of modeling clay were attached to the specimen at several places to damp out the long train of specimen oscillations following each acoustic emission. The signals from each transducer were amplified by wide band amplifiers and recorded on a magnetic tape. The recording for the upper transducer signals was made in two sensitivity levels in order to cover 60 dB of signal dynamic range. A low frequency cutoff at 100 kHz was provided by the preamplifiers, and the high frequency end of the overall system response was limited at 600 kHz by the tape recorder.

The load level was sensed by a load cell, amplified by a d-c amplifier, and recorded digitally on a punched paper tape. The crack opening displacement was sensed by a NASA type clip gage[5], amplified by a d-c amplifier, mixed with the load signal, and also recorded digitally on the punched paper tape. The mixer is a passive network which mixes two d-c signals in a set ratio. It was adjusted to approximately cancel the initial displacement signal by the initial load signal. By recording the load displacement signal differential rather than the load and displacement signals separately, a high degree of accuracy in the measurement of compliance variations was achieved. The magnetic tape and the punched paper tape recordings were synchronized through simultaneous recordings of a time code.

A pulse generator, an oscilloscope, and a transmitting transducer, T in Fig. 2, also of lead zirconate titanate, were used for checking the operation of the system. The magnet mounted transmitting transducer was removed from the specimen before the specimen was loaded. Throughout the experiment, the specimens were loaded following as closely as possible the ASTM Test for Plane Strain Fracture Toughness of Metallic Materials (E 399 – 70 T). The only exception to this was that the loading rate was maintained below the standard by a factor of three in most cases to avoid an excessive pile-up of acoustic emission signals.

After the setup was completed and the instruments were calibrated, the specimen was first cycled several times with a peak loading well below the final fatigue load. During this time, the load displacement signal mixing ratio was adjusted to obtain a null initial output from the mixer. Immediately following this initial cycling, the specimen was tensile loaded at a nearly constant loading rate of 75 N/s until complete failure occurred. The data were recorded continuously throughout this phase of the test.

The data recorded on a magnetic recording tape, in direct recording mode at a

tape speed of 3.048 m/s (120 in./s), were the following: (1) upper transducer signal at a high sensitivity, (2) upper transducer signal at a low sensitivity, (3) lower transducer signal at a high sensitivity, and (4) IRIG-A time code. Recorded on a punched paper tape, in digital form, were (5) frequency modulated load level signal, (6) load-displacement differential signal, and (7) time.

Data Playback

The data playback was done in three substeps. Setups for these substeps are shown in Fig. 3. The data recorded on a magnetic tape were played back at a tape speed of 1.524 m/s (60 in./s). The lower tape speed was necessitated by the limitations imposed by some of the equipment used for the playback.

In the first step, the output signals from the two matched high gain channels of the tape recorder were filtered through two electronic filters. The filters were adjusted to obtain the best possible signal to noise ratio. This was normally done by using relatively narrow band-pass filters centered around the fundamental resonant frequency of the transducers. In the present experiments, this range was between 100 and 240 kHz, corresponding to 200 to 480 kHz in real time. The filtered signals were applied to the inputs of the coincidence acoustic emission monitor (AEM)[2]. The coincidence AEM is an electronic logic unit which selects only those emission signals which arrive at the two inputs of the unit simultaneously and rejects all others. The unit produces an output pulse only when acoustic emission signals originating within a narrow region enclosing

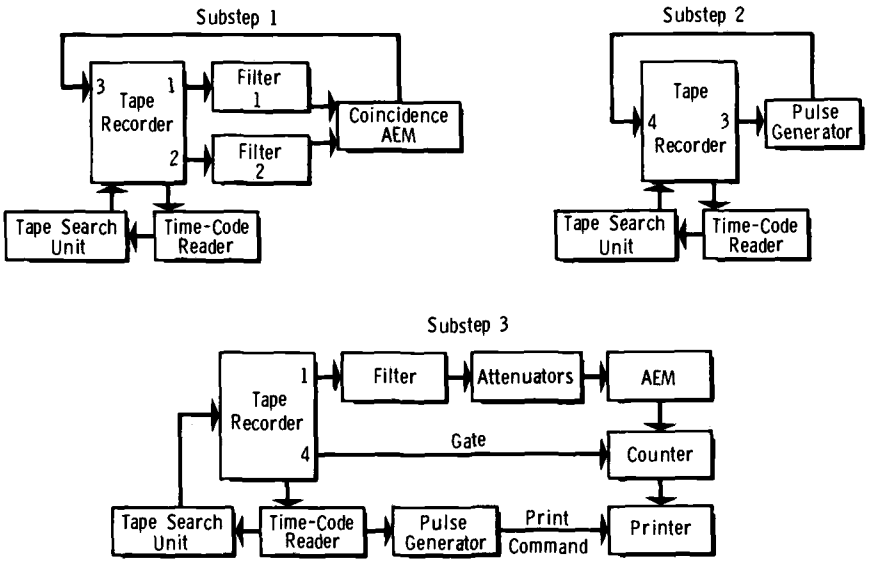

FIG. 3—*Block diagrams of experimental setups for data playback.*

the plane of the crack are detected, except for extremely rare instances when noise signals originating at two locations are detected simultaneously by two transducers. In this manner the unit performed a sort of spatial filtration to reject noise, which was necessary to prevent a large number of noise signals originating at the specimen pin contacts from being detected and contaminating the real emission signals from the crack front. The output pulse from the unit was recorded back on a vacant track of the same recording tape.

In the second step, the tape was turned around, and the pulses recorded in the first step were transferred to another vacant track after being lengthened to an appropriate pulse duration by a pulse generator. This process placed the pulse, which was to be used as a gate pulse in the next step, in the right location relative to the coincident emission signals. This process was necessary because the former pulses were displaced on the magnetic tape relative to the emission signals to which the pulses referred.

In the third step, the recorded emission signals were filtered and after being attenuated by step attenuators, were fed to an AEM unit. This AEM unit is an acoustic emission signal detection unit described by Nakamura[*1*]. Only one channel of the unit was used for this purpose. Used in this way, the AEM unit is essentially an adjustable threshold discriminator having a dead time following each signal detection that is adjusted to be slightly longer than the duration of the signal. Consequently, only one output pulse is produced for each signal train whose maximum amplitude exceeds the set threshold of the unit. This output was then gated by the gate pulse recorded in the preceding step and counted on a counter. The signal trains counted satisfy the following two conditions: (1) their peak amplitude must be greater than a given threshold and (2) they must arrive at the two transducers simultaneously. The accumulated count was then printed out by a digital printer. Periodic printouts of the data were controlled by the time code recorded on the tape. This process was repeated for each 3-dB step of the attenuator settings and for each of the high and low sensitivity channels, covering the entire usable range of the recorded signals.

Crack Growth Calculation

The amount of crack growth was calculated from the load-displacement differential data. The load-displacement differential, which is an accurate measure of the change of compliance of the specimen, yields an apparent crack growth. The apparent crack growth is the sum of the increment of the plastic zone radius at the crack tip and the amount of real crack growth. Since the former can be calculated from the stress intensity factor and the yield strength of the material, the latter can be obtained from the load-displacement differential data. Because the load-displacement differential is very sensitive to the change of compliance, a very small amount of crack growth, on the order of 10 μm, can be detected. A detailed derivation is given elsewhere[*6*].

Experimental Results

Crack Growth Behavior

The apparent crack growths of the specimens calculated from the change of compliance are shown in Fig. 4. The broken line indicates the increment of the plastic zone radius. The horizontal line at $\delta_a = 360\,\mu m$ corresponds to the 4 percent offset line on a conventional load-displacement diagram.

The crack growth behaviors of specimens 34C17 and 7H35 were similar to each other. The apparent crack growths of these specimens closely followed the increment of the plastic zone radius up to around $K_I = 70$ MN/m$^{3/2}$, and then deviated from it above this stress intensity level, indicating that an appreciable real crack growth started at this level and increased rapidly thereafter. Specimen 25A33 behaved in a similar manner except that the entire apparent crack growth curve was shifted somewhat towards smaller stress intensity levels.

The crack growth behaviors of specimens 3M8 and 6L49 were similar to the initial portions of the first two specimens. These two specimens, however, failed before the real crack growth became appreciable. Specimen 30B3 behaved differently from all the others. This was the only specimen which showed sudden increases of crack length with associated audible sounds before the final failure.

Electron micrographs of the crack surfaces just beyond the initial fatigue

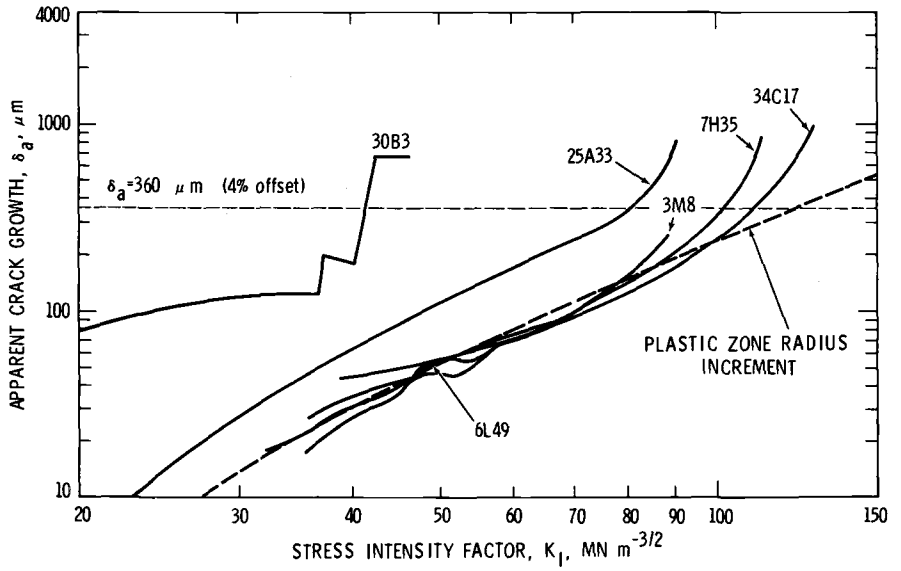

FIG. 4—*Apparent crack growths calculated from compliance of specimens.*

band, which represent the zone of slow crack growth, are reproduced in Fig. 5. Note that the fracture mode ranges from almost complete ductile, or dimple, fracture for specimen 34C17, to almost complete brittle, or cleavage, fracture for specimen 30B3.

Emission Count

Oscilloscope photographs of a typical acoustic emission event observed by the two transducers appear in Fig. 6. In the upper photograph, the entire signal is

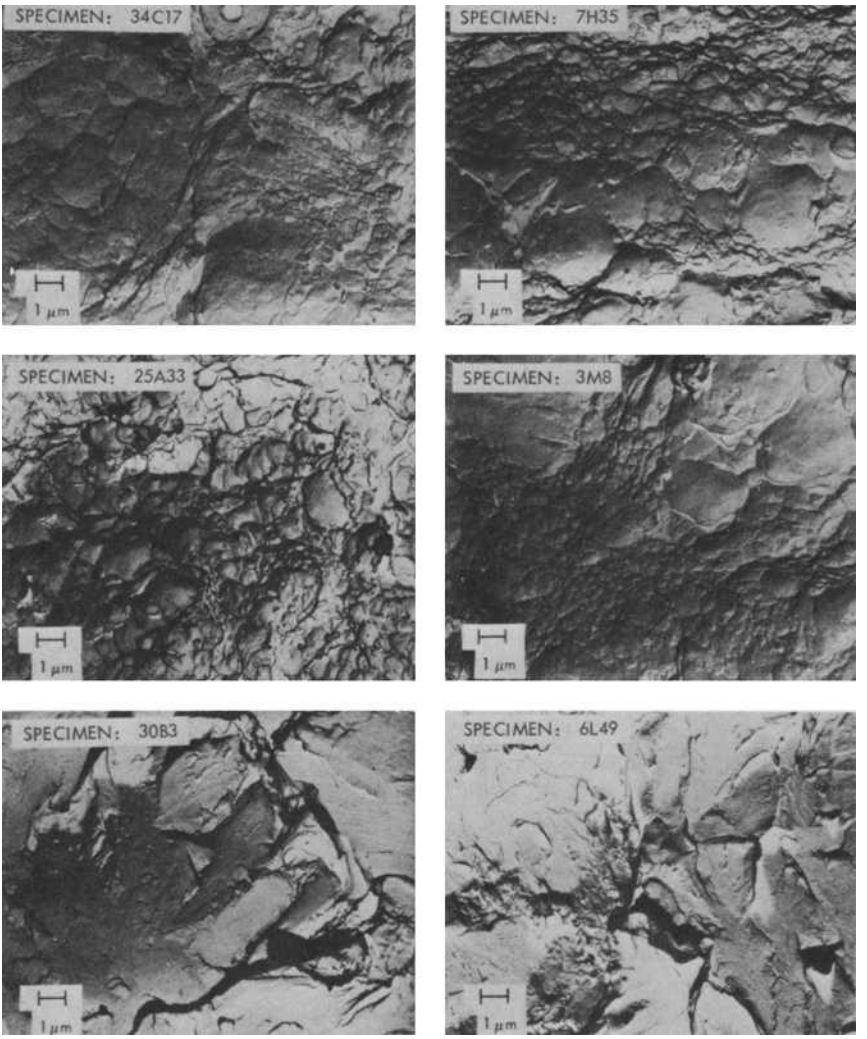

FIG. 5–*Electron micrographs of crack surfaces just beyond the fatigue zone.*

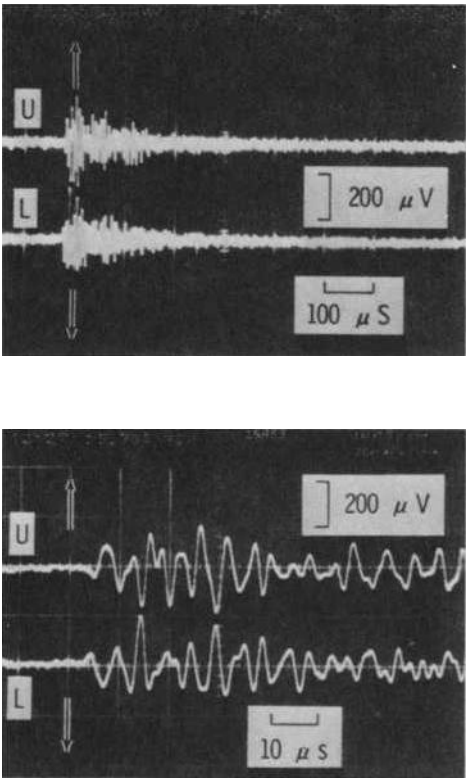

FIG. 6—*Oscilloscope photographs of typical acoustic emission event (specimen 25A33 at* K_I *= 62.5* $MN/m^{3/2}$*). U = upper transducer signal; L = lower transducer signal. Arrows indicate the direction of compressional force on the transducers.*

shown in a compressed time scale. The signal decay time of 100 to 200 μs is typical for a specimen of this size damped by modeling clay. If modeling clay were not attached, the specimen would vibrate for several milliseconds. In the lower photograph the beginning portion of the same signal is shown in an expanded time scale. The signal is observed in opposite phase between the transducers because of the opposite polarities of the two transducers.

In Fig. 7, the cumulative number of coincident acoustic emission events, which is the number of events originating around the crack plane, is plotted against the stress intensity factor at the crack tip. The dB figure on the right-hand side of each curve indicates the detection sensitivity; that is, each curve indicates the cumulative number of emission events of peak amplitudes greater than a certain given dB above 10 μV at the preamplifier input. The stress intensity factor is corrected for the amount of apparent crack growth.

These curves generally approach straight lines on these log-log plots. No clear

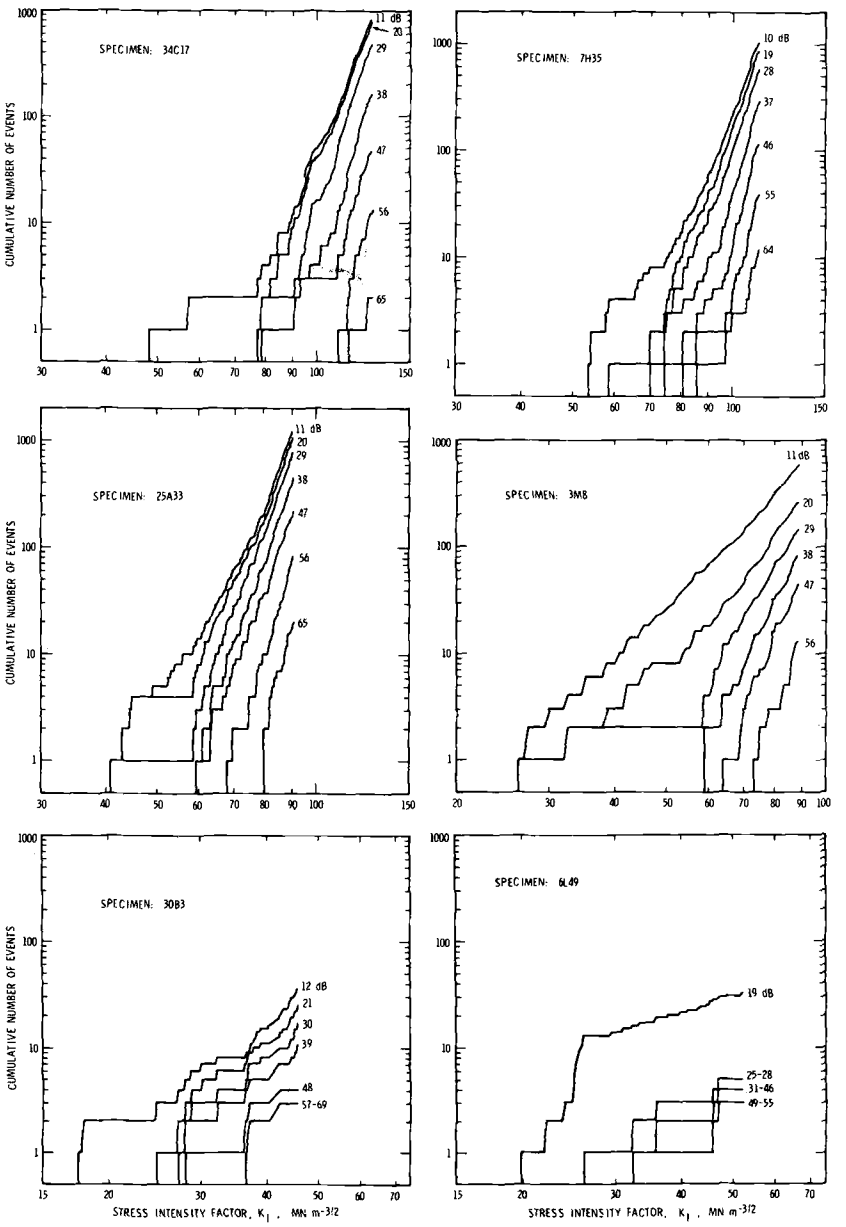

FIG. 7—*Cumulative number of acoustic emission events versus stress intensity factor, with detection threshold as a parameter. The detection threshold is given in decibels above 10 μV at the preamplifier input.*

deviations from a straight line are observed even when the critical stress intensity level is approached. This means that the cumulative number of emission events is nearly proportional to a constant power of the stress intensity factor. This power factor, however, varies from one specimen to another and also varies with the threshold of detection. The observed ranges of the power factors are listed in Table 2. Usually the power factor tends to increase with the increasing amplitude of emission signals, indicating that there are proportionately larger numbers of large amplitude emissions at greater stress intensity levels.

There is a definite correlation between the emission behavior and the crack growth behavior. Those three specimens which showed a large amount of slow crack growth, namely, specimens 34C17, 7H35, and 25A33, showed a rapid increase of the number of emission events starting at approximately the stress level where the crack growth curve deviated from the plastic zone radius curve. The other three specimens, which did not show appreciable slow crack growths, showed a relatively gradual increase of the number of emission events with increasing stress intensity factor, starting at a relatively low stress level compared with the other three specimens.

Amplitude Distribution

The amplitude distributions of emission events are calculated from the cumulative number of events measured at each 3-dB step of detection threshold. The total distributions for all the specimens, or the distributions of all the observed acoustic emission events throughout the slow crack growth up to but not including the final failure phase, are compared in Fig. 8. The abscissas are the peak emission amplitudes in decibels, with 10 μV peak amplitude at the preamplifier input arbitrarily set to 0 dB. The ordinates are normalized for each specimen.

The emission amplitude is distributed over a range of more than 60 dB, that is, the energy ratio of the largest to the smallest signal is more than 10^6. The

TABLE 2—*Power factor*[a] *of cumulative number of emission events with respect to the stress instensity factor.*

Speciman	Power Factor[a]
34C17	12–20
7H35	14–20
3M8	5–15
25A33	12–20
6L49	~3
30B3	~4

[a] Power factor, α, is defined by $N = kK_I^{\alpha}$, where N is the cumulative number of emission events and k is a proportionality constant. Therefore, $\alpha = (d \log N)/(d \log K_I)$.

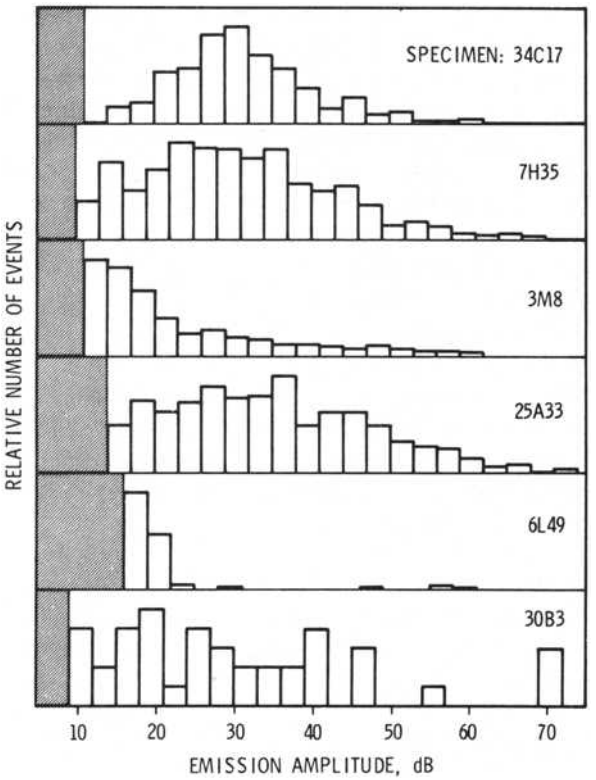

FIG. 8--*Amplitude distributions of acoustic emission events due to slow crack growth. The emission amplitude is given in decibels above 10 μV peak at the preamplifier input.*

correlation between the amplitude distribution and the crack growth behavior is again quite clear. Those three specimens which showed a large amount of slow crack growth, namely specimens 34C17, 7H35, and 25A33, show a peak of the distribution within the amplitude range of the present observation. Of these three specimens, specimen 34C17, which has the highest K_{Ic} of all, has the most distinct peak with almost complete lack of small amplitude emissions.

The two specimens which deviated little from the plastic zone curve in the apparent crack growth behavior, namely, specimens 3M8 and 6L49, have quite different amplitude distributions from the others. Their distributions decrease monotonically with increasing amplitude in this amplitude range, indicating that the major distribution peak is at some amplitude below the detection threshold of the present measurement. The distribution of specimen 6L49 clearly indicates a bimodal distribution with a major peak in the very small amplitude region and a minor peak in the large amplitude region. There are some suggestions of this bimodal distribution in other specimens, although they are not conspicuous.

The distribution function of specimen 30B3 is irregular. This is in agreement with the rather irregular crack growth behavior of the specimen. The peak at the extreme emission amplitude is due to emission events associated with two audible sound emissions which occurred before the final failure of the specimen.

In each diagram of Fig. 9, the change of the emission amplitude distribution

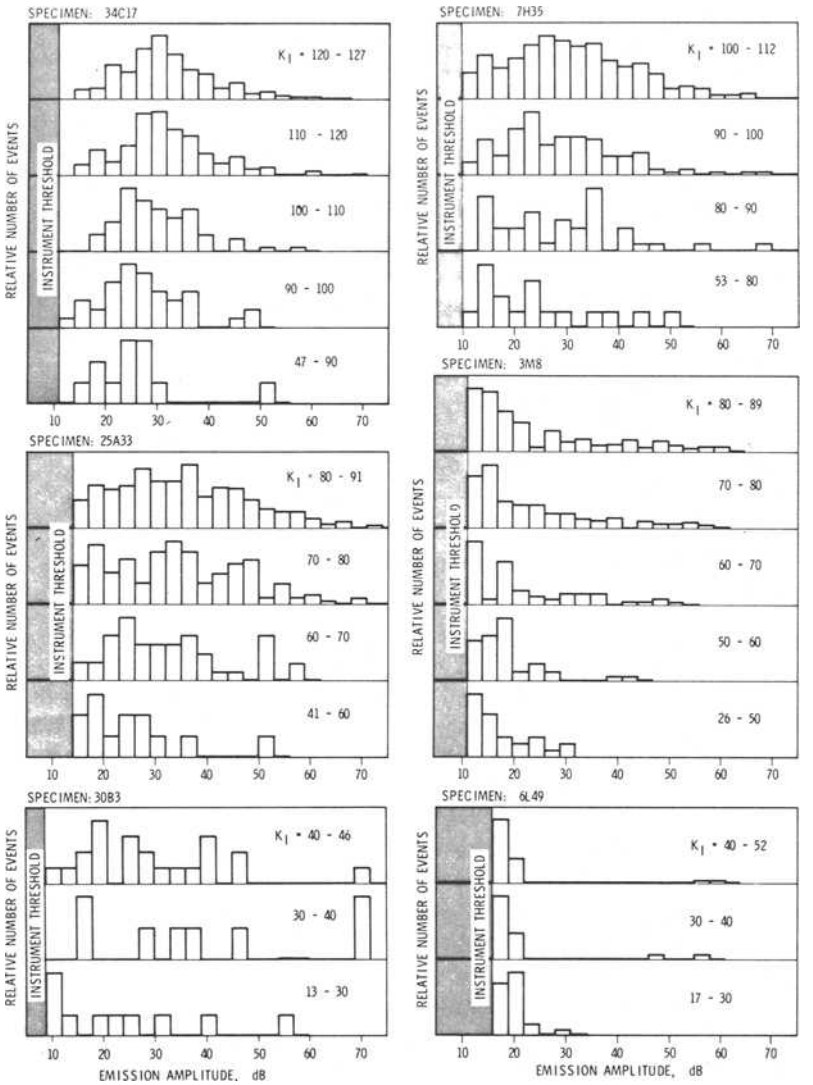

FIG. 9—*The change of acoustic emission amplitude distribution with stress intensity level. The stress intensity factors are given in* $MN/m^{3/2}$. *The emission amplitudes are in decibels above 10 μV peak at the preamplifier input.*

with the stress intensity level at the crack tip is shown for each specimen. The emission amplitude scale is the same as before, and the K_I levels are given in intervals in $MN/m^{3/2}$. The distribution is normalized for each K_I interval. A common trend seen on all of these diagrams is that the peak of the distribution shifts toward larger amplitude emissions as the stress intensity factor increases. The shift is not very large, amounting to 10 to 15 dB, but is consistently observed. The other trend seen in these distributions is that there are proportionately larger numbers of extremely large emissions observed as the stress intensity factor increases. This is also evident in Fig. 7.

Another convenient way of displaying the amplitude distribution data is to use a log-log plot of the cumulative number of events versus amplitude, as is commonly done in seismology. In Fig. 10, the same original data as those for Fig. 9 are plotted in terms of cumulative number of events versus amplitude. The cumulative number of events is the number of events of amplitude equal to or greater than a given amplitude. The curve is a monotonically decreasing function of amplitude and generally can be approximated by one or more straight line segments. The slope of the curve, which is called "*b* value" in seismology, is a manifestation of the amplitude distribution.

The slopes for these specimens are seen to be generally around 1 ± 0.5, although there are exceptional cases like specimen 6L49, where a bimodal distribution produces a step in its plot. One interesting feature of these plots is that the slope tends to decrease as the stress intensity factor increases. This is clear on some specimens, but not so clear on others. The slope changes from around 1.5 at very low stress levels to around 0.5 at stress levels approaching the critical level.

Noise

The results described so far are for acoustic emission signals originating from around the crack tip and detected by the coincidence logic. Even for these simple specimens, the noise generated by a very small mechanical movement of a loading pin relative to the specimen is not negligible. Particularly at a high gain, the noise accounts for more than half of the total number of events observed.

In Fig. 11, the cumulative number of all events, including both emission signals and noise, is plotted against load level at three different detection sensitivity levels. The data are for specimen 3M2, which received the same heat treatment as specimen 3M8, and thus has similar physical properties. Each curve has the same general shape where the cumulative number of events increases linearly with increasing load up to a certain level and then increases rapidly thereafter. The first portion is due almost entirely to the noise originating at the interfaces between the loading pins and the specimen, and the second portion is due both to noise and to real emission signals from the growing crack.

The amplitude distribution of noise signals, namely, those signals rejected by

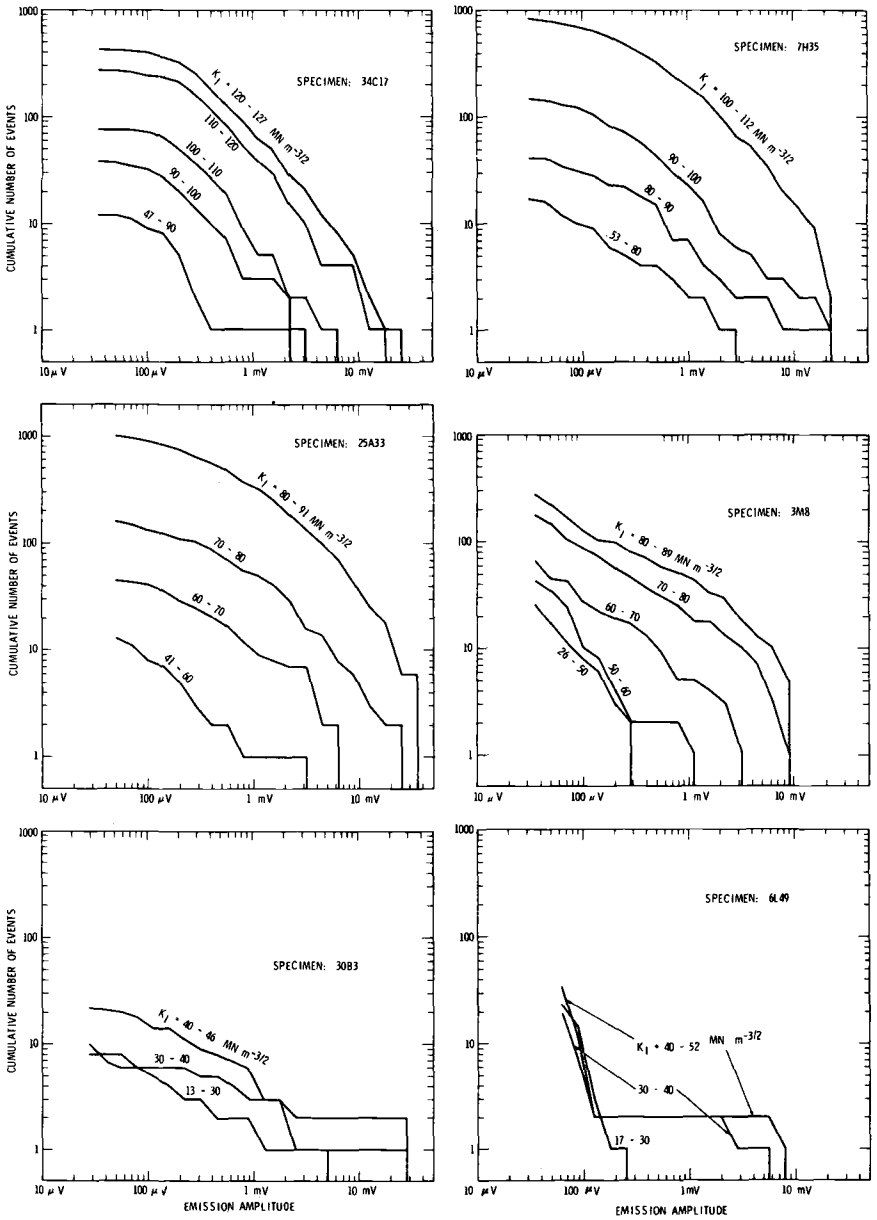

FIG. 10—*Log cumulative distribution of emission amplitude. For details, see text.*

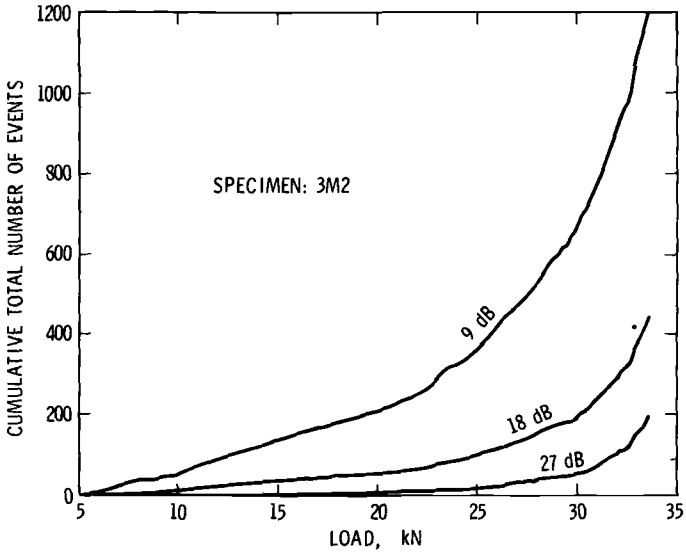

FIG. 11—*Cumulative number of all acoustic events, including both emission signals and noise, versus load level, with detection sensitivity in decibels above 10 μV at the preamplifier input as a parameter.*

the coincidence logic, is shown in Fig. 12 in the same scale used in Figs. 8 and 9. The distribution is clearly different from those of real acoustic emissions. Most noise events are concentrated in the very small amplitude region, indicating that it is emitted in a large number of very small events.

Figure 13 is the log-log plot of the cumulative number of these noise events versus amplitude in the same scales as those used for Fig. 10. These curves show steeper slopes than those for emission signals from crack growths. The slopes of these curves are around 1.5 and do not vary much with increasing load. This is in contrast to a similar plot for acoustic emission signals from crack growths, for which the slope is approximately unity and generally decreases with increasing load level.

Discussion

Before we discuss the physical meaning of the observed amplitude distributions, it is appropriate to consider the relationship between the observed amplitude and the amount of energy released at the crack tip. When a load is applied to a specimen, the supplied energy is first stored in the specimen in the form of strain energy. When this stored energy locally reaches a certain critical level, a sudden redistribution of the energy takes place. This may take place either in the form of a dislocation movement or in the form of a creation or a propagation of a crack in the material. When this happens, a small fraction of the

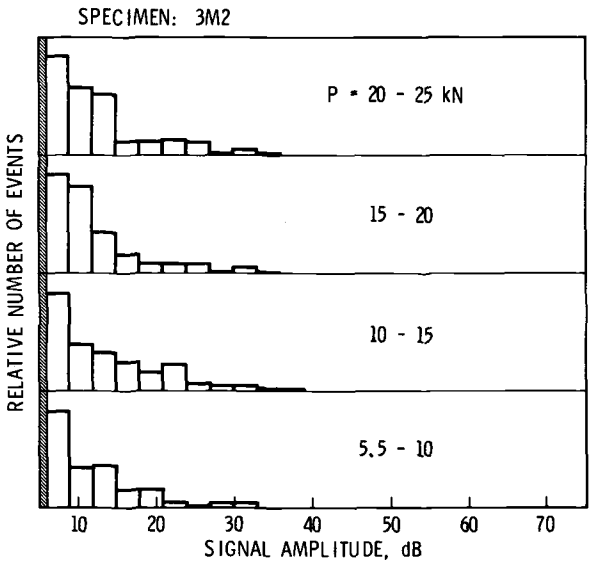

FIG. 12—*Amplitude distribution of noise due to rubbing of loading pin against specimen, at four different load intervals. The signal amplitude is given in decibels above 10 μV peak at the preamplifier input.*

strain energy is converted into acoustic energy, which is emitted from the region where the energy redistribution takes place. Since this initial energy conversion is a process of extremely short time duration compared with the resolution time of the equipment used for observing the acoustic emission signals, the emitted initial acoustic wave can be considered as being essentially a step function in displacement. (A crack propagation of several micrometers will normally take only a few nanoseconds to complete, whereas acoustic emission equipment typically has a time resolution on the order of a microsecond.) The observed acoustic emission signals, however, are not step functions, since several factors contribute to modify the emission waveforms. The major factors are the frequency dependent attenuation of acoustic waves in the material, the finite dimensions of the specimen, and the limited pass band of the acoustic instrumentation. Consequently, what is observed is a narrow band representation of an initially wide band signal.

Even with these restrictions, the observed amplitude can be considered to be a measure of the released energy. This is because, in general, the greater the energy released, the greater the energy observed within a given narrow band of frequencies. Furthermore, the observed amplitude is proportional to the square root of the energy incident on the sensor within the frequency band of the instrument response; thus, the square of the observed amplitude is a rough measure of the energy released at the emission source.

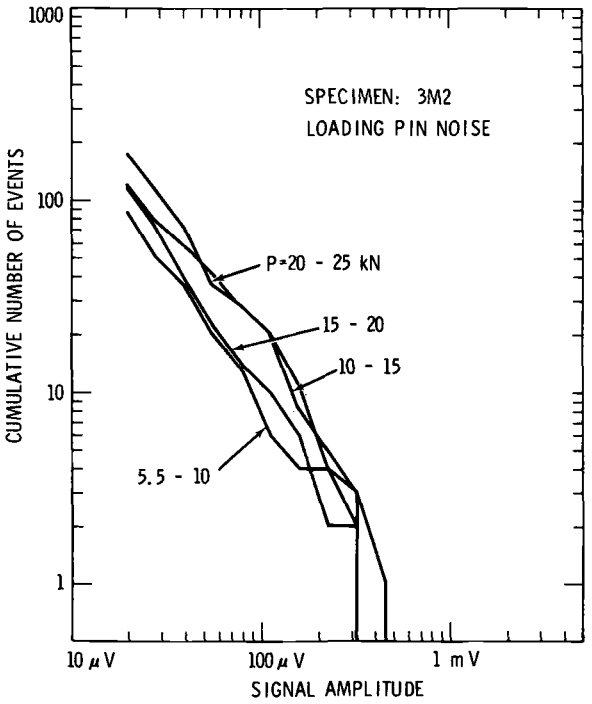

FIG. 13–*Log cumulative distribution of noise events.*

The amplitude distributions observed in this study have a great significance in terms of the fracture properties of the material. The fact that the observed emission amplitudes are distributed over a range of 60 dB or more (10^6 or more in energy range) is evidence that a fracture of a polycrystalline material is essentially a stochastic process. When viewed microscopically, a polycrystalline material is heterogeneous and, thus, the local stresses and strengths of the material are not uniformly but more or less randomly distributed near the crack tip. When the local stress exceeds the local strength of the material somewhere in the crack tip region, a sudden energy redistribution starts and proceeds, until there is no more energy available to sustain this energy redistribution process and equilibrium is reached. How much energy is redistributed and how much energy is released into acoustic energy in a single such process can only be estimated statistically by the heterogeneity of the material.

The observed amplitude distributions, Fig. 8, seem to be classifiable into two groups. One group, represented by specimens 34C17, 7H35, and 25A33, shows a peak of the distribution within the amplitude range of this experiment. This means that a moderate amount of energy can be stored locally in the crack tip

region of these specimens and then released without causing unstable crack growth. The fact that these specimens also showed a large amount of slow crack growth before the final failure agrees with this interpretation. Specimen 34C17, which has the highest fracture toughness of all the specimens tested, shows a relatively narrow peak. This indicated that this specimen has a less heterogeneous and more ordered microstructure than other specimens. The almost complete lack of small amplitude emissions for this specimen is evidence that the energy cannot be released in a small amount, which thus indicates that the material can store a relatively large amount of strain energy without causing a local instability anywhere in the material. The electron micrograph of this specimen shows a completely ductile failure mode.

The other group, represented by specimens 3M8 and 6L49, shows most of the emissions to be concentrated in the very small amplitude region. This means that the material cannot sustain a large amount of energy locally, and a small amount of accumulated energy will cause a local instability, resulting in a small amount of acoustic energy released for each acoustic emission. In contrast to the first group of specimens, which showed very few emissions during the plastic deformation at the crack tip, this group showed emissions starting at a very low stress level. This may be interpreted as a result of brittle cleavages developing in grains in the plastic zone before general crack growth begins. The results of electron fractography support this interpretation. The observation that the cumulative number of very small emissions for specimen 3M8 increases in approximate proportion to the fifth power of the stress intensity factor, which is not too far from the fourth power relation between the volume of the plastic zone and the stress intensity factor, also supports this interpretation[7]. Note that these small emissions at low stress levels are not observed for the first group of specimens. This indicates that the observed emissions are not likely to be from the plastic deformations (dislocations).

The bimodal distribution observed clearly on specimen 6L49, and also less clearly on some others, suggests that two different mechanisms of crack propagations may be taking place in these specimens. We have not yet attempted to interpret this distribution.

Returning to a general discussion of crack growth, consider a case in which slow crack growth occurs when the stress intensity factor at the crack tip is increased from K_1 to K_2. Because of the heterogeneity of the material, the local strain energy level in a given microscopic region near the crack front when the stress intenstiy factor is K_1 has a probability density function of the form shown schematically by curve E_1 in Fig. 14, while the threshold energy level, or potential barrier, at which a local instability occurs has a probability density function resembling curve T of Fig. 14. When the stress intensity factor is increased from K_1 to K_2, the local strain energy level will increase, and the probability density function now takes the form shown by E_2. Then, the

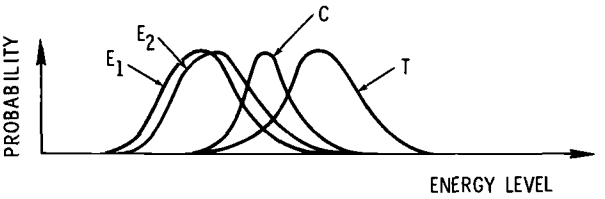

FIG. 14—*A schematic diagram of local energy distributions and threshold. See text for details.*

probability that the local strain energy exceeds the threshold in this region during this interval is given schematically by curve *C*. When this happens, crack growth occurs and proceeds until another equilibrium is reached, at that time the local strain energy will settle to another level. This latter level is nearly independent of the initial energy level except that it is lower than the initial level. The final strain energy level has a probability density function that is almost the same as E_2 because a minute growth of the crack will not change the macroscopic stress intensity level of the crack tip region appreciably. The amount of energy represented by the difference between the initial energy level, whose distribution is given by *C*, and the final energy level, whose distribution is given by E_2, will be released into other forms of energy, and a small fraction of it will be observed as an acoustic emission. Thus it is clear that the acoustic emission amplitude distribution is related to the distributions of the local strain energy level and the threshold level, which, in turn, are determined by the material properties.

The shift of the distribution peak towards larger emission amplitudes with increasing stress intensity factor, which was observed on all of the specimens tested, can be interpreted qualitatively as a result of the progressively larger amount of energy available locally as the stress intensity factor increases. Referring to Fig. 14, when the stress intensity factor increases, curves E_1 and E_2 shift to higher energy levels and so does the peak of curve *C*. If the average shift of curve *C* is greater than that of curve E_2, then a shift of the emission amplitude peak towards higher amplitude emissions will result.

The slope of the log cumulative distributions, Fig. 10, is directly related to the decay of the emission-amplitude distributions on the high amplitude side. Thus it is related to the material property as well as to the emission mechanisms. This slope is found to be generally around 1 ± 0.5 for acoustic emission signals from these specimens. Furthermore, the slope is found to decrease with increasing stress level, from around 1.5 at very low stress levels to around 0.5 at stress levels approaching the critical value. A similar effect was also noted by Scholtz[8] for microfracturing in rocks, which suggests that this effect may be a universal characteristic of brittle fracture. If this is true, it will be feasible to use the amplitude distribution of acoustic emission signals for determining the

criticality of defects in materials and structures under test. The definite difference observed between the amplitude distribution of rubbing noise and that of crack generated emission signals also has a great significance when the monitoring of a bolted structure is attempted.

Concluding Remarks

The present study clearly showed the importance of the amplitude distribution of acoustic emission signals in relation to the fracture properties of D6ac steel. In particular, the difference in the amplitude distribution between high and low fracture toughness specimens is noteworthy in connection with the physical meaning of the toughness of materials. Although only qualitative discussions of the results were attempted in this study, the type of information obtained can readily be used for quantitative interpretation of fracture mechanisms. Thus used, the acoustic emission technique will be a strong tool for the investigation of fracture mechanisms.

The observed shift in the amplitude distribution with stress intensity level at a crack tip indicates a potential use of this type information for nondestructive inspection. The observed difference between the amplitude distribution of emission signals from crack growth and that of rubbing noise will be a useful characteristic for separating significant emission signals from noise in complex structures. More experiments are needed, particularly with several other materials of practical interest, for further confirmation of the present results.

The experimental setup used and the procedures followed are not suited for accumulating data for a large number of other materials because of the extreme amount of time required. An electronic logic unit to take the amplitude distribution data similar to the results of the present experiment in real time has been developed for this purpose and is currently being evaluated.

Acknowledgments

We wish to thank J. W. Hagemeyer for his kind assistance and valuable discussions throughout the present experiment. The electron fractographs were taken and analyzed by Z. R. Wolanski, whose cooperation is also appreciated. This study was supported by an IRAD (Independent Research And Development) program of the General Dynamics Corporation.

References

[*1*] Nakamura, Yosio, *Materials Evaluation*, MAEVA, Vol. 29, 1971, pp. 8-12.

[*2*] Veach, C. L. and Nakamura, Yosio, "Development of Acoustic Emission Monitoring Techniques," in Research Summary ARR-15, General Dynamics, Fort Worth, Tex., 1971 (to be published).

[*3*] Pollock, A. A. and Radon, J. C., "Acoustic Emissions in the Fracture Toughness Test of a Mild Steel," Report FG-26, Department of Mechanical Engineering, Imperial College, London, 1970.

[4] Radon, J. C. and Pollock, A. A., "Acoustic Emissions and Energy Transfer during Crack Propagation," Report FRR-31, Mechanical Engineering Department, Imperial College, London, 1970.

[5] Fisher, D. M., Bubsey, R. T., and Srawley, J. E., "Design and Use of Displacement Gage for Crack-Extension Measurements," NASA Technical Note D-3724, National Aeronautics and Space Administration, Washington, D.C., 1966.

[6] Nakamura, Yosio, Veach, C. L., and McCauley, B. O., "Amplitude Distribution of Acoustic Emission Signals," Report ERR-FW-1176, General Dynamics, Fort Worth, Tex., 1971.

[7] Engle, R. B. and Dunegan, H. L., *International Journal of Nondestructive Testing*, IJNTA, Vol. 1, 1969, pp. 109-125.

[8] Scholtz, C. H., *Bulletin of the Seismological Society of America*, BSSAA, Vol. 58, 1968, pp. 399-415.

C. E. Hartbower,[1] *W. G. Reuter,*[1] *C. F. Morais,*[1] *and P. P. Crimmins*[1]

Use of Acoustic Emission for the Detection of Weld and Stress Corrosion Cracking

REFERENCE: Hartbower, C. E., Reuter, W. G., Morais, C. F., and Crimmins, P. P., "Acoustic Emission for the Detection of Weld and Stress-Corrosion Cracking," *Acoustic Emission, ASTM STP 505,* American Society for Testing and Materials, 1972, pp. 187-221.

ABSTRACT: This paper describes the utility of acoustic emission for the detection of weld and stress corrosion cracking. It includes a brief review of the history of acoustic emission, a selected bibliography, and the findings of two researches. It was found that a 100-ksi yield strength constructional alloy weldment produced bursts of acoustic emission for over 400 h after welding. This acoustic emission was correlated with the amount of cracking as determined by metallographic examination. With acoustic emission instrumentation, a convervative threshhold stress intensity for stress corrosion cracking was determined, based on crack propagation rather than on time to failure. A linear relationship is shown between acoustic emission count and stress intensity factor.

KEY WORDS: acoustics, emission, stress waves, stress corrosion cracking, crack propagation, fractures (material), weld defects, cracking (fracturing), nondestructive tests, acoustic detection

This paper reviews some applications of the acoustic emission technique to the detection of weld and stress corrosion cracking. In the welding of large structures involving high strength structural steel, fabricators sometimes are required to wait several days after welding to assure that cold (delayed) cracking is completed before nondestructive inspection. However, this time period is arbitrary because without the acoustic emission technique, there is no practical way to know when delayed cracking has finished. If the duration of cold cracking could be determined, then the time between fabrication and non-

[1] Associate scientist, senior engineer, liason engineer, and engineering supervisor, respectively, Metallurgy Section, Aerojet Solid Propulsion Company, Sacramento, Calif., 95813.

destructive inspection might be shortened, which would thus shorten the overall production time. Welding engineers are also concerned about the possibility of hot cracking (cracking which occurs above 400 F); if the temperature at which cracking occurs could be determined, it would be possible to gain insight into the mechanism of cracking and consequently have a basis for corrective action. Acoustic emission provides a means of detecting cracking as it happens so that it can be recorded as a function of time and temperature.

There are many other practical applications for a method capable of detecting stress corrosion cracking as it occurs. In a study of the metallurgical nature of slow crack growth in 18 Ni maraging steel, the use of acoustic emission revealed details of the subcritical crack growth process in far greater detail than theretofore possible. The mechanisms of subcritical crack growth under investigation included hydrogen embrittlement, stress corrosion cracking (distilled water at 65 and 165 F) and the combined effect of interstitial solid solution hydrogen and water.

Historical Background

Two Decades of Research and Development

The use of acoustic emission as a nondestructive inspection technique has been under development for approximately two decades. The technique is based upon the elastic energy which is spontaneously released when a material undergoes plastic deformation or cracking or both. In other words, a material undergoing crack growth both generates and transmits a signal (acoustic emission) which can then be detected by suitable instrumentation and whose source can be located by using seismic techniques. In Germany during 1950, Kaiser[*1*] reported what was apparently the first comprehensive investigation of acoustic emission. In the United States, the researches of Schofield et al[*2-4*], and studies at the Aerojet-General Corporation[*5-28*] were largely responsible for triggering the current increased activity in this new field of nondestructive inspection. At the University of California Lawrence Radiation Laboratory Dunegan[*29-32*] also did pioneering work in this area, but most of his early research was for the U.S. Atomic Energy Commission, so it was not publicized. Graduate students at Michigan State University started working in this field around 1960 and are continuing to work with the stress wave emission phenomenon[*33-36*]. Other colleges and universities have also been working with acoustic emission in the last five years[*37-45*].

Application to Stress Corrosion Cracking

In research sponsored by the U.S. Air Force[*14,23*], two particularly noteworthy observations were made: (1) a variation in temperature from 65 F to 165 F had a marked effect on the crack incubation time in distilled water; and

(2) the determination of threshhold stress intensity factor (K_{Iscc}) based on *time-to-failure* tests can be nonconservative for service involving long time exposure to a given stress corrosion environment. Acoustic emission permits the detection of crack incubation and measurement of the secondary incubation time; thus, it can provide a qualitative measure of the crack growth rate. When K_{Iscc} is determined on the basis of crack initiation, it is obviously a more conservative criterion than time to failure, particularly when the time to failure observations are based on test periods that are shorter than the service life. Acoustic emission has revealed cases where the primary incubation time was longer than the usual time to failure test periods. Even more important though, once cracking had begun, sometimes the secondary incubation time was short and failure occurred in much less than the intended service life.

Application to the Inspection of Welds

Notvest appears to be the first to have used stress wave emission in the study of weld cracking. His study was concerned with the crack susceptibility of D6aC steel during and after welding. A piezoelectric transducer attached to the weld plate detected signals associated with weld cracking which were then amplified and tape recorded. Recording was continuous through the welding and postheat cycles. With this technique, cracking was found to be associated with transformation reactions. The test welds were considered crackfree when adjustments in weld procedure eliminated the acoustic emission. The system used by Notvest ". . . was sensitive enough to detect the austenite-to-martensite transformation. . . . Without post heat, acoustic crack indications were detected as soon as the weld zone cooled below 500° F. Increasing preheat only served to delay cracking until an equivalent temperature was reached in the cooling curve. If sufficient weld preheat and post heat was provided, the cooling curve for a weld would intersect the region of bainite transformation and no visible or acoustic crack indications were detected"[*46*].

Jolly[*47*] has described the use of stress wave emission to detect weld cracking in stainless steel. He found that crack growth could be detected during tungsten inert gas welding without interference from the noise of the welding arc. Crack growth sometimes continued from the beginning of weld solidification until the weld approached thermal equilibrium with the welded structure, and the onset of emission occurred 20 to 45 s after the deposited weld metal began to solidify. The rate of emission from single-pass welds was about one order of magnitude less than that from multipass welds. Furthermore, the emission rate increased as the weld cooled; the normalized emission rate reached a maximum at approximately 400 C, indicating that a major portion of the emission in the stainless steel welds was due to hot cracking.

Hartbower[*25*] evaluated weld cracking in HY-80 steel based on stress wave emission. The tungsten arc process was used to produce a multipass square butt

weld with deliberately incomplete penetration to assure cracking. There was no attempt to record stress wave emission during welding. After welding, stress wave activity was greatest in the first seven h, with 7078 counts; in the following 24 h period, there was an increase of only 29 counts and in the next 24 h period there was only one additional count. This suggested that delayed cracking might be completed in approximately three days. However, it was noted that the gross cracking which occurred during welding may have largely stress relieved the weldment and in this way shortened the period of delayed cracking.

Navy Sponsored Study of Weld Cracking

The primary objective of the research described in the following paragraphs was to quantitatively measure the duration of delayed cracking in 100-ksi yield strength weldments as a function of constraint and welding conditions. Weld cracking was induced by use of the cruciform.

The cruciform has been discussed as a test for heat affected zone (HAZ) cracking by Poteat and Warner[*48*], Winterton and Nolan[*49*], and Rathbone et al[*50*]. All welding was done at Mare Island Naval Shipyard to ensure that the findings of the investigation would be representative of shipyard practice and skills. Both manual welding with covered electrodes and semiautomatic welding with the metal inert gas (MIG) process were investigated. With the exception of controlled experiments where the electrode was deliberately exposed to moisture, the covered electrodes were stored in an oven at 250 F up to time of use, in accord with approved shop practice. Moreover, to ensure that the findings would be meaningful in terms of heavy-construction practice, multipass welding was used along with controlled preheat and interpass temperature.

The objectives of the program were met by monitoring the weldments for acoustic emission during and immediately after welding and for periods up to 18 days. Stress wave indications of delayed cracking were subsequently correlated with metallographic findings in selected weldments.

Materials and Welding Procedure

One of the materials investigated in the Navy study was a 100-ksi yield strength constructional alloy supplied in two composition types as shown in Table 1. The weldments were made with both covered electrode and

TABLE 1–*Chemical composition and tensile properties.*

		Composition (Weight percent)											Tension (ksi)	
Heat	Code	C	Mn	P	S	Si	Ni	Cr	Mo	V	Ti	Cu	FTY	FTU
B7748	B	0.15	0.33	0.010	0.019	0.27	2.43	1.35	0.29	0.003	0.001	0.15	105	120
5P3524	P	0.10	0.79	0.005	0.010	0.28	3.36	0.90	0.41	0.09	...	...	110	124

semiautomatic MIG welding. The covered electrode was $^{3}/_{16}$-in.-diameter MIL-12018, and the bare electrode used in MIG welding was $^{1}/_{16}$-in.-diameter MIL-Type B88. Shop procedure calls for a maximum energy input of 55,000 J/in. of weld in thicknesses of ½ in. or greater. The welds were preheated to 150 F and the interpass temperature was held at approximately 250 F. Tack welding was not used; the weldments were dogged to the work table as shown in Fig. 1. Welding was done in a systematic manner, always proceeding from A to B to C to D (see Fig. 1) in accord with Army Ordnance procedure.

Acoustic Emission During and Immediately After Welding

One objective of this study was to determine the feasibility of using the stress wave analysis technique (SWAT) as a supplementary nondestructive inspection

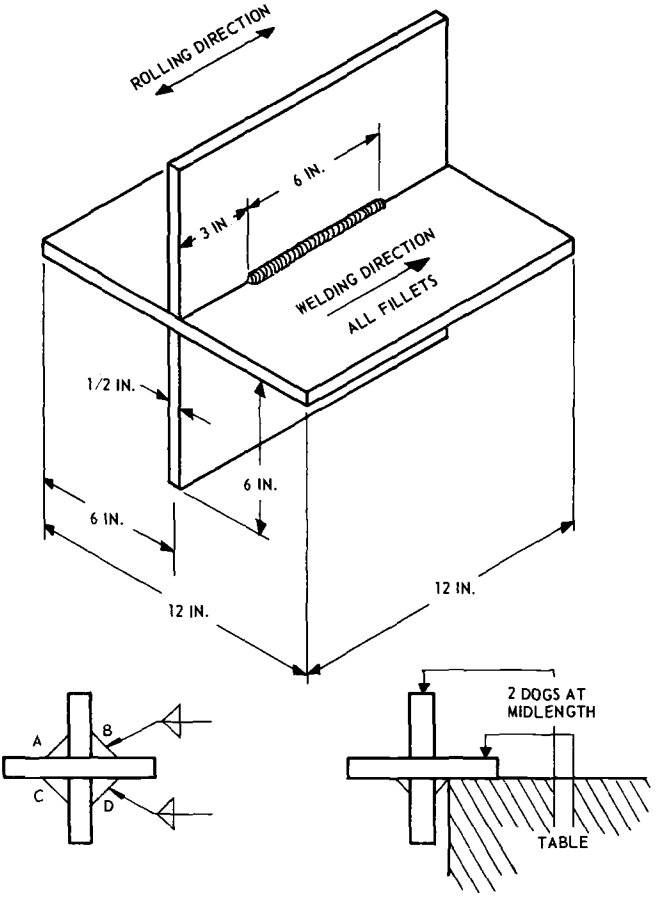

FIG. 1—*Typical cruciform details and clamping arrangement.*

procedure to detect cracking *during* welding. In general, the first weldment to be completed on a given day was monitored with the SWAT system shown in Fig. 2, starting with the last weld pass and continuing for approximately 2 h after the completion of welding. In the case of the cruciforms welded with covered electrode, data were collected from the as-deposited joint, then the slag was removed from the weld, and monitoring was continued for the remainder of the 2-h period.

For those cruciforms welded with a covered electrode, during welding and for the first few minutes after welding, there was a very large stress wave emission (SWE) count rate which was found to be in large part the result of cracking slag. For example, as shown in Fig. 3, during the first 5 min following welding, the cruciform generated over 1,500,000 counts; whereas, on removal of the slag, the count in the next 5-min period increased by only 70,000. The data as seen on an oscilloscope before and after removing the slag were typical of metal cracking. Thus, slag cracking was found to preclude the use of acoustic emission as an inspection method for cracking during welding with a covered electrode. After this fact had been established, the slag was removed immediately after welding. In the MIG welds, the data recorded during and immediately after completing the last weld pass are assumed to be the result of martensite transformation [*46*] or short time cold cracking or both [*51*].

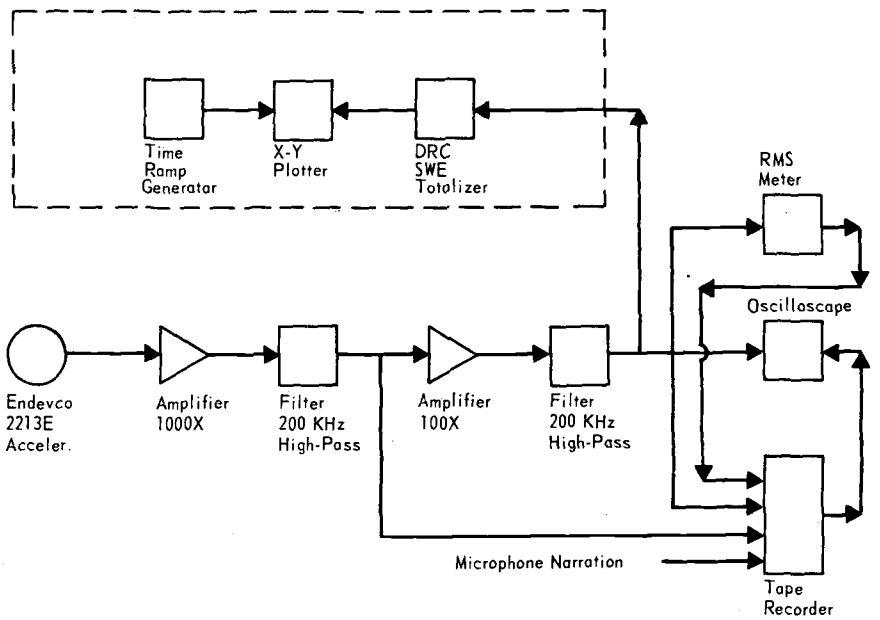

FIG. 2–*SWAT instrumentation used in monitoring cracking in the Fabrication Shop.*

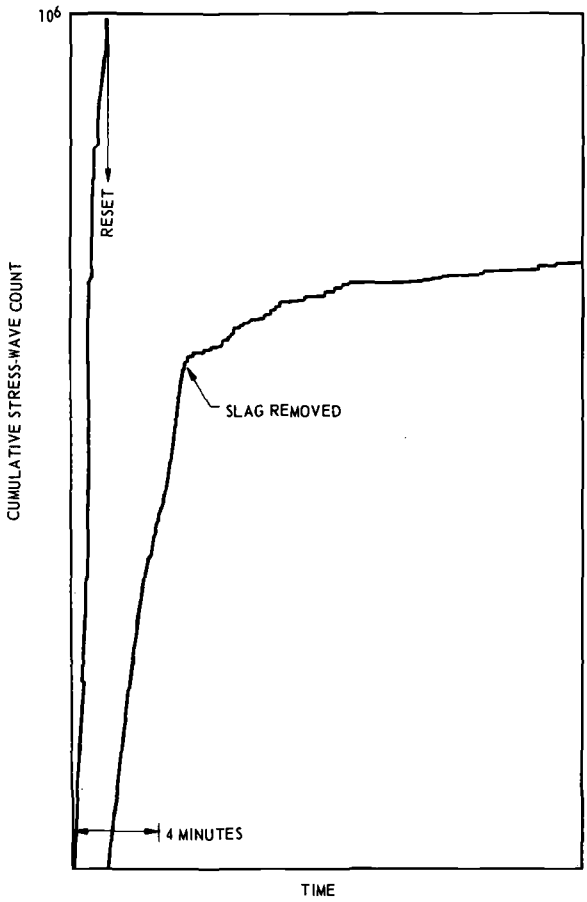

FIG. 3—*Cumulative stress wave count before and after slag removal.*

Figure 4 shows the data collected from the last two passes during MIG welding of a 1-in.-thick cruciform. Note that while the second pass was being deposited (200 kHz high pass filtering) approximately 2,500,000 counts were recorded over a period of 30 s. The signals observed on the oscilloscope were characteristic of stress wave emission; few electrical disturbances were observed with 200 kHz high pass filtering. When the weld pass was completed, the filtering was dropped to 100 kHz. The stress wave emission rate was very high for 22.5 s after the weld pass had been completed; this was followed by an abrupt reduction in the rate of stress wave emission.

Approximately 5 min after completing the second pass, the third pass was started. Again, the filter was set at 200 kHz during welding; approximately 5,000,000 counts were recorded over a period of 35 s while the third pass was

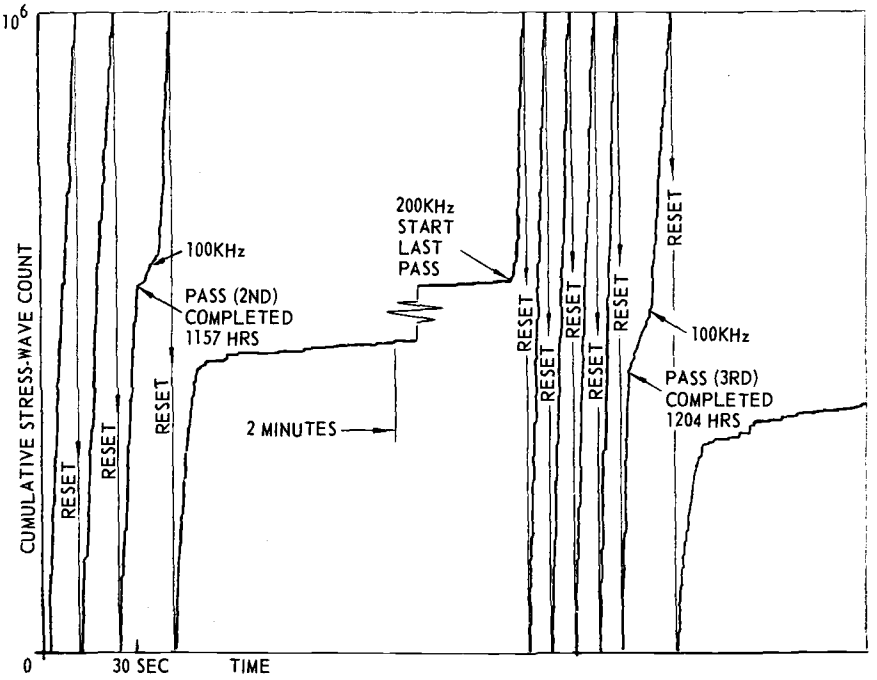

FIG. 4—*Cumulative stress wave count during and immediately after MIG welding the heat B Cruciform.*

being deposited. The filter was then dropped to 100 kHz; the stress wave emission rate continued to be very high for 21.5 s after the weld had been completed. Again, an abrupt decrease in the rate of stress wave emission followed.

Table 2 shows that when 1-in. thick heat B was welded with the MIG process, in the period between 5 and 10 min after the weld had been completed, the average SWE count rate was 14,000 per minute, and in the 10 to 15-min period, the count rate was 7400 per minute. When heat P was welded with the MIG process, in the 5 to 10-min period after welding was completed, the average SWE count rate was 31,400 per minute, and in the 10 to 15-min period, the count rate was 8600 per minute. When 1-in. thick heat P was welded with covered electrode, the average count rate was 44,600 per minute in the period between 5 and 10 min and 18,000 per min between 10 and 15 min after welding. When the same heat was welded as 2-in. thick plate, approximately the same rates were observed as for 1-in. thick plate.

Figure 5 shows the stress wave activity recorded as soon as the slag was removed from the last pass of 2-in. heat P cruciform welded with covered electrode. Note that the activity was high at first but then decreased rapidly over

TABLE 2–*Summary of stress-wave count rate between 5 and 15 min after welding.*

Date	Plate Thick.	Plate Code	Electrode	Joint	Test	Time after Welding, min	SWE Count Increase, count	SWE Count Rate, SWE/min
20 Aug.	1-in.	B	bare	IP[a]	26	5–10	70 000	14 000
						10–15	37 000	7 400
27 Aug.	1-in.	P	bare	IP	27	5–10	157 000	31 400
						10–15	43 000	8 600
10 Sept.	2-in.	P	covered	IP	30	5–10	232 500	46 500
						10–15	78 000	15 600
17 Sept.	1-in.	P	covered	IP	32	5–10	223 000	44 600
						10–15	90 000	18 000

[a] Incomplete penetration fillet weld.

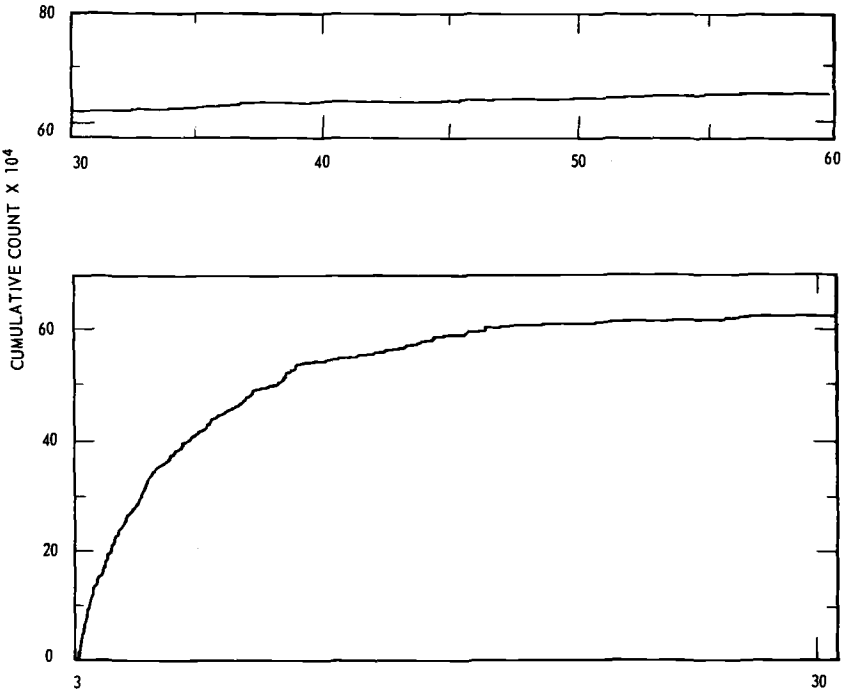

FIG. 5–*Cumulative stress wave count in the first hour after welding the heat P cruciform with covered electrode (incomplete penetration cruciform, slag removed).*

a period of approximately 15 min. Thereafter, as seen in Fig. 5 (10^6 full scale), there were only occasional bursts of stress wave activity. In the second and third hours of recording, as seen in Fig. 6, the record was 10^5 full scale; again occasional bursts of stress wave emission were evident, with the cracking continuing at a more or less constant rate over the 2-h period recorded.

Delayed Crack Detection

After approximately 2 h of continuous monitoring immediately after welding, the cruciforms were moved from the fabrication site to the Aerojet plant in Sacramento, a distance of approximately 75 miles. During this period, no data were taken; the time lost traveling between the fabrication site and setting up in the Aerojet plant was about 4 h.

Upon return to the Aerojet plant, the program plan called for continuous monitoring from 1600 hours Thursday until 0800 hours Monday, a total of 88 h. The SWAT system used in this data collection is shown in Fig. 7. Note that the filter level used after welding was finished was lower than that used during welding (see Fig. 2).

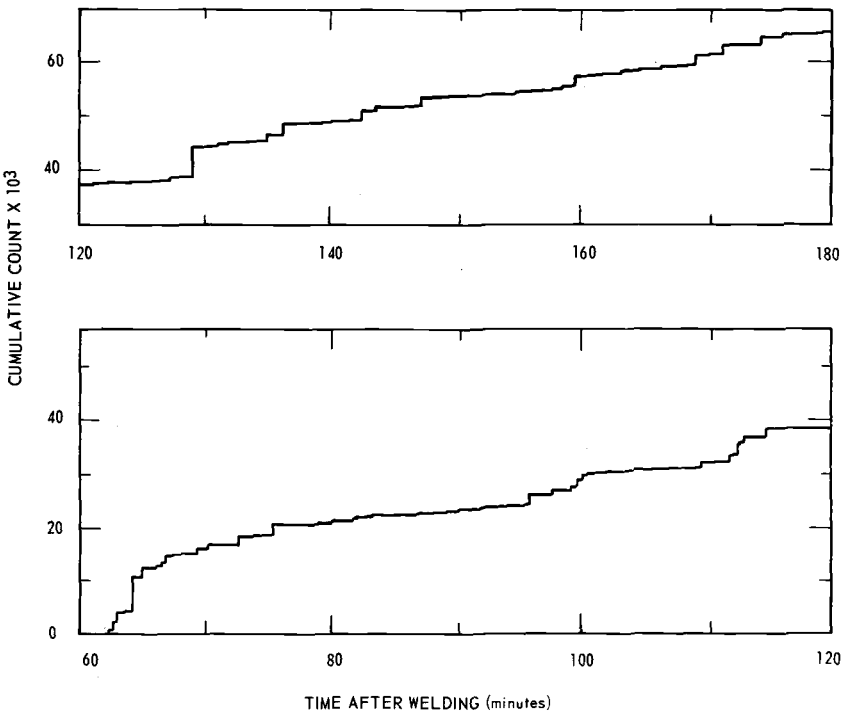

FIG. 6—*Cumulative stress wave count in the second and third hour after welding heat P with covered electrode (same cruciform as Fig. 5).*

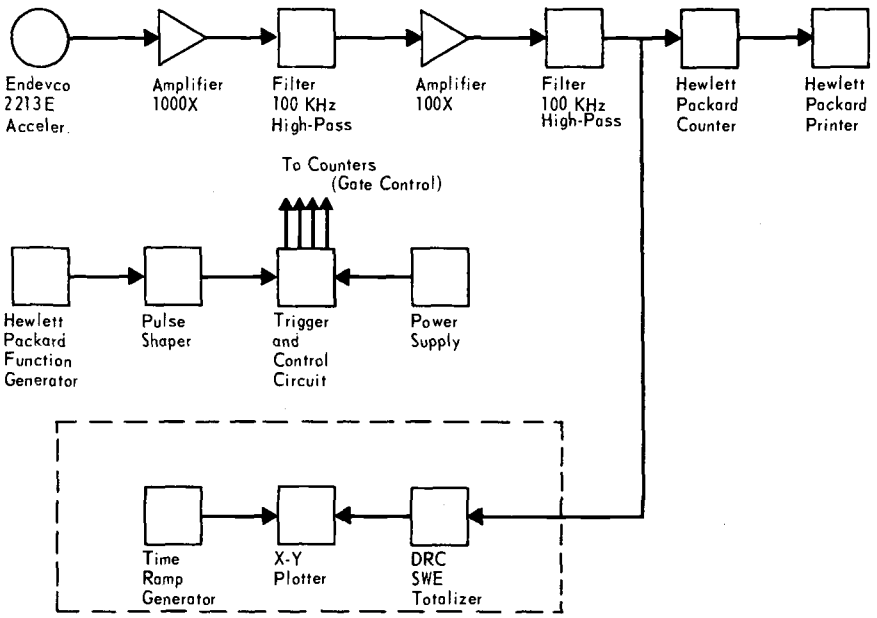

FIG. 7—*SWAT instrumentation used in monitoring delayed cracking at Aerojet.*

Figure 8, a plot of cumulative stress wave count versus time, is typical of these data; the material in Fig. 8 is 2-in.-thick plate welded with a 12018 electrode. Note that with delayed cracking the data are predominantly of the burst type. The data in Fig. 8 are from cruciform 30; see Figs. 5 and 6 for the data recorded immediately after welding.

In addition to being displayed on an X-Y plotter, the data were printed on a strip chart showing the number of counts recorded in each 1-min period. Table 3 illustrates the detailed information that can be obtained from the acoustic emission strip chart. The time between stress wave bursts (ΔT) provides a measure of crack incubation time. In that the electronic counter system integrates the number of stress waves and the size of the stress wave, the rate of stress wave emission (number of counts per minute) is considered to be an indication of the size of the crack increment. The cumulative (total) count provides an overall indication of the amount of cracking. The time period count provides an overall indication of the amount of cracking. The time period over which the stress wave activity occurs gives the duration of cold cracking. Note the large number of occurrences in the first 10 h and the long intervals between bursts toward the end of the data collection period (for purposes of illustration, only the data in the first 10 h and after 350 h are tabulated here). To summarize the strip chart data, tables were prepared to show the activity occurring in successive 10-h periods.

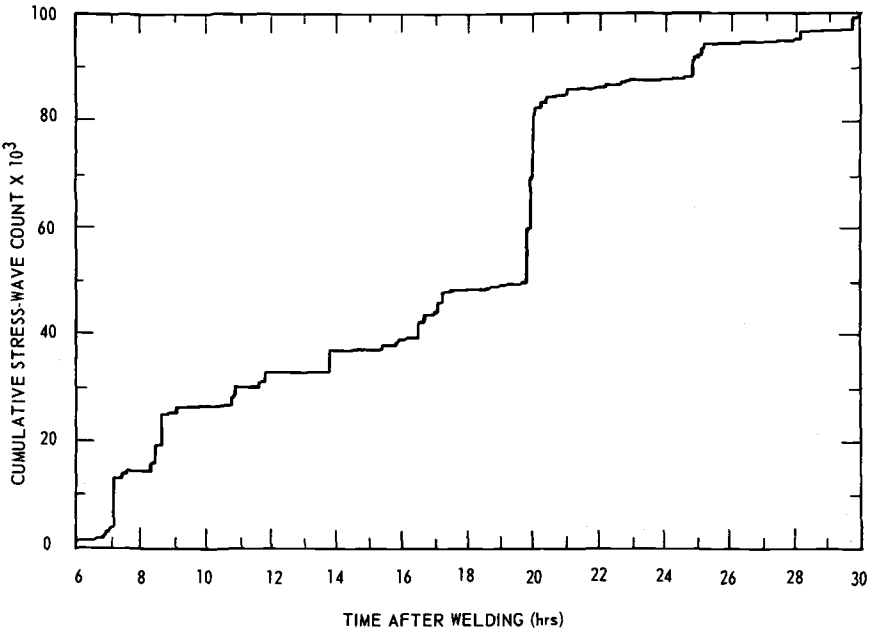

FIG. 8–*Cumulative stress wave count from 6 to 30 h after welding heat P with covered electrode.*

Table 4 summarizes the data presented in Table 3, based on count rates of 100 and 500 per minute. A change in count rate is tantamount to changing the sensitivity of the system; that is, if counts of 500 or greater are used, the smallest increments of crack growth are disregarded. Until a thorough metallographic investigation is made of the extent of actual cracking in each weldment, the size of the burst that is associated with meaningful crack extension is not known. Note, from Table 4, that the cruciform prepared from heat B using stick electrode generated a much higher count than the cruciform prepared from heat P regardless of the count rate used.

To eliminate the complication of different data collection periods, the average count per burst was calculated on the basis of counts of 500 per minute or greater. Table 5 shows that the average count per burst was remarkably constant; this can be attributed to either a characteristic of the system or a characteristic of the type of cracking. If the latter is correct, this would indicate that each of the conditions and materials tested generated the same size of crack increment per burst.

Correlation of Acoustic Emission and the Extent of Cracking

This study showed that stress wave emission occurred in some weldments throughout the entire period of investigation, and this appeared to be

TABLE 3—*One-inch plate welded with 12018 covered electrode, incomplete penetration fillets.*

Date 1970	Code B, Heat B7748				Code P, Heat 5P3524			
	Time		Emission		Time		Emission	
	Clock	ΔT	Rate	Total	Clock	ΔT	Rate	Total
17 Sept.					1 002	Welding complete		
	1 117	Welding complete						
	1 440	System on			1 440	System on		
					1 450		147	147
					1 458	8	130	277
					1 500	2	100	377
					1 501	1	779	1 156
					1 508	7	1 485	2 641
					1 511	3	660	3 301
	1 512		1 293	1 293	1 512	1	894	4 195
					1 513	1	1 656	5 851
					1 514	1	237	6 088
	1 518	6	5 242	6 535	1 518	4	2 939	9 027
					1 519	1	357	9 384
					1 524	5	754	10 138
					1 526	2	130	268
	1 527	9	145	6 680				
					1 544	18	190	458
					1 549	5	2 581	13 039
	1 550	23	722	7 402				
					1 551	2	685	724
					1 552	1	2 307	16 031
	1 553	3	1 163	8 565	1 553	1	1 396	17 427
					1 660	7	480	907
					1 604	4	3 199	21 106
					1 606	2	1 980	23 086
	1 608	15	230	8 795	1 608	2	253	339
	1 610	2	1 089	9 884	1 610	2	8 516	31 855
	1 611	1	2 949	12 833				
					1 612	2	139	994
	1 614	3	6 692	19 525	1 614	2	188	32 182
					1 622	8	368	550
	1 625	11	117	19 642				
					1 628	6	213	763
	1 630	5	102	19 744				
					1 632	4	161	32 924
	1 634	4	12 208	31 952				
					1 636	4	1 046	33 970
					1 645	9	432	34 402
	1 651	17	1 608	33 560	1 651	6	3 764	38 166
					1 701	10	100	266
					1 735	34	157	423
					1 739	4	797	39 220
					1 744	5	1 199	40 419
					1 747	3	303	722
					1 808	21	367	41 089
	1 820	89	894	34 454	1 820	12	175	264
					1 827	7	306	570

TABLE 3–(*Continued*)

Date 1970	Code B, Heat B7748				Code P, Heat 5P3524			
	Time		Emission		Time		Emission	
	Clock	ΔT	Rate	Total	Clock	ΔT	Rate	Total
	1 841	21	142	34 596				
	1 846	5	157	34 753				
					1 856	29	2 394	43 964
					1 858	2	180	44 144
					1 859	1	1 008	45 152
					1 902	3	1 568	46 720
	1 907	21	410	35 163	1 907	5	724	47 444
					1 918	11	620	48 064
					1 927	9	1 199	49 263
	1 942	35	1 510	36 673				
	1 950	8	972	37 645				
					2 002	– 10 h after welding		
					2 019	52	688	49 951
	2 032	42	102	37 747				
					2 033	14	1 944	51 895
	2 035	3	687	39 434				
					2 044	11	669	52 564
	2 047	12	6 990	45 424				
					2 105	21	212	776
	2 117	– 10 h after weld completion						
2 Oct.					0 002	– 350 h after welding		
	0 117	– 350 h after welding						
					1 002	– 360 h after welding		
	1 117	– 360 h after welding						
	1 308	1 518	168	875				
					1 730	1 308	109	811
					1 737	7	152	963
	1 839	331	783	323 658				
					2 002	– 370 h after welding		
	2 117	– 370 h after welding						
3 Oct.	0 215	456	634	324 292				
	0 216	1	3 755	328 047				
					0 602	– 380 h after welding		
	0 717	– 380 h after welding						
	1 105	529	154	201				
	1 111	6	103	304				
	1 410	179	177	481				
					1 602	– 390 h after welding		
	1 717	– 390 h after welding						
					1 952	135	176	100 139
	2 012	362	140	621				
					2 028	36	727	866
	2 056	44	104	725				

TABLE 3–(*Continued*)

Date 1970	Code B, Heat B7748				Code P, Heat 5P3524			
	Time		Emission		Time		Emission	
	Clock	ΔT	Rate	Total	Clock	ΔT	Rate	Total
4 Oct.	0 055	239	126	851				
					0 202	– 400 h after welding		
	0 254	119	1 881	330 732				
	0 317	– 400 h after welding						
	0 507	133	136	868				
	0 512	5	121	989				
	0 520	8	125	331 114				
					1 202	– 410 h after welding		
	1 301	461	472	586				
	1 317	– 410 h after welding						
					1 501	1 113	125	991
	1 506	125	192	778				
					2 202	– 420 h after welding		
	2 317	– 420 h after welding						
5 Oct.	0 128	622	144	331 922				
					0 812	– 430 h after welding		
	0 917	– 430 h after welding			0 917	1 096	305	101 296
					0 924		121	417
					0 932		227	644
					0 940		109	753
	1 010	System Off			1 010	System Off		
					1 802	– 440 h after welding		
	1 917	– 440 h after welding						

irrespective of constraint or welding process. Without metallographic examination, a question remained as to the size of the defect source generating the stress wave emission. Moreover, with more than one weld in the cruciform, there could have been multiple stress wave sources, which would preclude meaningful incubation time measurements. In other words, the high count rate observed during the first several hours after welding could have been the result of (1) discontinuous growth of a few large cracks, (2) grain-by-grain cracking along an enlarging crack envelope, (3) a myriad of small cracks, or any combination of the three. Moreover, while the weldment was cooling but still hot, microcracking may have been occurring in the weld metal over the entire length of the deposit, and after the weld had become cold the stress wave emission may have come from one or more cracks in the weld or HAZ or both. Also, with high amplification and sensitivity in the SWAT system, the count rate observed during welding, and continuing for a short time after the welding, may have been, at least in part, generated by the martensite transformation[*46*].

Two weldments were selected for metallographic examination. The sectioning

TABLE 4—*Stress-wave emission from 1-in. Code B and Code P cruciforms welded with 12018 covered electrode.*

Period, h	Based on a rate of 500 counts/min or greater				Based on a rate of 100 counts/min or greater			
	Plate B		Plate P		Plate B		Plate P	
	No. Bursts	SWE Count	No. Bursts	SWE Count	No. Bursts	SWE Count	No. Bursts	SWE Count
10–20	2	1 700	9	21 637	4	2 279	14	22 892
20–30	19	29 513	7	15 407	50	36 319	16	17 587
30–40	8	14 702	1	1 641	28	18 715	4	2 133
40–50	5	86 791	0	0	18	90 197	0	0
50–60	4	5 798	0	0	6	6 106	0	0
60–70	6	17 109	0	0	14	19 037	0	0
70–80	0	0	0	0	7	1 351	0	0
80–90	1	508	0	0	5	1 202	0	0
90–100	4	20 395	1	1 050	10	22 048	1	1 050
100–110	2	7 363	0	0	6	8 469	0	0
110–120	2	1 054	0	0	3	1 234	0	0
120–130	8	25 652	0	0	15	27 099	1	200
130–140	0	0	0	0	0	0	0	0
140–150	5	3 242	1	956	18	5 593	1	956
150–160	0	0	0	0	5	1 339	0	0
160–170	1	1 554	0	0	3	1 846	0	0
170–180	2	2 763	0	0	4	3 339	1	111
180–190	0	0	0	0	3	938	0	0
190–200	1	953	0	0	1	953	0	0
200–210	1	881	0	0	3	1 311	0	0
210–220	7	13 272	0	0	8	13 612	0	0
220–230	1	1 554	0	0	7	3 010	0	0
230–240	0	0	0	0	2	333	0	0
240–250	0	0	0	0	0	0	0	0
250–260	0	0	0	0	0	0	0	0
260–270	0	0	0	0	0	0	3	503
270–280	2	1 911	0	0	9	3 738	10	1 838
280–290	2	3 084	0	0	5	3 997	5	946
290–300	0	0	0	0	3	553	0	0
300–310	1	769	0	0	3	1 481	0	0
310–320	0	0	1	694	0	0	2	803
320–330	1	668	0	0	1	668	0	0
330–340	0	0	0	0	2	612	0	0
340–350	0	0	0	0	0	0	9	1 420
350–360	0	0	0	0	1	168	0	0
360–370	1	783	0	0	1	783	2	261
370–380	2	4 389	0	0	2	4 389	0	0
380–390	0	0	0	0	3	431	0	0
390–400	1	1 881	1	727	4	2 251	2	903
400–410	0	0	0	0	4	854	0	0
410–420	0	0	0	0	1	192	1	125
420–430	0	0	0	0	1	144	0	0
430–440	0	0	0	0	0	0	4	762
Total	89	248 289	21	42 112	260	286 590	76	52 490

TABLE 5—*Number of bursts, total count (bursts of 500 or more counts), and average count per burst.*

Weldment		Plate B			Plate P		
Thickness	Process	No. Bursts		SWE Count	No. Bursts		SWE Count
1 in.	Stick	89		248 289	21		42 112
			Avg	2 790		Avg	2 000
2 in.	Stick	30		58 188	27		54 052
			Avg	1 980		Avg	2 000
1 in.	MIG	68		111 575	97		169 323
			Avg	1 640		Avg	1 750
2 in.	MIG	35		57 410	29		40 801
			Avg	1 640		Avg	1 410

was in accord with the procedure used by Army Ordnance [*48*] except that the weldments were not stress relieved and the etchant had to be modified. Two percent nital was used. The weldments selected were cruciforms 31 (heat B) and 32 (heat P); these were 1 in. thick, welded with covered electrode and monitored for 440 h (approximately 18 days). Based on macroexamination, weldment 31 with over 200,000 counts was found to be cracked over the entire sectioned length of the *D* weld. Based on a decreasing depth of crack in each successive section, the cracking began at the starting end of the D weld. Figure 9 shows the

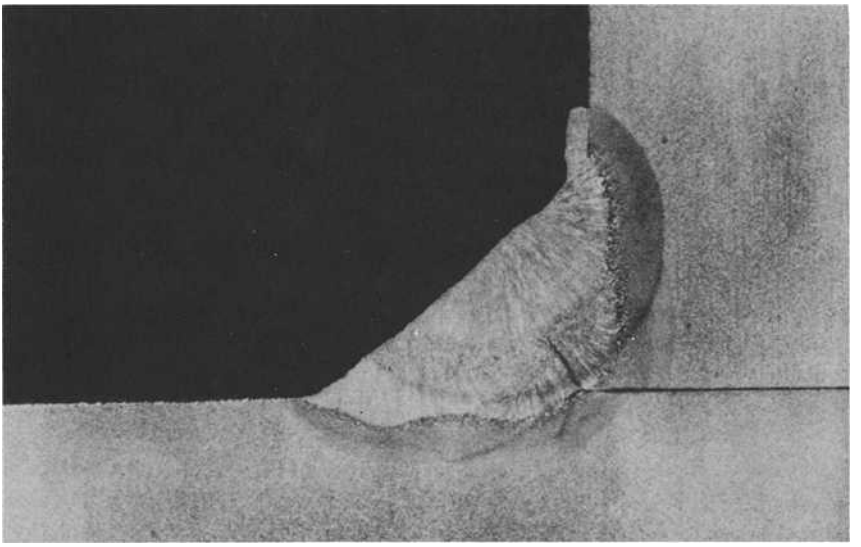

FIG. 9—*D weld cracking at approximate midlength of cruciform No. 31* (×3).

crack at approximately midlength of the D weld (section 31-D4). Weldment 32, on the other hand, with approximately 40,000 counts was found to have macrocracking only in the section nearest the finishing end of the D weld. Figure 10 shows microcracking (X250) in the next to the last section (32-D5). Microexamination revealed crack initiation in several of the welds examined, namely, in welds A, B, and C, as well as D, starting at the root of the incomplete penetration fillet welds.

Air Force Sponsored Study of Stress Corrosion Cracking

The primary objective of the research described in the following paragraphs was to investigate the effects of circulating, distilled water on slow crack growth in 250 grade 18 Ni maraging steel, at 65 and 165 F, as a function of melting practice. The steel consisted of an air melted (AM) heat (induction stirred, ladle vacuum degassed) and a vacuum-arc remelt (VAR) heat. The VAR heat was produced by remelting a portion of the air melted heat. The breakdown and conversion practices employed in producing the AM and the VAR sheet products were the same; furthermore, the steel from both melting practices was heat treated in the same manner; that is, solution treated at 1625 F and aged at 925 F for 3 h.

Test Procedure

The single-edge notched (SEN) tension specimen used to investigate subcritical crack growth in an aqueous environment is shown in Fig.11 together

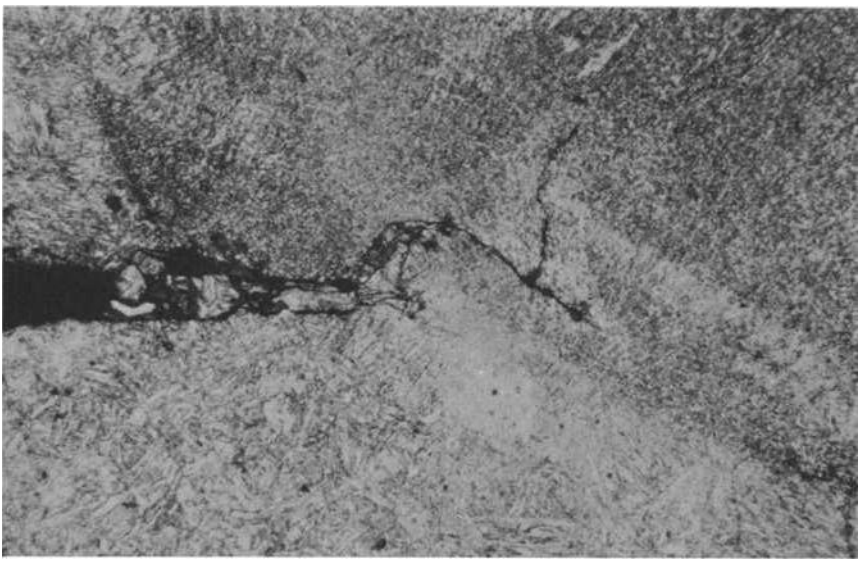

FIG. 10–*Microcracking in section 5 of cruciform 32 (X190).*

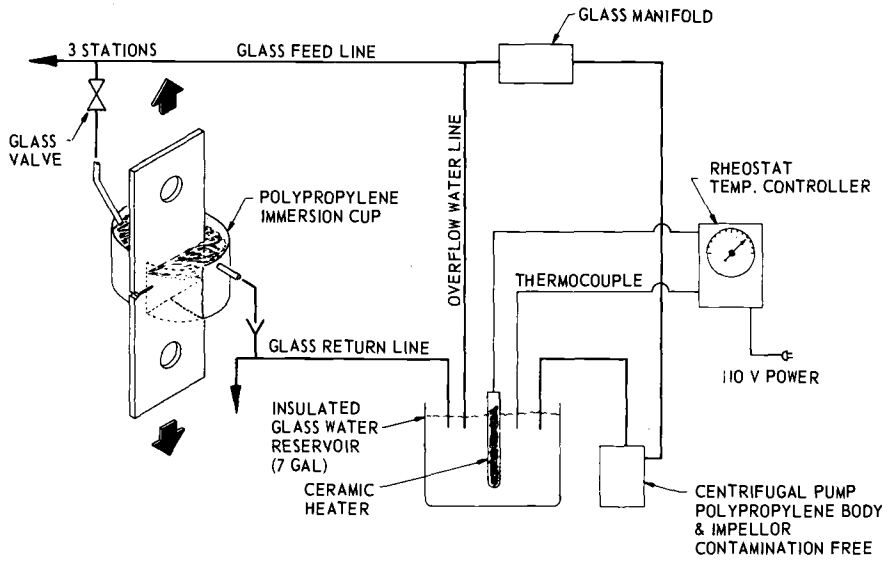

FIG. 11—*Water circulation system.*

with the water circulating system. In anticipation of the long test times in this investigation, to maintain the chemistry of the distilled water as constant as possible, the entire system was made of glass and chemically stable plastics and utilized a 7-gal reservoir. The K calibration was as published by ASTM [*52*].

A crack opening displacement (COD) gage was used for detecting pop-in and following the crack growth. The gage was positioned to bridge the specimen preflaw by positioning the gage between the lips of the specimen notch. The COD gage used in this investigation has been developed specifically for pop-in and slow crack growth measurements where small changes in crack opening are anticipated [*53*]. The signal from the gage went to a bridge balancing unit, to a d-c amplifier, and then to a d-c millivolt recorder. For the stress corrosion studies, the unit was operated at a gain of 1200, with less than 1 percent peak-to-peak instability. The system also had a zero suppression capability, which allowed the gain of 1200 to be fully utilized even if the crack opening were to increase as much as 0.05 in., although such displacements were usually not encountered.

The stress wave analysis technique (SWAT) was employed to detect pop-in and to monitor the occurrence of subsequent slow crack growth by recording acoustic emission. The SWAT system (Fig. 12) used in this study, which utilized an electronic counter, had the capability of long-time automated data collection. One characteristic of the system was that, if the electronic counter trigger was set just above the background noise level, a large amplitude burst type stress wave with its exponential decay provided several counts from the one stress

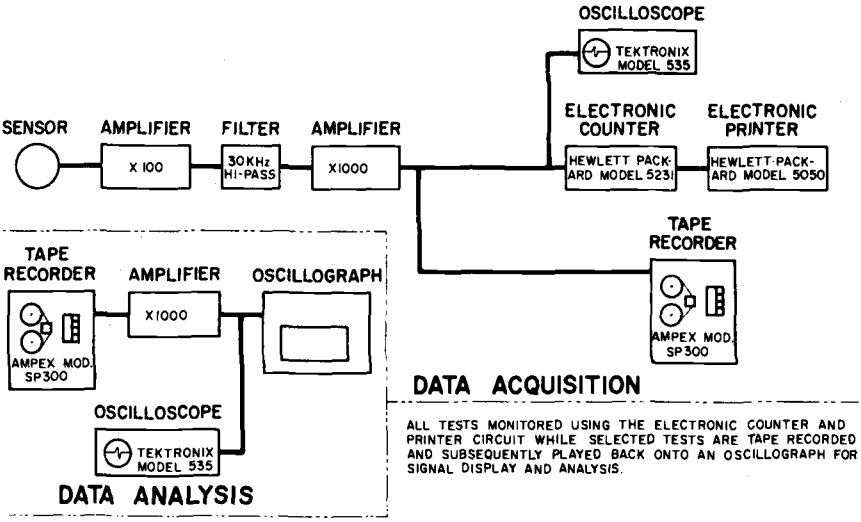

FIG. 12—*Schematic of SWAT data acquisition and data analysis instrumentation.*

wave. Thus, the electronic counting system provided a value weighted by the stress wave amplitude and, consequently, was more a qualitative measure of energy released than the number of stress waves. As indicated in this figure, the SWAT system consisted of accelerometers, amplifiers, filters, and an electronic counter digital printer. The accelerometers were attached to the specimens using a linear-force, coiled spring technique.

As indicated in Fig. 12, the electronic counter system provided a real-time automatic count of the stress wave emission throughout each test period. The high pass filter in the system eliminated a major portion of the extraneous low frequency noises which tend to mask very small amplitude stress waves. In the research reported here, a high sensitivity SWAT system was used; with an amplification of 100, followed by 30-kilocycle high pass filtering and then an amplification of 1000, a 38-kilocycle input signal (approximately the resonance frequency of the mounted accelerometer) was amplified approximately 5000 times.

Specimens were loaded in a test machine actuated by a two-way air cylinder. The essential feature of the system was its ability to hold a constant load over extended test periods. Each material condition tested was loaded in water to approximately 0.7 of the critical stress intensity (K_c) previously determined for each material in a conventional fracture test.

Stress Corrosion Cracking in Maraging Steel

Specimen VAR-10, 0.175 in. thick, was tested at room temperature at a K/K_c ratio of 0.74. Figure 13 is a plot of cumulative SWE count versus time at hold

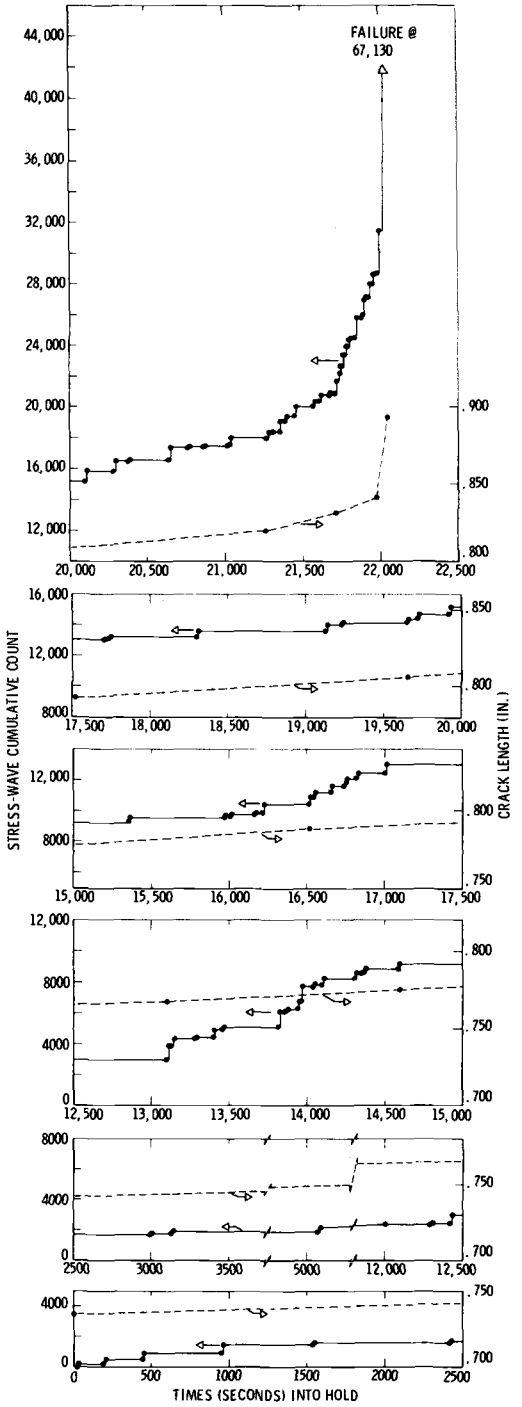

FIG. 13–*Details of subcritical crack growth in 18Ni maraging steel in 70 F, circulating, distilled water (specimen VAR-10).*

for specimen 10. Figure 13 also shows flaw length versus time; generally, there was a good correlation between this relationship and SWE count plotted versus time. However, it should be noted that SWE was more sensitive to crack growth than the COD measurement.

Specimen VAR-9, tested in 165 F water at K/K_C of 0.68, failed in a shorter time than specimen VAR-10, tested at 70 F at a similar K/K_C value. Note in Table 6 that the primary incubation time was less for specimen 9 (tested at 165 F) than for specimen 10 (tested at 70 F and approximately the same stress intensity level). Figure 14 is a plot of cumulative SWE count versus time at load for specimen 9. Unlike the room temperature tests, the steplike, crack growth process was continuous until the specimens failed. Note that there was good correlation between crack length as determined by COD measurements and SWE count plotted versus time.

Acoustic Emission as a Measure of Slow Crack Growth

The data plotted in Figs. 13 and 14 indicate good agreement between acoustic emission and crack length as determined from crack opening displacement (COD) measurements; where there was a large increase in flaw size, there was also a jump in the cumulative stress wave emission count. The behavior at 165 F consisted of a succession of four jumps; the first occurred after a primary incubation period of approximately 3700 s, the second occurred approximately 3300 s later, the third occurred approximately 2000 s later, and the fourth occurred less than 1000 s later. Figure 15 is a schematic of the crack jump progression in terms of cumulative stress wave count versus time at constant load. Note from the schematic that primary incubation time was defined as the time from the start of hold to the first rapidly increasing slope (jump) in the plot of cumulative stress wave emission count versus time. Secondary incubation time was defined as the average time between successive rapidly increasing slopes (jumps) after primary incubation. The behavior at 70 F, in contradistinction to that at 165 F, consisted of a gradually increasing slope until just prior to failure; that is, there was a single jump at failure.

TABLE 6—*Stress corrosion cracking incubation time for flaw growth in 18Ni maraging steel.*

Specimen No.	K/K_C	Test Temperature, deg F	Primary Δt_P, s	Secondary, s			Total Time to Failure, min
				Δt_{S1}	Δt_{S2}	Δt_{S3}	
VAR-10	0.74	70	21 970				371
VAR-9	0.68	165	3 710	3 350	2 060	640	176

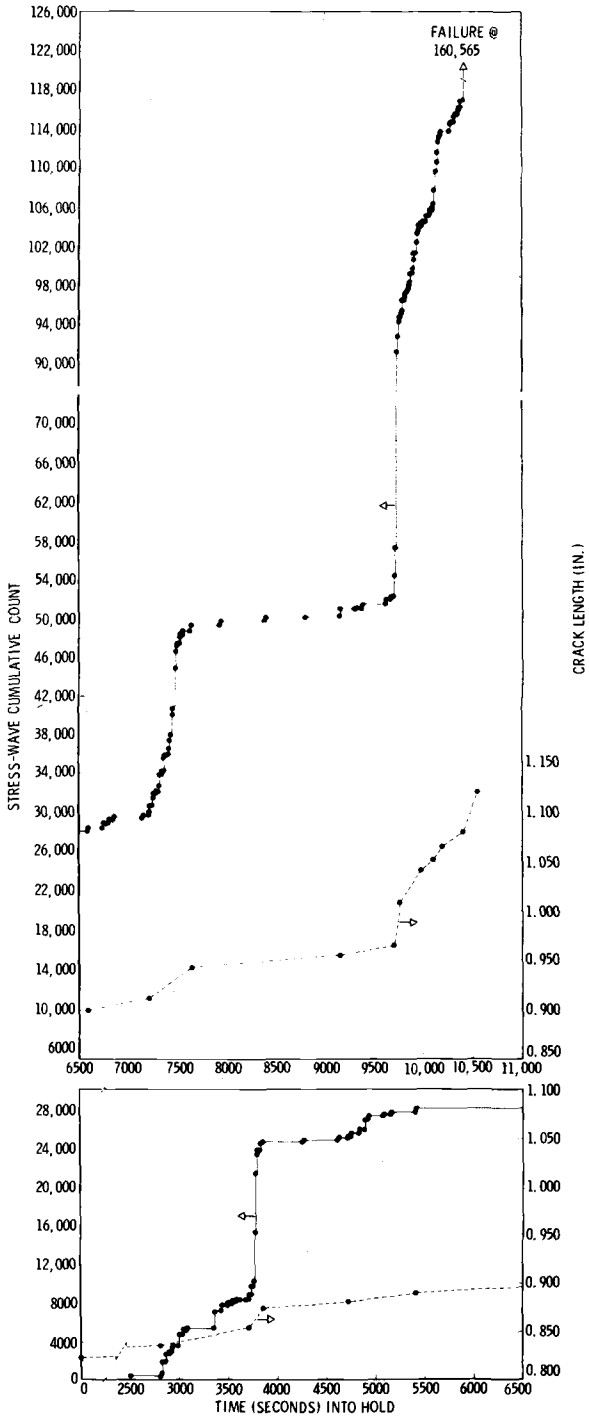

FIG. 14—*Details of subcritical crack growth in 18Ni maraging steel in 165 F, circulating, distilled water (specimen VAR-9).*

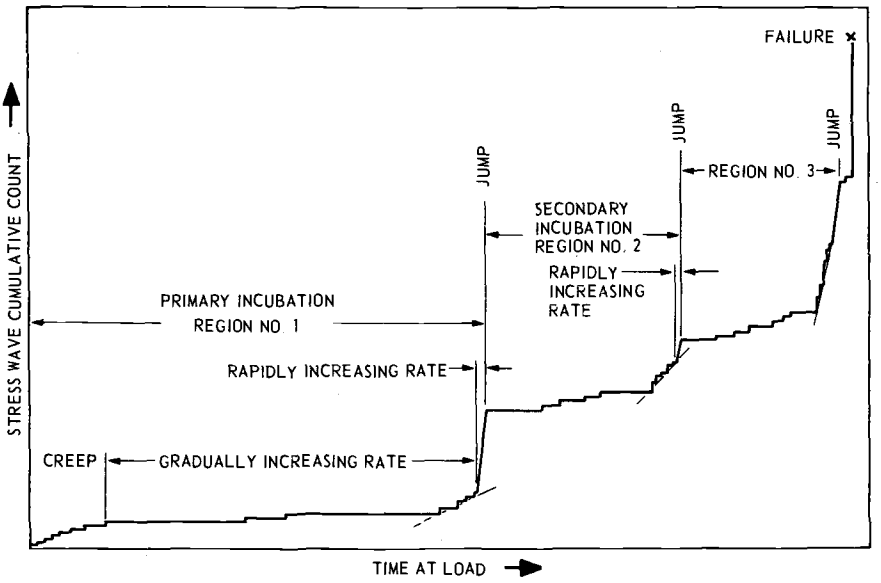

FIG. 15—*Schematic showing subcritical crack growth process and terminology.*

An attempt was made to relate SWE occurrences to actual flaw growth for a given time interval by determining the flaw growth per SWE count (μin./SWE). The results shown in Table 7 were obtained from several 250 grade maraging steel specimens. Note that the crack growth per stress wave was essentially constant regardless of whether it was measured in the region of gradual or rapid crack growth. The range and average value for 25 observations was

0.8 to 13.1
Avg(25) 3.4 μin./SWE

whereas, the crack growth rate *da/dt* in the periods of gradual increase was

1.0 to 53.2
Avg(13) 12.0 μin./s

and *da/dt* in the periods of rapid increase was

133 to 2187
Avg(12) 814 μin./s

The essentially constant value of crack growth per stress wave count simply reflects the fact that the stress wave count was higher in periods of rapid crack

TABLE 7—*Stress corrosion cracking of 250 grade 18 Ni maraging steel in circulating, distilled water (0.175 in thick).*

Specimen No.	Test Condition	Subcritical Cracking Region	K/K_c at Start of Each Region	Rate of Slow Crack Growth				Failure K_c, ksi $\sqrt{\text{in.}}$	Time to Failure, min
				Gradual Periods		Rapid Periods			
				μ in./s	μ in./SWE	μ in./s	μ in./SWE		
AM-6	70 F	1	0.70	4.9	13.1	1720	2.8	304	1582[a]
AM-8	70 F	1	0.72	1.0	8.9	276	2.1	295	1344
AM-10	70 F	1	0.75	1.6	2.7	2187	1.0	284	678
AM-9	165 F	1	0.70	3.8	2.8	700	1.6		
		2	0.84	2.3	5.4	[b]	[b]		
		3	[b]	[b]	[b]	[b]	[b]	274	442
VAR-6	70 F	1	0.81	35.2	2.9	260	0.9	326	168
VAR-10	70 F	1	0.74	4.8	3.7	1325	2.8	255	371
VAR-8	165 F	1	0.77	8.4	3.0	742	2.4		
		2	0.90	53.2	2.1	675	1.0	258	98
VAR-9	165 F	1	0.68	8.6	3.8	133	1.2		
		2	0.73	10.4	7.0	745	1.6		
		3	0.79	10.7	7.9	733	1.2		
		4	0.87	11.3	3.2	273	0.8	344	176

[a] Did not fail. Load was increased slightly ($K/K_c = 0.82$) and failure occurred in 1.5 min.
[b] COD strip chart ran out of travel.

growth and lower in periods of gradual crack growth. Thus, the stress wave count was verified as a measure of crack growth.

Another important observation from Table 7 is the length of time required for failure in some of the specimens exposed to 70 F distilled water. The primary incubation time for specimen AM-8 at $0.72K_c$ was 1298 min (21.6 h) and failure occurred in 1344 min (22.4 h). Of two companion specimens, AM-6 did not fail in 26 h at $0.7\,K_c$ and AM-10 required 663 min (11 h) for primary incubation and 678 min (11.3 h) for failure at $0.75K_c$. Thus, if the threshhold stress intensity factor were determined based on time-to-failure observations, a test period of less than 11 h at 70 F would have indicated the K_{Iscc} value to be $0.75K_c$. Note the relatively short interval of time between primary crack incubation and failure in these specimens. Figure 16 was based on time-to-failure observations[*54*]; based on these data, it was observed that the K_{Iscc} was 10 to 15 ksi$\sqrt{\text{in.}}$ If acoustic emission had been used, and crack propagation rather than time to failure were the criterion, the K_{Iscc} values for the material aged at 800 F for 10 h and 900 F for 100 h might have been below 10 ksi$\sqrt{\text{in.}}$

Relationship to Stress Intensity Factor

Potentially one of the most important observations derived from acoustic emission technology is that the emission characteristics of flawed specimens are

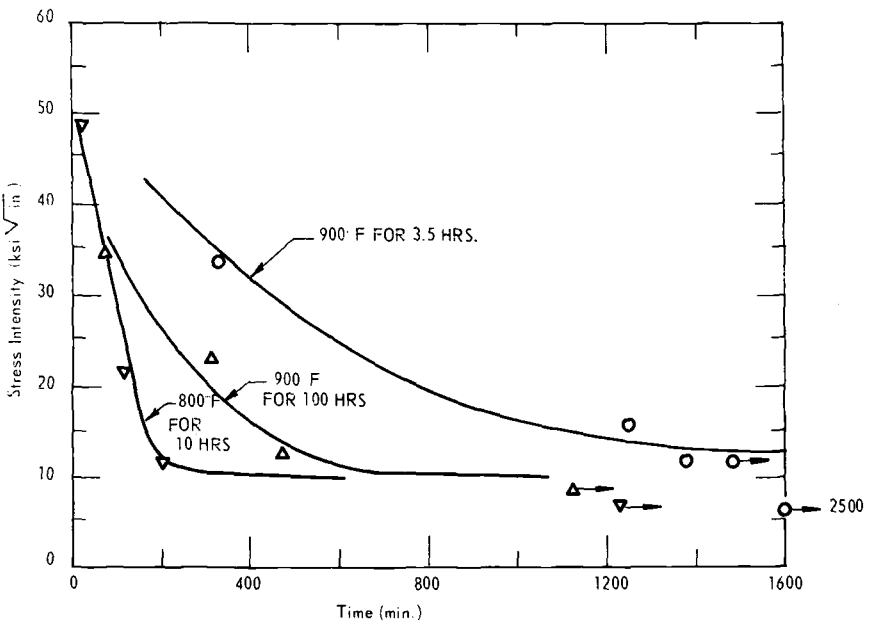

FIG. 16–*Effect of aging treatment on stress corrosion susceptibility in 3 percent NaCl at pH 1.7 of 18Ni maraging steel austenitized 1 h at 2300 F*[*54*].

highly dependent upon the stress intensity of the flaw present. The first evidence obtained at Aerojet of a relationship between stress wave emission and stress intensity factor came from a study of fatigue cracking in ⅛ by 8 by 24-in. D6aC through cracked, center notched panels[55]. As shown in Fig. 17, the crack growth rate in low cycle high stress intensity fatigue was shown to be directly proportional to the summation of stress wave amplitude in each cycle.

At about the same time, Dunegan, Harris, and Tatro at the University of California Lawrence Radiation Laboratory (LRL) showed that, with the counter trigger level set to record plastic deformation (dislocation activity), most of the emission occurs during and shortly after yielding, then decreases as further straining takes place. Based on the volume of metal being strained in the plastic zone at the tip of a crack, Dunegan assumed that the acoustic emission count rate would be proportional to the rate of increase of the volume of metal producing the acoustic emission. This led to the prediction that if all the acoustic emission pulses are added up as the test proceeds then at any time the total number of counts will be proportional to the fourth power of the stress

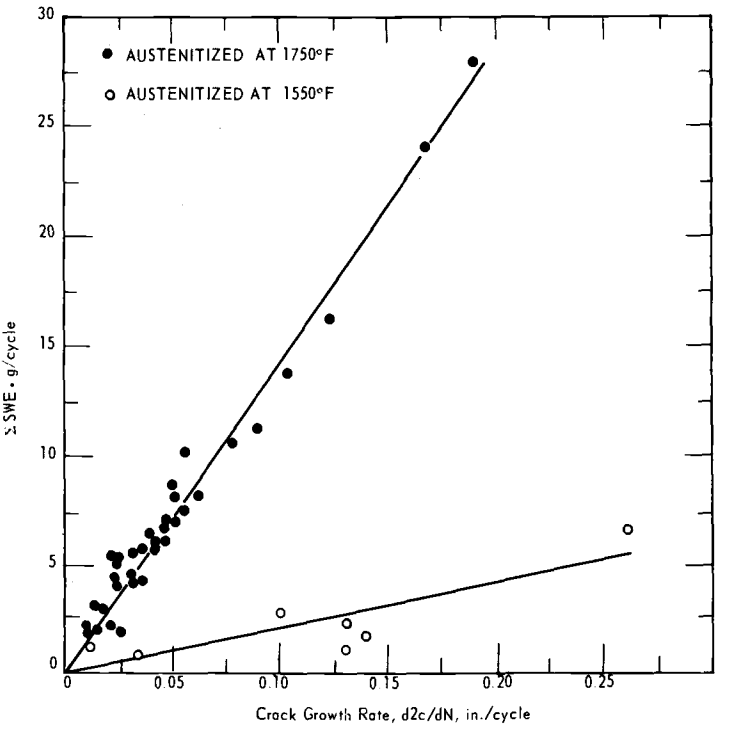

FIG. 17—*Relationship between crack growth rate and stress wave emission for two conditions of D6aC steel.*

intensity factor associated with the flaw at the time. Figure 18, which was taken from the work of Dunegan and Harris, shows the relationship between stress intensity factor and acoustic emission cumulative count in rising load-to-failure tests of 7075-T6 aluminum. Note that data were obtained from four initial crack lengths grouped into a single curve fitting the theoretical fourth power curve. Unfortunately such data did not always conform to a fourth power curve; in another study, Dunegan and Harris reported the exponent to vary between 6 and 8. Later studies at Aerojet indicated a direct proportionality between stress intensity factor and cumulative stress wave count in single-edge notched tension specimens. It was hypothesized that the difference between the LRL and Aerojet test results could be the result of a differenc in triggering level. At LRL the counter triggering level was set to include the continuous emission produced by plastic deformation; whereas, in most Aerojet studies, the triggering level was set above the continuous emission, focusing on the burst-type stress wave emission associated with incremental crack growth. However, differences from test to test, even with a supposedly constant data acquisition system, have been encountered and are as yet unexplained.

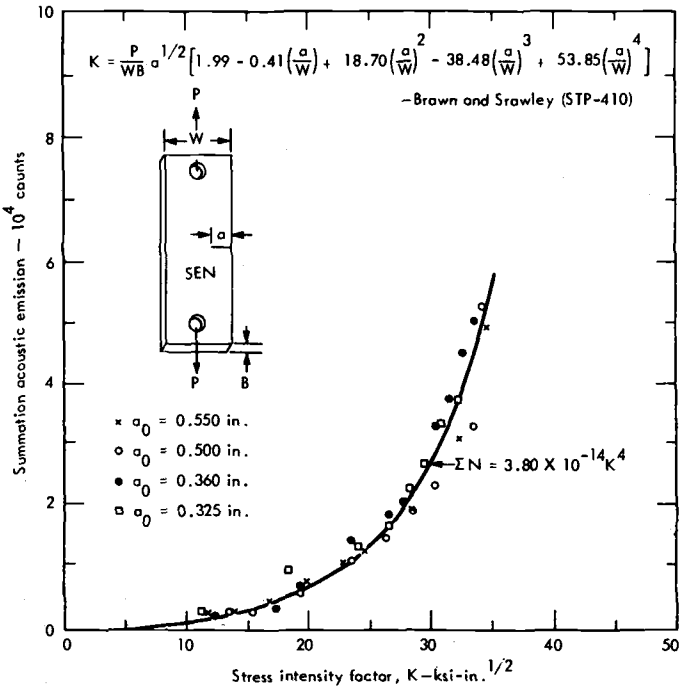

FIG. 18–*Summation acoustic emission as a function of stress intensity factor for rising load-to-failure tests of 7075-T6 aluminum; a best fit fourth power curve was drawn through the data points* [31].

The importance of the relationship between the stress intensity factor and acoustic emission lies in the possibility of estimating flaw sizes and failure load based on in-service, real-time, nondestructive inspection of a flawed structure utilizing acoustic emission. However, before this can be realized, much has to be learned about the variables affecting the count versus K relationship. To facilitate comparisons between results obtained in the various studies at Aerojet, a computer program was used to calculate stress intensity values from empirically determined values of load and COD and to plot various relationships. These relationships are based on the following fracture mechanics parameters [*56*]:

$$G = K^2/E$$

$$(COD)E/(1-\nu^2) = \frac{2K}{\pi}(2\pi r)^{1/2}$$

$$r = \frac{1}{2\pi}\left(\frac{K}{FTY}\right)^2$$

where G is the stress-field energy release rate (in.·lb/in.^{2}), K is the stress intensity factor (ksi$\sqrt{\text{in.}}$), E is the modulus (psi), COD is crack opening displacement (in.), ν is Poisson's ratio, r is the plastic zone size (in.), and FTY is the 0.2 percent offset yield strength (psi).

It is hypothesized that, if the electronic counter integrates size and number of the stress wave emission, the count can be assumed to be proportional to the stress field energy release rate, G. Based on this assumption, it can be shown that the above fracture mechanics parameters should provide the following relationships:

$$TSWE \propto K^2/E$$
$$COD \propto (1-\nu^2)\, TSWE/FTY$$

where $TSWE$ is the cumulative stress wave emission count.

Figure 19 is an example of the simple empirical relationship found between stress intensity factor and cumulative stress wave count. Figure 20 is a plot of the same empirical relationship as printed out by the computer for four other test specimens. Figures 21 and 22 are the computer printout plots for the same data but based on the assumption of a proportionality between the stress field energy release rate, G, and the cumulative acoustic emission count. Each of these plots indicates a relationship between the respective fracture mechanics parameters and acoustic emission count.

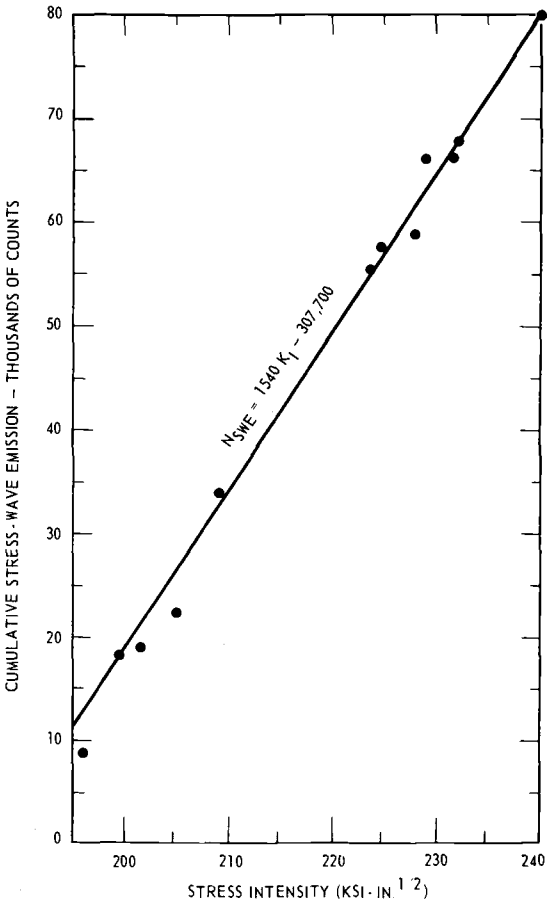

FIG. 19–*Relationship between* K *and count for 18Ni maraging steel specimen VAR-8 under constant load in 70 F circulating water.*

Summary

Stress waves were emitted from all of the weldments tested both during and immediately after welding and for prolonged periods after the weldments had cooled to room temperature. The maximum rate of emission occurred during welding and immediately after the last pass was completed; the continuous nature of the emission during and immediately after welding suggests that the source may have been (1) a growing crack, (2) a myriad of microcracks, (3) a transformation of austenite to martensite, or (4) any combination of these. All would have occurred progressively as an isotherm followed the welding arc down the length of the weldment.

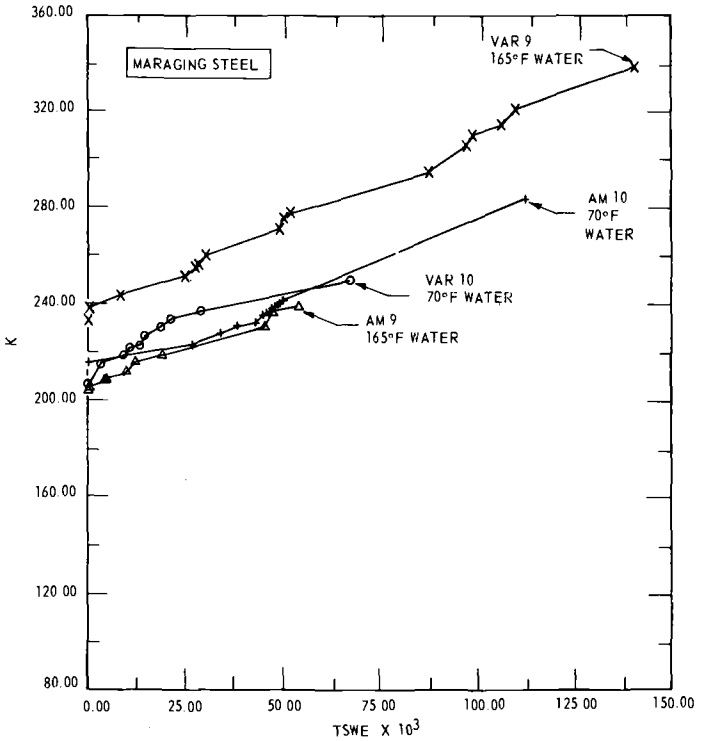

FIG. 20—*Relationship between cumulative stress wave emission count and stress intensity factor for various test conditions, traced from computer printout.*

Within 15 min to 2 h after welding was completed, the continuous high level acoustic emission changed to discontinuous bursts of stress wave activity, with progressively longer time intervals between bursts. Marked differences in stress wave activity were observed between cruciforms welded with a given electrode but involving different base metal chemistry. One pair of such weldments were examined metallographically and the extent of cracking was found to correlate with the cumulative SWE count.

Acoustic emission occurring as the result of stress corrosion cracking has been shown to provide information on the crack growth process in greater detail than is otherwise available. Moreover, the data show that for service involving long exposure times, threshhold stress intensity values, K_{Iscc}, based on time-to-failure observations are nonconservative when test periods are shorter than the service life. Data are also presented showing a linear relationship between acoustic emission and stress intensity factor. The importance of this relationship lies in the possibility of estimating flaw sizes and failure stress based on real-time nondestructive inspection of a flawed structure utilizing acoustic emission.

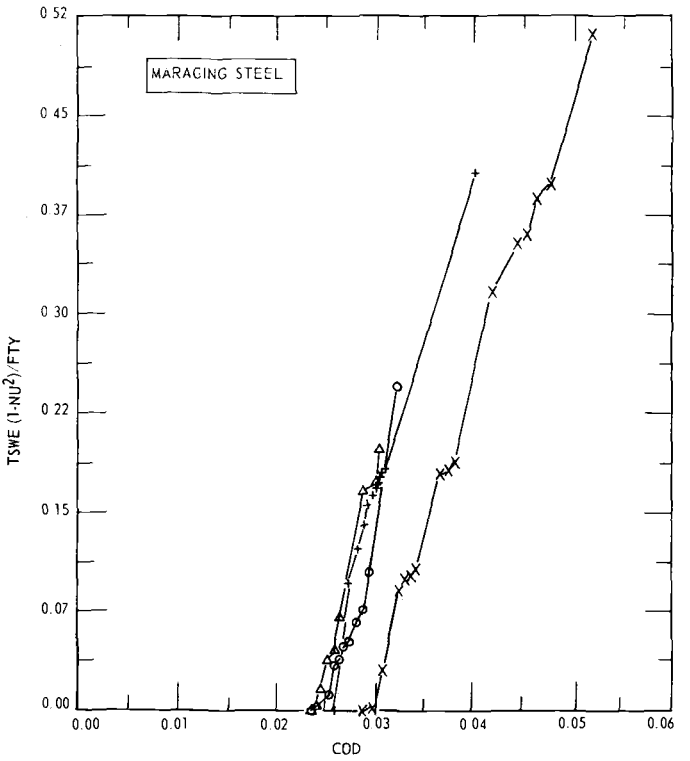

FIG. 21—*Relationship between measured crack opening displacement and calculated COD based on stress wave emission (same steels and test conditions as in Fig. 20).*

Acknowledgments

The research on stress corrosion cracking described in this paper was supported by the Metals and Ceramics Division of the Air Force Materials Laboratory, Contract AF 33(615)-2788, under the direction of K. L. Kojola, WP-AFB project engineer. The research on weld cracking was supported by the Naval Ship Systems Command (Code 03422), Contract N00024-70-C-5215, under the direction of B. B. Rosenbaum and John Gleim (Code 6101D). Also, we gratefully acknowledge the many helpful suggestions and the substantial contributions of R. L. Baker, R. T. Dahl, A. T. Green, and W. R. Phillips, all of Aerojet, who were responsible for the instrumentation used in this work.

References

[*1*] Kaiser, J. "Untersuchungen über das auftreten Geräuschen beim Zugversuch," Ph.D. thesis, Technische Hochschule, Munchen, 1950; also, *Arkiv für das Eisenhuttenwesen*, AREIA, Vol. 24, No. 1/2, Jan./Feb. 1953, pp. 43-45.

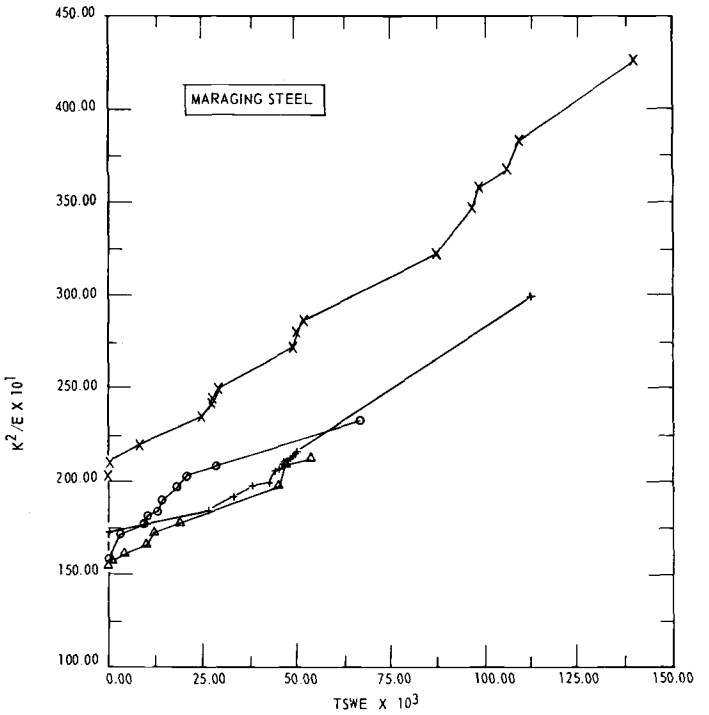

FIG. 22—*Relationship between cumulative stress wave count and stress field energy release rate.*

[2] Schofield, B. H., Bareis, R. A., and Kyrala, A. A., "Acoustic Emission Under Applied Stress," WADC Technical Report 58-194, April 1958.

[3] Schofield, B. H., "Acoustic Emission from Metals, Its Detection, Characteristics, and Source," Proceedings of the Symposium on Physics and Nondestructive Testing, Southwest Research Institute, San Antonio, Tex., Oct. 1963.

[4] Schofield, B. H., "Acoustic Emission Under Applied Stress," ASD-TR-53-509, Part 1, April 1963, Part 2, May 1964.

[5] Green, A. T., Lockman, C. S., and Steele, R. K., *Modern Plastics*, MOPLA, Vol. 41, July 1964, pp. 137-139.

[6] Green, A. T., Hartbower, C. E., and Lockman, C. S., "Feasibility Study of Acoustic Depressurization System," Report NAS 7-310, Aerojet-General Corporation, Feb. 1965.

[7] Hartbower, C. E., Gerberich, W. W., and Crimmins, P. P. in *Weld Imperfections*, Addison-Wesley, Menlo Park, Calif., 1968, pp. 371-389.

[8] Steele, R. K., Green, A. T., and Lockman, C. S. in *Weld Imperfections*, Addison-Wesley, Menlo Park, Calif., 1968, pp. 361-370.

[9] Hartbower, C. E., Gerberich, W. W., and Crimmins, P. P., "Characterization of Fatigue-Crack Growth by Stress-Wave Emission," NAS 1-4902, June 1966.

[10] Green, A. T., Lockman, C. S., Brown, S. J., and Steele, R. K., "Feasibility Study of Acoustic Depressurization System," NASA CR-55472, March 1966.

[11] Green, A. T., "Stress-Wave Detection, Saturn S-II," NASA CR-61161, Dec. 1966.

[12] Gerberich, W. W. and Hartbower, C. E., *International Journal of Fracture Mechanics*, IJFMA, Vol. 3, No. 3, Sept. 1967, pp. 185-192.

[13] Gerberich, W. W. and Hartbower, C. E., "Monitoring Crack Growth of Hydrogen Embrittlement and Stress Corrosion Cracking by Acoustic Emission," Conference on Fundamental Aspects of Stress Corrosion Cracking, Ohio State University, Sept. 1967.
[14] Hartbower, C. E., Gerberich, W. W., and Crimmins, P. P., "Mechanisms of Slow Crack Growth in High-Strength Steels," AFML-TR-67-26, Vol. 1 Aerojet-General Corp., Feb. 1967; also, *The Welding Journal*, WEJOA, Vol. 47, No. 1, Jan. 1968, pp. 1-18.
[15] Green, A. T., "Testing of 10-inch Glass Hemispheres Using Stress-Wave Analysis Technique," N00014-67-C-0333, Naval Ship Research and Development Center, Sept. 1967.
[16] Green, A. T. and Hartbower, C. E., "Stress-Wave Analysis Technique for Detection of Incipient Failure," Aerojet-General Corp., Proceedings of the ORNL Conference on Incipient Failure Diagnosis for Assuring Safety and Availability of Nuclear Power Plants, Gatlinburg, Tennessee, Oct. 1967.
[17] Reuter, W. G., Green, A. T., Hartbower, C. E., and Crimmins, P. P., "Monitoring of Crack Growth in Ti-6Al-4V Alloy by the Stress Wave Analysis Technique," Report on NASA Houston Contract NAS 9-7759, Dec. 1968.
[18] Hartbower, C. E., Gerberich, W. W., and Crimmins, P. P., *The Welding Journal*, WEJUA, Vol. 47, No. 10, Oct. 1968, pp. 443-443s.
[19] Hartbower, C. E., Gerberich, W. W., and Liebowitz, H., *Engineering Fracture Mechanics*, EFMEA, Vol. 1, No. 2, Aug. 1968, p. 291; also, "Stress-Wave Characteristics of Fracture Instability in Constructional Alloys," AD-674-881, Aerojet-General Corp., July 1968.
[20] Baker, G. S., "Acoustic Emission and Prefracture Processes in High-Strength Steels," AFML-TR-67-266, Aerojet-General Corporation, Wright-Patterson AFB, March 1968.
[21] Hartbower, C. E. and Crimmins, P. P., "Fracture of Structural Metals as Related to Pressure-Vessel Integrity and In-Service Monitoring," presented at the ICRPG/AIAA Third Solid Propulsion Conference AIAA Paper 68-501, Atlantic City, June 1968.
[22] Gerberich, W. W. and Reuter, W. G., "Theoretical Model of Ductile Fracture Instability Based on Stress-Wave Emission," ONR Contract Report N00014-66-C0340, Aerojet-General Corp., Sacramento, Calif., Feb. 1969.
[23] Hartbower, C. E., Reuter, W. G., and Crimmins, P. P., "Mechanisms of Slow Crack Growth in High Strength Steels and Titanium," Contract AF 33(615)-2788, Final Technical Report AFML-TR-67-26, Vol. 2, June 1969.
[24] Green, A. T., "Development of a Nondestructive Testing Technique to Determine Flaw Criticality," ARPA Contract F33615-68-C-1705, Aerojet-General Corp., Sacramento, Calif. Aug. 1969.
[25] Hartbower, C. E., *The Welding Journal*, WEJUA, Vol. 49, No. 2, Feb. 1970, p. 54s.
[26] Hartbower, C. E., Climent, F. J., Morais, C., and Crimmins, P. P., "Stress-Wave-Analysis Technique Study of Thick-Walled Type A302-B Steel Pressure Vessels," NASA NAS9-7759, Aerojet-General Corp., July 1969.
[27] Green, A. T., *Nuclear Safety*, NUSAA, Vol. 10, Jan.-Feb. 1969, pp. 4-18.
[28] Green, A. T., and Hartbower, C. E., "Development of a Nondestructive Testing Technique to Determine Flaw Criticality," ARPA Contract F33615-68-C-1705, Interim Technical Report, ARPA Order No. 1244, Code 8D10, May 1970.
[29] Dunegan, H. L., Harris, D. O., and Tatro, C. A., "Acoustic Emission Research Status Report, Dec. 1963-Aug. 1964," UCID-4868 Rev. 1, Lawrence Radiation Laboratory, Nov. 1964.
[30] Dunegan, H. L. and Tatro, C. A., *Reviews of Scientific Instruments*, RSINA, Vol. 38, No. 8, Aug. 1967.
[31] Dunegan, H. L., Harris, D. O., and Tatro, C. A., *Engineering Fracture Mechanics*, EFMEA, Vol. 1, No. 1, June 1968, pp. 105-122.
[32] Dunegan, H. and Harris, D., *Ultrasonics*, ULTRA, Vol. 7, July 1969, pp. 160-166.
[33] Tatro, C. A., "Sonic Techniques in the Detection of Crystal in Metals," Progress Report, Division of Engineering Research, Michigan State University, East Lansing, Mich., Jan. 1959.

[34] Tatro, C. A. and Liptai, R. G. in *Proceedings of the Symposium on Physics and Nondestructive Testing*, Southwest Research Institute, San Antonio, Texas, Oct. 1962, pp. 145-174.
[35] Liptai, R. G., "An Investigation of the Acoustic Emission Phenomenon,' Ph.D. thesis, Michigan State University, East Lansing, Mich., 1963.
[36] Engle, R. B., "Acoustic Emission and Related Displacements in Lithium Fluoride Single Crystals," Ph.D. thesis, Michigan State University, East Lansing, Mich., 1966.
[37] Mitchell, L. D., "An Investigation of the Correlation of the Acoustic Emission Phenomenon with the Scatter in Fatigue Data," Ph.D. thesis, University of Michigan, Ann Arbor, Mich., 1965.
[38] Kerawalla, J. N., "An Investigation of the Acoustic Emission from Commercial Ferrous Materials Subjected to Cyclic Tensile Loading," Ph.D. thesis, University of Michigan, Ann Arbor, Mich., 1965.
[39] Argarwall, A. B. L., "An Investigation of the Behavior of the Acoustic Emission from Metals and a Proposed Mechanism for its Generation," Ph.D. thesis, The University of Michigan, Ann Arbor, Mich., 1968.
[40] Frederick, J. R., "Use of Acoustic in Nondestructive Testing," Semi-Annual Report 01971-2-T, March-Aug. 1969, University of Michigan, Ann Arbor, Mich., Nov. 1969.
[41] Sankar, N. G., "Unload Emission Behavior of Material and Its Relation to the Bauschinger Effect," Ph.D. thesis, University of Michigan, Ann Arbor, Mich., 1969.
[42] Egle, D. M., "A Comprehensive Analysis of an Acoustic Emission Detection System," Ph.D. thesis, Tulane University, New Orleans, La., 1965.
[43] Chambers R. H., "New Techniques in Nondestructive Testing by Acoustical and Exo-electron Emission," AD-691-230, Arizona University, Tuscon, Ariz., July 1969.
[44] Day, C. K., "An Investigation of the Plastic Bursts of Microstrain in Zinc As Sources for Acoustic Emission," M.S. thesis, Washington State University, Pullman, Wash., 1969.
[45] Spanner, J. C., "A Selective Review on the Utilization of Acoustic Emission Techniques for Materials Research and Structural Integrity Analysis," M.S. thesis, Washington State University, Pullman, Wash., 1970.
[46] Notvest, K., *The Welding Journal*, WEJUA, Vol. 45, No. 4, April 1966, pp. 173-178s.
[47] Jolly, W. D., *The Welding Journal*, WEJUA, Vol. 48, No. 1, Jan. 1969, pp. 21-27.
[48] Poteat, L. E. and Warner, W. L., *The Welding Journal*, WEJUA, Vol. 39, No. 2, Feb. 1960, pp. 70-76s.
[49] Winterton, K. and Nolan, M. J., *The Welding Journal*, WEJUA, Vol. 39, No. 2, Feb. 1960, pp. 77-82s.
[50] Rathbone, A. M., Conner, L. P., and Gross, J. H., *The Welding Journal*, WEJUA, Vol. 43, No. 12, Dec. 1964, pp. 551-563s.
[51] Kammer, P. A., Masubuchi, K. and Monroe, R. E., "Cracking in High-Strength Steel Weldments–Critical Review," DMIC Report 197, 7 Feb. 1964.
[52] Brown, W. F. and Srawley, J. E., *Plane-Strain Crack Toughness Testing of High-Strength Metallic Materials, ASTM STP 410*, American Society for Testing and Materials, 1967, p. 12.
[53] Fisher, D. M., Bubsey, R. T., and Srawley, J. E., "Design and Use of Displacement Gage for Crack Extension Measurements," Technical Note D-3724, NASA, Nov. 1966.
[54] Stavros, A. J. and Paxton, H. W., "Stress-Corrosion Cracking Behavior of a 18 percent Ni Maraging Steel," Contract Nonr-760 (31), ARPA Order #878, April 1970.
[55] Hartbower, C. E., Gerberich, W. W., and Crimmins, P. P., "Characterization of Fatigue Crack Growth by Stress Wave Emission," NASA Langley Research Center Contract NAS 1-4902, Final Report CR-66303, June 1966; see also *International Journal of Fracture Mechanics*, Vol. 3, Sept. 1967, p. 185.
[56] Irwin, G. R., *Engineering Fracture Mechanics*, EFMEA, Vol. 1, No. 2. 1968, 241-257.

K. A. Fowler[1] *and E. P. Papadakis*[1]

Observation and Analysis of Simulated Ultrasonic Acoustic Emission Waves in Plates and Complex Structures

REFERENCE: Fowler, K. A. and Papadakis, E. P., "**Observation and Analysis of Simulated Ultrasonic Acoustic Emission Waves in Plates and Complex Structures,**" *Acoustic Emission, ASTM STP 505*, American Society for Testing and Materials, 1972, pp. 222-237.

ABSTRACT: Experiments have been performed with the Panametrics acoustic emission simulation test set which show that acoustic emission signals in plates and shells travel in the plate modes supported by these shapes. The first longitudinal plate mode has the highest group velocity in its low-frequency limit, and signals in that mode and frequency range arrive first, followed by strong signal at the velocity of the first flexural mode in its nondispersive region. In some cases the flexural signal is much stronger than the longitudinal signal. In general, the received signals are dispersed. The time-frequency-energy output matrix tends to be complicated, as energy of different frequencies is spread over time by the various dispersive modes. Special transducers can be used to discriminate against certain particle motions, suppressing the reception of certain modes, and may be useful in triangulation studies.

KEY WORDS: acoustics, emission, triangulation surveys, elastic waves, shear properties, piezoelectric transducers, dispersing, wave dispersion, plates (structural members), ultrasonic frequencies, Lamb waves, crack propagation

Acoustic emissions are generally thought of as step or delta functions due to the nature of the generating source, and as such the emissions contain a broad spectrum of frequencies[*1*]. If the propagation medium is nondispersive, the entire burst arrives at the receiver undistorted. However, if the propagation medium is dispersive, some frequencies arrive later than others[*2*]. The pulse is spread out into an FM signal with both frequency and amplitude varying with time at the receiver.

Most materials in the form of bulk samples are nondispersive except near

This work was supported in part by the Office of Naval Research, Acoustics Programs.

[1] Chief, Materials Evaluation Branch, and department head, Physical Acoustics Department, respectively, Panametrics, Waltham, Mass.

phase transitions. Metals, for instance, are nondispersive except near Curie temperatures, superconducting critical temperatures, martensitic phase transition temperatures, order-disorder transition temperatures, and the like [3]. In other words, engineering materials at their operating temperatures are nondispersive. Structures, however, can be dispersive. Geometrical boundary conditions applied to solids, in particular, rods and plates [4], make the resultant shape dispersive. A spectrum of frequencies applied as an impulse to a point on or within a plate will arrive at another point on the plate later, strung out in time with a time-varying amplitude and frequency content. The maximum amplitude may appear far into the FM burst on the time scale, and the first-arrival signal may not be at the center frequency of the spectrum of the burst.

The fact that plates are dispersive is particularly significant to the test engineer because so many structures are fabricated from plates or plate-shaped sections. Pressure vessels have received much attention recently [5] because they have simple shapes and can be easily pretested in their mode of operation. While internal pressure is being applied, the acoustic emission can be monitored. Triangulation schemes locate cracks from the time of arrival of emission signals [5]. In this context, the importance of dispersion in the structure becomes obvious.

Theory

This paper deals with dispersive wave propagation in plates. The theory follows the treatment of Meeker and Meitzler [4]. The elastic wave energy in the plate can be divided up into an infinite number of modes, all but one of which are dispersive for some range of frequencies. The modes comprise dilatational, flexural, and shearing strains. It is likely that an acoustic emission from a propagating crack will excite all the modes which will propagate within the frequency range in the emission spectrum. Higher modes have cutoff frequencies below which they do not propagate, so the spectrum of the acoustic emission will not excite them. The cutoff frequency depends upon a normalized, dimensionless frequency

$$\tilde{f} = hf/v_s \tag{1}$$

where h is the plate thickness, f is the frequency, and v_s is the shear wave velocity in the bulk material. In Fig. 1 we plot the normalized group delay

$$\tilde{D} = Dv_s/L \tag{2}$$

versus the normalized frequency for four modes in aluminum. The group delay is D, and L is the path from transmitter to receiver. A wave packet of center frequency f will traverse a distance L such that its center arrives after a delay D.

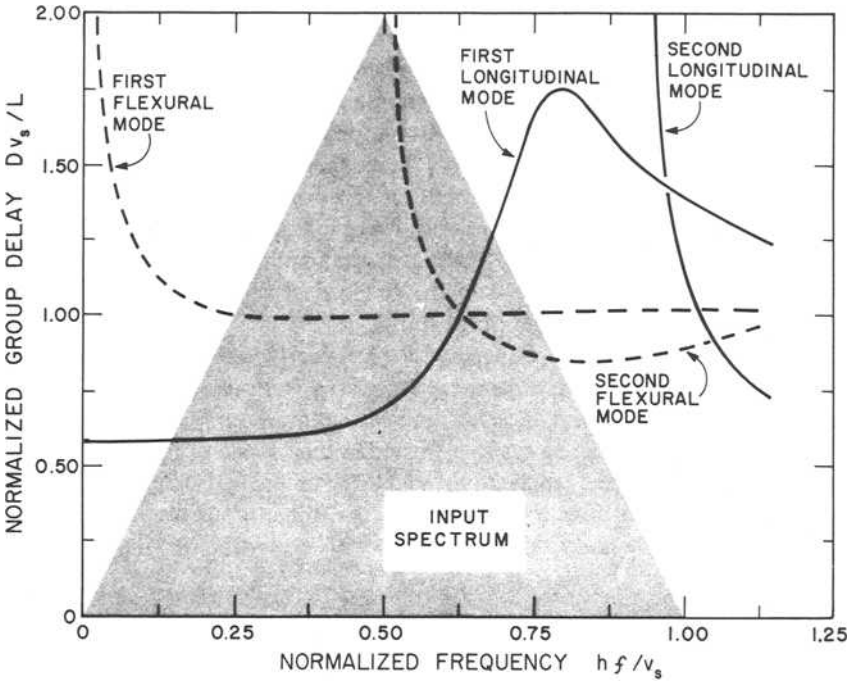

FIG. 1–*Normalized group delay as a function of normalized frequency for the lower longitudinal and flexural modes in plates. Calculation for Poisson's ratio = 0.35 after Meeker and Meitzler[4]. Superimposed is a hypothetical input spectrum for an acoustic emission. The energy at any frequency, divided among the propagating modes, arrives at a receiver at times corresponding to the group delay.*

As an example, if it were possible to excite only the first longitudinal mode at $\tilde{f} = 0.80$, then the energy would arrive at the receiver with a relative delay $\tilde{D} = 1.75$, or a delay of $D = 1.75\ L/v_s$. If all three possible modes at $\tilde{f} = 0.80$ were excited, then energy would arrive at times $0.85\ L/v_s$, $1.00\ L/v_s$, and $1.75\ L/v_s$.

For simplicity the horizontal shear modes were omitted from the following analysis, although it was recognized that energy would go into those modes. The receiver used in the experiment discriminated against the horizontal shear motion; thus, the results are qualitatively accurate because no energy traveling at the horizontal shear velocity could be received.

Again, for simplicity, a triangular frequency spectrum $B(f)$ centered at $hf/v_s = 0.5$ was chosen. The spectrum is superimposed upon the mode curves in Fig. 1. It represents a unit of energy input because

$$\int_0^1 B(hf/v_s)\, d(hf/v_s) = 1 \tag{3}$$

The energy was divided equally among the modes present, assuming equipartition of energy. Then the abscissa hf/v_s of Fig. 1 was divided into eight increments for numerical analysis, and the time of arrival of the energy in each mode was found from the curves. In Table 1 the energy density in the various frequency intervals is given versus relative arrival time $\tilde{D}$. This time-frequency-energy matrix is examined below.

Experiments

Equipment

The Panametrics acoustic emission simulation test set (AESTS)[6] was used with a spectrum analyzer system to test the theory outlined above. The AESTS consists of a Panapulser 5050M pulser, a magnetostrictive transducer driving a wire delay line with a needlepoint, a receiving transducer (in this case a Panametrics 5070 VIP-5-½-L broadband NDT transducer, although other types can be used), and a Panametrics 5050 AE-160 preamplifier. A broadband pulse simulating the acoustic emission is generated by the pulser and introduced into the specimen by the magnetostrictive transducer and wire. The pulse travels in the plate as acoustic energy, which is picked up by the receiving transducer and displayed on an oscilloscope. A block diagram of the entire system is given in Fig. 2. The received signal is also sent to a stepless gate, which is adjustable in

TABLE 1—*Time-frequency-energy matrix.*

$D=\frac{Dv_s}{L}$	hf/v_s							
	0.125	0.250	0.375	0.500	0.625	0.750	0.875	1.000
0.1	...	...	...	...	...	...	...	...
0.2	...	...	...	...	...	...	...	...
0.3	...	...	...	...	...	...	...	...
0.4	...	...	...	...	...	...	...	...
0.5	0.016	0.047	0.078	...	...	...	...	...
0.6		...	...	0.109	...	...	...	...
0.7		...	...	...	...	...	...	...
0.8		...	...	...	0.074	...	...	...
0.9		...	...	...	...	0.052	0.031	0.010
1.0		...	0.078	0.109	0.074	0.052		
1.1		0.047	...	...		...	0.031	0.010
1.2	↑	...	...	...	↑	...	...	...
1.3	|	...	...	...	|	0.052	...	...
1.4	|	...	...	...	|	...	...	0.010
1.5	0.016	...	...	...	0.074	...	...	...
1.6	spread	...	...	...	spread	...	...	...
1.7	↓	...	...	...	↓	...	0.31	...
1.8		...	...	...		...	...	...
1.9		...	...	...		...	...	...
2.0		...	...	...		...	...	...

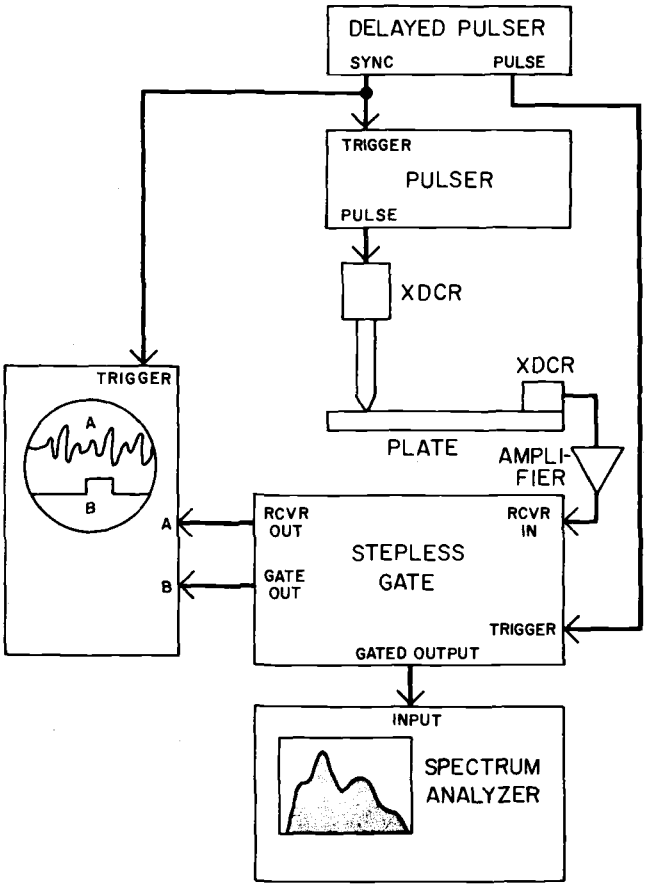

FIG. 2–*Block diagram of the electronic system used to sample the frequency spectrum of the simulated acoustic emission signal. The gate sends segments of the signal in the time domain to the spectrum analyzer.*

position and width so that different parts of the acoustic signal can be sampled. The gate signal is also displayed on the oscilloscope to show the portion of the acoustic signal being sampled. (See Fig. 3 for a typical oscillogram.) The sampled portion of the signal is sent to a Hewlett-Packard Spectrum Analyzer #140T which displays the frequency spectrum on a built-in cathode ray tube. Figure 4 is the spectrum of the grated portion of the signal in Fig. 3. The block diagram of Fig. 2 shows how the range of the instrumentation can be extended to lower frequencies (with the Panapulser 5050M) and to longer delay times with the auxiliary delayed pulser.

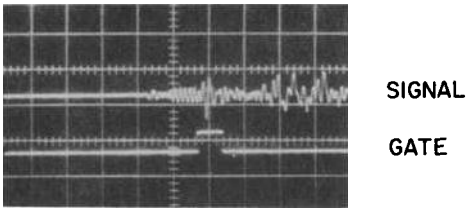

FIG. 3—*Typical simulated acoustic emission signal after dispersion in an aluminum plate. The gate pulse is also shown.*

Materials

The experiment to test the time-frequency-energy matrix of Table 1 was performed on an aluminum plate ½ in. (1.27 cm) thick and about 28 in. (71 cm) square. The VIP-5 receiving transducer was located on one major face near the center of one edge, and the point of the wire from the magnetostrictive input transducer was located at various points along a line passing through the VIP-5 position and bisecting the plate (see Fig. 5). This plate was ideal for demonstrating the dispersion from the triangular spectrum in Fig. 1, because the normalized frequency hf/v_s is 1.0 at a frequency of 240 kHz. Essentially all the energy fell below 300 kHz in the experiment.

Another experiment was performed to give a qualitative illustration of dispersion in engineering structures. A tank with a wall 0.25 in. (0.635 cm) thick for holding compressed gas was investigated with the AESTS system. While a monitoring oscilloscope (see Fig. 6) was used, the spectrum analyzer was not.

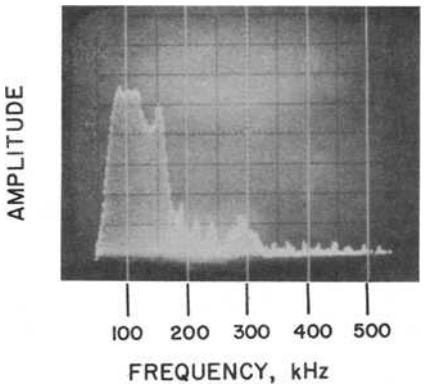

FIG. 4—*Spectrum of the gated portion of the signal in Fig. 3.*

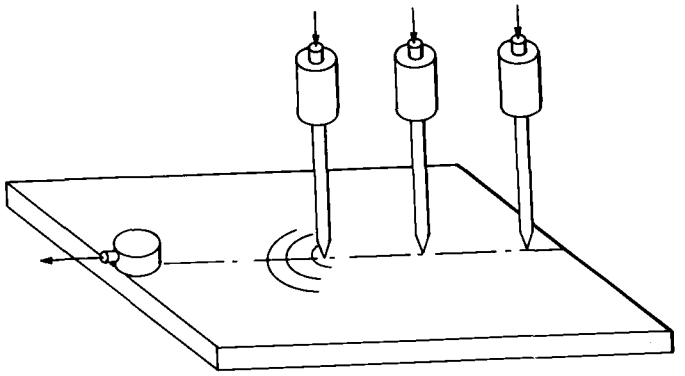

FIG. 5–*Geometry of the experiment on the aluminum plate. The magnetostrictive transducer with the pointed leadin wire was placed at several positions, while the VIP-5 broadband transducer was kept at the edge of the plate.*

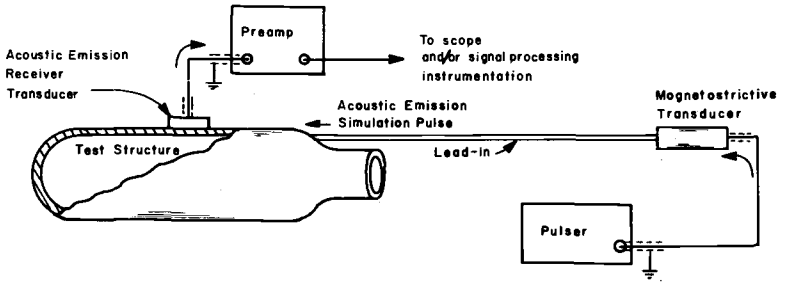

FIG. 6–*Geometry of the experiment on the steel gas cylinder.*

Results

Aluminum Plate

The experiment on the aluminum plate was divided into three sections, as follows:

1. Measure the frequency content of the entire received acoustic signal for various distances between transmitter and receiver.
2. Measure the frequency content of the leading edge of the received acoustic signal for various distances between transmitter and receiver.
3. Measure the frequency content of portions of the received acoustic signal gated out as a function of arrival time for various distances between transmitter and receiver.

Frequency Content of Entire Pulse–The frequency content of the entire pulse was measured at various transmission distances to detect attenuation (if

present) as a function of frequency. Signals from two paths, 1 in. (2.54 cm) and 14 in. (35.6 cm), are shown in Fig. 7. The pulse spreads out in time but the frequency spectrum is almost constant when the entire dispersed pulse is gated into the spectrum analyzer. The attenuation is independent of frequency, being due to circular spreading from the point source. Note that the frequency

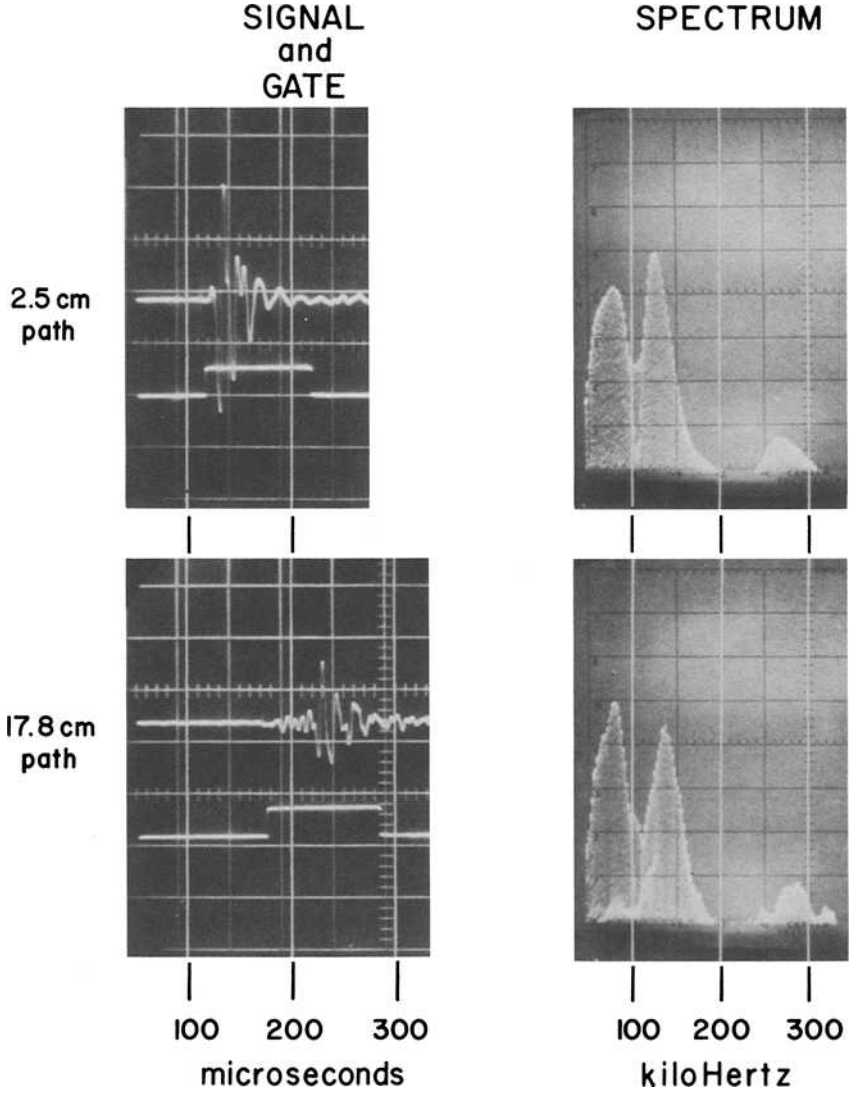

FIG. 7—*Simulated acoustic emission signals and their spectra when the entire dispersed signal is sent to the spectrum analyzer. The spectrum is essentially unchanged with path length, although the pulse shape in the time domain is altered drastically.*

spectrum is not a perfect triangle as used in the theory, so the later results will be qualitative.

Frequency Content of Leading Edge–For triangulation with emission sources, experimenters have proposed using the leading edge of the pulse to determine the pulse travel time from the defect to the transducer. It is important to measure the frequency content of the leading edge versus distance to ascertain that the disturbance represents a specific mode of propagation with a definite velocity. If it has a definite velocity, then triangulation will yield a true position of the defect.

The leading edge spectra for various distances between transmitter and receiver are shown in Fig. 8, along with the pulse and gate pictures. The spectra are fairly sharp, centered around 100 to 110 kHz, whereas the amplitudes of the total spectra (Fig. 7) are greater elsewhere. The velocity of the mode carrying the leading energy was found from the travel time as measured on the oscilloscope traces. The delay in the input wire was subtracted out. The measurements and results are given in Table 2. The average velocity, 0.508 cm/μs, is between the free-field plane wave velocity v_l of 0.642 cm/μs for longitudinal waves and $v_s = 0.304$ cm/μs for shear waves as given by Mason [7] for rolled aluminum. However, the velocity does correspond, within experimental error, to the velocity of the first longitudinal plate mode in Fig. 1 at $hf/v_s = 0.45$ on the abscissa, which corresponds to 100 to 110 kHz. ($hf/v_s = 1.0$ is 240 kHz as mentioned earlier.) At $hf/v_s = 0.45$, the group velocity of the first longitudinal plate mode is about 9 percent lower (because the group delay, Fig. 1, is 11 percent higher) than the plate velocity v_p, which is its low-frequency limiting velocity. The formula [4] for v_p is

$$v_p = v_s \left[2/(1 - \sigma)\right]^{1/2} \tag{4}$$

where v_s is the bulk shear velocity and σ is Poisson's ratio. Using the ASM values [8] for modulus of rigidity, density, and Poisson's ratio for the actual alloy investigated (6061), the shear velocity is found to be $v_s = 0.312$ cm/μs and the plate velocity to be $v_p = 0.540$ cm/μs. The velocity is $v_{1L} = 0.491$ cm/μs which is 9 percent lower for the first longitudinal mode. This value differs from

TABLE 2–*Delay and velocity of leading edge.*

Length, cm	Delay, μ		Velocity, cm/μ
17.8	37		0.480
35.6	65		0.546
53.3	107		0.498
71.1	140		0.508
		Avg	0.508

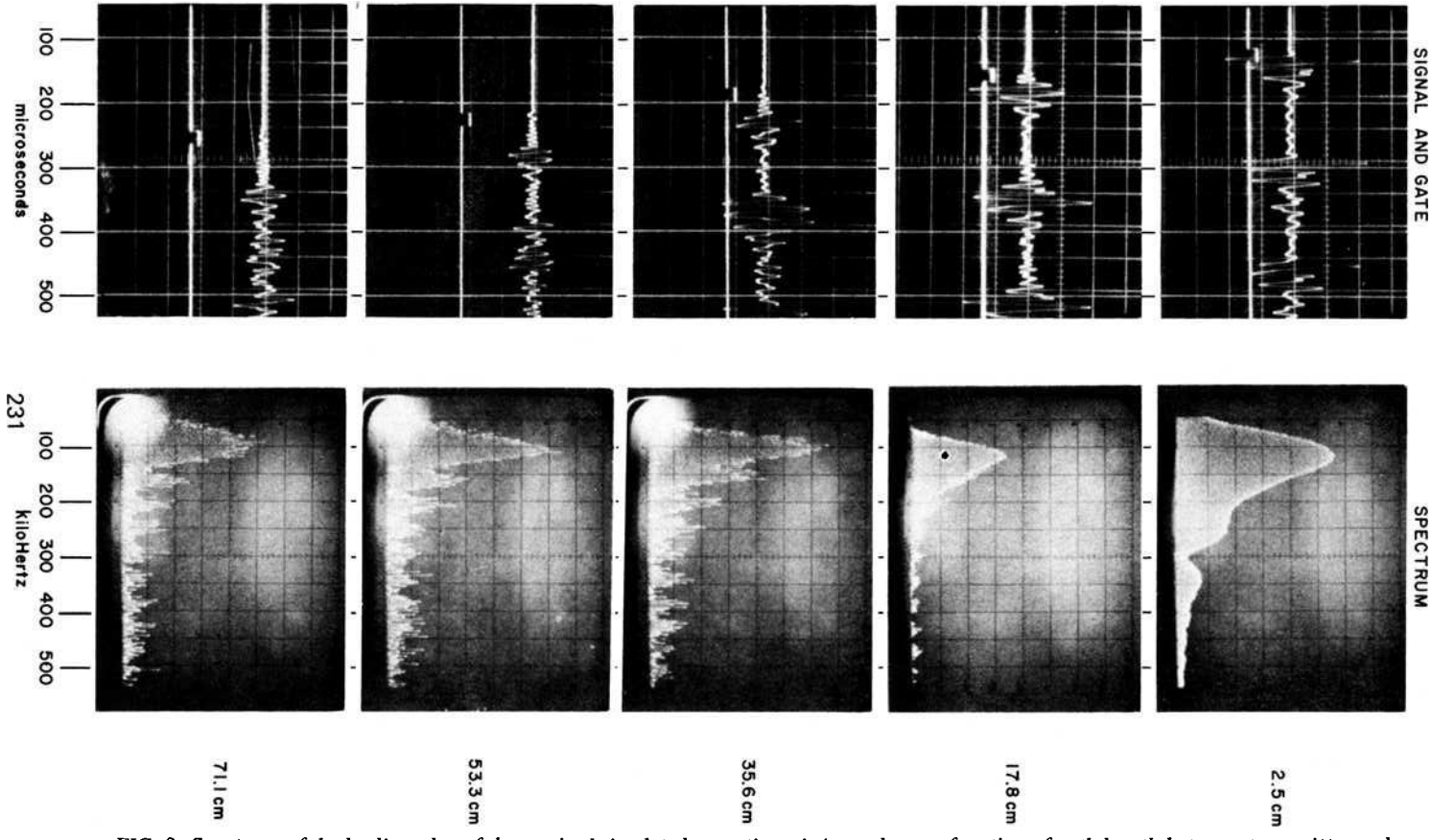

FIG. 8—*Spectrum of the leading edge of the received simulated acoustic emission pulse as a function of path length between transmitter and receiver. The spectrum holds constant with distance and is different from the spectrum of the whole pulse, Fig. 7. It is thought that the first longitudinal mode in its low-frequency limit carries this energy.*

the velocity measured experimentally by only 3.3 percent. This velocity correspondence confirms that the earliest arriving energy is carried by the first longitudinal mode in the plate. It is clear from Fig. 1 that the earliest arriving energy should indeed be carried by the first lontigudinal mode and should be centered below 120 kHz; there, the group delay is lowest. The results in Table 1 showed that the earliest arriving energy should be below 120 kHz ($hf/v_s = 0.500$) and should be most intense between $hf/v_s = 0.375$ and 0.500. This was found to be the case experimentally, tending to verify the hypothesis of energy transport by plate modes.

Frequency Content within Dispersed Pulse–For a complete test of the time-frequency-energy matrix of Table 1, the frequency content of small portions of the dispersed pulse were gated out in the time domain and fed to the spectrum analyzer. The pulse oscillograms and spectra are shown in Fig. 9 for the 28-in. propagation path. The spectrum of the first-arrival energy, Fig. 9*a*, was centered at 100 to 110 kHz, as noted above, and had little energy above 120 kHz. This spectrum corresponds to a relative time between $\widetilde{D} = 0.5$ and 0.6 in Table 1. The spectrum of the second portion of the pulse, Fig. 9*b*, (appearing as a clean 4-cycle burst of rf) is centered at 130 kHz and corresponds to $\widetilde{D} = 0.8$. According to Fig. 1, the first longitudinal mode carries most of this in its curved region between $hf/v_s = 0.500$ and 0.625. The higher frequency tail in the spectrum around 170 to 220 kHz is carried by the second flexural mode and corresponds to $\widetilde{D} = 0.9$. The third portion of the pulse, Fig. 9*c*, resembles a 1½-cycle broadband pulse and contains a broad spectrum of frequencies. The time slot corresponds to $\widetilde{D} = 1.0$, where the first longitudinal and the first and second flexural modes cross simultaneously in Fig. 1. The energy distribution in the spectrum corresponds closely to the row $\widetilde{D} = 1.0$ in the time-frequency-energy matrix, except for the high-frequency peak around 280 kHz which may be carried by the second longitudinal mode or possibly by the first flexural mode above $hf/v_s = 1.0$, the upper limit of the spectrum $B(f)$ considered here. The fourth and fifth portions of the pulse (Figs. 9*d* and 9*e* unfortunately may contain reflected energy from the lateral edges of the square specimen. From geometrical considerations it is apparent that the 120-kHz energy may contain a reflected portion of the first longitudinal mode, which was the first-arrival signal at the lateral edges; however, the second flexural mode can also carry that frequency in the time interval under consideration. The high-frequency components are possibly direct rays carried by the first and second longitudinal modes in the range $\widetilde{D} = 1.3$ to 1.7.

The velocity of the mode carrying the energy in the third segment of the received signal was calculated by measuring the time to the center of the 1½-cycle strong video pulse (see Fig. 9*c*. The measurements were made on the oscillograms in Fig. 8. The delay in the input wire was again subtracted out. The measurements and results are given in Table 3. The average velocity,

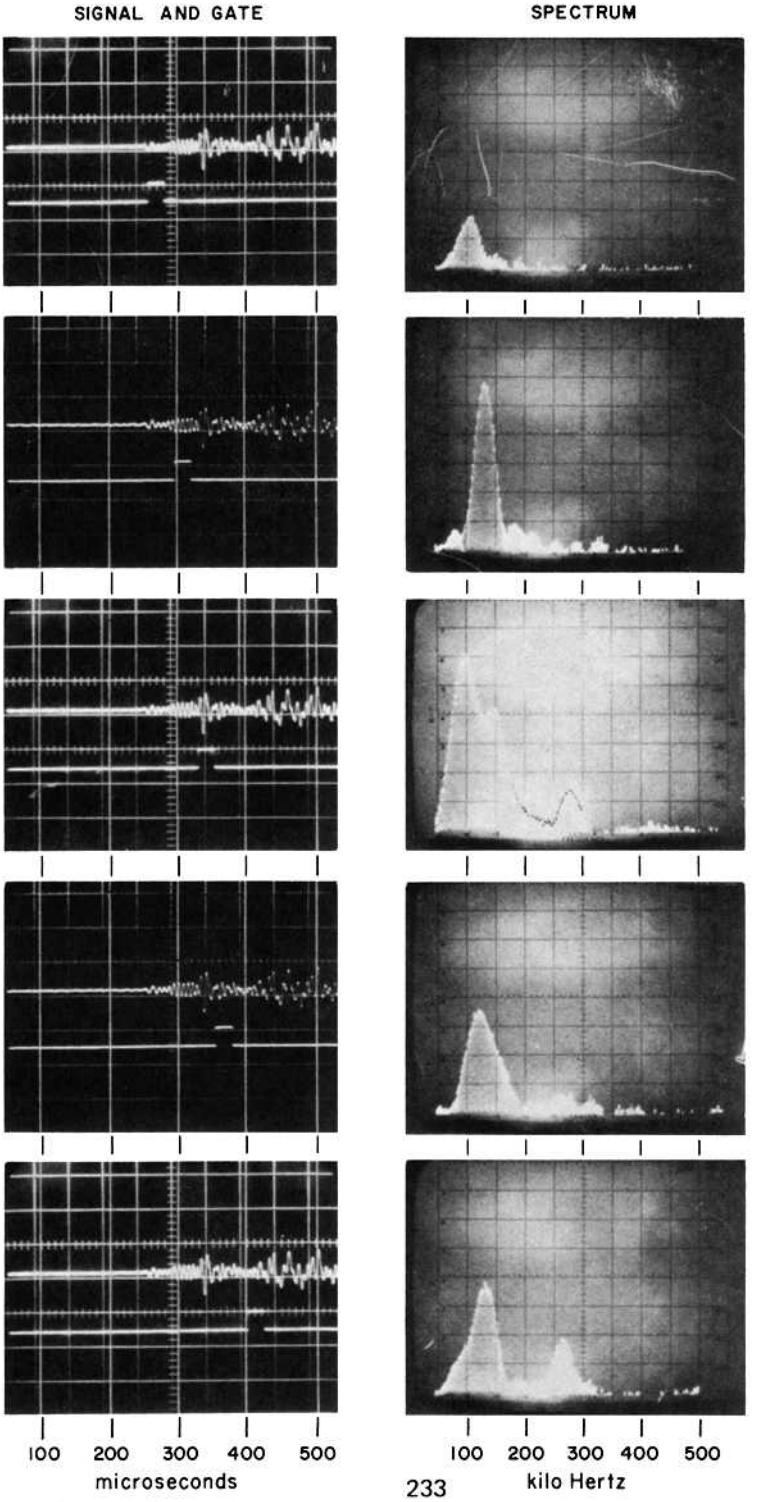

FIG. 9—*Spectrum of the various segments of the simulated acoustic emission pulse versus delay after a 28-in. path. The spectrum varies with delay time in the received signal as explained in the text. The analysis is consistent with the mode picture of Fig. 1.*

TABLE 3–*Delay and velocity of the major video spike.*

Length, cm	Delay, μs	Velocity, cm/μs
17.8	60	0.297
35.6	110	0.322
53.3	165	0.322
71.1	225	0.315
	Avg	0.314

0.314 cm/μs, agrees almost exactly with the shear velocity of 0.312 cm/μs calculated earlier. In reality, however, the energy was traveling in the first flexural mode, which has the same velocity between $hf/v_s = 0.25$ and 1.00 since it is essentially nondispersive in that region. Thus, the first flexural mode carries a definitely discernible broadband pulse in the nondispersive region of the mode.

In general, the measured frequency spectra of the various time-domain segments of the dispersed pulse agree qualitatively and in some cases semiquantitatively with the time-frequency-energy matrix of Table 1. It can be stated that plate mode analysis is a valid way of describing the dispersive nature of acoustic emission pulses.

Pressure Cylinder

Longitudinal Wave Receiver–When the magnetostrictive extensional wave wire input and the broadband pressure-sensing receiver were used, signals resembling those of Fig. 10 were obtained. There, the signals are shown for various distances between input and output. The first-arrival signal is a chirped pulse with the high frequency portion toward the leading edge. The leading edge arrives after a delay corresponding to a group velocity of 0.318 cm/μs. This velocity is close to the bulk shear velocity [6] and the group velocity of the first flexural mode in its nondispersive region, that is, for $hf/v_s > 0.25$ in Fig. 1. Since the VIP-5-½ transducer when used as receiver will respond to flexural motion in the tank wall, but not to horizontal shear, the received energy must be traveling in a flexural mode, probably the first. For $h = 0.635$ cm and $v_s = 0.318$ cm/μs, the frequency f must be greater than 125 kHz. Thus, in the first flexural mode, the energy above 125 kHz would arrive first at a velocity of about 0.318 cm/μs, while the energy at lower frequencies would arrive later, with a longer delay as shown in Fig. 1. The appearance of the chirped pulses in Fig. 10 is consistent with propagation in the first flexural mode, since the high frequencies arrive first and the low frequencies arrive later.

In the region below $hf/v_s = 0.50$ (equivalent to f below 250 kHz in the steel wall), where most of the energy resides, only the first flexural and the first longitudinal modes propagate (discounting horizontal shear which will go undetected). It is not clear why a longitudinal wave does not appear before the

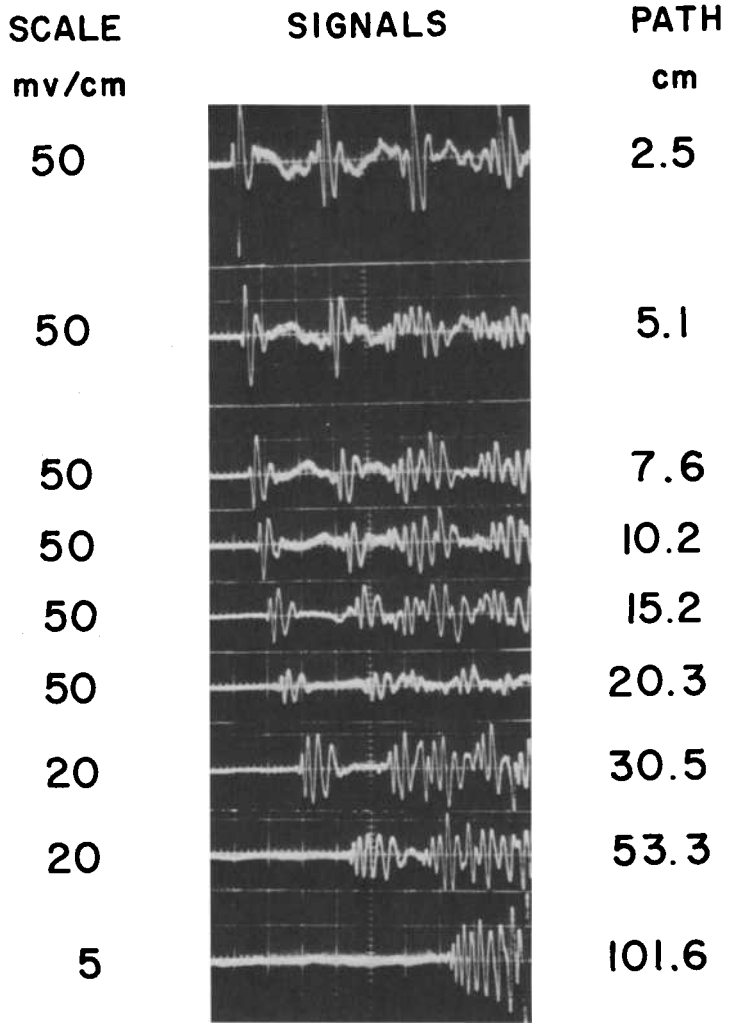

FIG. 10—*Dispersed signals from the simulated acoustic emission test set used on the steel gas cylinder of Fig. 6. (Multiple echoes are reverberations in the input wire.) The signals are chirped with the high frequencies arriving first. Most of the energy is in the first flexural mode.*

flexural pulse. The plate velocity is 0.540 cm/μs (Eq 4), so longitudinal motion, if present, should manifest itself well ahead of the fastest flexural signal. It may be that the curvature of the cylinder mitigates against the generation or propagation of a longitudinal plate displacement. Further work should be performed to investigate this question, because the experiment suggests that the first-arrival acoustic emissions travel by flexure in curved shells, not by the first

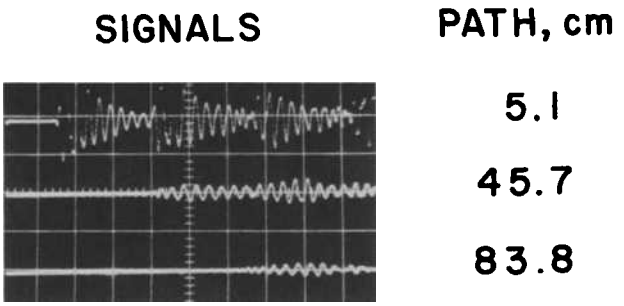

FIG. 11–*Simulated acoustic emission signals as received by cross-coupled transducers which tend to receive all modes. The energy is in the first flexural or zeroth shear modes, which have almost the same velocity over a large frequency range.*

longitudinal plate mode as found in flat plates. If the longitudinal motion is present, its amplitude relative to the flexural amplitude should be studied as a function of hf/v_s and as a function of radius of curvature of the shell.

Other Receiving Transducers–Experiments were also performed with three other types of receiving transducers, designated AE-0.1-L (longitudinal), AE-0.1-S (shear), and AE-0.1-CC (cross-coupled). The designation 0.1 refers to 0.1 MHz = 100 kHz, the approximate resonant frequency. The L type will respond to longitudinal and flexural waves, the S type to horizontal shear waves, and the CC type to all types. Their common characteristic is high sensitivity achieved through undamped, resonant piezoelectric elements.

Results of cementing CC-type probes to the cylinder at three different distances from the magnetostrictive wire input are shown in Fig. 11. The velocity of earliest arrival is 0.33 cm/μs, proper for the nondispersive portion of the first flexural mode and for the zeroth shear mode which is intrinsically nondispersive. Careful study of the photograph reveals that the earlier part of

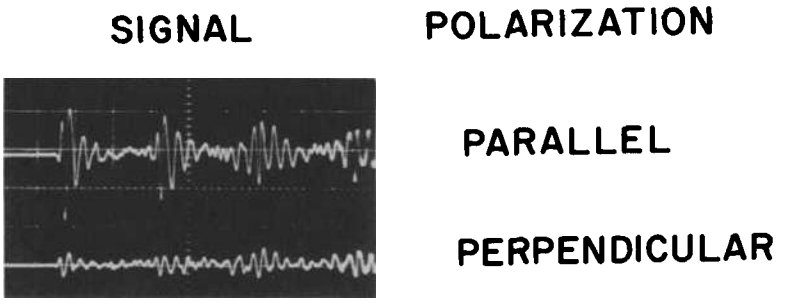

FIG. 12–*Simulated acoustic emission signals as received by shear mode transducers. With the shear polarization of the piezoelectric ceramic parallel to the input wire carrying an extensional wave, the signal is maximized as expected.*

the signal contains the higher frequencies, while the lower frequencies are delayed to a later point in the signal. This chirping is consistent with propagation in the first flexural mode.

The directivity of the S-type transducers is demonstrated in Fig. 12. Horizontal shear motion was imparted by attaching the magnetostrictive transducer at grazing incidence to the cylinder. The AE-0.1-S transducer yielded the largest signal when its polarization was in line with the wire. A minimum signal was received at 90 deg to this direction.

Acknowledgments

We wish to acknowledge the assistance of James Bradshaw in arranging the electronics and carrying on many of the measurements reported here. The continued interest of Marvin Lasky and Robert Faires of the Office of Naval Research is greatly appreciated.

References

[1] Lindsay, R. B., *Mechnical Radiation*, McGraw-Hill, New York, 1960, pp. 105-109.
[2] Lindsay, R. B., *Mechanical Radiation*, McGraw-Hill, New York, 1960, pp. 109-112.
[3] Garland, C. W. in *Physical Acoustics: Principles and Methods*, Vol. 7, W. P. Mason, Ed., Academic Press, N. Y., 1970, pp. 52-148.
[4] Meeker, T. R. and Meitzler, A. H. in *Physical Acoustics: Principles and Methods*, Vol. 1, Part A, W. P. Mason, Ed., Academic Press, N. Y., 1964, pp. 111-167.
[5] Hutton, P. H. and Parry, D. L., *Materials Research and Standards*, MTRSA, Vol. 11, No. 3, March 1971, pp. 25-32.
[6] Fowler, K. A., *Materials Research and Standards*, MTRSA, Vol. 11, No. 3, March 1971, pp. 35-36.
[7] Mason, W. P., *Physical Acoustics and the Properties of Solids*, D. Van Nostrand Co., Inc., Princeton, N. J., 1958, p. 17.
[8] *Metals Handbook*, Vol. 1, eighth edition, American Society for Metals, Novelty, Ohio, 1961, p. 946.

D. O. Harris,[1] *A. S. Tetelman,*[2] *and F. A. Darwish*[3]

Detection of Fiber Cracking By Acoustic Emission

REFERENCE: Harris, D. O., Tetelman, A. S., and Darwish, F. A., "**Detection of Fiber Cracking By Acoustic Emission,**" *Acoustic Emission, ASTM STP 505,* American Society for Testing and Materials, 1972, pp. 238-249.

ABSTRACT: A theoretical model is presented that relates acoustic emission to fiber cracking which occurs during a rising load tension test on a fiber reinforced composite. The percentage of broken fibers in an Al_3Ni fiber reinforced aluminum was measured as a function of tensile strain by optical inspection of the polished surface of strained specimens. This information was used in conjunction with the proposed model to predict the acoustic emission response of the composite material. These predictions were compared with experimental observations, and a good agreement was obtained between the two sets of results. These results indicate that it is possible to relate acoustic emission quantitatively to the micromechanics of the deformation processes occurring within fiber reinforced composites, thereby demonstrating the applicability of acoustic emission to materials studies and also to nondestructive evaluation of the integrity of composite materials.

KEY WORDS: nondestructive tests, composite materials, fiber composites, cracking (fracturing), tension tests, strains, deformation, acoustics, emission, elastic waves, failure, fractures (materials), stress waves

Nomenclature

a, b, c = Numerical constants

B, C_1, C_2, C_3 = Proportionality constants

E_f = Young's modulus of fiber

$E_1(x)$ = An exponential integral, defined as $\int_x^\infty \frac{e^{-y}}{y} dy$

Portions of this work were performed under the auspices of the United States Atomic Energy Commission. The National Aeronautics and Space Administration also provided financial support under contract NSG-622.

[1] Director of Research, Dunegan Research Corp., Livermore, Calif.

[2] University of California at Los Angeles, Los Angeles, Calif.

[3] Cairo, United Arab Republic.

N = Total number of acoustic emission counts observed since beginning of test
n = Number of acoustic emission counts observed from a single "event"
t = Time
t^* = Time for amplified acoustic emission signal to ring down below the trigger level of the counter
U = Energy released during an acoustic emission "event"
V = Voltage of amplified and filtered acoustic emission signal
V_t = Minimum voltage required to trigger the counter
V_o = Initial voltage of acoustic emission signal due to a single event
β = Time constant of exponential decay of sensor signal due to a single event
ϵ = Tensile strain
ϵ_f = Strain in fiber
ϵ_o = Threshold strain for detection of acoustic emission
λ = Frequency of the acoustic emission signal in rad/s
σ_f = Stress in fiber
ω = Percentage of cracked fibers

The increased need for high strength, low weight materials with sufficient ductility for structural applications has recently led to a rapidly expanding interest in composite materials. These materials show great promise for the development of materials which are tailor-made for specific critical applications. However, there are problems in the use of composites, such as the relative difficulty encountered in studying deformation characteristics, and in non-destructive evaluation of the integrity of the material. Acoustic emission is a relatively new technique that appears well suited for application to these problem areas, and the purpose of this investigation is to demonstrate this applicability. The acoustic emission observed from a whisker reinforced metal tension specimen during a rising load test is investigated and correlated with fiber breakage characteristics of the material as determined from independent tests.

Experimental Techniques

Material

The material selected for this investigation was a unidirectionally solidified Al-Al_3Ni eutectic alloy. This material was prepared by the carefully controlled, unidirectional solidification of an aluminum nickel alloy of eutectic composition. This technique results in the growth of the second phase in a regular form such as rods or platelets aligned in a matrix of the other phase [*1-4*]. The

Al-Al_3Ni material used in this investigation was produced at a solidification rate of 2 cm/h, which resulted in a microstructure of rodlike Al_3Ni whiskers embedded in a continuous matrix of aluminum containing about 0.045 percent Ni in solid solution.

The fiber diameter was 1.42 μm, and the average distance between centers of nearest neighbor fibers was 3.4 μm. References *4* and *5* provide a detailed description of the solidification procedure.

Specimen

A flat pin-loaded tension specimen was used in this investigation. The 1-in.-long gage section had a cross section of 0.40 by 0.040 in. Aluminum reinforcements were bonded to the faces of the specimen with epoxy in the region around the pins in order to eliminate pull-out of the loading pins. The regions around the pins were preloaded to values greater than the load required to break the specimen in the gage length. This procedure eliminated extraneous noise that could originate from the highly stressed regions and the epoxy bond. Reference *6* provides details of the preloading procedure. The tension tests were performed on an Instron machine and strain was measured by use of a strain gage.

Direct Measurement of Fiber Cracking

Tension specimens were polished and electropolished, loaded to various strain levels, and then unloaded. The number of cracked fibers on the specimen surface was then determined by scanning the surface with an optical microscope at a magnification of 1000 in slightly overlapping passes. Figure 1 presents a photomicrograph of the surface of a specimen that has been strained. It shows the fibers embedded in the matrix with a broken fiber clearly visible. Some observations were also made at various positions through the thickness of the specimen and no significant variations were observed. Hence, surface observations were felt to be representative of the material as a whole.

Figure 2 presents the experimental results for the percentage of cracked fibers, along with a plot of the following equation which was curve fitted to the experimental data

$$\omega(\epsilon) = 0.427\,(1 - e^{-b\epsilon^c}) \tag{1}$$

where $b = 2.590$, $c = 0.5385$. This equation fits the experimental data very well; its similarity to a Weibull distribution is the reason it was selected. The results show that only a small fraction of the total fiber population cracked prior to final failure of the composite; for example, the number of cracked fibers at 90 percent of the failure strain is less than ½ percent. Typical failure strains were around 2 percent, with some scatter in the data. Similar results were observed on

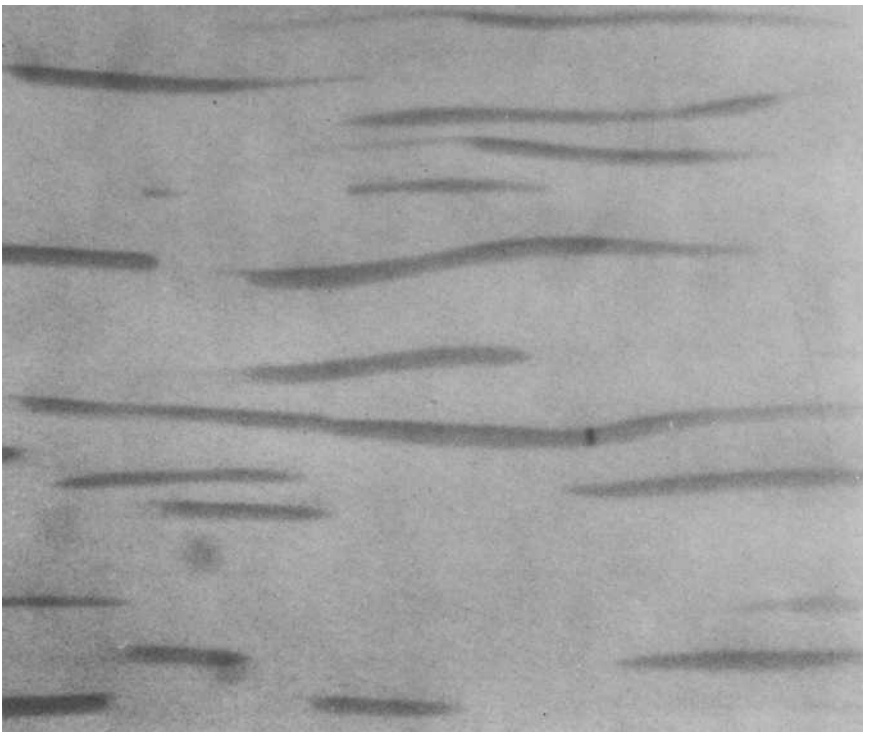

FIG. 1--*Photomicrograph of strained material showing cracked fiber* (× *2000*).

tests conducted at temperatures of −120 C and −196 C [7]. These observations indicate that in this material premature cracking does not set up a chain reaction that leads to failure on a large scale in the remaining fibers. Premature fiber fracture does not, therefore, lead to instability, and the composite strength is determined primarily by the average fiber strength.

Acoustic Emission Tests

Acoustic emissions are the stress waves spontaneously generated within the volume of a material being deformed. Extensive literature on the subject is now available [*6,8-14*], but only a brief review will be presented here. Acoustic emission techniques have been applied to studies of processes ranging from dislocation movements in single crystals to crack extension in large metallic pressure vessels [*11*]. Hence, they appear well suited to studies of the deformation characteristics of composite materials, including the detection of fiber breakage and nondestructive evaluation of material integrity. Most acoustic emission studies have been performed on metals, but some work has been

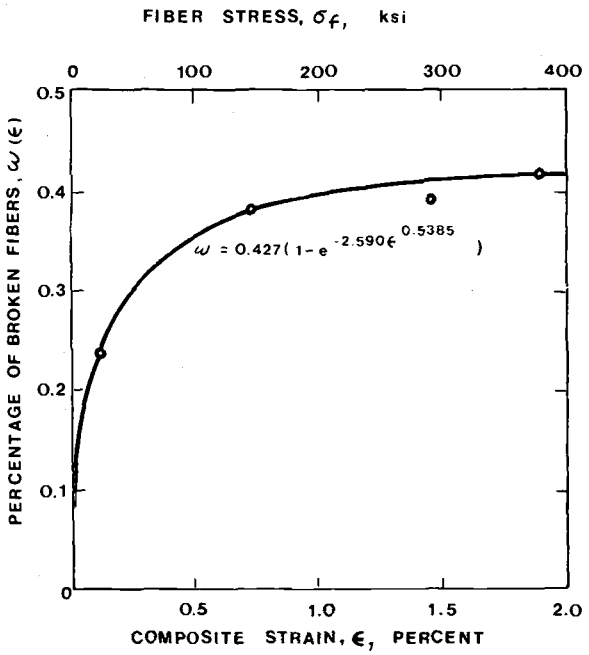

FIG. 2–*Percentage of cracked fibers as a function of tensile composite strain.*

conducted on composites [*15-18*]. The work reported in Refs *15* to *17* did not attempt to relate the acoustic emission to the deformation mechanisms occurring within the material. Reference *18* contains a study of acoustic emission due to crack extension in Charpy type specimens, and is somewhat related to the present investigation. However in that study the problem of fiber breakage due to an advancing crack front was considered, rather than the statistical variation of fiber strength as observed during a rising load tension test of an initially flawfree material.

The acoustic emission was detected by coupling a lead zirconate titanate (PZT) sensor directly to the specimen with viscous resin. The signal from the sensor was preamplified and filtered before being inserted into the secondary amplifier and filter. The amplified and filtered signal was then fed into a counter which monitored the number of times the signal exceeded a certain threshold level for triggering the counter. An overall system gain of 95 dB, and bandpass of 100-150 kHz was utilized.

In the type of instrumentation used, the amplified and filtered signal consisted primarily of damped sinusoids with a frequency corresponding to the resonant frequency of the sensor, as shown schematically in Fig. 3. The number of acoustic emission counts measured in the course of a test is the number of times that the amplified sensor signal exceeds the trigger voltage of the counter.

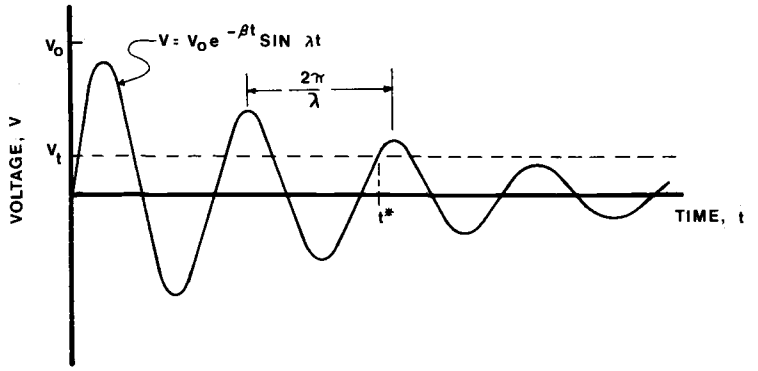

FIG. 3–*Schematic of a damped sinusoid signal, showing threshold voltage, and the multiple counts resulting from a single event within the test piece.*

Three counts would result from the signal shown in Fig. 3. In this way, a single event within the test piece does not produce a single count, but may result in several counts. A larger event will produce a signal that requires more cycles to "ring down" to a voltage below the trigger level. Hence, a larger event will give more counts than a small one, producing some measure of the amplitude of the events occurring within the material.

The results of a rising load test on a tension specimen are presented in Fig. 4. Stress and summation acoustic emission are presented as a function of strain. This data was collected in real time as the test proceeded. The percentage of broken fibers, ω, is also replotted in this figure.

Theoretical Development

The relationship between the events occurring within the material and the acoustic emission counts is necessary in order to predict theoretically the acoustic emission characteristics of a given material. Such a relationship will be outlined in this section. The following steps are used in this development:

(1) Assume that the voltage of the amplified sensor signal inserted into the counter is a damped sinusoid of the form

$$V = V_o e^{-\beta t} \sin \lambda t \tag{2a}$$

and that t^*, the time required for the signal to ring down to the threshold voltage (V_t), is long compared to the period of the oscillations. Hence, n, the number of counts from a given event, will be

$$n = \frac{\lambda t^*}{2\pi} \tag{2b}$$

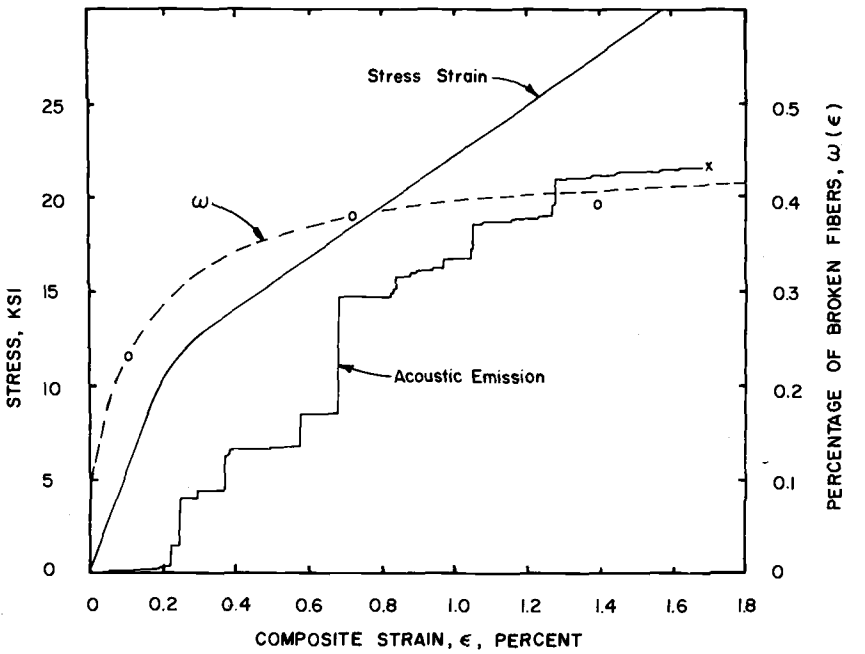

FIG. 4–*Summation acoustic emission, percentage of cracked fibers, and stress as a function of strain for a rising load tension test on whisker reinforced metal composite.*

Also, from Eq 2a,

$$V_t \cong V_0 e^{-\beta t^*} \tag{2c}$$

Solving this equation for t^*, and inserting the result into Eq 2b yields the following result

$$n = \frac{\lambda}{2\pi\beta} \ln \frac{V_0}{V_t} \tag{3}$$

This equation relates the number of counts observed from a single event to the initial amplified and filtered voltage resulting from that event, and the threshold voltage of the counter.

(2) Assume that the energy released during an event is proportional to the square of the initial voltage resulting from that event:

$$U \propto V_0^2 \tag{4}$$

or

$$V_0 = C_1 \sqrt{U}$$

where C_1 is a proportionality constant. This assumption is based on the fact that the voltage output of a piezoelectric disk is proportional to the stress on the disk face, and the energy density of an elastic stress wave is proportional to the square of the stress. This relationship could be generalized to $U \propto V^p$, where p is some constant. However, as will be noted later, the end result of the theoretical development is independent of the value of the exponent p, and the plausible value of 2 will be used in the following development. An assumption similar to that expressed in Eq 4 was used by Gerberich and Hartbower [*19*] in their model relating acoustic emission to the energy released during crack extension. However, this assumption was empirically modified to improve correlations with experimental data.

(3) Assume that all of the observed emission comes from fiber cracking. This is a plausible assumption, since the low strength, high purity aluminum matrix will be relatively "quiet," and should not contribute much emission compared to the "noisier" cracking of fibers.

(4) Assume that the energy released when a fiber breaks is proportional to the square of the stress in the fiber, that the fiber remains elastic until it fails, and that the strain in the fiber is the same as the strain in the composite (isostrain assumption). These assumptions lead to the following results

$$U \propto \sigma_f^2 / E_f = E_f \epsilon_f^2 = E_f \epsilon^2 \tag{5}$$

or

$$U = C_2{}^2 E_f \epsilon^2$$

where C_2 is a proportionality constant. Combining Eqs 3, 4, and 5, leads to the following result

$$n = \frac{\lambda}{2\pi\beta} \ln \frac{V_o}{V_t} = \frac{\lambda}{2\pi\beta} \ln \frac{C_1\sqrt{U}}{V_t} = \frac{\lambda}{2\pi\beta} \ln \frac{C_1 C_2 E_f^{1/2}}{V_t} \tag{6a}$$

This equation gives the number of counts observed when a fiber breaks at a strain ϵ. Note that this equation holds only for $(C_1 C_2 E_f{}^{1/2} \epsilon)/V_t > 1$. For smaller values of this parameter n will be zero, because the energy released in the event will be too small to give voltages of sufficient amplitude to trigger the counter. Let ϵ_o be the strain corresponding to this threshold condition, which will be equal to $V_t/C_1 C_2 E_f{}^{1/2}$). Equation 6a can then be rewritten as

$$n = \frac{\lambda}{2\pi\beta} \ln \frac{\epsilon}{\epsilon_o} \quad (\epsilon > \epsilon_o) \tag{6b}$$

It is worth noting that, because of the presence of the log in Eq 6b, the form of this equation is not altered by assuming an exponent other than 2 in Eqs 4

and 5. Changing these exponents would only alter the multiplying constant ahead of the logarithm term in Eq 6a, and this term multiplied by a proportionality constant will be varied in later steps of the development in order to obtain an agreement between the theoretical and experimental results.

The parameter measured during the acoustic emission test was the total number of counts observed since the beginning of the test. Denote this as N, and consider it to be a function of the strain, ϵ. N will be related to n, the number of broken fibers, and the strain at which they break in the following manner

$$dN \propto n(\epsilon)\, d\omega = n(\epsilon)\frac{d\omega}{d\epsilon}\, d\epsilon = \frac{\lambda}{2\pi\beta}\frac{d\omega}{d\epsilon}\ln\frac{\epsilon}{\epsilon_0}\, d\epsilon \tag{7a}$$

Introducing the proportionality constant B allows this to be rewritten as

$$dN = B\frac{d\omega}{d\epsilon}\ln\frac{\epsilon}{\epsilon_0}\, d\epsilon \tag{7b}$$

N can now be determined by integration of this differential equation

$$N = B\int_{\epsilon_0}^{\epsilon}\frac{d\omega}{d\epsilon}\ln\frac{\epsilon}{\epsilon_0}\, d\epsilon \tag{8}$$

This equation can be used in the following two ways:

(1) To predict N once ω is known. This is of use in being able to predict the acoustic emission response of fiber composite material knowing its fiber cracking characteristics.

(2) To determine ω once N is known. It is usually much easier to perform the acoustic emission test than to measure directly the number of broken fibers. Hence, it would be desirable to measure the fiber cracking by acoustic emission techniques.

Comparison of Theory and Experiment

Equation 8 can be used to predict the acoustic emission once the fiber cracking characteristics are known. For the particular case under consideration, this can be accomplished by inserting Eq 1 into Eq 8 and carrying out the integration. Differentiating Eq 1

$$\frac{d\omega}{d\epsilon} = 0.427\, e^{-b\epsilon^c} bc\epsilon^{c-1} = a\epsilon^{c-1}\, e^{-b\epsilon^c} = a\frac{e^{-b\epsilon^c}}{\epsilon^{1-c}} \tag{9}$$

where $a = 0.427bc = 0.5955$. Inserting this into Eq 8

$$N(\epsilon) = aB\int_{\epsilon_0}^{\epsilon}\frac{e^{-bx^c}}{x^{1-c}}\ln\frac{x}{\epsilon_0}\, dx \tag{10}$$

Making the change of variable $u = (x/\epsilon_0)^c$, integrating by parts, and using the definition of the exponential integral[*20*] leads to the following result

$$N(\epsilon) = \frac{aB}{bc^2}\left[E_1(b\epsilon_0{}^c) - E_1(b\epsilon^c)\right] - \frac{aB}{bc} e^{-b\epsilon^c} \ln\frac{\epsilon}{\epsilon_0} \tag{11}$$

There are two disposable parameters in this equation, B and ϵ_0. The parameter ϵ_0 will be in the range 0.05 to 0.25 percent. The ratio N/B was calculated for various ϵ_0, and a value of 0.10 percent selected as the one that most nearly gave a curve that fit the experimental results. The scale factor B was then selected to provide an optimum curve fit; a value of B of 1.90×10^5 counts resulted. The calculations were performed on a computer using the polynomial approximation for $E_1(x)$ included in Ref *20*. Figure 5 presents the results calculated from Eq 11 using these values of ϵ_0 and B. The experimental results are also included.

Discussion of Results and Conclusions

The agreement between the theoretical and experimental acoustic emission results presented in Fig. 5 is very good. It is interesting to note that about half of the fibers that broke during the test did so at strains less than the threshold strain ϵ_0 of 0.1 percent. There is believed to be no inconsistency in these results; fibers that broke prior to 0.1 percent released insufficient energy to give voltages of large enough amplitude to trigger the counter.

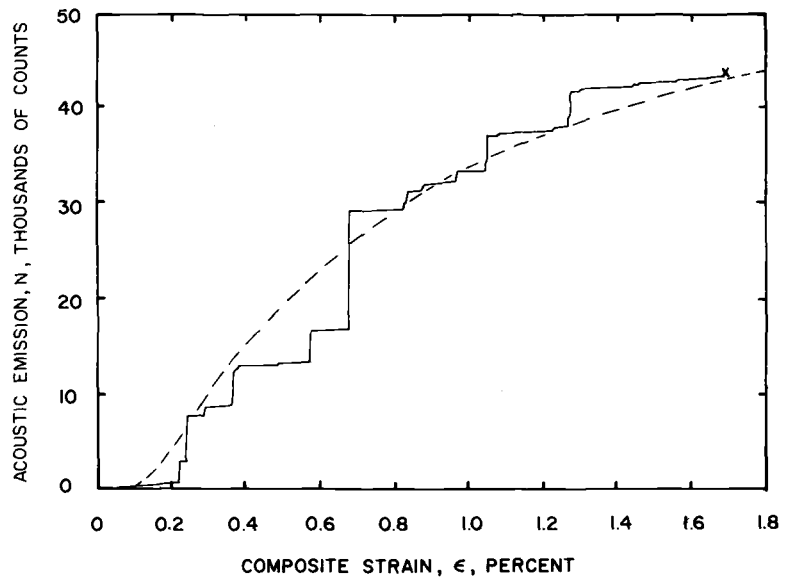

FIG. 5–*Results of theoretical calculations of summation acoustic emission as a function of strain.*

The jumps in the experimental acoustic data can never be reproduced theoretically when ω is considered to be a continuous function of ϵ. This good agreement demonstrates that it is possible to relate acoustic emission characteristics quantitatively to the deformation processes occurring within the material. The model presented can be used to predict the acoustic emission response from fiber composites once the fiber cracking characteristics of the material are known. The demonstrated ability to monitor acoustic emission from composites and to relate it to deformation occurring within the material indicates the applicability of acoustic emission testing to the nondestructive evaluation of composite materials. Other deformation modes, such as delamination and plastic deformation or crazing of the matrix, should also be detectable by use of acoustic emission. However, plastic deformation and matrix crazing will usually give emission signals of a much lower amplitude than fiber cracking and delamination, and will therefore be difficult to detect if these lower amplitude events occur simultaneously with one of the noisier processes. This is felt to be the case in the whisker reinforced material considered here, since plastic deformation of the high purity aluminum matrix would be expected to be quiet relative to the cracking of the high strength fibers.

The model presented could also be used to theoretically calculate ω from the observed acoustic emission characteristics. It would often be easier to perform an acoustic emission test and relate the results to the process of interest, than to examine the material directly. In the case considered here, the acoustic emission test is much easier to perform than the tedious optical measurements of the number of broken fibers.

In conclusion, the results presented demonstrate the applicability of acoustic emission to studies of the micromechanics of deformation of composites. It is not only possible to detect fiber breakage by use of acoustic emission, but also to obtain quantitative relationships. These results also show that acoustic emission can be used to advantage in the nondestructive evaluation of composite materials, since details of the deformation characteristics of the material are readily obtained.

Acknowledgments

We would like to take this opportunity to thank G. I. Latter, formerly of the Lawrence Radiation Laboratory, Livermore, California, for his assistance in curve fitting the experimental fiber cracking data, and also the United Aircraft Research Laboratories for supplying the material used in this investigation.

References

[*1*] Chadwick, G. A., *Journal of the Institute of Metals*, JIMEA, Vol. 91, 1963, pp. 169-173.

[*2*] Yue, A. S., *Transactions of the Metallurgical Society of AIME*, TMSAA, Vol. 224, Oct. 1962, pp. 1010-1015.

[3] Tiller, W. A. and Mrdjenovich, R. W., *Journal of Applied Physics*, JAPIA, Vol. 34, No. 12, Dec. 1963, pp. 3639-3460.
[4] Salkind, M. J. and Lemkey, F. D., *International Science and Technology*, ISCTA, No. 63, March 1967, pp. 52-64.
[5] Salkind, M. J., George, F. D., Lemkey, F. D., and Boyles, B. J., "Investigation of the Creep, Fatigue, and Transverse Properties of Al_3Ni Whisker and $CuAl_2$ Platelet Reinforced Aluminum," United Aircraft Research Laboratories Final Report E910344-4, 11 May 1966.
[6] Dunegan, H. L., Harris, D. O., and Tatro, C. A., *Journal of Engineering Fracture Mechanics*, EFMEA, Vol. 1, No. 1, June 1968, pp. 105-122.
[7] Darwish, F. A. "The Effect of Temperature and Fiber Orientation on the Strength and Deformation Characteristics of Fiber Composites," Ph.D. thesis, Department of Materials Science, Stanford University, Stanford, Calif., Oct. 1969.
[8] Dunegan, H. L. and Harris, D. O., *Ultrasonics*, ULIQA, Vol. 7, No. 3, July 1969, pp. 160-166.
[9] Dunegan, H. L. and Tatro, C. A., in *Techniques of Metals Research*, Vol. 5, Part 2, R. Bunshah, Ed., Wiley, New York, 1971, pp. 273-312.
[10] Dunegan, H. L. and Harris, D. O., "Acoustic Emission Techniques," to be published in SESA Monograph *Experimental Techniques in Fracture Mechanics*, A. S. Kobayashi, Ed.
[11] Liptai, R. G., Harris, D. O., Engle, R. B., and Tatro, C. A., "Acoustic Emission Techniques in Materials Research," Lawrence Radiation Laboratory Report UCRL-72582, Livermore, Calif., July 1970; to be published in *Advanced Experimental Techniques in the Mechanics of Materials*.
[12] Liptai, R. G. and Harris, D. O., *Materials Research and Standards*, MTRSA, Vol. 11, No. 3, March 1971, p. 8.
[13] Tatro, C. A., *Materials Research and Standards*, MTRSA, Vol. 11, No. 3, March 1971, p. 17.
[14] Frederick, J. R., *Materials Evaluation*, MAEVA, Vol. 28, No. 2, Feb. 1970, pp. 43-47.
[15] Green, A. T., Lockman, C. S., and Steele, R. K., *Modern Plastics*, MOPLA, Vol. 41, July 1964, pp. 137-139.
[16] Dunegan, H. L. and Green, A. T., *Materials Research and Standards*, MTRSA, Vol. 11, No. 3, March 1971, p. 21.
[17] Liptai, R. G., "Acoustic Emission from Composite Materials," Lawrence Radiation Laboratory, Report UCRL-72657, Livermore, Calif., Feb. 1971.
[18] Fitz-Randolph, J. M., "Acoustic Emission Characterization of the Fracture Process in a Boron-Epoxy Composite," M.S. thesis, School of Engineering, University of California at Los Angeles, 1971.
[19] Gerberich, W. W. and Hartbower, C. E., *International Journal of Fracture Mechanics*, IJFMA, Vol. 3, No. 3, Sept. 1967, pp. 185-192.
[20] Abramowitz, M. and Stegun, I. A. in *Handbook of Mathematical Functions*, National Bureau of Standards Applied Mathematics, Series 55, 1964.

T. T. Anderson,[1] *A. P. Gavin,*[1] *J. R. Karvinen,*[1] *C. C. Price,*[1] *and K. J. Reimann*[1]

Detecting Acoustic Emission in Large Liquid Metal Cooled Fast Breeder Reactors

REFERENCE: Anderson, T. T., Gavin, A. P., Karvinen, J. R., Price, C. C., and Reimann, K. J., **Detecting Acoustic Emission in Large Metal Cooled Fast Breeder Reactors,"** *Acoustic Emission, ASTM STP 505*, American Society for Testing and Materials, 1972, pp. 250-269.

ABSTRACT: Research at Argonne National Laboratory on acoustic emission and closely related areas is oriented to goals of the liquid metal cooled fast breeder reactor (LMFBR) program. These goals include acoustic monitoring of reactor core and power plant components, acoustic detection of boiling in liquid sodium, and acoustic emission testing of materials at elevated temperatures. For monitoring of sodium-filled components, several types of acoustic emission sensors are being developed for operation in sodium at temperatures to 650 C. These sensors contain the high temperature, radiation resistant, piezoelectric material, lithium niobate which is clamped or bonded to the sensor housing.

Reactor components have been monitored acoustically with both high temperature (620 C rating) accelerometers and with standard accelerometers. The acoustic surveillance tests have shown: (1) flowrate-dependent noise in a sodium-cooled nuclear reactor (EBR-II) and in a sodium component test facility (CCTL); (2) sodium-oxide binding within an EBR-II primary pump; and (3) a loose drain tube in the EBR-II primary sodium to secondary sodium intermediate heat exchanger.

KEY WORDS: breeder reactors, acoustics, emission, piezoelectric transducers, acoustic surveillance, liquid metal cooled reactors, power reactors (nuclear), high temperature tests, ultrasonic tests, niobates, cracking (fracturing), plastic deformation, cavitation noise, elastic waves, crack initiation, crack propagation

Operating conditions of a liquid metal cooled fast breeder reactor (LMFBR), and behavior of materials used in its construction at high temperature, can be

Work performed under the auspices of the U. S. Atomic Energy Commission.

[1] Argonne National Laboratory, Argonne, Ill. 60439.

determined by acoustic monitoring. In many cases the observed phenomena are classed as acoustic emission, since elastic waves are generated by short duration (millisecond and microsecond) events such as material fracture, vapor generation and collapse, and mechanical abrading. In the nuclear heated core of the Dounreay fast reactor in Scotland, for example, boiling of the sodium potassium eutectic coolant (NaK) has been monitored using accelerometers mounted on long rods (acoustic waveguides)[*1,2*]. These rods transmit sound from the core, through the reactor cover, and into the room environment. From sound intensity and time of arrival, the location of a sound source, such as gas leaking from a ruptured fuel pin, is determined from triangulation. Abnormal sounds such as entrained gas carried along in the sodium lines generate characteristic emissions. In the sodium-heated steam generator, should wastage of sodium into water occur, the size of the leak could be determined acoustically[*4*].

In relation to these various applications of acoustic emission surveillance, programs at Argonne National Laboratory include reactor diagnostics, acoustic boiling detection, and high temperature acoustic emission.

Detection Methods

Off the shelf acoustic transducers are not readily available for high temperature monitoring. If the transducer is externally cooled to permit contact with system components, conventional coolants such as water or organics are eliminated because of possible reaction with the sodium. If the cooled transducer is exposed to the sodium, its external surfaces accumulate impurities from the sodium.

For transducers mounted on the system exterior, standoffs isolate the transducer thermally at the cost of reduced sensitivity and narrower frequency response. For instance, a member of uniform cross section could extend into the sodium system through an acoustically isolated seal, acting as a mechanical (acoustic) waveguide for transmission of vibrations to the transducer located external to the system.

Another approach, simpler conceptually but harder to put into practice, is to build transducers which will withstand both elevated temperature and the nuclear radiation. Possible transducer types include capacitive, inductive, magnetostrictive, and piezoelectric. We have chosen the piezoelectric type because of its typical broad frequency response.

Acoustic Waveguides

An acoustic (mechanical) waveguide is a mechanical structure along which an elastic wave can propagate from a sensing location contacting the medium being monitored to a receiving location for transmitting or converting the elastic energy[*5*]. Types of waveguides applicable to reactor monitoring take the form of metal rods, tubes, or wire bundles[*6*]. Solid rods have compared favorably

with hydrophones in detecting audio-range sounds. Mechanical resonances occurring within an acoustic waveguide determine the frequency response limits (Fig. 1). For a rod, the lowest frequency limit is determined by the first longitudinal resonances frequency, $f_1 = c_1/2L$, where c_1 is the extensional velocity in the rod and L is the length of the rod. Below that frequency, the entire rod moves as a single mass. When the acoustic frequency is high enough that a wavelength is comparable to rod diameter[*8*], acoustic energy is converted into shear wave modes travelling at 60 percent of the extensional velocity to cause dispersion of the wave.

A tubular waveguide with a closed end or a rod attached to a diaphragm can be made to match the acoustic impedance of the liquid for higher acoustic sensitivity (Fig. 2). A tube exhibits radial and flexural resonances, which cause the tube to act as a bandpass filter[*9*]. The sound is received at the end and also at preferred angles along the tube as a function of frequency[*10*].

The high frequency limitation of the radial modes is avoided through transmission of the sound along wire bundles functioning as acoustic pipes, which are analogous to fiber-optic light pipes. The fiber waveguides beside

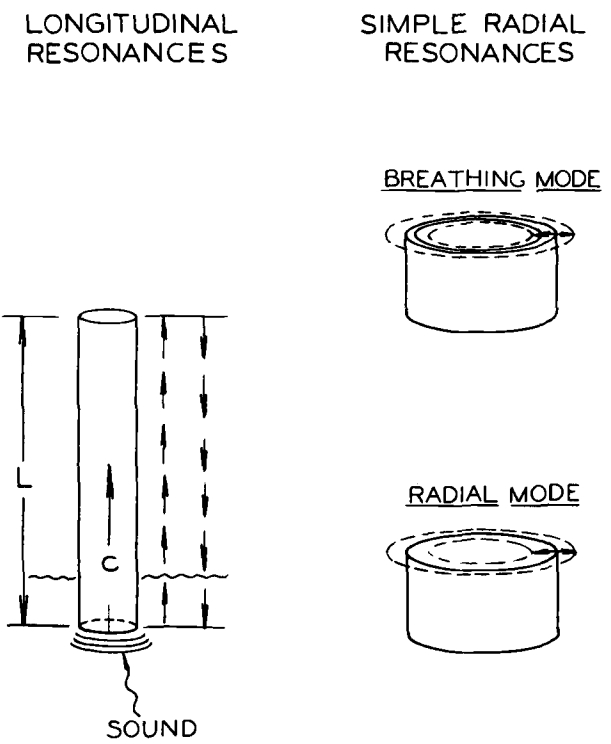

FIG. 1—*Typical longitudinal and radial resonances of acoustic waveguides.*

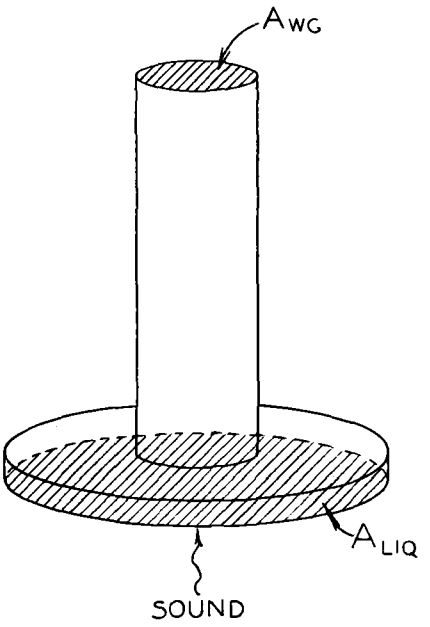

FIG. 2—*Acoustical matching between the waveguide and the liquid medium. The product ρc (density times sound velocity) is specific acoustic impedance and* A *is cross-sectional area.*

having greater mechanical flexibility have fairly high sensitivity over a wide frequency range.

High Temperature Acoustic Sensors

Acoustic sensors which can be immersed in the sodium coolant relatively close to the sound source, offer the advantage of wider frequency bandwidth to discriminate both pressure pulsations and high frequency boiling emissions. In this application, the sensor must produce a stable, reliable output in the presence of intense gamma and neutron radiation and at temperatures up to 650 C.

We have undertaken the development of acoustic sensors designed to withstand this high temperature, radioactive, sodium-immersed environment (Figs. 3, and 4)[*12*]. Our development work has been limited to a piezoelectric transducer incorporating lithium niobate as the active element. Lithium niobate is one of a very few piezoelectric materials which possess a Curie point above 650 C. Two major areas of concern with the use of this material in a fast reactor

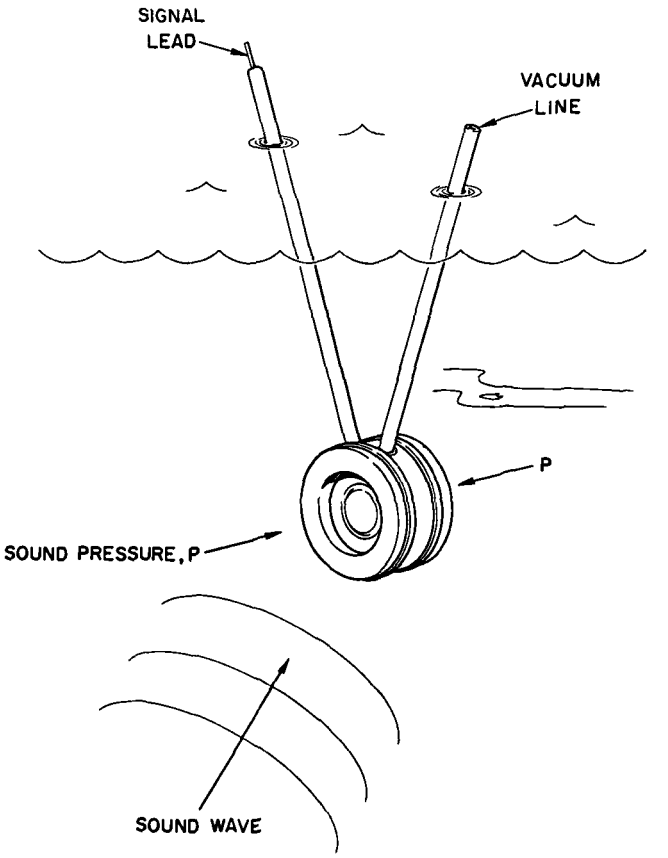

FIG. 3–*High temperature acoustic transducer for operation in liquid sodium.*

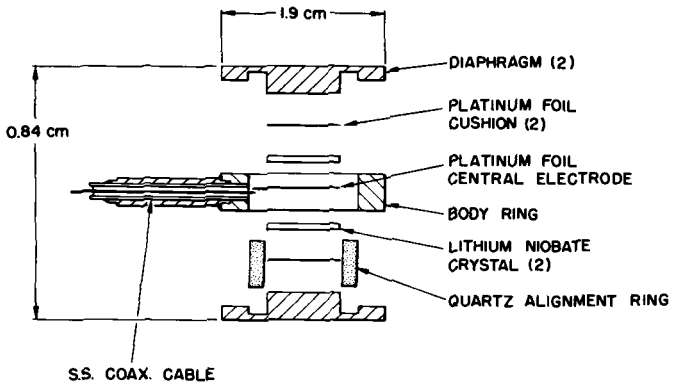

FIG. 4–*Assembly of ANL high temperature acoustic transducer.*

environment are its resistance to radiation and its electrical resistance in a sealed unit at the temperatures required.

The ability of lithium niobate to withstand irradiation has been demonstrated by several investigators. Single crystals of the material exposed to 1-2 MeV electrons from a Van de Graaff at equivalent dose rates up to 10^5 R/s to a maximum total dose of 10^{10} R demonstrated little damage to the crystal due to this exposure to ionizing irradiation[*13,14*]. Similarly a crystal exposed to a total dose of 10^{10} R gamma rays from a Co^{60} source showed no significant changes in piezoelectric properties[*15*]. Exposure of a crystal to gamma irradiation at a dose rate of 1.75×10^7 R/h for a total dose of 2×10^9 R at 280 C plus 2×10^9 R at 537 C did not cause significant changes in its piezoelectric properties[*16*]. Neutron irradiation at low dosage (4×10^{17} neutrons/cm^2) caused a slight expansion[*17*]. The effect of fast neutron irradiation has not been investigated, however thermal neutron irradiation to 3×10^{17} neutrons/cm^2 demonstrate only slight changes in optical absorption and dielectric constant. We have irradiated a Y-cut specimen to 6×10^{17} neutrons/cm^2 without detectable change of piezoelectric properties.

The electrical resistivity of lithium niobate decreases with temperature to the extent that the resistance at 650 C of crystals of the size and configuration used in our sensors is only slightly higher than the minimum required input impedance of available charge amplifiers. In addition to this the resistance is decreased further by loss of oxygen from the crystal in gaseous atmospheres containing low concentrations of oxygen[*18,19*].

As shown in Fig. 4, our transducer design is based on the symmetric drive concept in which two crystals in the form of circular plates are arranged with faces of like polarity facing a central electrode in a housing between flexible diaphragms. A change of pressure in the liquid in which the unit is immersed produces an electrical charge at the surfaces of the crystals which is transmitted to the read out instrumentation via the high temperature coaxial cable attached to the sensor housing. Development units of this design have been tested for response to low frequency sound waves in air up to 650 C and have produced satisfactory results. Their high frequency response in room temperature water is also satisfactory. Future tests in 650 C sodium are planned.

Acoustic Emission at Elevated Temperatures in Stainless Steel Fatigue Test Specimen

The technology developed for measuring acoustic emission at elevated temperatures is directly applicable to the monitoring of reactor components which are situated in the radioactive liquid sodium environment. Detection of crack initiation and propagation in stainless steel specimens subjected to cyclic fatigue at elevated temperatures constitutes a part of acoustic emission applicable to problems in materials evaluation. Establishment of a correlation

between crack size or growth rate and amplitude of acoustic emission pulses, determination of minimum detectable crack size, and prediction of incipient failure are the main objectives of this program.

Z-cut lithium niobate crystals with baked on, platinum-palladium-gold electrodes were silver brazed to stainless steel rods acting as transducer housings and mounting supports (Fig. 5). Gold wires silver brazed to the other electrode supplied the second electrical contact. Stainless steel cylinders with coaxial connectors at one end surrounded the crystals providing the necessary shielding. The other end of the mounting rods were flattened, slotted, and fitted with a hole matching the diameter of the test specimens, thus enabling a quick interchange of samples. This construction proved more stable in prolonged operations at elevated temperature than pressure-contact piezoelectric transducers. Brazing also eliminated the necessity of matching the flatness of the support mounting to the flatness of the crystal surface for maximum transfer of acoustical energy. The intimate contact between the crystal and the support structure in a brazed transducer gave rise to large amplitude electrical activity during a fast heating cycle, probably caused by temperature gradients and a mismatch in expansion coefficients of the two materials. This electrical activity

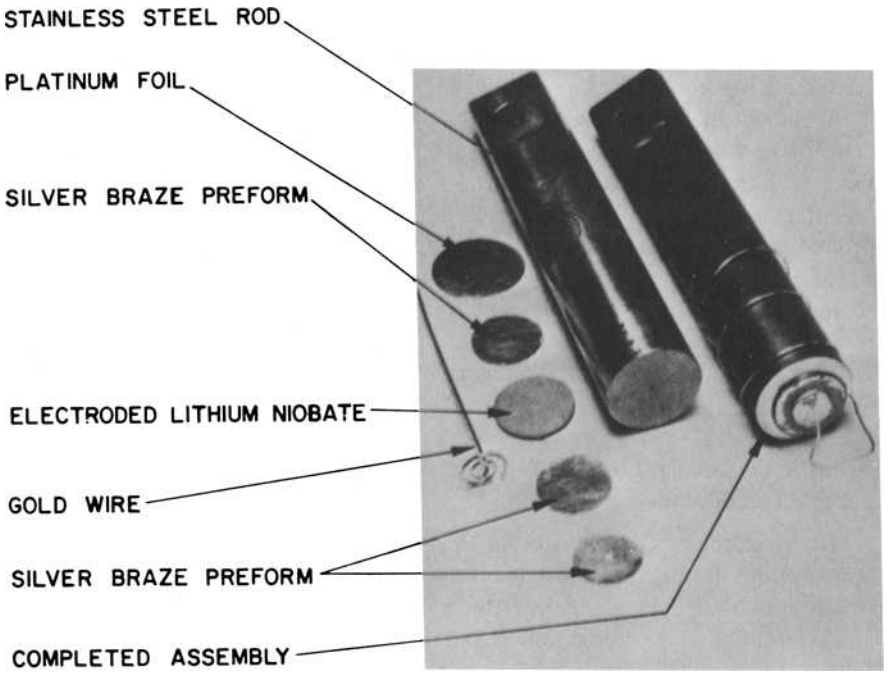

FIG. 5—*Assembly of ANL high temperature ultrasonic transducer.*

consisted of large voltage spikes which reverse polarity during a fast cooling cycle. Once the temperature stabilized the activity ceased. A heating or cooling rate of 100 to 150 C/h assured a completely quiet transition. Transducers constructed in the described way have exhibited a sensitivity in the order of −110 dB below 1V/μbar at 1 MHz.

The outlined goal necessitates continuous recording of acoustic emission signals (Fig. 6). Emission pulses in the utilized test facility are detected with the piezoelectric transducers, mounted at one end of an hourglass-shaped test specimen. The transducer signal, after amplification and filtering, is recorded with a visicorder and simultaneously monitored with an oscilloscope (Fig. 7). The test specimen, mounted in a tensile machine, is inductively heated to 800 F while alternately undergoing compression and tension at a rate of 0.1 Hz. Capacitive feed through of the 450 kHz heating supply voltage and noise of the tensile machine force the implementation of a bandpass filter in order to obtain a satisfactory signal to noise ratio. The optimal bandpass for the utilized setup was experimentally determined to be from 10 to 200 kHz.

From preliminary results the following general observations can be made:

(1) Most of the acoustic emission occurs toward the end of the fatigue test, shortly before failure.

(2) There usually is more activity during the tension than during the compression cycle.

(3) Interruption of the fatigue test after the appearance of the first few pronounced emission peaks reveals under microscopical examination a number

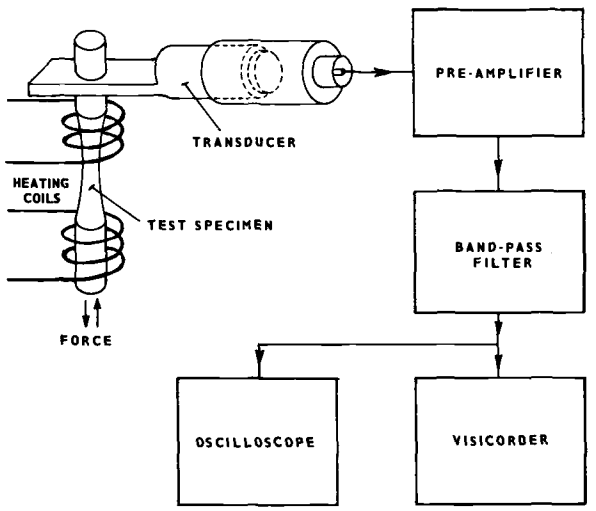

FIG. 6—*Block diagram of test facility for investigating high temperature crack propagation.*

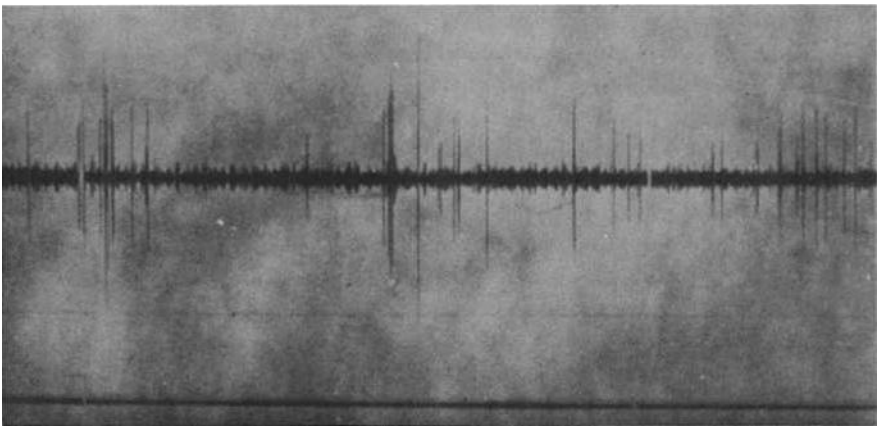

FIG. 7—*Visicorder record of acoustic emission.*

of sizable microcracks. The surface of the test specimen appears wrinkled but wrinkle formation was not indicated by acoustic emission.

The last observations indicate the multitude of yet unsolved problems and unanswered questions. What is the minimum plastic deformation detectable by acoustic emission? Are the detected surface cracks the only ones or are there more cracks inside the test specimen?

The continuing program is directed to answering these questions. Frequent interruptions of the fatigue cycling, microscopic surface examination, and cross-section micrographs of the test specimens should enable one to find the desired correlations.

Acoustic Boiling Detection: A Review

Sodium boiling in the core of a fast breeder reactor can be hazardous for two principal reasons: first, a blockage of flow in a coolant channel within the core could lead to overheating and failure of the fuel pins, and second, the possibility exists of a local positive void-reactivity coefficient, by which the presence of sodium vapor could lead to an increase in power with resulting generation of more vapor. Good mechanical and neutronic design will minimize the likelihood of boiling but surveillance of the operating reactor is required to initiate control action if boiling should occur.

Boiling in the core of a nuclear reactor might be detected by a variety of methods, including acoustic attenuation between two points[*20,21*], coolant thermocouple signal[*22*], neutron detector signal[*23*], and acoustic detector signal[*24,25*]. The tendency to boil can be measured through a change of the threshold for acoustically induced cavitation[*26*]. Neutronic and acoustic methods have an advantage of monitoring the overall core region. However,

neutron methods have varying response versus position and have low sensitivity. The acoustic methods, although fast and sensitive, must discriminate boiling from competing acoustic sources[*27*].

For a large accident type excursion, an analysis of sensor performance characteristics has been presented for use in protection systems of LMFBRs[*28*]. Systems for monitoring of the reactor, employing pressure pulse sensors in inlet and exit plenums to the core, or employing neutron sensors, are concluded to be more adaptable to the plant protective system than would be individual subassembly sensors.

Early work on acoustic boiling detection, performed for water reactors, encountered excessive system noise[*29,30*]. In the high-flux research reactors, coolant flow rates can be high enough to produce cavitation within the coolant channels[*31*]. To minimize effects of noise, frequency "windows" were sought to discriminate boiling from other signals. The observed resonances were found to depend on system geometry[*32*] rather than on boiling resonances, although these same geometric effects assisted in the transmission of sound through the reactor[*33*]. Therefore, all broadband noise would excite the same resonances. In addition, experiments with boiling sodium disclosed high frequency components up to 400 kHz[*34*].

Acoustic discimination of cavitation noise from boiling noise appears to be much less effective than elimination of cavitation noise from the reactor[*35*]. Cavitation occurs in liquid metal cooled systems as demonstrated for small space power plants[*36*]. At an inlet restriction of the Phoenix reactor, cavitation was equivalent to that obtained in a water mockup[*37*]. This similarity of water model testing to actual sodium systems may be expected for the same cavitation number[*38*]. Locally occurring cavitation at restrictions and orifices will affect background noise level. The unambiguous detection of a given amount of boiling above background noises may require reducing self generated acoustic emissions.

Boiling of the liquid metal coolant has been detected quite sucessfully at the relatively quiet Dounreay fast reactor (DFR)[*39*]. Other applications of acoustic diagnostics to the DFR have included detection of a sodium leak in the primary circuit, gas entrainment in the primary circuit, void fraction measurement, and performance of electromagnetic pumps[*40*]. In the prototype fast reactor (PFR), currently under construction in the United Kingdom, monitors will be installed to detect onset of cavitation within components. Design of PFR sodium pumps has included minimizing noise generation from cavitation and from impeller blade passing frequency[*41*].

Acoustic Monitoring of Two Large Sodium Systems

The primary sodium circuit of the Experimental Breeder Reactor No. II (EBR-II) was monitored[*42*] to obtain acoustic backgrounds on a large sodium system whose flow is produced by two large (4200 g/m, 0.265 m^3/s at 50

megawatts thermal) centrifugal pumps. The tests consisted simply of monitoring vibrations with accelerometers attached to reactor component structures at the operating floor level, approximately 30 ft (9.1 m) above the nuclear core. The most direct acoustic paths to the reactor core were via each of three holddowns (Fig. 8). Accelerometers, having 125-kHz resonance frequency, were attached to the upper end of a 3-in (7.6-cm) diameter tie rod in each reactor cover holddown assembly. The lower end of the tie rod attaches permanently to the top of the reactor vessel. The acoustic path to the core is completed via sodium and

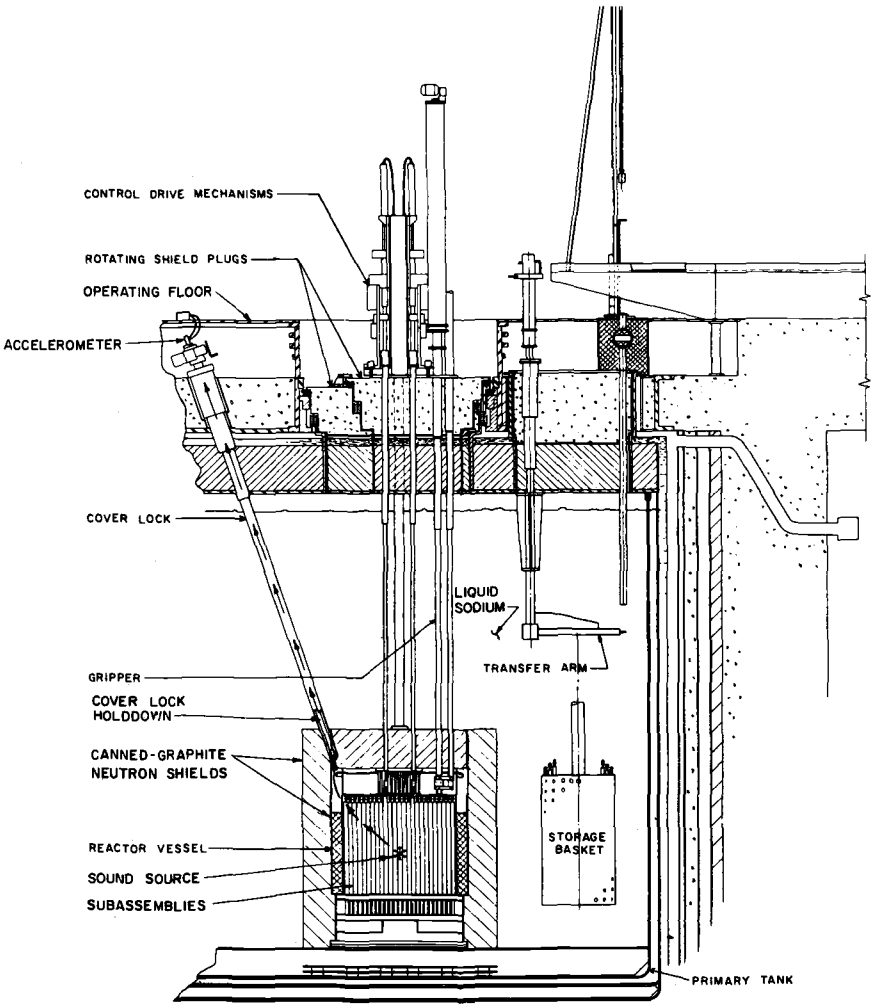

FIG. 8—*Acoustic monitoring location on cover lock holddown at the EBR-II reactor.*

internal components. Other monitoring locations were the top of the valve stem to a primary system throttle valve and the upper motor flange of each primary system pump. The vibration measurements consisted of audio monitoring, oscilloscope traces, and swept-frequency spectra from 1 to 10 kHz (audio) and from 10 to 100 kHz (ultrasonic).

For this type of passive monitoring, there is but indirect evidence for the origin and transmission of sounds. However, the holddown tie rods appeared capable of acting to some extent as acoustic waveguides, since tapping on one tie rod caused a signal delayed by 5 ms on another, compared to calculated delays of 4 ms for an extensional wave and 6 ms for a shear wave via the reactor vessel.

The tie rod could be expected to transmit vibrations at frequencies from the first longitudinal mode (0.33 kHz) to the first radial mode (50 kHz). In this frequency range, the transmission of sound will be nonuniform due to several causes, including: reflections from ends of the tie rod, connection of the tie rod to the holddown mechanism, and transmission paths through structure and liquid sodium from sound sources. At frequencies above 50 kHz, the acoustic signal would be distorted by conversion of acoustic energy in the tie rod from longitudinal waves to shear waves.

Amplitudes of vibration on the holddowns and on the throttling valve remained constant with changing reactor power, but diminished rapidly with flow to a threshold at 54 percent of the 50 MW th flow rate. At this threshold, the sounds were like popping corn, increasing to a continuous static at 100 percent flow. Spectra of the three holddowns were quite different in the ultrasonic range, although each maintained its spectral shape despite the dramatic change of level with flow (Figs. 9 and 10). The first holddown signal contained appreciable components to 50 kHz; the second, to 20 kHz, and the third, to 90 kHz. At full flow, vibration spectrum level varied from 0.01 to 0.03 g (1 g = 9.8 m/s) for an ultrasonic spectrum window of 1 kHz on the holddowns and on the throttling valve.

As an independent check on the flow-dependent background noise at EBR-II, tests were performed on another large sodium system at Argonne, the core components test loop (CCTL). This test facility was being used to pump 1050 F (520 C) sodium through an experimental flow assembly at 400 g/m ($0.025 m^3/s$), at 125-ft head (3.7 atm), and 1000-rpm pump speed. For this test, high temperature accelerometers, rated to 620 C, were mounted on a base support of the test vessel and on the sodium pump discharge line (Fig. 11). The CCTL reduced flow tests showed the same flow-dependence as found for the accelerometers on the EBR-II primary flow system (Fig. 12). In both cases, wide band acceleration levels were of the order of 0.1 g rms at rated flow. At CCTL, individual sounds making the popping were observed to be ringing pulses decaying with a time constant of 20 to 30 ms. From Sabine reverberation theory, this decay time would correspond to an effective acoustic energy

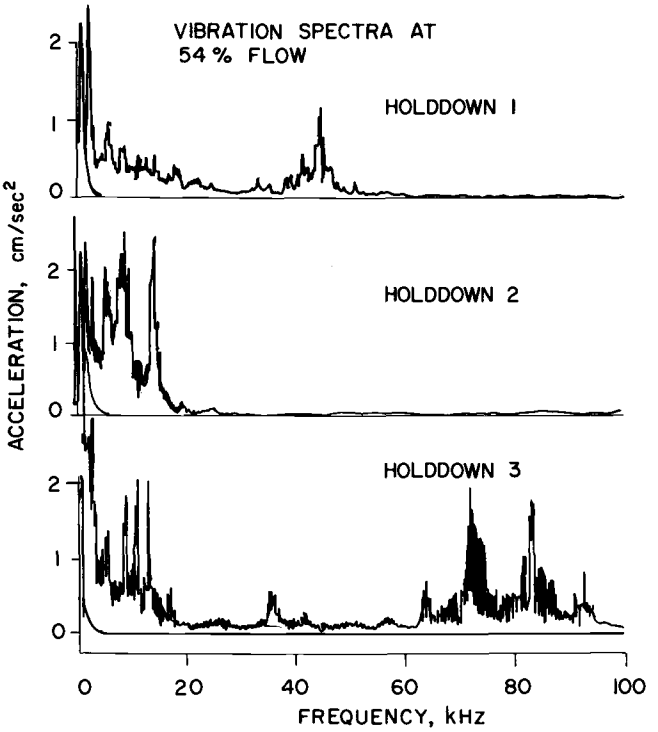

FIG. 9—*Frequency spectra for vibrations sensed on EBR-II holddowns at 100 percent primary sodium flow rate.*

absorption coefficient of 2 to 4 percent at the vessel wall. This is apparently a reasonable value for the relatively undamped liquid-filled system. Increased dispersion by piping should diminish the decay time. On the pump discharge line, decay time was only 10 ms.

Reactor Diagnostics by Noise Signature

Reactor diagnostics employing Fourier spectrum analysis and power spectral density have been employed to establish operating characteristics of the reactor and its auxiliary systems. Parameters include mechanical vibrations, neutron flux noise, and thermocouple temperature indications. Signatures have been established for a limited number of components[*43*].

These signatures are obtained by (1) recording on magnetic tape the output signals from accelerometers, thermocouples, and neutron detectors; (2) obtaining the averaged power spectral density by analog computation; and (3) obtaining the real-time spectrum with a real-time analyzer. The signatures have been obtained at much lower frequencies (10^1 to 10^3 Hz) compared to acoustic

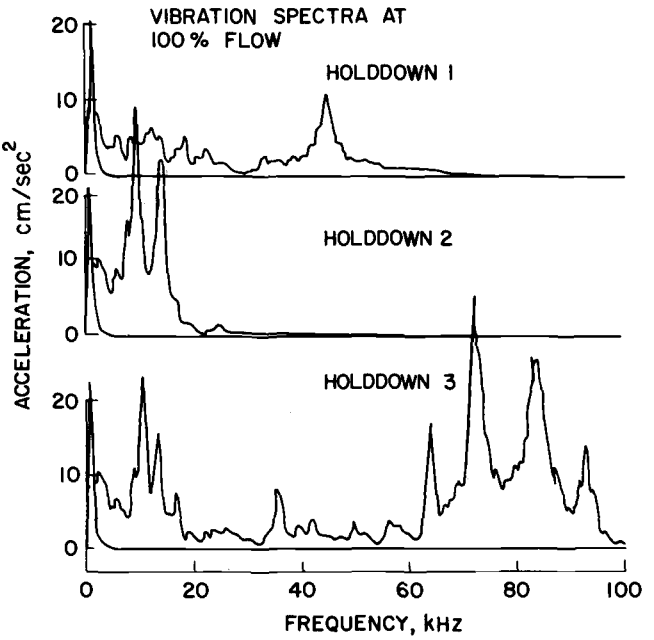

FIG. 10—*Frequency spectra for vibrations sensed on EBR-II holddowns at 100 percent primary sodium flow rate.*

emission signals usually associated with much higher frequencies (10^4 to 10^6 Hz). Nevertheless, many of the phenomena exhibit similar characteristics associated with high frequency acoustic emissions; that is, they can occur as random impulses to herald the onset of mechanical failure.

The diagnostic studies are concerned with identifying the origin of a low frequency oscillation (of approximately 10 Hz) in the reactor ion chambers, which measure the reactor neutron flux. The initial studies led to a conclusion that origin of the oscillation must be in or very near the reactor core. Since there is a possibility that the oscillation is mechanically or hydraulically stimulated, mechanical signatures are being made of components in or near the (primary) sodium coolant circuit which removes heat from the core. Thus far, no correlation has been found between the neutron flux and mechanical vibration of components which extend outside of the sodium system.

The mechanical signatures have proved useful on two occasions. On 17 May 1970, the EBR-II reactor power was set to zero (reactor scram) when operating conditions of one of the two primary sodium pumps indicated that continued operation might lead to seizure. A substantial change in the vibration signature was noted in the second harmonic of rotational speed. Gradually, the mechanical signature returned to the prescram pattern. On 19 September 1970, a similar

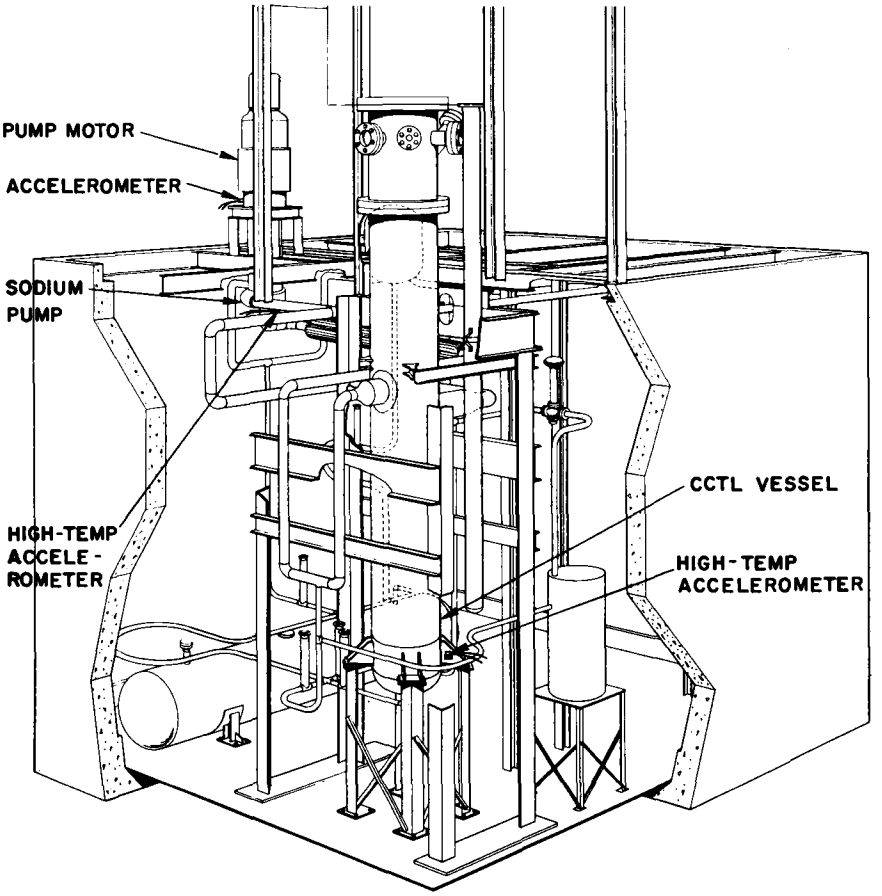

FIG. 11—*Acoustic monitoring locations on the core components test loop.*

disturbance of the pump occurred. Subsequent pump disassembly revealed a defective lower labyrinth seal. Possibly, deposits of sodium oxide scale above the seal had been breaking off, falling into the seal, and causing eccentric shaft motion to excite the second harmonic.

Mechanical signatures from the limited diagnostics again proved useful on 14 November 1970, when audible noises were detected coming from the sodium-to-sodium intermediate heat exchanger (IHX). Accelerometers, including high temperature (1150 F) models, were installed on or near secondary sodium inlet and dischange lines at the top of the heat exchanger (Fig. 13). Analysis of the noises and their dependence on secondary sodium flow indicated a loose member within the secondary side. Entry into the IHX, and extensive remote TV monitoring of the interior, confirmed that a drain tube had been the source

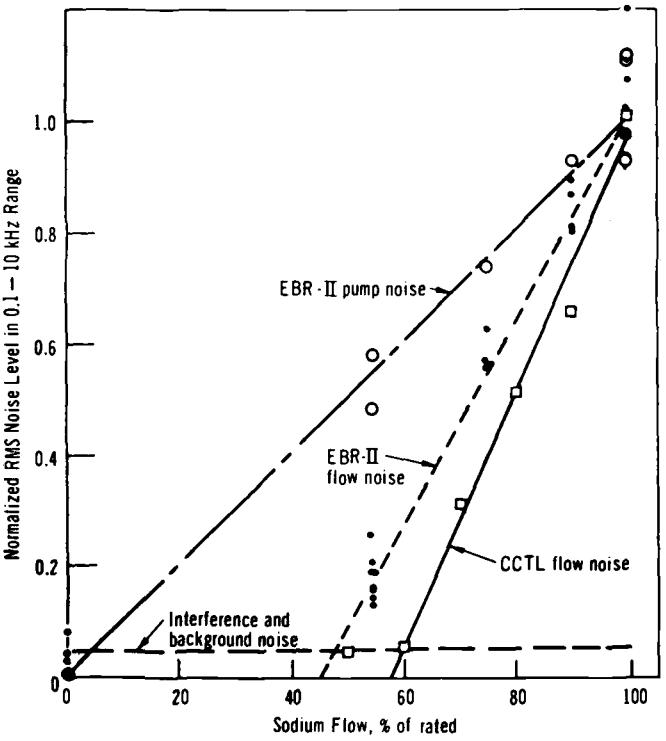

FIG. 12–*Noise level as a function of flow rate for large sodium systems.*

of the noise. The tube had been held in place by two J clips, of which one was completely broken off and the other was distorted. The tube was then excited and signatures were taken which were compared to calculations for a beam fixed at both ends (Fig. 14). This comparison verified that both ends were indeed fixed and that when the tube was clipped the remaining portion would be firmly fixed. After removal of the drain tube and additional testing, the IHX was placed back into service. Mechanical signatures taken on the IHX showed the source of noise to be eliminated.

Conclusions

The usefulness of acoustically monitoring large liquid metal coolant systems has been demonstrated for obtaining information on plant operation and plant repairs. In addition, technology and devices are being developed for direct monitoring of hot surfaces and of the internal sodium environment. The imminent combination of monitoring with these devices is expected to permit *in situ* acoustic surveillance and acoustic emission testing within and on a liquid sodium system.

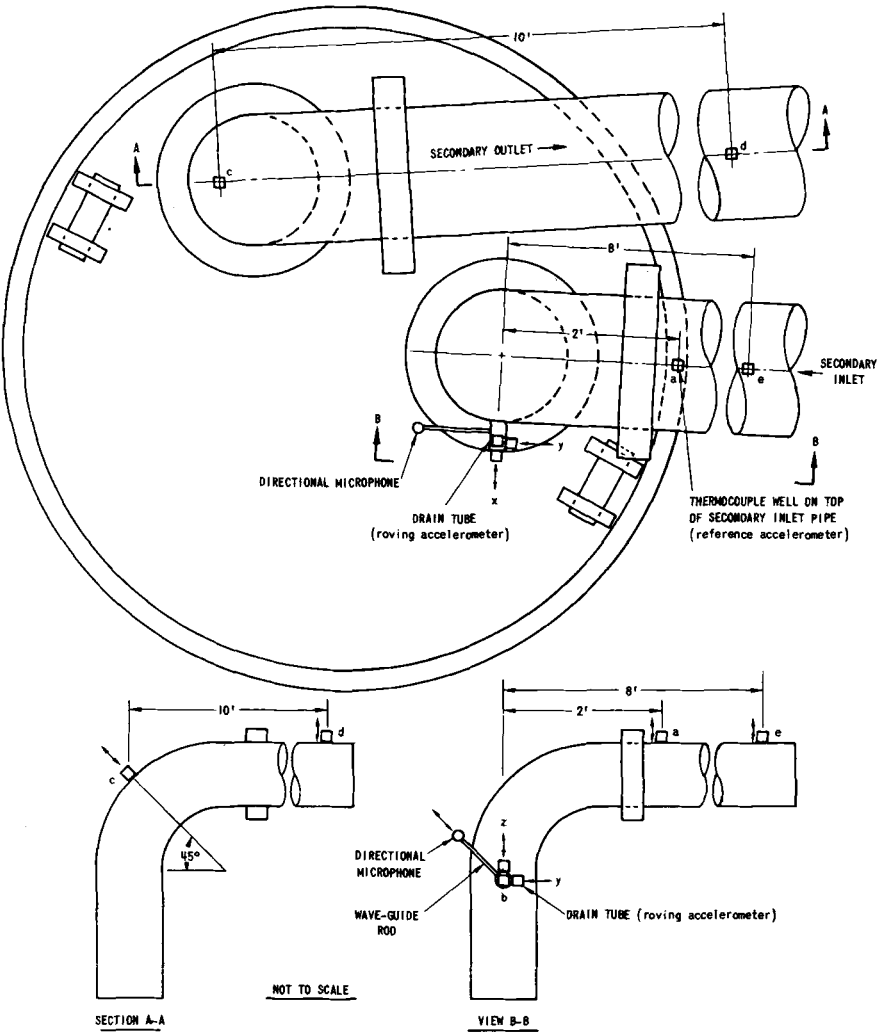

FIG. 13–*Monitoring locations on the EBR-II intermediate heat exchanger (IHX).*

References

[1] James, L. C., *Nuclear Engineering,* NUCEB, Vol. 10, Jan. 1965, pp. 18-22.

[2] Ledwidge, T. J., "Detection of Liquid Boiling in a Nuclear Reactor," British Patent 1,052,239, 1966.

[3] Matthews, R. R. and Henry, K. J., *Nuclear Engineering,* NUCEB, Vol. 13, Oct. 1968, pp. 840-844.

[4] Barkhoudarian, S. and Scott, C. C., "Preliminary Study of Feasibility of Acoustic Detection of Small Sodium-Water Reactions in LMFBR Steam Generators," APDA-256, Atomic Power Development Associates, Detroit, Mich., May 1970.

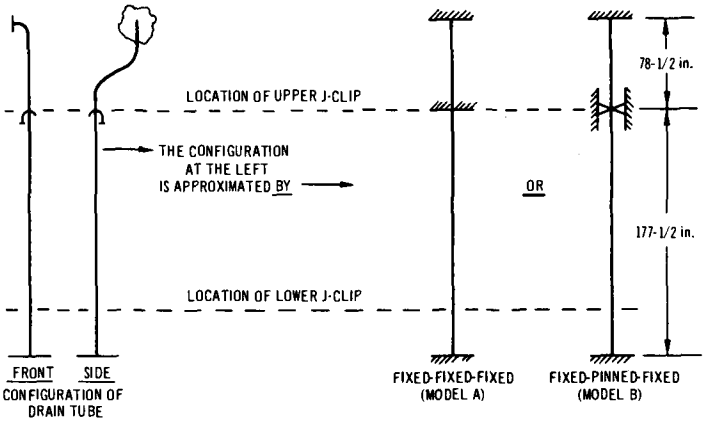

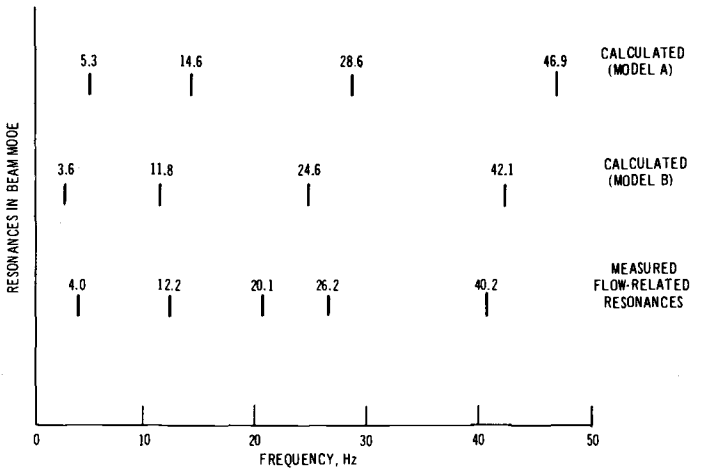

FIG. 14—*Resonances of the IHX drain tube immersed in liquid sodium, with upper J clip in place and lower J clip removed.*

[5] Redwood, M. R. in *Mechanical Waveguides*, Pergamon Press, New York, 1960.
[6] Woodward, B. and Stephens, R. W., *Ultrasonics*, ULTRA, Vol. 9, Jan. 1971, pp. 21-25.
[7] Woodward, B., *Acustica*, ACUSA, Vol. 24, No. 3, 1971, pp. 117-125.
[8] Bunney, R. E., Goodman, R. R., and Marshall, S. W., *Journal of the Acoustical Society of America*, JASMA, Vol. 46, No. 5, 1969, pp. 1223-1233.
[9] Junger, M. C. and Rosato, F. J., *Journal of the Acoustical Society of America*, JASMA, Vol. 26, No. 5, Sept. 1954, pp. 709-713.
[10] Liamshev, L. M., *Soviet Physics-Acoustics*, AKZHA, Vol. 2, 1956, pp. 198-203.
[11] Murry, E. J., *Ultrasonics*, ULTRA, Vol. 8, No. 3, July 1970, pp. 168-173.

[12] Gavin, A. P. and Anderson, T. T. *I.E.E.E. Transactions on Nuclear Science*, (Institution of Electrical and Electronic Engineers), IETNA, Vol. NS-18, No. 1, Feb. 1971, pp. 340-344.

[13] Primak, W., Anderson, T. T., and Halverson, S. L. *Nuclear Technology*, NUCEB, Vol. 10, Jan. 1971, pp. 76-84.

[14] Primak, W. and Anderson, T. T., *Journal of Applied Physics*, JAPIA, Vol. 41, No. 11, Oct. 1970, pp. 4745-4746.

[15] Smith, R. W., in *Proceedings of the I.E.E.E.* (Institute of Electrical and Electronic Engineers), IEEPA, Vol. 59, No. 4, April 1971, pp. 712-713.

[16] Halverson, S. L., Anderson, T. T. Gavin, A. P., and Grate, T., *I.E.E.E. Transactions on Nuclear Science*, (Institute of Electrical and Electronic Engineers), IETNA, Vol. NS-17, No. 6, Dec. 1970, pp. 335-340.

[17] Dowell, M. B. and Lefkowitz, I., *Journal of the Physiological Society of Japan*, NISEA, Vol. 28, Supp., 1970, p. 442.

[18] Bergmann, G., *Solid State Communications*, SSCOA, Vol. 6, 1968, pp. 77-79.

[19] Jorgensen, P. J. and Bartlett, R. W., *Journal of Physics and Chemistry of Solids*, JPCSA, Vol. 30, 1969, p. 2642.

[20] Technological University of Einhoven, "Study of Possible Application of Acoustical Methods for Determining Void Fraction in Boiling Water Reactors," EURAEC-366, Feb. 1962.

[21] Bonnet, J. A., Jr. and Osborn, R. K., *Transactions of the American Nuclear Society*, TANSA, Vol. 14, No. 1, 13-17 June, 1971 pp. 309-310.

[22] Fry, D. N., Kryter, R. C., Robinson, J. C., *Transactions on Nuclear Science*, (Institute of Electrical and Electronic Engineers), IETNA, Vol. NS-18, No. 1, Feb., 1971, pp. 345-350.

[23] Marciniak, T. J., Habegger, L. J., and Greenspan, H., "Summary Review of Neutronic Noise Techniques for Incipient Boiling Detection in Liquid Metal Fast Breeder Reactors," ANL-7652, Argonne National Laboratory, Argonne, Ill., Jan. 1970.

[24] Anderson, T. T., Mulcahey, T. P., and Hsu, C., "Survey and Status Report on Application of Acoustic-Boiling Detection Techniques to Liquid-Metal-Cooled Reactors," ANL-7469, April 1970.

[25] Cothren, R. K., "The Acoustical Characteristics of Boiling Bubbles," M.S. thesis, Department of Nuclear Engineering, University of North Carolina at Raleigh, 1969.

[26] Kartluke, H., Wichner, R. P., and Hoffman, H. W., "An Acoustic Instrument for Measuring Subcooling in Boiling Systems," ORNL-P-1678, Sept. 1965.

[27] Saxe, R. F., "Survey of Boiling Detection Methods in Reactors," Incipient Failure Diagnosis for Assuring Safety and Availability of Nuclear Power Plants," CONF-671011, Jan. 1968, pp. 41-57.

[28] Van Erp, J. B., Macfarlane, D. R., and Fauske, H. K., *Nuclear Engineering and Design*, NEDEA, Vol. 15, 1971, pp. 441-457.

[29] Hogan, J. M. and Boyd, L. R., "Joint Bettis-KAPL Nucleate Boiling Detection Experiment," WAPD-168, Feb. 1957.

[30] Colomb, A. L. and Binford, F. T. "The Detection of Boiling in a Water-Cooled Nuclear Reactor," ORNL-TM-274, 1962.

[31] Saxe, R. F. and Lau, L. W., *Nuclear Engineering and Design*, NEDEA, Vol. 8, pp. 229-240, 1968.

[32] Mac Leod, I. D., "Some Measurements of the Acoustic Spectrum Produced by Sub-Cooled Nucleate Boiling," TRG Report 1205 (R), 1966.

[33] Anderson, T. T. and Grate, T. A., *I.E.E.E. Transactions on Nuclear Science*, (Institute of Electrical and Electronic Engineers), IETNA, Feb. 1969, pp. 260-265.

[34] Le Gonidec, Rouvillois, Semeria, R., Lions, N., Robin, M., Simon, "Experimental Studies on Sodium Boiling," *Paper II-B/5, Conference Internationale sur la Surete des Reacteurs a Neutrons Rapides*, Aix-en-Provence, France, 19-22 Sept. 1967.

[35] Saxe, R. F., "The Detection of Boiling in Nuclear Reactors," *I.E.E.E. Transactions on Nuclear Science*, (Institute of Electrical and Electronic Engineers), IETNA, Vol. N.S.-18, No. 1, Feb. 1971, pp. 337-339.

[36] Hammitt, F. G., "Cavitation Phenomena in Liquid Metals," Report No. 01357-1-T, University of Michigan, Ann Arbor, Dec. 1967.

[37] Duquesne, J. C., Elie, X., and Constantin, J. P., in *1970 Cavitation Forum*, The American Society of Mechanical Engineers, New York, 1970, pp. 33-34.

[38] Bomelburg, H. J., "An Evaluation of the Applicability of Water Model Testing to Liquid Metal Engineering Problems," LMEC-68-4, Liquid Metals Engineering Center, Atomics International, Canoga Park, Calif., 26 Feb. 1968.

[39] Ledwidge, T. J., "The Detection of Local Overheating in Liquid Metal Cooled Fast Neutron Reactors," Doctoral thesis, University Aston in Birmingham, July 1969.

[40] Barclay, F. J., Hale, J. C., Ledwidge, T. J., Burton, E. J., and Jones, C. H., *Conference on Acoustics as a Diagnostic Tool*, Institution of Mechanical Engineers, London, 20 Oct. 1970, pp. 47-63.

[41] Bowles, L. F. and Taylor, D., *Nuclear Engineering*, NUENA, Vol. 12, May 1967, pp. 361-366.

[42] Anderson, T. T. and Just, F. H., in *Abstract Bulletin, TMS Fall Meeting and ASM Materials Engineering Congress*, Philadelphia, Pa., 13-16 Oct. 1969, p. 170. Available from American Society for Metals, Metals Park, Ohio 44073.

[43] Price, C. C. and Karvinen, J. R., *Transactions of the American Nuclear Society*, TANSA, Vol. 14, No. 1, 13-17 June 1971, pp. 303-304.

N. O. Cross,[1] *L. L. Loushin,*[1] *and J. L. Thompson*[1]

Acoustic Emission Testing of Pressure Vessels for Petroleum Refineries and Chemical Plants

REFERENCE: Cross, N. O., Loushin, L. L., and Thompson, J. L., "**Acoustic Emission Testing of Pressure Vessels for Petroleum Refineries and Chemical Plants,**" *Acoustic Emission, ASTM STP 505,* American Society for Testing and Materials, 1972, pp. 270-296.

ABSTRACT: Acoustic emission testing (AET) is being used by fracture mechanics and nondestructive test engineers to establish the design adequacy, structural integrity, and operating safety of petroleum and petrochemical equipment. Used as a tool in the application of fracture mechanics concepts, AET of heavy wall pressure vessels during hydrostatic testing also provides the means of assuring against catastrophic brittle fracture by locating growing defects. The state-of-the-art in developing effective electronic instrumentation and flaw site triangulation methods has reached the point where AET should be considered competitive with other, more commonly specified test methods.

For onstream surveillance, AET has the potential for the detection of service induced flaws and for detecting potentially detrimental changes in material properties. The amplitude and frequency content of environmental noise can however, limit applications of this type. Although techniques are available for minimizing the reception of unwanted electrical and mechanical sources of noise, additional effort is needed in this area to facilitate widespread inservice use.

Other areas requiring further research and development effort and the development of standards, include flaw signature analysis, signature analysis characteristics for various materials, simplified instrumentation, acoustic parameter selection, the effect on signals of environmentally induced materials property changes, and data display.

KEY WORDS: acoustics, noise (sound), fracture strength, toughness, brittle fracturing, pressure vessels, nondestructive tests, hydrostatic tests, stress waves, acoustic signals, data processing, computers

Acoustic emission techniques (AET) and instrumentation have developed to the point where this method can be practically applied for the nondestructive

[1] Senior engineer and project engineers, respectively, Esso Research and Engineering Co., Florham Park, N.J. 07932.

inspection of process vessels used in petroleum refineries and chemical plants[*1*]. High quality commercial electronic components, operable outside of laboratory environments, which fulfill specific AET requirements are readily available. Experience reported from tests under a variety of field environments has resulted in quantitive information on undesirable sources of noise and methods for improving signal/noise ratio or minimizing noise sources. Trends have evolved which favor certain types of AET data display and parameter relationships. More work has to be done in this area however, before generally accepted data reporting standards are established.

Acoustic testing of pressure vessels can be performed during the initial hydrostatic acceptance test while the vessel is in service, and during shutdown periods after intervals of service. Some of the reasons for AET of vessels are as follows:

(1) To locate fabrication flaws not discovered by the more common nondestructive testing (NDT) methods such as radiography and ultrasonic inspection.

(2) To prevent catastrophic loss of heavy wall vessels which could fail in a brittle fashion if a small undiscovered flaw were to propagate to critical size during hydrostatic testing.

(3) To find service induced flaws (that is, stress cracks, fatigue cracks, embrittlement areas) in the vessel.

(4) To requalify existing vessels for more severe operating conditions.

The single, most significant advantage of AET as an NDT method is its capability for locating structural discontinuities and flaws without resorting to a point-by-point search over the entire surface of the vessel. Radiography, ultrasonic testing (U.T.), magnetic particle, eddy current, and other NDT methods supply information about the part only at the point where they are applied. AET, on the other hand, being a passive test, can provide complete, flaw site information throughout the entire volume of the vessel.

Application of AET Specified by Fracture Mechanics

Studies of the fracture behavior of commonly used pressure vessel steels has led to the development of toughness criteria which were established to resist catastrophic brittle fracture.

Conventional design standards and practices which have been used in the past have rarely considered the possibility of catastrophic failure at design stress levels which are generally at or below yield strength of materials. Such failures are not unique to any individual type structures. Classic examples of catastrophic brittle failures range from the Boston molasses tank and Cleveland methane storage tank to the World War II Liberty ships, and even old iron bridges. These failures were all caused by some sort of mechanical or metallurgical notch or defect. In each case, the design criteria which were based

on strength properties alone were inadequate to prevent failure in the presence of a defect[2]. As a result, the interrelationship of material strength, toughness, and defects was recognized and an understanding of the mechanics of the fracture process was developed[3]. The fact that fracture mechanics could mathematically express the criteria for brittle fracture has been perhaps the most significant contribution to the state-of-the-art. Now with the ability to calculate critical defect sizes, inspection standards can be related directly to design criteria.

There are two criteria used in the industry to eliminate brittle fracture; prevention of fracture initiation and prevention of fracture propagation. Experience has shown that designing for the prevention of crack initiation is not always sufficient to assure freedom from brittle fracture in a heavy wall fabricated vessel. The presence of defects and flaws in a vessel is almost certain regardless of the care exercised during fabrication. Consequently, the potential for fracture initiation is always present. If pressure vessel designs are based on the prevention of fracture propagation, the severe limitations are encountered if high strength materials or thick sections are involved.

Of the several fracture criteria which have been established in the past, the most generally adopted has been based on a minimum charpy V impact energy which must be exhibited by the material at the minimum service temperature. Until recently, such a criterion had been considered adequate for all types of pressure vessels being used throughout the industry. However many petroleum and petrochemical processes have dictated increasingly higher design pressures and capacities. This has resulted in a substantial increase in the number of pressure vessels built in heavy section (that is, wall thicknesses in excess of 2 in.). Several catastrophic failures of heavy wall pressure vessels during hydrotest have shown that currently accepted "fracture-safe" criteria do not provide adequate safeguards against brittle fracture for such vessels at hydrotest temperatures. Although the materials were thought to have sufficient notch toughness in each case, the effect of increasing wall thickness on toughness requirements for the prevention of brittle fracture was not recognized.

The problem of brittle fracture poses a continuing threat to users of steel products without proper precautions. As the metal temperature is lowered, ferritic, bainitic, and martensitic steels become susceptible to brittle fracture at relatively low imposed stress levels. That is, below certain temperatures, these materials go through a ductile-brittle transition and become highly notch sensitive. Of the great number of factors which can contribute to brittle fracture, only three are considered critical. These factors are: (1) high stresses; (2) low toughness; and (3) critical defects. The threat of brittle fracture can be reduced, if not totally eliminated, if any one of these dominant factors can be eliminated or effectively controlled.

Thick sections and complex designs in pressure vessels have a tendency to

result in greater constraint on the material. Very little can be done to eliminate this condition.

The impact requirements associated with a leak-before-break toughness criterion or any other fracture-safe design basis increase significantly with material strength and thickness until they exceed the values that can be obtained with commercially available materials. As a result, there are limits to the application of toughness criteria in controlling brittle fracture. The general tendency had been to utilize higher strength materials in order to reduce section size but these materials usually have less tolerance for cracks and linear type flaws. As a result the pressure vessel has less tolerance for possible fabrication defects or for those which may develop during service and more intense inspection is required.

Advances in the state-of-the-art of steel technology have resulted in materials with improved notch toughness. However, the toughness of a material is always found to decrease as the thickness increases because of metallurgical variations. Compounding the problem of reduced toughness is the effect of increased constraint at a defect in heavy section plates. This condition significantly increases the likelihood of unstable crack propagation from existing flaws or defects.

Although the nature of fracture initiation can be extremely complicated, the conditions of continued propagation or fracture arrest are more complex because of several factors. Factors which are very important in the analysis of fracture arrest are the critical elastic strain, energy release rate, and the plastic work or energy dissipated at the crack surface. In heavy wall pressure vessels, design concepts for fracture arrest are extremely limited in scope and application. Therefore, materials must be capable of providing for fracture arrest in pressure vessels. If the material is capable of preventing catastrophic brittle fracture from full thickness defects, then one form of fracture arrest is said to have been achieved. This has become known as the leak-before-break fracture toughness criterion.

The leak-before-break fracture criterion received considerable attention by various industries because the criterion can be used to establish material requirements based on fracture mechanics concepts. The application of fracture mechanics to the prevention of brittle fracture can provide assurance to the pressure vessel designer or operator that an ordinarily detectable defect could be supported by the material without resulting in a catastrophic failure. From experience in fracture testing of thin wall (thicknesses less than 2 in.) pressure vessels it was shown that a defect could grow to a through-the-thickness crack before it could reach the critical size necessary to cause failure. However, as the toughness requirements increase because of size or strength, the material may lack sufficient notch toughness to tolerate a critical defect which is smaller than the wall thickness. When problems of brittle fracture have been encountered, the

generally accepted fracture-safe criteria which are based on Charpy V impact energy have been incapable of estimating limiting thicknesses.

Because there are limits to the action that can be taken by the designer or fabricator of heavy wall pressure vessels to affect either the stress and toughness factors in the brittle fracture control problem, control of critical defect size appears to be the only technically feasible method of solving this problem. Standard inspection techniques such as radiography and ultrasonics lose their capability of detecting the small cracks and defects that can easily propagate to critical size as the thickness increases. In addition, the most severe type of defect, linear cracks, can go largely undetected because they appear nearly transparent to X rays and are at times capable of transmitting sound waves across the interface.

Basis for Application of AET to Heavy Wall Vessels

If the design criterion requires standards for crack detection and notch toughness which are beyond technical capabilities, then maximum use of acoustic emission monitoring is recommended.

For heavy wall pressure vessels, the impact requirements associated with the leak-before-break toughness criterion cannot be satisfied beyond a certain thickness. As indicated earlier, this is because of the inherently poor notch toughness properties in a heavy section of steel plate and the high toughness requirements for thicker sections. The impact energy which a material must exhibit so that leak-before-break behavior would be attained is shown as the upper boundary in Fig. 1 as a function of wall thickness for vessels up to 6 in. thick. The lower boundary is a less conservative criteria based on a modification of the leak-before-break concept known as "through-thickness-yielding". Impact requirements commonly used for heavy wall vessels and applied to materials in thicknesses above 2 in. are generally below the upper boundary. This is due to the necessity to compromise between available guaranteed properties for commercial materials and reasonable levels of toughness for safe design.

On many occasions the higher quality steels which have been purchased for heavy wall pressure vessels exhibited considerably more toughness than that guaranteed by the steel producer. Recognizing that this can be a frequent occurrence, the requirements for application of acoustic emission testing of heavy wall pressure vessels are based on actual Charpy-V impact test data rather than specified properties.

The upper boundary in Fig. 1 represents a separation of conditions where acoustic testing is considered desirable or mandatory from those where it is not required.

It is generally agreed that the leak-before-break toughness criterion is the most conservative fracture-safe design basis and as such provides maximum

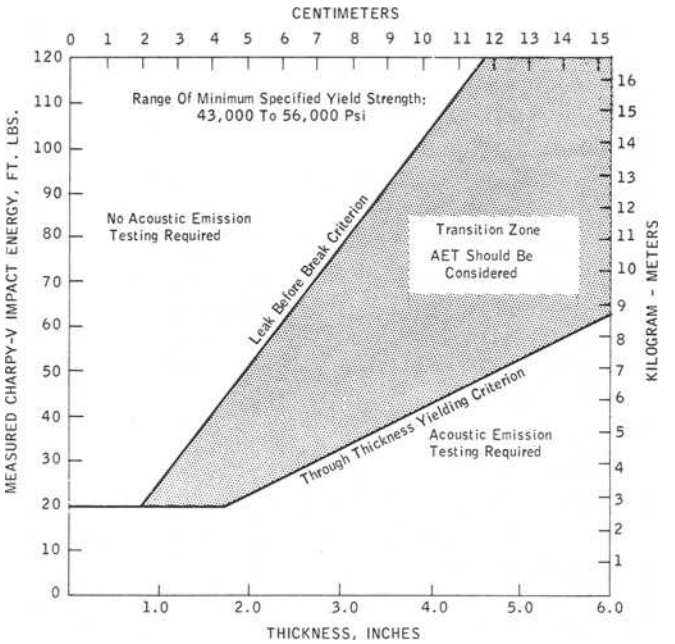

FIG. 1—*Requirements for acoustic emission testing of fully killed and medium strength carbon and low alloy steels.*

assurance against brittle fracture under all circumstances. Because the toughness requirements associated with this criterion are conservative there are cases where adequate protection can be achieved with lower notch toughness properties. Therefore, a second criterion has been utilized to establish a reasonably lower boundary based on the plastic zone associated with a central flaw just touching the surfaces and to provide a "transition zone" in which the probability of brittle fracture can be reduced by other factors such as design, inspection and operating conditions, and measured physical properties. In cases where the service of a heavy wall pressure vessel is not considered severe or where the exhibited toughness may be adequate when coupled with stringent inspection by conventional techniques, the need for applying acoustic emission testing may not be necessary.

Where a vessel falls on or within the transition zone a careful review and consideration of all factors should be made before deciding whether to require acoustic emission testing or not. The refinement of this gray zone and perhaps its ultimate elimination is possible as technology develops. In the meantime, it is best to review specific situations which fall within that zone.

It must be recognized that if a critical size flaw exists in a vessel, it is improbable that AET can prevent catastrophic failure. In this case, the only

physical change associated with flaw growth immediately prior to fracture initiation is plastic deformation of the material near the end of the flaw tip and it is highly unlikely that the very low level acoustic emission associated with this plastic deformation would be detected by the AET system. A subcritical flaw, on the other hand, will propagate toward critical size in steps of ever increasing size and, therefore, increasing energy release per event. It is this increasing energy content which can be recognized and allow for a safe termination of the test. Since the acoustic emission characteristics of construction materials vary over several orders of magnitude, it is necessary to acoustically evaluate the material being studied prior to the test if judgments of severity are to be made during a vessel hydrostatic test. Even then the interpretation will be rather qualitative. Further research in acoustic emission testing and fracture mechanics may be expected to reduce the subjectivity of flaw analysis.

AET Instrumentation System

A block diagram of an experimental AET system is shown in Fig. 2. The system was designed for general research work so flexibility beyond that needed for pressure vessel testing alone has been incorporated. The physical appearance of the system except for sensors and preamplifiers is shown in Fig. 3.

For vessel testing, up to 10 sensors and preamplifiers are positioned on the test vessel at selected locations. Detected emission stress waves are amplified by a factor of 100 to 2000 and sent via coaxial cables to the signal processing unit located up to 400 ft away. In the signal conditioning unit the signals are filtered

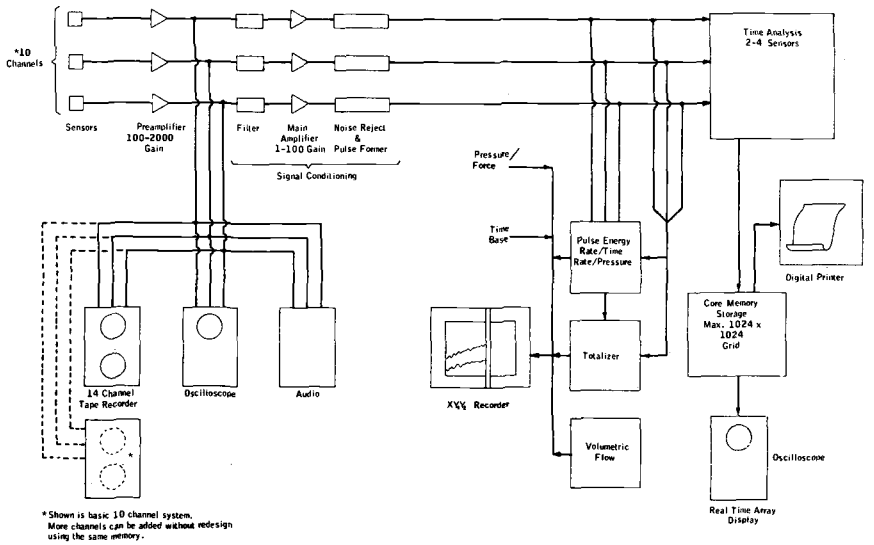

FIG. 2—*Acoustic emission system block diagram.*

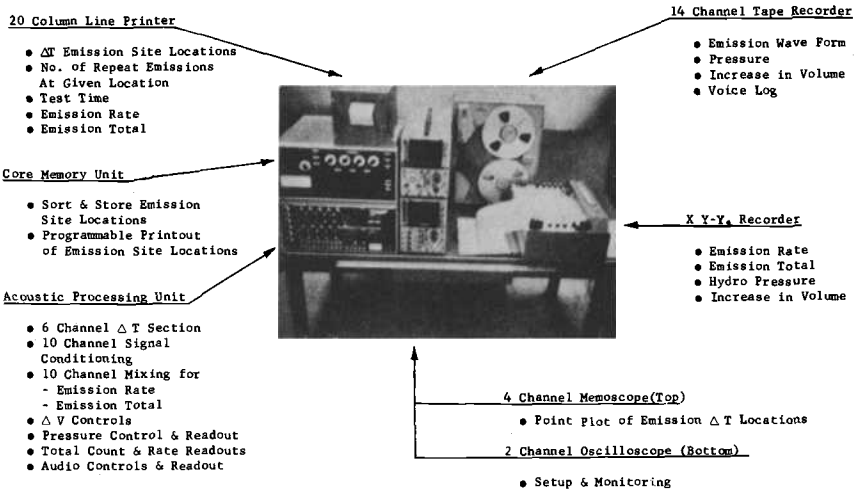

FIG. 3—*Acoustic emission system.*

to reduce the masking effects of signals from bolt creep, flange noise, and vibration or shock from nearby machinery. After filtering, the signals are further amplified up to 100 times and a single pulse is formed indicating time of arrival of the emission signal.

The pulses generated by 2 to 4 sensors are selected for input to the time analysis logic which generates the time of arrival differences, or ΔT, used in flaw triangulation. The time analysis section also performs certain validity checks so that obviously invalid data may be discarded. Valid ΔT's are stored in the core memory unit, sorted by location and, if a location is assuming statistical significance, it is published by the digital printer. The core memory uses sparse array storage techniques common to the data processing industry so that a grid of 1024 by 1024 points may be stored in a 4096 word memory. By this technique up to 1200 valid, significant, sites may be stored at one time. An oscilloscope is used to display an isometric plot of the stored data so that an operator may make a real time evaluation of emission sites as they accumulate. An additional feature will permit display of a selected ΔT location on the same oscilloscope screen in numeric form.

The pulses from the signal conditioners are also used to derive emission rate, total, and energy. Emission rate may be either in emissions per unit time or emissions per psi, pound, temperature increment, etc. where a 0 to 1-V signal proportional to the parameter is available. This form of rate measurement evolved as variations in vessel pressurization rate were found to cause annoying distortions in emission rate data per unit time. This method extracts emission rate per unit stress which is the most meaningful information.

The emission rate, emission total, or pressurizing fluid volumetric flow may

be plotted versus time or pressure, on an XYY′ recorder so that trends may be seen as they develop.

The raw data from the preamplifiers is stored on a 14-track tape recorder so that it may be replayed and triangulation performed on a different set of sensors on a posttest basis. The raw signals are also displayed on an oscilloscope and converted to the audible range through a loudspeaker. These two outputs are mainly signal quality checks and can pinpoint problems such as the development of leaks, and sensor, preamplifier or cable grounding problems, should they develop.

System Characteristics and Description

Perhaps the most critical portion of the system is the sensor preamplifier pair. To detect the extremely low level emission signals, it is necessary to convert the mechanical stress wave to an electrical signal as efficiently as possible, then amplify that feeble signal with a minimum of noise addition by the preamplifier circuitry. Further, the preamplifier and sensor must reject low frequency noise and recover from large signal overloads promptly and cleanly.

The frequency range chosen for pressure vessel AET lies between 100 and 250 kHz. This range is the usual compromise between low frequency mechanical noise rejection and increasingly severe high frequency attenuation losses over long distances [*4,5*]. The first piezoelectric transducer sensors were made of two longitudinally poled pieces of (PZT-5), soldered together to form a cylinder slightly shorter in length than its diameter. The arrangement simultaneously offered both high sensitivity and broad bandwidth [*6*]. Unfortunately, it was very difficult to fabricate this composite element consistently, so a solid piece of PZT-5, about the same size as the dual element, has been adopted for the present. The signal versus frequency response of the transducer is shown in Fig. 4*a*. This stack is mounted in a copper shield tube such that physical damping of the piezoelectric crystal is minimized. Finally, the shield tube is terminated in a short length of coaxial cable and spring mounted in a magnet assembly which permits simple attachment to the vessel.

A low electrical noise preamplifier was developed with frequency response tailored to complement that of the sensor. This 5-transistor preamplifier is powered by either a 22½-V battery or from a central power supply, and achieves noise performance equivalent to a noise source at the input of 10 μV rms. The frequency response of the preamplifier is shown in Fig. 4*b*, and the response of the sensor preamplifier pair in Fig. 4*c*. The broadband acoustic transducer input for the above frequency spectra was achieved by impinging the grit stream from a small sandblaster onto a piece of 1-in.-thick steel plate.

Signal Conditioning

The preamplified signals are received via coaxial cables at the signal processing unit and put through an active filter to further reduce low frequency signals and

a. FREQUENCY SPECTRUM - AET SENSOR

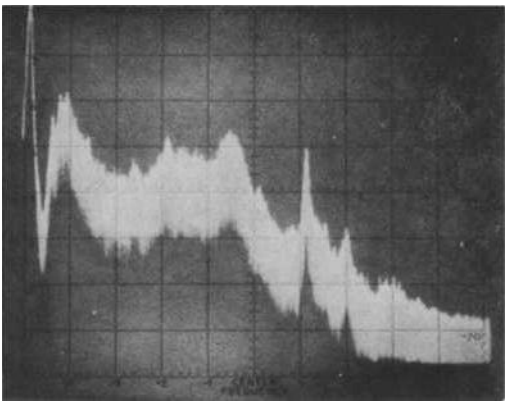

b. FREQUENCY SPECTRUM AET PREAMPLIFIER

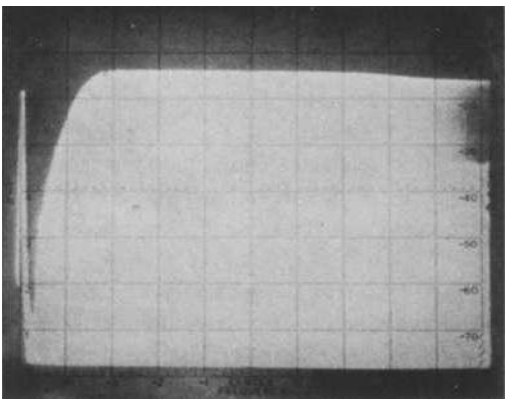

c. FREQUENCY SPECTRUM AET SENSOR + PREAMPLIFIER

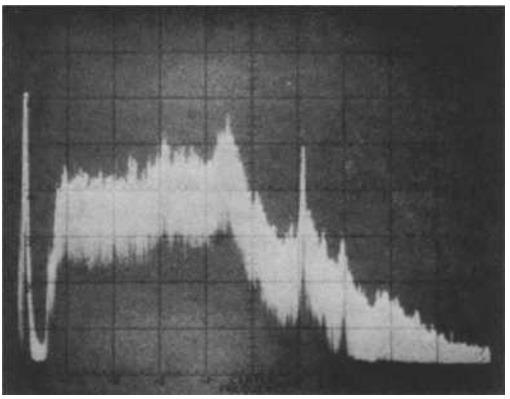

FIG. 4—*Frequency responses. All spectra: 50 kHz/Div.*

also eliminate stray pickup from any nearby radio transmitters. The frequency determining elements of the active filter are on a small removable plug allowing simple frequency changes for use up to 2 MHz. After filtering, the signal is further amplified and a minimum threshold is set so that subsequent circuitry will not be affected by low level random noise produced by the amplifier chain.

The final step in the conditioning of the signal is determination of arrival time. A single digital pulse is derived for each emission which lasts 2 ms longer than the received emission. For accurate event rate counting and triangulation it is mandatory that only one pulse be generated per emission event.

The same digital pulses are also used to determine emission rate and total emissions detected. The totalizer is a straight forward counter with 6 digits displayed out of a possible 9 and an analog output switchable to any pair of digits in the display. The input to the totalizer may be pulses from any or all channels. The ratemeter is designed as an all digital unit to eliminate problems associated with long time constant analog smoothing filters which must be employed at low event rates. Such filters are undesirable since they mask the contribution of short length bursts, which are often of importance. The derived rate may be in terms of events per unit time—the usual meaning of rate—or in terms of events per unit parameter. This parameter may be any quantity such as pressure, load, strain, or temperature. The only requirement is that the quantity be presented to the ratemeter as a linear analog voltage of at least 1-V range. By removing time as the rate parameter, testing may be done without concern about data distortion caused by variations in the time rate of pressurization, cooling, etc.

A digital output volumetric flowmeter is included to allow detection of nonlinearity in the pressure-volume relationship due to plastic yielding in a vessel. Currently, flaw emission rate or total count are plotted against time or pressure on a 2-pen XYY′ recorder. Data are thus preserved on paper and trends such as increase in emission rate or vessel yielding may be readily seen in real time.

Time Analysis

The time analysis and storage section of the system determines time differences between several sensors, stores valid ΔT pairs in a core memory, prints ΔT pairs which are developing significance, and creates a real time oscilloscope display of all ΔT pairs stored in core so an operator can see qualitatively the current results of the test as they accumulate.

The time analysis section digitially generates one or two ΔT's associated with 2 to 4 sensors. Tests for validity of ΔT include a maximum distance test and a time correlation check between the pair of ΔT's and length of event. ΔT combinations which fail these tests are discarded. The time analysis unit also contains one of the two interfaces with the core memory and the digital printer interface.

The core memory unit is a special purpose device built around a commercial core memory module. The core interfaces with the time analysis unit and the file sort/display unit. The time analysis interface accepts ΔT's, synchronizes the ΔT counters, and controls the printer. The file sort/display interface provides the display of all data in core on a time sharing basis with the time analysis interface, and switches to a high speed mode to sort incoming data to the proper storage address. The data are stored in core as an associated pair of ΔT's to simplify triangulation. To assign each possible ΔT pair a unique core address would limit resolution to an unacceptably coarse grid on a larger vessel, that is, about a 32 by 64 point grid. The evident need for a much larger memory is circumvented by using a common data processing technique for storing only meaningful data called sparse array storage[7]. By this technique 3 core memory words are assigned to each data point. The first word stores ΔT_1, the second holds ΔT_2 while the third stores the number of times the particular ΔT_1, T_2 combination has been detected. The memory is thus like a file drawer. The file sort/display unit receives a valid ΔT pair from the time analysis interface and sorts through the file seeking an entry under that ΔT pair. If one exists, the count in the third word is incremented by 1. If an entry does not exist, one is inserted in the proper numerical order. Should the file be full, an entry with only 1 count is selected at random, destroyed, and the new entry placed in file. Such random action does not affect test data validity since the file contains space for 1200 entries.

The display function generates a 3-dimensional isometric visual view of a plane corresponding to the 1024 by 1024 possible points the ΔT pair can occupy. Actual counts in a location appear to be elevated above the base plane. Due to the statistical nature of signal detection, a defect location will not correspond to a given single point but rather a narrow mountain peak which will be statistically centered at the ΔT coordinates. An addition to the display will allow the operator to move an intensified spot on the display to a peak of interest, then display, at the bottom on the oscilloscope screen, the time coordinates and count magnitude corresponding to that location. Real time triangulation may thus be performed while the data accumulates. Since ΔT's are stored as related pairs, and only those pairs assuming statistical significance need to be considered, the data handling problem has been significantly reduced.

Field Application Considerations

The foremost problem associated with field acoustic emission testing is unwanted noise arising from mechanical and electrical sources. A brief summary of these is given in Tables 1 and 2. The present AET system is designed to filter out most ambient mechanical noise, however, certain types such as caused by impact, cavitating or very turbulent flow, sealing flange stick-slip, or vessel mount motion may be detected. It is not possible to completely eliminate these, but their contribution may be reduced considerably by a few precautions. These

TABLE 1—*Mechanical/liquid noise sources—AET vessel testing.*

Cause	Possible Corrective Measures
Movement on supports	Place vessel on wood blocks or other quiet material
Movement of internals—trays, rings, baffles, girders, etc.	Remove internals or place on wood blocks. Shim with soft plastic if bolted in place
Rain, snow, sleet	Move vessel under cover or reschedule test
Leaks in gaskets or screwed fittings	Seal off leak
Flange gaskets and bolting	Tighten bolting
Hydrostatic test pump and liquid lines to vessel	Increase inside diameter of outlet to reduce noise from flow and cavitation
	Use high pressure reinforced hose between pump and vessel. Do not pipe pump to vessel
Mechanical vibration of flow noises transmitted through supporting structure or attached piping	Band pass filter at frequency outside of offending noise spectrum
	Disconnect vessel from structure or reduce flow rates, or both
	Conduct test when vessel is out of service
Nearby sources of mechanical noise (overhead cranes, punch presses, railways, rolling mills, etc.)	Band pass filtering
	Conduct test at a time when noise source is not operative

TABLE 2—*Electrical noise sources—AET vessel testing.*

Cause	Possible Corrective Measures
Nearby welding especially high frequency start on TIG and MIG	Stop the welding or wait until a time when welding is not scheduled
Power line noise such as caused by large motors and controllers	Extensive filtering of instrument power or use of a portable generator (usually simplest)
Radio station and other detected interference (ground loops)	Shielding of transducer and cable to preamplifier
	Special care in grounding of all system components. Sometimes use of braided wire or welding cable is necessary between all preamplifiers and then to signal conditioner chassis ground.

include protection from rain, mounting on wood or padded cribbing, using hose rather than pipe from the pump to the vessel, removing members in contact with both the vessel and a noise producing structure, and securing all vessel connections against liquid leakage.

Electrical noise is a function of instrument shielding and good electrical grounding, which is often more of an art than a science. Good shielding practice demands that the voltage drops caused by currents in ground conductors be less than signal voltages. It is important to note that as frequency increases, the current in a conductor tends to flow more on the surface—the so called skin effect. At the frequencies under discussion, the effect is not pronounced; however the types of electrical noise encountered in the field demand consideration of this skin effect. Sharp pulses contain much of their energy in the high frequency range. Hence if a poor high frequency ground is used, a voltage drop due to the noise will exist with the result that the ground at the preamplifier will not be 0 V referred to the signal processor, but will swing about 0 V. This has the same effect as placing the voltage excursion on the signal lead, causing the energy content of the noise to be detected at the signal processor. Keeping the skin effect in mind, as well as the fact that the signals are being detected at a level of only tens of microvolts at the sensor, a very low impedance ground is needed for a broad frequency band; for example, a large surface area. Either welding cable or braided wire ground strap have been found to work well. Figure *5a* and *5b* schematically illustrate grounding schemes which often work well for this arrangement. Note that all heavy external grounding cables and chassis interconnection grounds are common to only one point. The input ground on the signal processor is the optimum place since this point is most sensitive to ground current induced voltages.

Evaluating Sources of Noise

Before undertaking an AET in the field or shop it is necessary to estimate or measure the effect of environmental noise sources on the test results. Noises of concern are those of sufficient amplitude and frequency content to be confused with true emissions from the vessel and could thus introduce spurious information for the real time evaluation and into the recorded data. Band pass filtering to a large extent can eliminate much of the low frequency mechanical noise sources and some of the higher radio frequency (R.F.) electrical signals. Under certain conditions however, particularly for onstream monitoring, broadband noise sources such as liquid cavitation or vibrating pumps and motors, can be of such high amplitude that it is impossible to conduct a successful AET.

Quantitive evaluation of noise sources at the test site is highly desirable and can save much time and expense involved in the shipment and setting up of a rather bulky AET system.

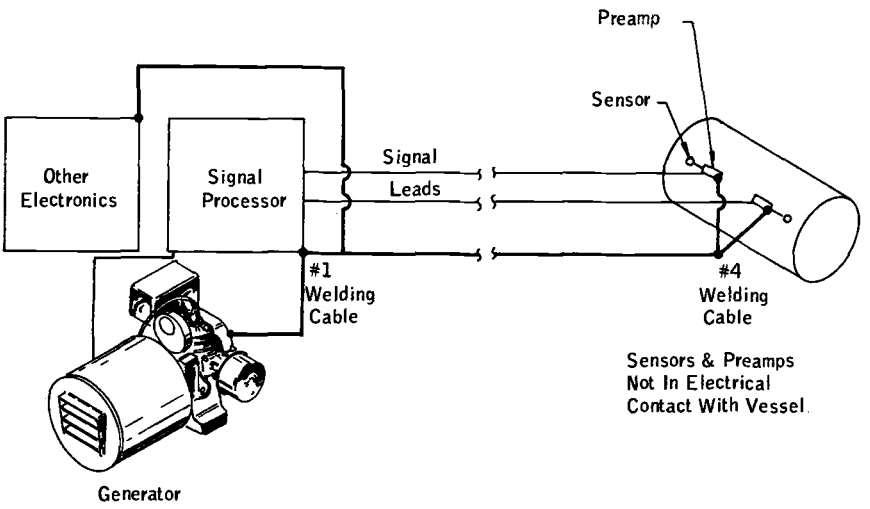

Welding cable offers good, high frequency, low impedance ground. All chassis grounds made to one point, preferably near signal processor input ground.

FIG. 5a—*System grounding configuration.*

One test method successfully used consists of inserting a signal of known amplitude into the vessel and appraising the detectability of this signal against the existing background noise. Since there is no currently available standard emission source, the injected pulse is usually generated from a pulser and transducer which laboratory studies have shown to approximate a true emission in signal shape and amplitude.

The inserted signal can conveniently be detected by an acoustic sensor and preamplifier normally used for the vessel AET work. Display of the received signal is readily accomplished on a portable oscilloscope. To simulate the proposed field test conditions, the inserted signal should be put into the vessel at the maximum spacing to be used between sensors.

Emission Site Triangulation Techniques

The primary purpose for applying AET during the hydrostatic test of a vessel is to pinpoint flaw locations in the structure and make necessary repairs at these spots. As previously discussed, the significance of the displayed ΔT coordinates is determined by the number and coincidence of similar ΔT locations presented in the printout. Identification of a resolved ΔT location, as "A" in Table 3 and in Fig. 6 is needed before this point can be plotted on the vessel.

One system for triangulation involves constructing two intersecting hyperbolas representing the loci of points having a constant time difference from the

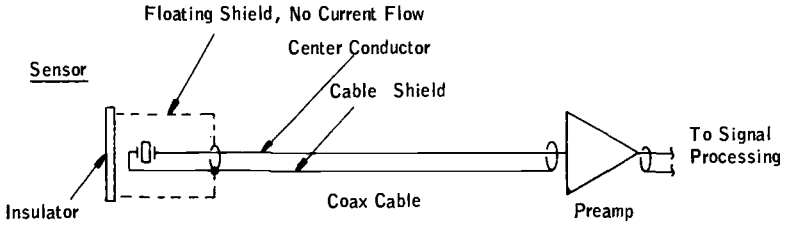

a) Moderate shielding, floating shield carries no signal currents, hence no resistive voltage drop due to noise induced current.

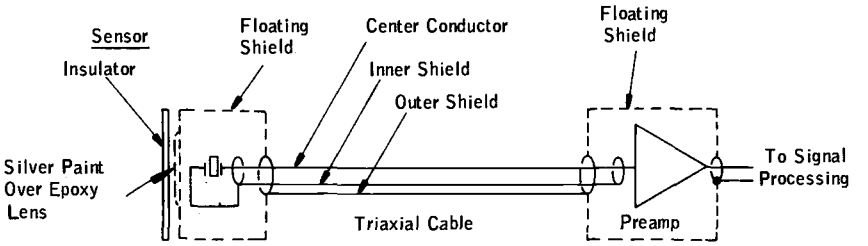

b) Severe service shielding.

FIG. 5b—*Sensor preamp shielding.*

two fixed points where the sensors are located. The manner in which these hyperbolas are constructed is described in the example shown in Figs. 7, 9, and Table 4. An important point to note is the significance of the (+) and (−) signs associated with the ΔT values and hyperbola index. This is explained in Figs. 7 and 8. In practically all cases, there will be only one intersection for a pair of hyperbolas, however spurious emission sites can be identified if no intersection occurs for the particular ΔT combination. Figure 9 shows the hyperbolas and emission site found for a combination of positive and negative ΔT values. The emission site "A" identified in Table 3 and Fig. 6 was located in the vessel in Fig. 10. Ultrasonic inspection at the triangulated point confirmed the presence of several discontinuities in a longitudinal seam at point A on the sketch of the vessel shown in Fig. 11.

A second method for locating an emission site employs the Apollonian construction discovered by Appolonius of Perga, a 3rd century B.C. Greek mathematician. This construction locates the center of a circle which passes through a fixed point and is tangent to two given circles. Figure 12 shows this

TABLE 3—*Real time* ΔT *printout.*

ΔT × 10^{-1} μ SEC			
1→4	1→5		
042	047	A = 650 PSIG	
042	047	A	
037	041	A	
039	041	A	
−083	−119		
042	047	A	
269	268		
048	051	A	
039	047	A	
047	041	A	
046	042	A	
038	041	A	
050	060	A	
034	047	A	
036	040	A	
039	040	A	
−371	−370		
−088	−098		
045	041	A	INCREASING
050	053	A	PRESSURE
326	320		
305	126		
298	290		
307	125		
047	047	A	
047	041	A	
052	053	A	
−138	−125		
047	041	A	
047	041	A	
−138	−117		
−141	−115		
047	040	A	
042	046	A	
−136	−119		
−117	−122		
−396	−381		
−139	−118		
043	047	A	
−138	−120		
−093	−097		
054	063	A	
050	053	A = 90 PSIG	

type of construction for the same ΔT combination used in the example of Fig. 9. Actual construction of the unknown circle with radius e is not necessary. A much simpler method consists of drawing a series of concentric circles on a thin clear plastic overlay sheet and by observation and trial and error find the circle

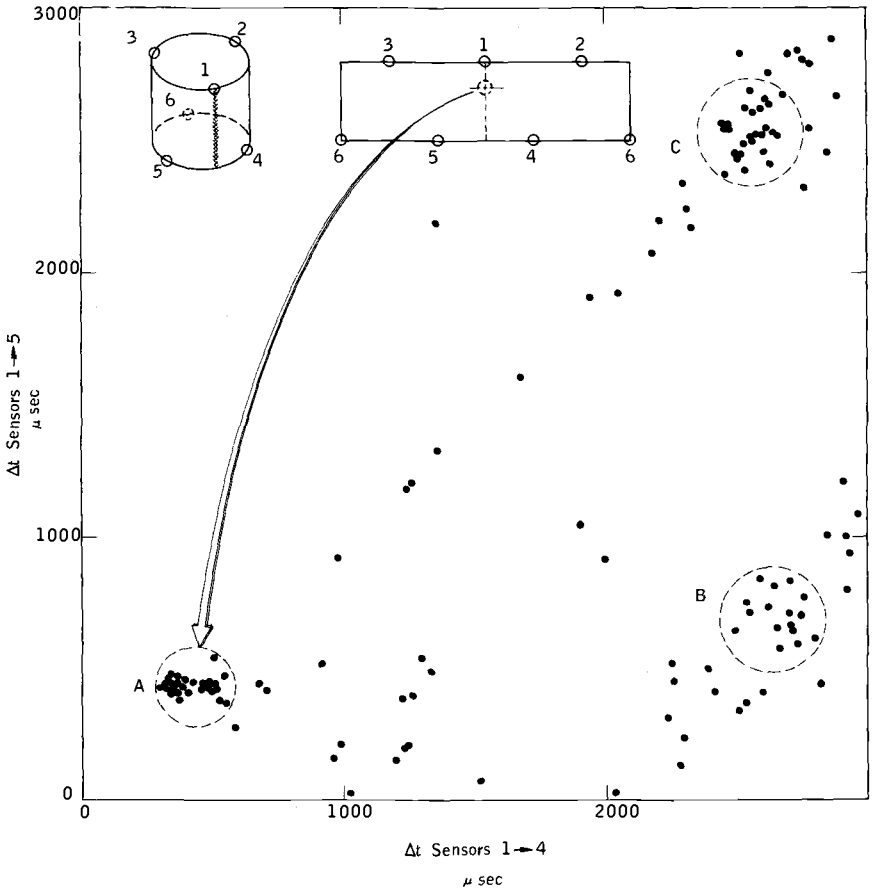

FIG. 6—Δt *plot of (+, +) locations on a pressure vessel.*

which is the best fit for the conditions. The center of this circle is the emission site. It should be noted that there are usually four possible solutions to the Appolonian construction. The correct solution is obtained by noting the order in which the emissions are received at each sensor and assigning the proper (+) or (−) sign to the ΔT's according to the convention observed when using hyperbola method.

Use of Look-Up Tables

Triangulation by means of intersecting hyperbolas or the Apollonian construction is applicable to vessel surfaces which can be developed into a flat plane, such as a cylindrical shell section. The same methods are not applicable to curved surfaces such as spheres or semielliptical heads. One direct method of

TABLE 4—*Instructions for constructing the* ΔT *hyperbola (refer to Fig. 7).*

GIVEN

Sensors 1 and 2 spaced 10 ft apart
Measured velocity = 0.1 in./μs

Measured transit time $1\rightarrow2 = \frac{\mu s}{0.1 \text{ in.}} \times \frac{12 \text{ in.} \times 10 \text{ ft}}{1 \text{ ft}} = 1200\ \mu s$

Emission $\Delta T 1\rightarrow2 = +300\ \mu s$

ΔT sign logic: if emission is detected by 1 before 2, ΔT is positive (+).
if emission is detected by 2 before 1, ΔT is negative (−).

METHOD

1. Draw a line between sensors 1 and 2.
2. Mark center at C.
3. Find hyperbola index; He

$$He = \frac{10\Delta T 1\rightarrow2}{\text{Transit Time}_{1\rightarrow2}} = \frac{10(+300)}{1200} = \frac{3000}{1200} = +2.5$$

4. Divide $1C$ into 10 equal parts (hyperbola index is positive (+) and is therefore, constructed to the left of C since emission is first detected by sensor 1).
5. From C mark off +2.5 divisions—point P.
6. With P as a center, lay off $\overline{P1}=\overline{1m}=\overline{mn}=\overline{pr}=\overline{rs}=\overline{st}$ on line $\overline{12}$.
7. With 1 as a center draw arcs $1\rightarrow r$, $1\rightarrow s$, $1\rightarrow t$.
8. With 2 as a center draw arcs $2\rightarrow1$, $2\rightarrow m$, $2\rightarrow n$.
9. Mark intersecting points of arcs $1\rightarrow r$ and $1\rightarrow s$, $1\rightarrow t$, and $2\rightarrow1$, $2\rightarrow m$, $2\rightarrow n$.
10. Through arc intersecting points and P draw hyperbola.

handling these shapes is by laying out the surface in some uniform grid pattern and recording the ΔT coordinates printed out when an inserted pulse signal is applied to the head at the grid intersection points. In this fashion a map of ΔT values and corresponding locations on the vessel is developed.

Figure 13 pictures the semielliptical head on a pressure vessel on which a 120 deg sector has been layed out preparatory to making a ΔT "look-up" table. Here, the 120 deg sector was divided into eight 15 deg intermediate sectors. These intermediate sectors were intersected by concentric circles increasing in 6-in. radius increments. The actual recorded ΔT values for a 10 ft diameter semielliptical head are given in Fig. 14.

Hide and Seek Emission Location Method

This is a variation of the "look-up" technique and is useful for precisely positioning an emission site which has been approximately located. It can be used at any accessible location on the vessel surface but is most appropriate on the heads and around nozzles, manways, and other connections. This method consists of inserting an artificial signal at the estimated emission site location on the vessel and comparing the ΔT printout from this point with the actual ΔT

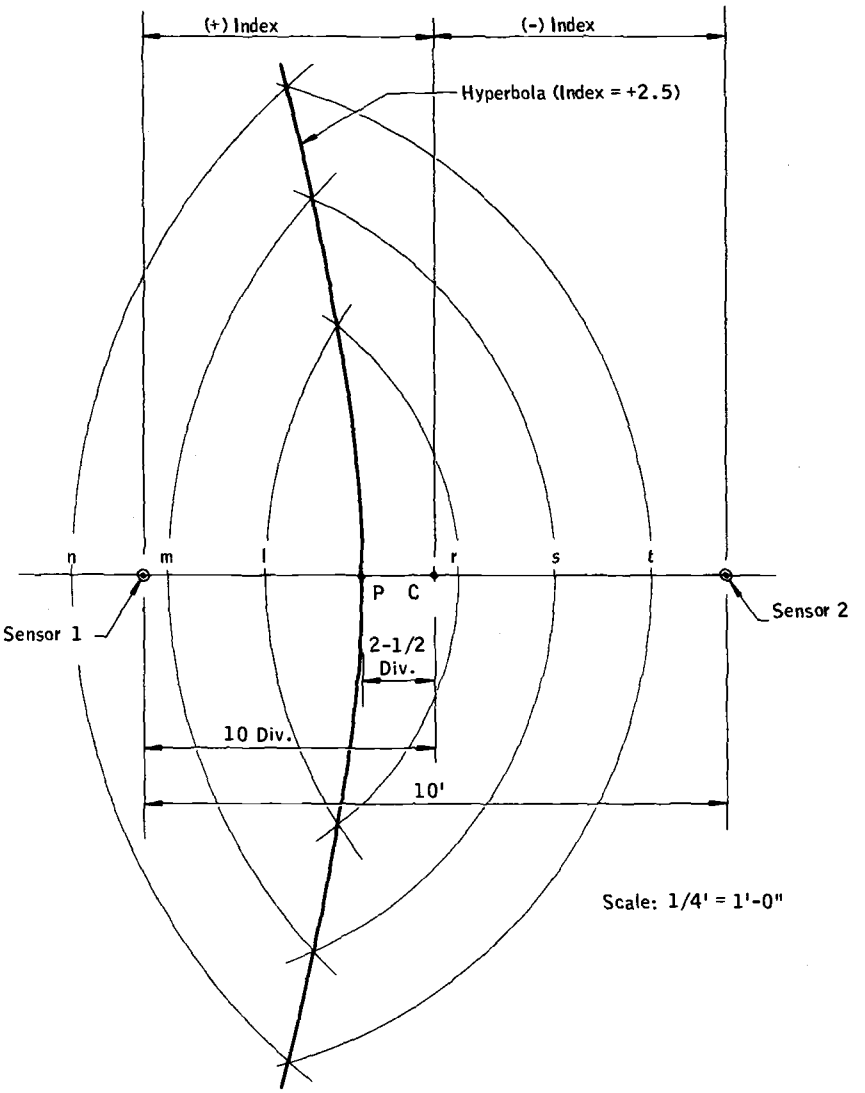

FIG. 7—*Construction of the* Δt *hyperbola.*

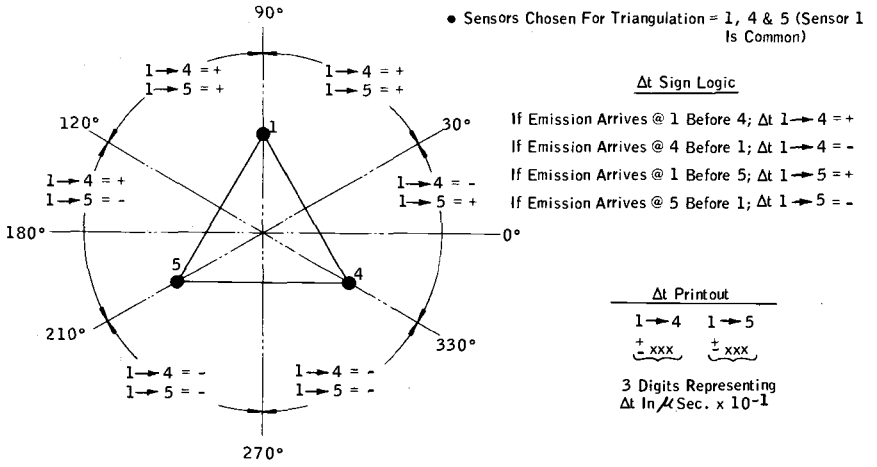

FIG. 8—Δt *printout and display logic.*

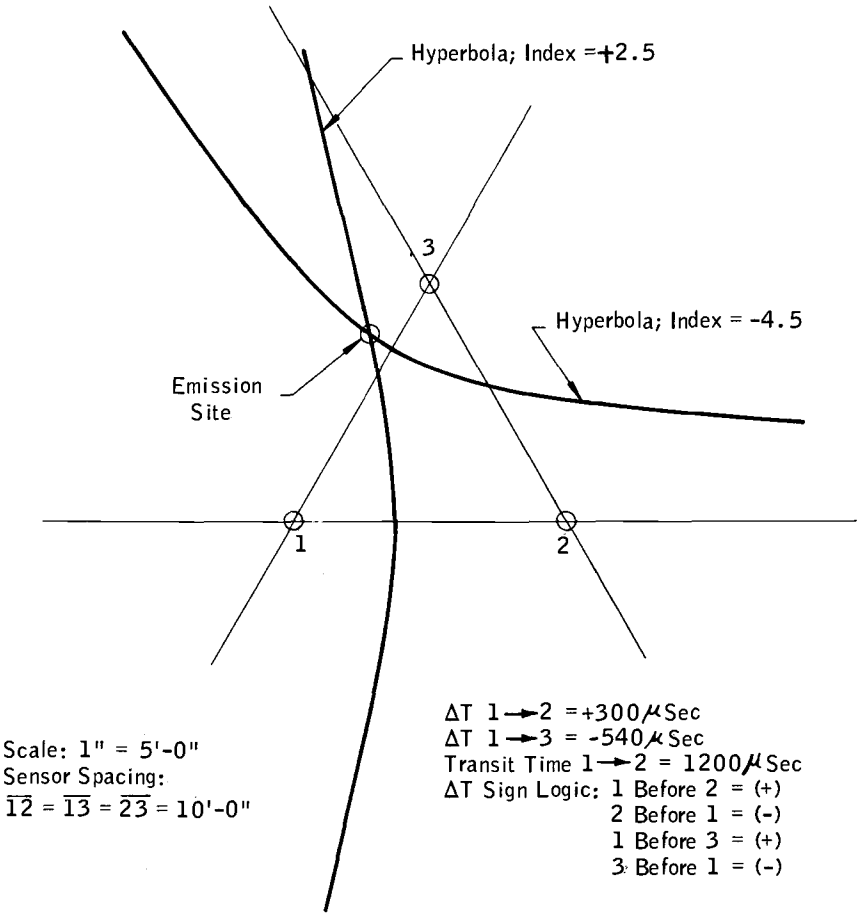

FIG. 9—*Emission triangulation using intersecting hyperbolas.*

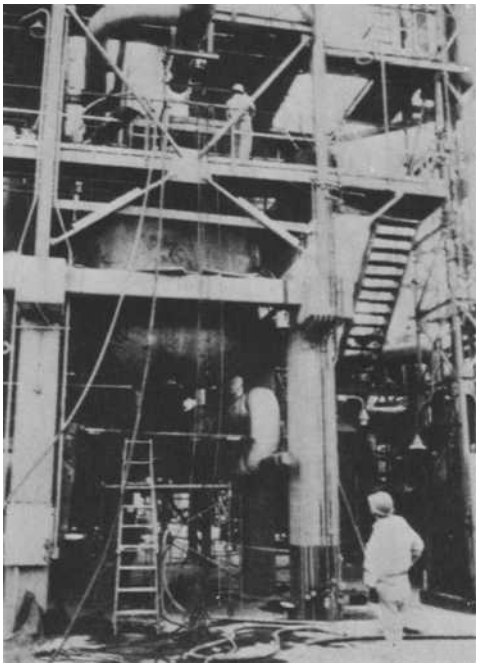

FIG. 10–*Refinery pressure vessel prepared for acoustic emission testing.*

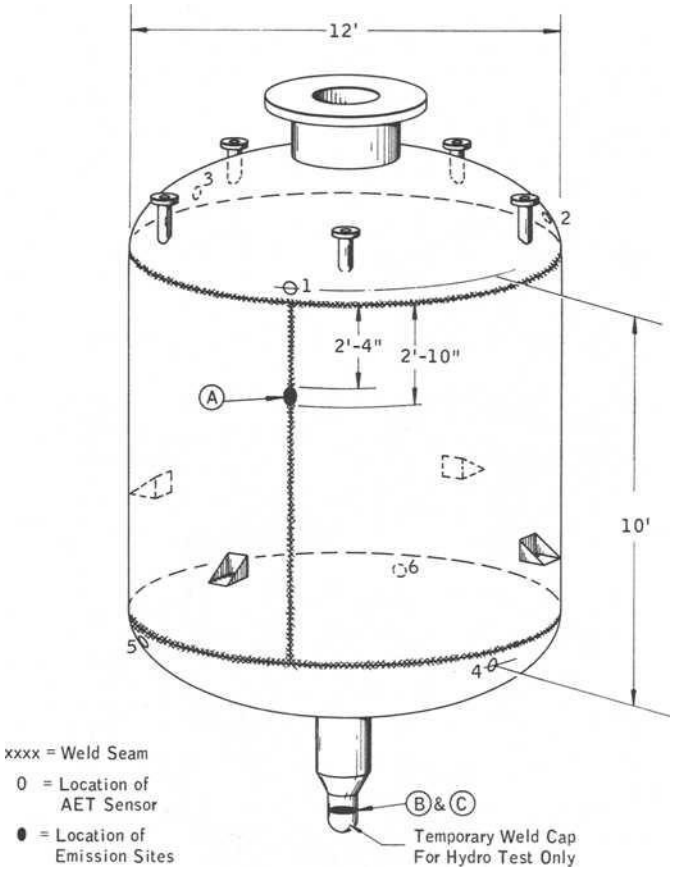

FIG. 11—*Sensor layout and emission site locations on a pressure vessel.*

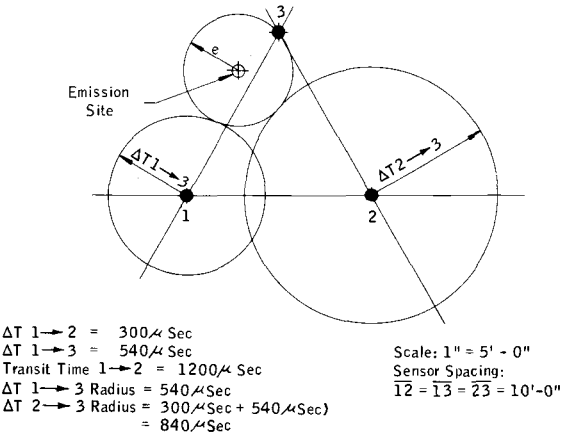

FIG. 12—*Emission triangulation using the Appollonian construction.*

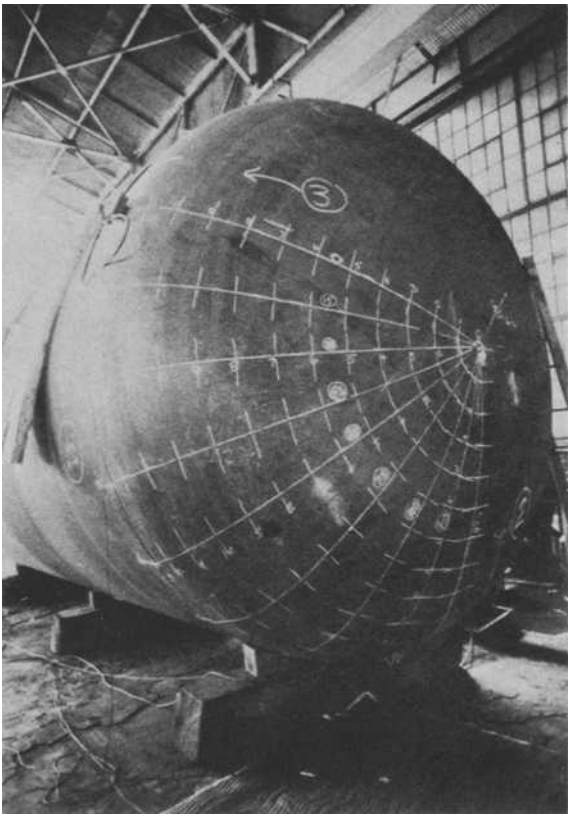

FIG. 13—*Vessel head laid out for preparation of look up table.*

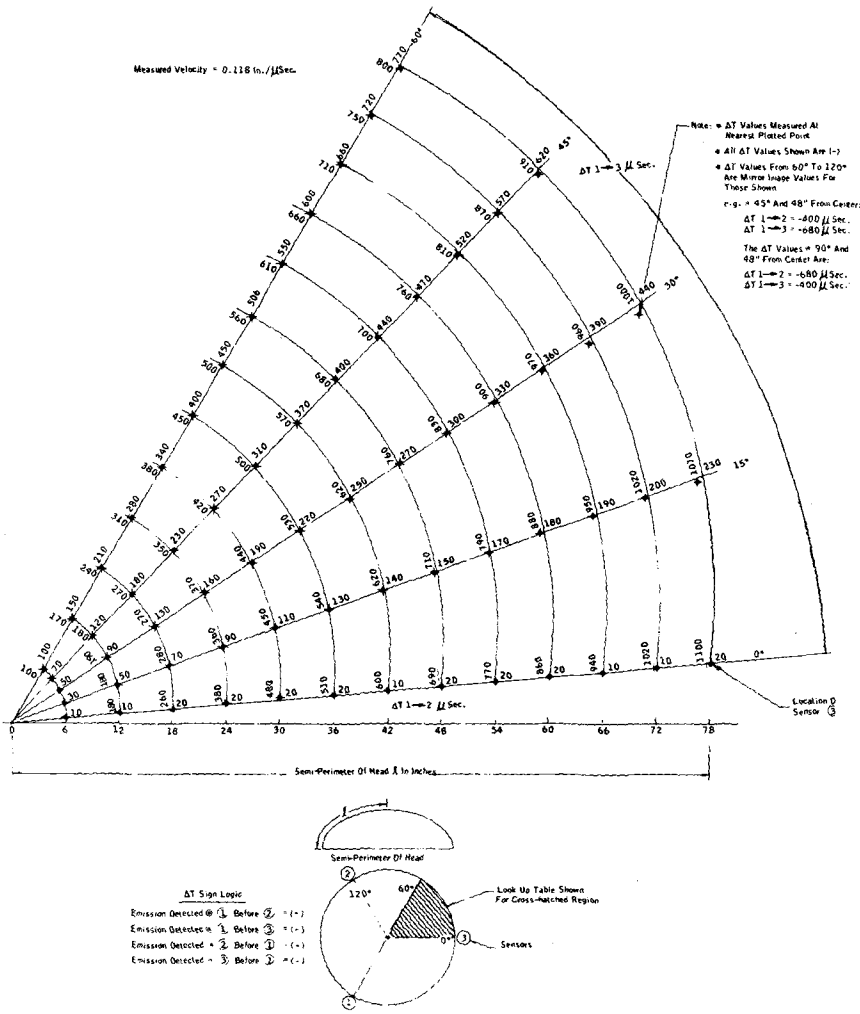

FIG. 14—Δt *look up table for carbon steel 1:2 semielliptical head.*

values obtained from the AET. By moving the position of the inserted signal to various nearby locations and comparing the ΔT printout, this "hide and seek" process can pinpoint the actual emission site within an accuracy of one or two inches.

Conclusions

Acoustic emission testing is becoming a practical NDT technique for the volumetric inspection of pressure vessels used in the petroleum and chemical industries. Specifically, AET fulfills needs in the following areas:

(1) To locate fabrication flaws not discovered by the more common NDT methods such as radiography and ultrasonic inspection.

(2) Prevention of catastrophic loss of heavy wall vessels which, could fail in a brittle fashion if small undiscovered flaws were to propagate to critical size during hydrostatic testing.

(3) To find service induced flaws (namely, stress cracks, fatigue cracks, embrittlement areas) in a vessel.

(4) To requalify existing vessels for more severe operating conditions. The state-of-the-art in developing effective electronic instrumentation and flaw site triangulation methods has reached the point where AET should be considered competitive with other more commonly specified test methods for onstream surveillance. AET also has the potential for the detection of service induced flaws; the amplitude and frequency content of environmental noise can however, limit applications of this type. Techniques are available for minimizing the reception of unwanted electrical and mechanical sources of noise. Considerable additional work is needed, however, to facilitate widespread inservice use. Other areas where additional research and development efforts and test standards are required include flaw signature analysis, materials effects, instrumentation, parameter selection, and data display.

References

[1] Cross, N. O., "Acoustic Emission Technique for Insuring Safe Hydrostatic Tests of Pressure Vessels," American Society of Mechanical Engineers, Report 70-PET-31.

[2] Bedesem, W. B. and Clarke, J. S., "Prevention of Catastrophic Brittle Fracture of Heavy-Wall Pressure Vessels," American Society of Mechanical Engineers, Report 68-PUP-4.

[3] Irwin, G. R., *Engineering Fracture Mechanics*, EFMEA, Vol. 1, No. 2, Aug. 1968.

[4] Hutton, P. H., "Detection of Incipient Failure in Nuclear Reactor Pressure Systems Using Acoustic Emission," 1969, BNWL-997, Battelle Memorial Institute, Pacific Northwest Laboratory, Richland, Wash.

[5] Waite, E. V. and Parry, D. L., *Materials Evaluation*, MAEVA, Vol. 29, No. 6, June 1971.

[6] Lucey, G., Jr., *Journal of the Acoustical Society of America*, JASMA, Vol. 43, No. 6, 1968.

[7] Flores, Ivan in *Computer Sorting*, Prentice-Hall, New York, 1969.

H. L. Balderston[1]

The Broad Range Detection of Incipient Failure Using the Acoustic Emission Phenomena

REFERENCE: Balderston, H. L., "The Broad Range Detection of Incipient Failure Using the Acoustic Emission Phenomena," *Acoustic Emission, ASTM STP 505*, American Society for Testing and Materials, 1972, pp. 297-317.

ABSTRACT: The broad range detection of incipient failure in structural, mechanical, hydraulic, pneumatic, electrical, and electronic systems is based upon the detection of the two basic causes of failure. These causes are structural degradation and chemical contamination occurring in the structure of the material of which the systems listed above are composed. The detection of incipient failure allows maintenance to be programmed at the convenience of the user, thus preventing down time of equipment during use periods.

The acoustic emission phenomena are employed in the detection of incipient failure in all types of equipment covered in this report. Specifically, the examples chosen are structural, mechanical, pneumatic and hydraulic components, subassemblies, or specimens as applicable. From these examples the broad range incipient failure detection concept based on the acoustic emission phenomena is developed. The experiments covered include detection of incipient failure in bearings, hydraulic assemblies, pneumatic subsystems, stress corrosion in aluminum, ductile tensile failures in carbon steel, 4330M steel, and in boron-epoxy composite material.

KEY WORDS: failure, detection, acoustics, emission, resonant frequency, frequencies, fatigue (materials), spalling, stress corrosion, yield, phase transformation, crack propagation, crack initiation, cavitation, coronas

The broad range detection of incipient failure in structural, mechanical, hydraulic, pneumatic, electrical, and electronic assemblies evolved as a result of a long study of the basic causes of failure. As a result of these studies and experience in the detection of failure over the past twenty years and, more specifically, during the development of the Boeing Microelectronic Integrated Test Equipment (BOMITE) concept, an important discovery was made. All failures in all types of equipment are the direct result of two basic causes of

[1] Consultant, The Boeing Company, Seattle, Wash. 98116.

failure–structural degradation and chemical contamination–occurring at the atomic level within the structure of the material of which the assembly is composed. Failure was also found to have a beginning, a period of growth, and an ending which resulted in such great damage to the assembly that no further use or operation was possible.

Research has shown that failure can be detected incipiently; that is, at an early stage in its development. Action can be taken to prevent the failure from occurring by elimination of the cause very early before significant damage occurs, or by replacement of the component or subassembly before failure occurs. In the second case, where replacement is involved, the incipient failure is detected or monitored up to the point when failure is near, but sufficient time must be allowed to replace the assembly involved. To the extent that progressive failures can be detected incipiently and monitored during progression, these failures can be eliminated.

That is not to say that all failures will be eliminated, since in some the progression from start to failure is so fast that there is no time for preventive or maintenance action. Most catastrophic failures are caused by extremely great forces such as lightning, hurricanes, heavy loads, or by catastrophic human error. Although we can do little to prevent failures caused by natural disasters or human error, we can take action to prevent the bulk of all failures, provided we can detect these failures incipiently.

Incipient failure detection (IFD) is based upon the detection of the basic causes of failure–structural degradation and chemical contamination–in the structure of material. Among the phenomena found usable in the detection of incipient failure are the acoustic emission phenomena, the resonant frequency phenomena, the exoelectron emission phenomenon, and electromagnetic energy in the form of electrical noise. Of these, the ones most universally applicable to materials are the acoustic emission phenomena. This paper will cover the detection of incipient failure through the use of the acoustic emission phenomena in a selection of structural, mechanical, pneumatic and hydraulic components, assemblies or specimens, as applicable.

Procedure

The acoustic emission phenomena originate in the form of burst pulses or continuous energy emissions of acoustic energy emanating from the atomic structure of material while under load, deformation, stress, or during change in crystal structure. They also originate during change in state, as in solid to liquid to gas and vice versa. They originate during the formation of chemical compounds and during change; that is, a hot concentrated solution of sodium chloride will emit during cooling as the sodium chloride crystals are being formed. They will also emit as the sodium chloride is dissolved in water. Other

chemicals which dissolve in water exhibit the same characteristics when going in and out of solution, but this latter research has not been reported on to date.

In structural materials under stress the principal degradation processes which produce acoustic emission are deformation, yield, initiation, and propagation of cracks. Other degradation processes are oxidization, combustion, electrolysis, abrasion, wear, and chemical attack, as in corrosion. All these processes produce detectable acoustic emission. Typical burst emission produced by these processes in structural materials is essentially as shown in Fig. 1. Each rise above the trigger level in the burst pulses is counted in the count rate technique (Table 1). The trigger level is set close to the threshold or noise level. The count period may range from 0.1 to 10 s and the count per unit time, providing an indication of energy content per unit time, is directly related to the degradation occurring per unit time. Specifically, the count rate per unit time is related to the speed at which a crack initiates and propagates. It is related to the volume of material transforming per unit time in martensite transformations, as in the heat treatment of steel. It is also related to the number of crystals that form per unit time during the crystallization process of sodium chloride and other chemical compounds. The total count technique is also employed. Total count is related to total damage or change occurring over the period of observation. In some cases a better relationship is obtained utilizing count rate; in others, total count provides a more accurate indicator of incipient failure. For the most part, these are the techniques employed in incipient failure; however, in special cases, as in

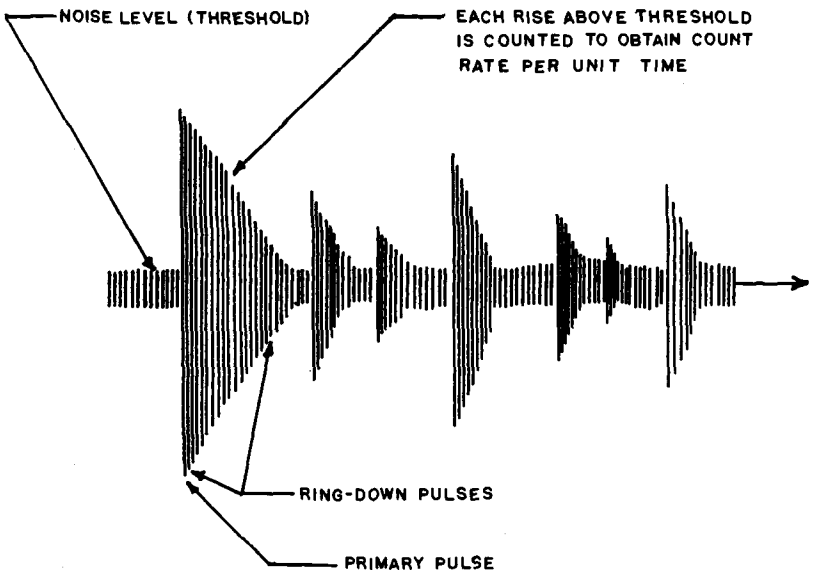

FIG. 1—*Typical acoustic emission pulses.*

TABLE 1—*Usable IFD techniques with rated applicability to equipment.*

Technique	Equipment		
	Structural	Mechanical	Hydraulic and Pneumatic
Acoustic Emission Phenomena			
Count rate/unit time	1	6	3
Total count	2	5	4
RMS energy in a bandwidth	3	4	2
Peak energy in a bandwidth	4	...	1
Resonant Frequency Phenomena			
RMS energy in a bandwidth	...	2	...
Power spectral density in a bandwidth	...	1	...
Peak energy in a bandwidth	...	3	...

rotational equipment, another form of acoustic energy exists when a failure mechanism is in process or has created a very small defect. This is the resonant frequency phenomenon[*1*] and is created by shock excitation of a rotational mass passing over a defect, as a ball in a ball bearing rolling over a spall. All components of the mechanical equipment resonate when shock-excited. Thus, a wide band of frequencies exists. Since these latter phenomena will not be discussed extensively in this report, see Ref *1* for further information. For the mechanical experiments reported here, the rotational and resonant frequencies were filtered out to enable utilization of acoustic emission.

Table 1 shows usable IFD techniques. The two basic phenomena are covered—acoustic emission and resonant frequencies. Note that in structural equipment, count rate per unit time is the most valuable technique, while in mechanical equipment, power spectral density in a bandwidth is the most valuable. In hydraulic and pneumatic equipments, peak energy over a relatively narrow bandwidth is the most valuable. It should be emphasized that these ratings are based upon the detection of incipient failure, not necessarily extremely small events. The detection of incipient failure at the so-called red line condition, when an actual warning or decision with respect to maintenance action is required, can be handled by any of the techniques listed. In hydraulic and pneumatic equipments, internal leakage flow under cavitation or turbulence, as applicable, is the basic source of acoustic emission. The size of the flow through the orifice in a servo valve at the null position, for example, is related to the amount of wear or damage which has occurred to the orifice. In hydraulic systems, particularly servo valves, the cavitation phenomena gives off tremendous bursts of acoustic emission during the implosion of cavitation bubbles. In a 3000 psi system, the forces exerted by the implosion of cavitation bubbles may be as high as 50,000 psi. The amplitude of the burst acoustic emission

emanating from a severe cavitation situation can create energy levels 10 billion times above the zero level[3].

The equipment utilized in the detection of incipient failure through the acoustic emission phenomena is shown in block diagram form in Fig. 2 and consists of transducers (special design), amplifiers, filters, counters, etc. The family of transducers have frequency capabilities from 50 kHz to 20 MHz. A photograph of a family of transducers is shown in Fig. 3.

A single line diagram would consist of a transducer, amplifier, bandpass filter to eliminate unwanted noise; another amplifier, if necessary, depending upon level of signal; counter, a/d converter, and strip chart recorder. The root mean square value of acoustic emission energy, total count and tape recorder setups are also shown. A photograph of a typical test equipment setup is shown in Fig. 4. The preparation of specimens, where involved, is covered under the individual experiments. The best technique for detection of incipient failure in each of the experiments covered will be indicated under each experiment.

Experimental Work

A number of selected experiments in separate categories will be described in this section. Although a number of experiments in each category have been performed, only a selected group of experiments in each chosen category will be detailed for mechanical, hydraulic, pneumatic, and structural assemblies. The results of each experiment will be described, and the discussion following will cover the broad range applicability of the acoustic emission phenomena.

Indication of Incipient Failure in Mechanical Subsystems

To illustrate the applicability of the acoustic emission phenomena to mechanical subsystems, the detection of incipient failure in a bearing has been selected. Much of the work done in this area has been accomplished by utilizing the power spectral density in a bandwidth technique and the RMS energy in a

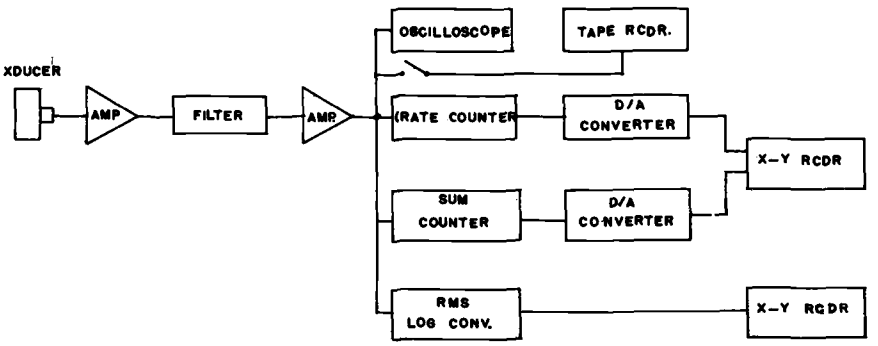

FIG. 2—*Test equipment setups.*

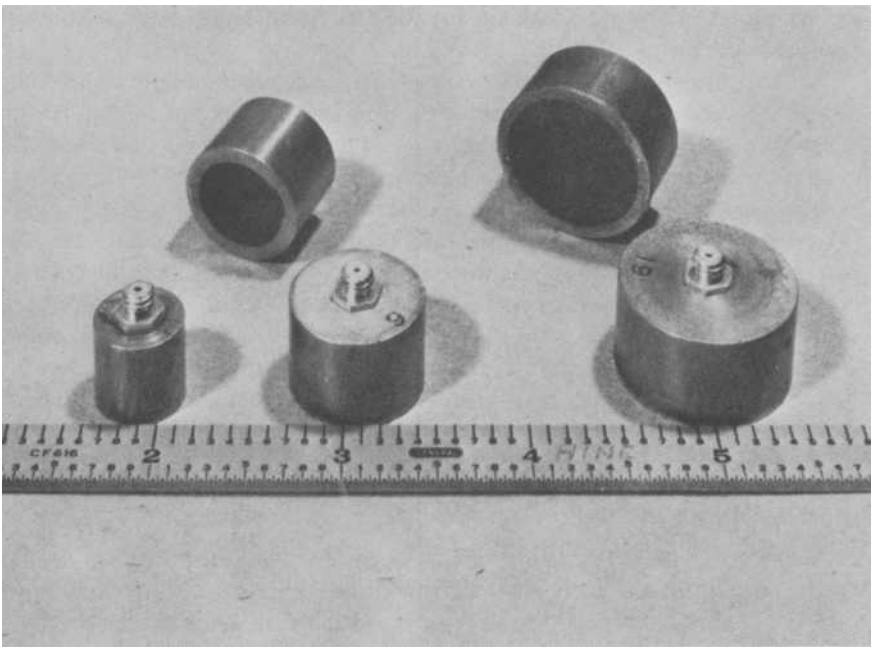

FIG. 3—*An assortment of acoustic emission transducers.*

bandwidth technique[*1*]. For this experiment we shall utilize the count rate per unit time and the acoustic emission phenomena. The equipment setup employed in this experiment is shown in Fig. 2. The transducer was a 1-MHz design with the filter set to eliminate frequencies below 100 kHz to eliminate the rotational and resonant frequencies. The usable frequencies through the transducer and filter combination covered a band of frequencies from 100 kHz to 2 MHz. The bearing was a Barden size 204 Class 7. It was pressure lubricated with oil and was placed in a bearing test machine operated with 1000-lb. radial and 1000-lb. axial loads. The rotational speed was 11,250 rpm. Prior to installing the bearing in the bearing test rig, the bearing was nicked 0.005 in. in depth and width on the inner race to artificially create a minor defect. The bearing was operated in the test rig a total of 10 min when catastrophic failure occurred. A plot of count rate during the interval from start to failure is shown in Fig. 5. The initial count rate was 50,000 counts/s. The data is shown on the chart, the initial data being relatively steady at the 50,000 count rate. Note that there was a gradual rise in the count rate until approximately 1.4 min before failure when the count rate rose to a peak of approximately 85,000 counts/s. Count rate lowered slightly and failure occurred. In our observations we have found that count rates above 70,000 are indicative of rapid crack initiation and spalling. We have also observed visible

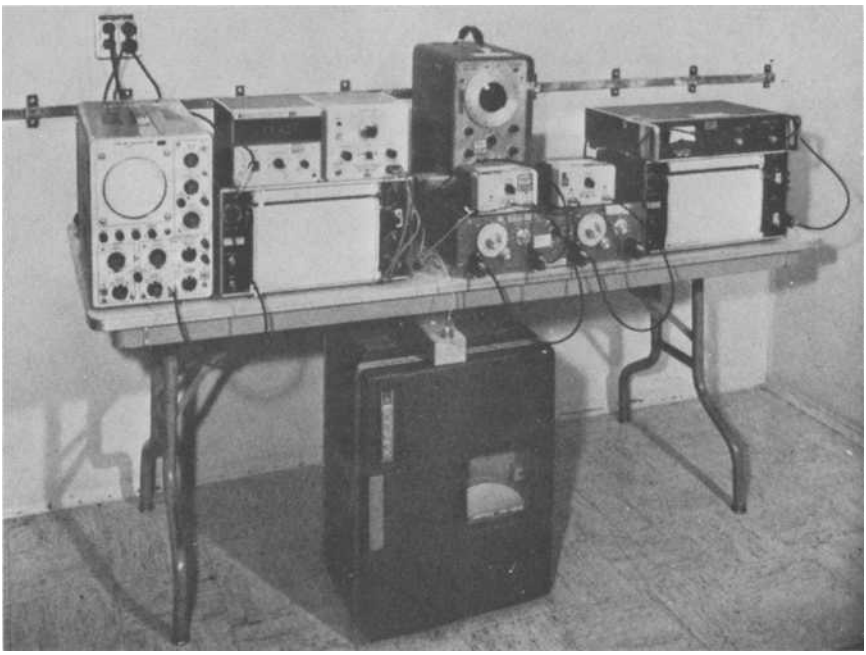

FIG. 4—*Typical acoustic emission test equipment.*

defects at count rates as low as 30,000 when an extremely rapid rise occurs. Accordingly, both the rate of increase in count rate as well as the count level are significant in determining incipient failure. In bearings, the actual point at which a warning signal is given is dependent upon the maintenance concept of the user. When it is desirable to obtain as much use as possible from the bearing before replacement, very often the bearing will be allowed to deteriorate to the point where a substantial amount of metal is removed by spalling. In other instances, as in employment in space where immediate maintenance action can not be taken, a very small spall would be considered the red line condition; that is, the condition at which a warning signal is given. In any event, the technique reported here as well as the RMS energy in a bandwidth, power spectral density in a bandwidth technique reported in Ref *1* are all capable of detecting very minor to major degradation in bearings as well as detecting when failure occurs and allowing prediction of when failure will occur.

The use of resonant frequencies[*1*] have some advantages over the employment of the acoustic emission phenomena in that the rate at which the bearing components are shock excited into their resonant frequencies is related to the rotational frequency of the bearing, which can be calculated, and which in turn allows identification of the component which is becoming defective. Utilizing

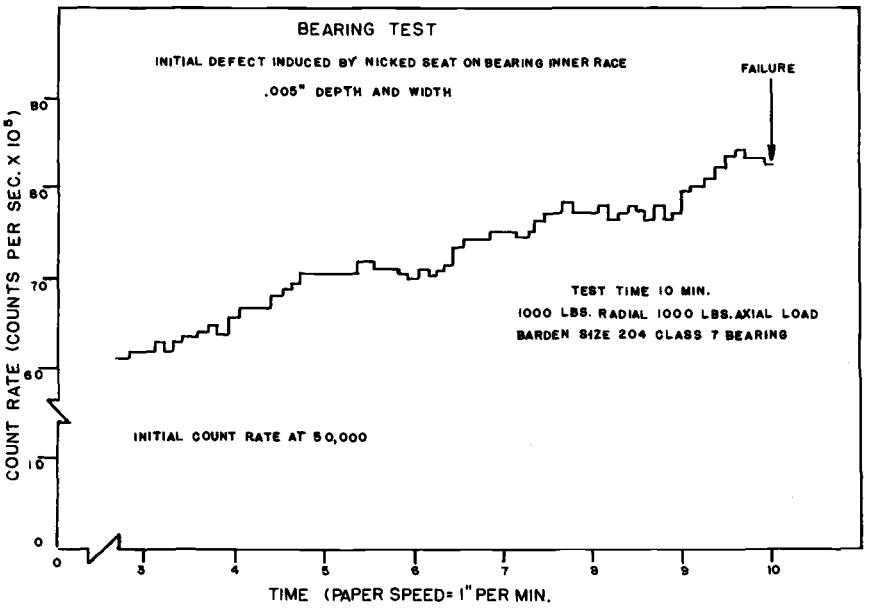

FIG. 5–*Plot of count rate during the interval from start to failure.*

the acoustic emission phenomena as reported here will not allow ready identification of the source unless triangulation techniques are employed[*2*]; however, in rotating devices where the bearing is the prime source of problems, such as in fans, blowers, generators, motors, and other simple rotating mechanisms, the employment of the acoustic emission phenomena does not require the employment of the triangulation technique to locate the source.

When maximum sensitivity is required, it is necessary to use the acoustic emission phenomena; therefore, the rotational and resonant frequencies are filtered out to pick up the lower level acoustic emissions. This must be done by filtering out all frequencies below approximately 100 kHz. If these frequencies are not eliminated, the sensitivity to crack initiation and very small spalls is greatly reduced due to the interference of these frequencies, since the acoustic emission information for very small cracks is hidden in the higher amplitude rotational and resonant frequencies.

Indication of Incipient Failure in Hydraulic Assemblies

Internal leakage is utilized to indicate wear or damage to the orifices in hydraulic components. In laminar flow, as in a needle valve, the acoustic emission is a continuous type showing relatively stable amplitude and frequency content at each flow rate. As the leakage flow increases, the amplitude also increases, while frequency tends to decrease. In the case of a servo valve wherein

cavitation is present, the energy levels for similar flow rates are approximately 1000 times greater, and the frequency content is extremely wide band. Frequencies have been observed as high as 40 MHz.

A complete presentation of incipient failure detection in hydraulic components utilizing the power spectral density in a selected frequency bandwidth is covered in Ref *3*. In this experiment the count rate technique was utilized, and count rate per unit time was related to internal leakage flow in a Moog 35-100 servo valve. Cavitation in this valve is quite severe. To simulate the damage to the orifice by cavitation, the spool lands were lapped to obtain successively higher flow rates. The transducer was mounted on the valve manifold. The test equipment setup was as shown in Fig. 2. Both count rate and RMS energy outputs were recorded. The curve shown in Fig. 6 relates acoustic emission

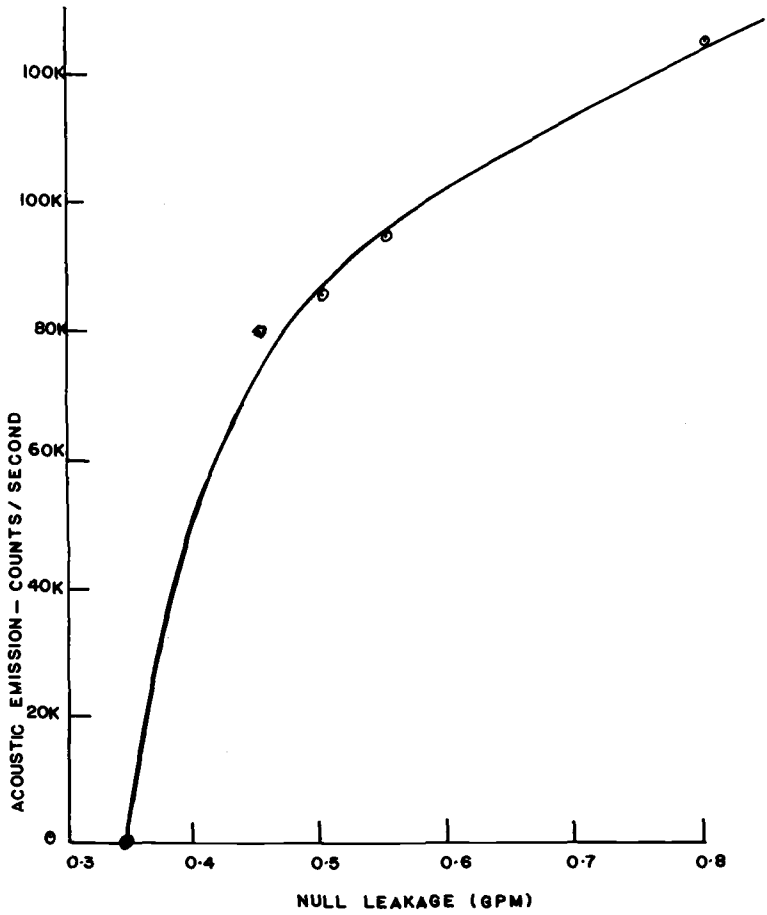

FIG. 6–*Acoustic emission versus leak rate.*

counts per second to leakage in gallons per minute at null. No two valves would give the same identical curve since no two valves would wear exactly alike in use; however, there is an increase in count rate with increase in leakage. The point at which a red line condition is established would be different depending upon the user; however, for most cases, it would be something near the capacity of the hydraulic pump serving the system and could be as high as 4.5 gal/min. It is expected that a red line condition would be established much below this figure. In some valves it has been observed that with large leakage flows and with certain types of wear, the cavitation actually decreases. This results in a decrease in the count rate. This, however, can provide another indication of valve wear and points up the necessity for monitoring these components on a periodic basis. Both the extent of cavitation present at any time of observation and the internal damage sustained by the component as shown by the increased internal leakage flow are significant in the detection of incipient failure. The peak energy in a bandwidth as shown by power spectral density plots in Ref *3* appears to be a more sensitive indicator of incipient failure in hydraulic components. Considering, however, the gross nature of the point at which an incipient failure warning would be given, the RMS energy in a bandwidth and the count rate per unit time techniques are equally effective.

Both cavitation and internal leakage flows can be measured precisely by the acoustic emission phenomena and can be used as an indicator of internal damage. When the internal leakage flows reach a selected level, maintenance action can be programmed at the convenience of the user.

Indication of Incipient Failure in Pneumatic Subsystems

The primary incipient failure mechanism in pneumatic subsystems is external leakage. In this experiment we shall demonstrate that the acoustic emission phenomena and the count rate technique can be utilized to detect leakage in pneumatic subsystems.

The emphasis is on the determination of the smallest possible leak under the worst possible condition; that is, a low pressure system. A hole was drilled electrically in the end of a test cap, 0.004 in. in diameter, another 0.0135 in. The other two specimens reported on were prepared as shown in Fig. 7. The caps were threaded to a length of 2-in. pipe which served as the pressure chamber. A maximum pressure of 60 lb. was employed, and the pressure was allowed to bleed down to zero. The flow rate in ml per minute was determined by displacement of water by the leakage air in a burette.

The equipment setup is shown in Fig. 2. A 300-kHz transducer was utilized. The filter was set to eliminate all frequencies below 100 kHz. The total amplification in the system was 50-dB gain. The data is shown in Fig. 7 covering four different test orifices.

The smallest flow which could be consistently measured under the very low

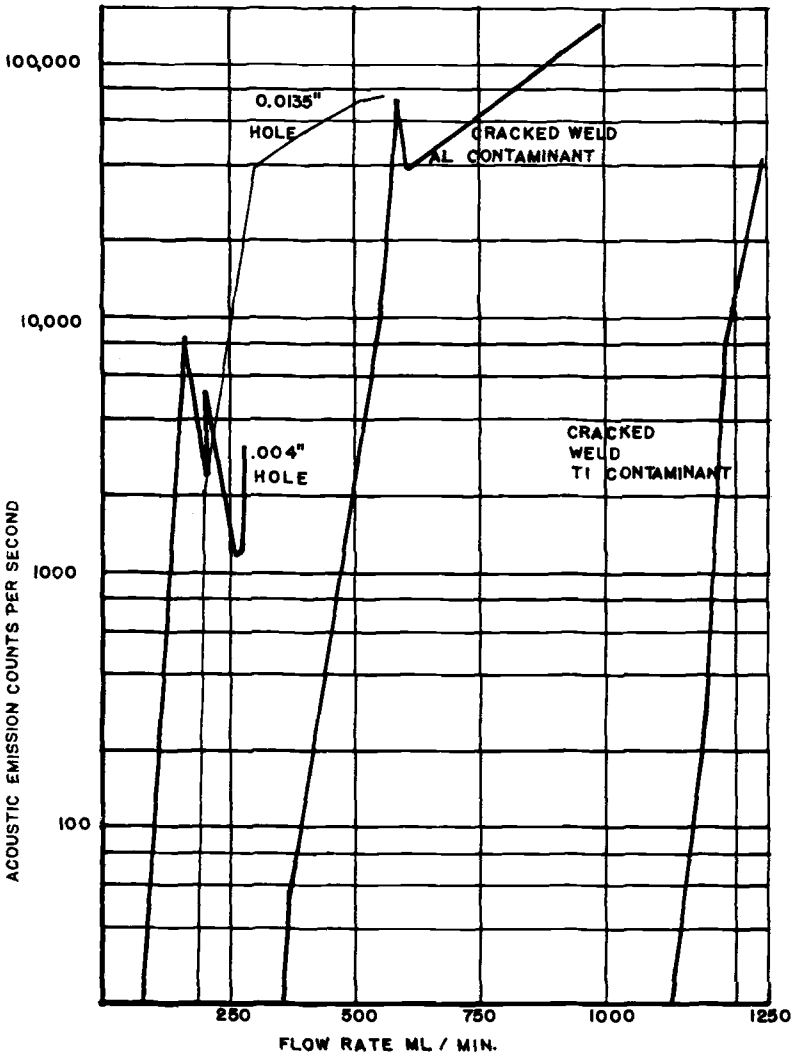

FIG. 7—*Pneumatic leakage versus acoustic emission.*

pressure environment was 80 ml/min, corresponding to about 0.2 atm cm^3s. This appears to be the point where turbulence ceases.

Indication of Incipient Failure in Stress Corrosion of Aluminum

A number of different double cantilever (DCB) beam specimens were examined; one was highly susceptible to stress corrosion cracking (Al 7079-T651); one was moderately susceptible (Al 7075-T651); and one was

highly resistant (Al 7075-T73). These specimens were prepared as shown in Fig. 8.

The specimens were cut using 1-in. thick material, such that the crack would run parallel to the grain direction of the metal. The double cantilever beam specimens were stressed by torquing the bolt to the point of crack pop-in and then were wetted with a 3 percent saline solution. The crack length and acoustic emission were monitored by an equipment setup as shown in Fig. 2 in an attempt to examine the correlation between emission history and crack propagation rate.

Figure 9 is a reproduction of strip chart data showing the relationship between acoustic emission and crack growth for the Al 7079-T651 specimen. From these data, it can be seen that the stress cracked specimen emitted no acoustic energy until the saline solution was added. At this point, the acoustic emission rose from 0 to 8000 counts/s. However, the crack indicator circuitry showed no measurable crack growth. The high rise in accoustic emission energy indicated that corrosive action was occurring. The acoustic emission continued actively for about 6 min prior to any detectable crack growth. Once the crack started, it exposed fresh metal to the corrosive solution and the acoustic emission increased again. As the crack increased, the stress decreased, and as one would expect, the stress corrosion activity indicated by acoustic emission also decreased. These data show that acoustic emission does provide a sensitive indicator of corrosive action and stress corrosion cracking. The crack history between the data points was sketched on the figure in accordance with the acoustic emission data. This crack growth history agrees with the general theory that cracks do not always progress at a uniformly predictable rate but will extend themselves in intermittent bursts.

During this test, it was observed that acoustic emission energy was emitted both as a result of the chemical attack upon the aluminum, as well as the result of the initiation and propagation of surface and subsurface cracks within the materials. Incipient failure indicators in the case of the cantilever beam

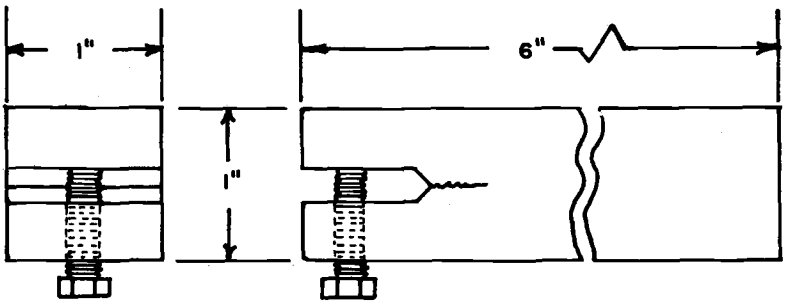

FIG. 8–*DCB stress corrosion specimen.*

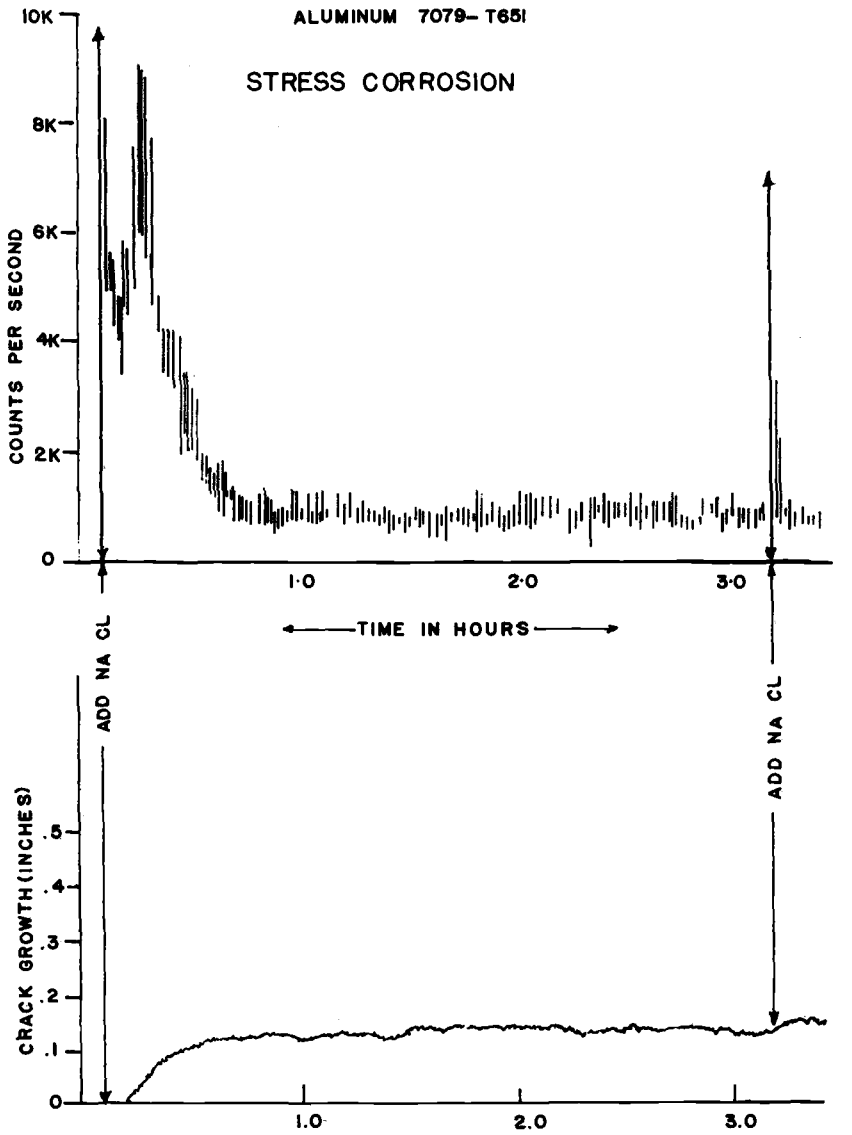

FIG. 9–*Reproduction of strip chart data showing the relationship between acoustic emission and crack growth for the Al 7079-T651 specimen.*

structures appear at the very exposure of the corrosive saline solution to the bare metal and are indicators of crack growth and propagation. For detailed information relating to initial attack as well as the following crack initiation on various specimens, see Ref *4*.

Indication of Incipient Failure in Ductile Tensile Failure of Carbon Steel

Tests have been conducted on specimens of SAE 1020 steel. These tests involved the subjection of the individual tension specimens to a constantly increasing strain and were performed on an Instron tension test machine. Throughout the tests, the individual specimens were monitored for stress and for acoustic emission. The bandwidth or "window" for monitoring acoustic emission was selected between 20 and 300 kHz. All frequencies below 10 kHz were filtered out.

Figure 10 shows the physical configuration of the specimens tested; Fig. 2 indicates the test equipment monitoring setup. The results of these tests were all consistent in showing that a very pronounced peak occurred at the engineering yield point (see Fig. 11), that is, the point at which yield occurred in the material. The acoustic emission phenomena at this point saturated the monitoring equipment. The interval of time subsequent to yielding was characterized by either a relatively constant rate of emission or very little emission. Just prior to failure, a small peak in acoustic emission occurred coincident with crack initiation with the number of counts first increasing then holding relatively steady as the crack propagated, decreasing, and rising to a second peak, at which time the specimen failed. This latter peak may be due to the necking down of the test specimen just prior to failure. This latter peak did not occur in all specimens.

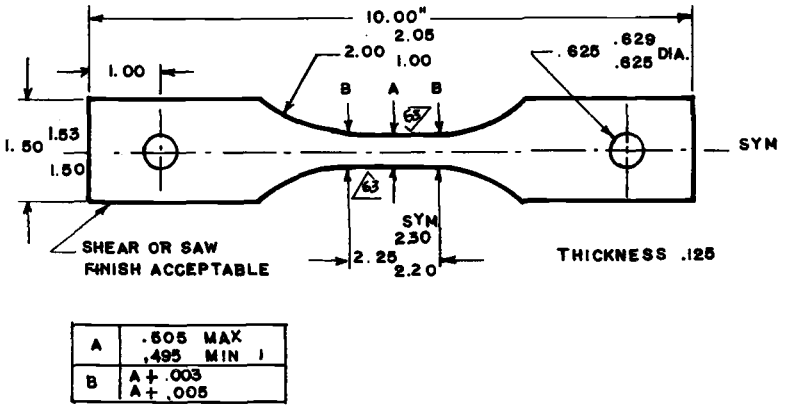

FIG. 10–*Ductile tension specimen of 1020 carbon steel.*

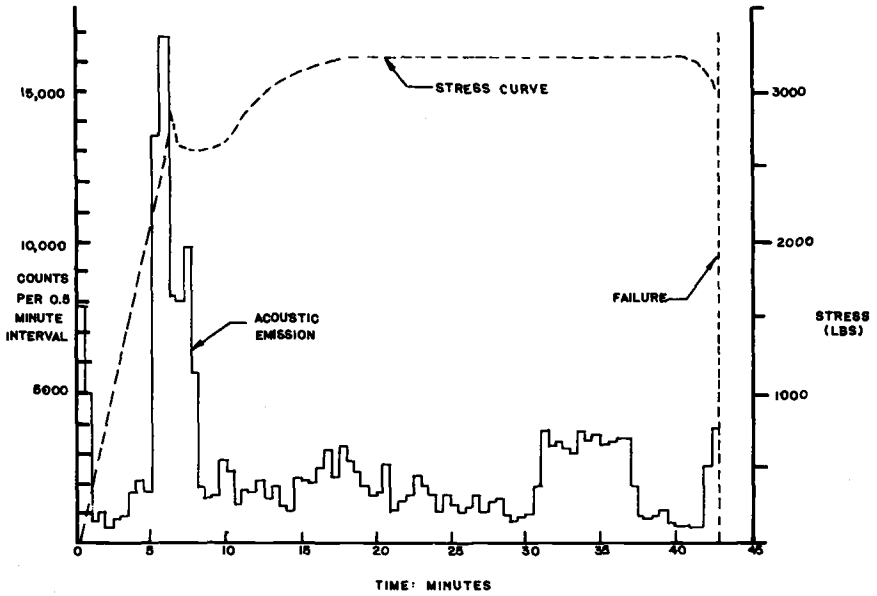

FIG. 11—*Ductile tensile loading showing carbon steel stress versus acoustic emission.*

The data taken are shown in Fig. 11. The rapid increase in acoustic emission shown has been demonstrated by several diverse tests and seems to be extremely well founded. The second trend covering the more or less constant emission which followed the yielding appears very plausible. The final rise, or double peak, which occurred just prior to failure in some specimens—indicates that some specimens may not have necked down prior to failure. This was confirmed in some instances by metallurgical examination. Crack initiation and propagation are shown by the large count between 30 to 38 min on the data. In some cases, the yield point would be selected as the indication of incipient failure and, in other cases, the point of crack intiation and propagation would be selected.

Indication of Incipient Failure in Ductile Tensile Failure in 4330M Steel

Tests were conducted on 4330M steel and the specimens were prepared similarly to a specimen of carbon steel, as shown in Fig. 10. The equipment employed for count rate was as shown in Fig. 2. Unlike the tests for carbon steel, which show a definite yield point occurring in a relatively small period of time, the yield in 4330M steel occurs over a wide range, starting at approximately the 1.25 min point as indicated on the data in Fig. 12, and extending to approximately the 8 min point at which crack initiation took place. The dotted line shows the time during which crack initiation and propagation

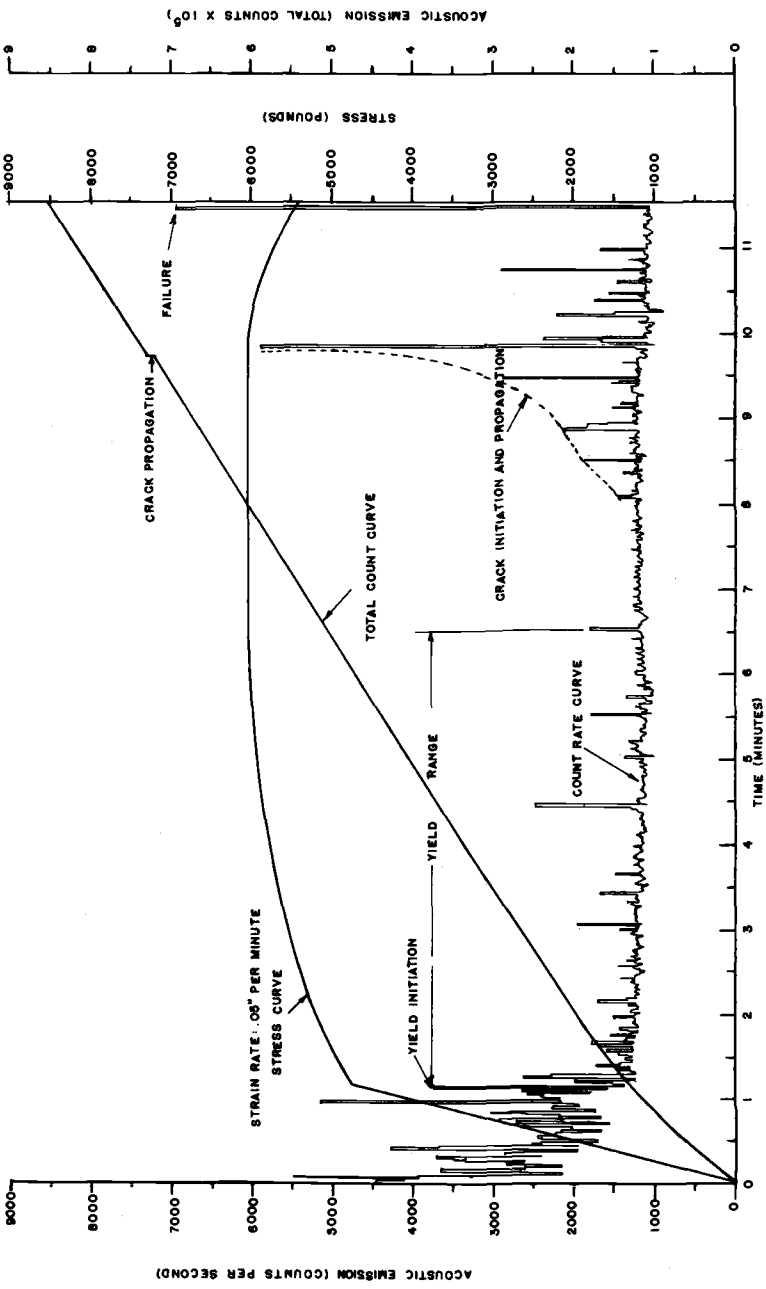

FIG. 12—*Count rate and total count acoustic emission plots, 4330M steel.*

took place, rising to a peak at approximately the 9.8 min point. At this point a drop in the stress curve shows a necking down of the specimen is occurring. This process continued and is shown by sporadic increases in the count rate to show that the crack is continuing to propagate, followed by a quiet period starting at 11 min and ending with a large rise which occurred at failure—approximately 11.5 min. These quiet periods are significant and may be utilized for incipient failure detection, depending on final design of detection equipment. The total count curve is included on this plot as well as the stress curve. Both the total count curve and the count rate information indicate the yield range. Yield point is readily identifiable on the count rate curve, and is clearly shown on the stress curve. RMS plots have also been obtained on 4330M steel and, in general, correlate well with the count rate and total count plots. The incipient failure warning could be given at any time during the yield range or at the crack initiation point, or during the crack propagation range, depending upon the maintenance concept of the user and how soon maintenance needed to be programmed.

Indication of Incipient Failure in Ductile Tensile Failure of Boron Epoxy Composite Material

Structural elements composed of boron epoxy composite material emit acoustic emission at much higher levels than is evidenced in the metals. This emission has been shown to increase characteristically with load beginning in significant amounts when the specimen is loaded to approximately 50 percent of ultimate. Emissions continued at an increasing rate until just prior to failure when a decrease in count rate was observed followed by a rapid rise to failure. The notched specimens employed in this series of tests are shown in Fig. 13. The equipment is the same as that shown in Fig. 2 for ductile tensile failure of metals.

The failure of individual filaments or groups of filaments is characterized by very high bursts of acoustic emission, while the failure of the epoxy material between filaments is characterized by lower bursts of energy.

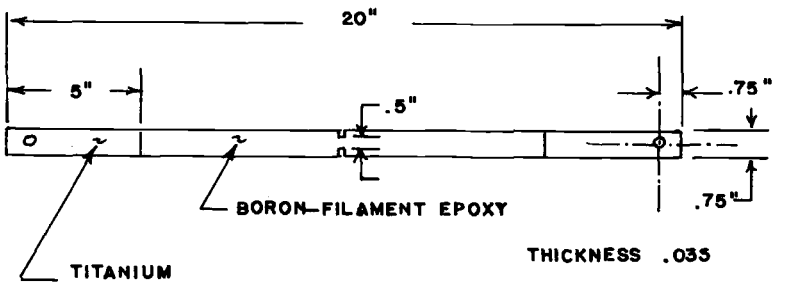

FIG. 13—*Boron epoxy composite specimen.*

The data for a typical specimen are shown in Fig. 14. The plot shows the initial quiet period, the rise in count rate of acoustic emission which occurred prior to failure, and a second characteristic which occurred in most of the tests. When significant amounts of acoustic emission occur (Fig. 14) during the early (first 50 percent of load), normally quiet portion of the loading cycle, the specimen fails sooner and shows less total emission during the rise to failure. This indicates the presence of defects in those specimens which emit early in the test. A good correlation between total count and total life has been observed. Life can be predicted at, or very near, the 50 percent point. The warning point can be established at the first major rise in count rate or at a total count level, which is more accurate.

Discussion

A selection of experiments have been included to demonstrate the broad range capabilities of the acoustic emission phenomena in the detection of incipient failure. It has been shown that incipient failure can be detected in mechanical, hydraulic, pneumatic, and structural assemblies. The crack initiation and propagation in all areas has been detected as well as other degradation processes which lead to failure. The techniques employed include the count rate per unit time and total count of the burst emission pulses originated when stress is applied to material and a degradation process takes place. The RMS value of

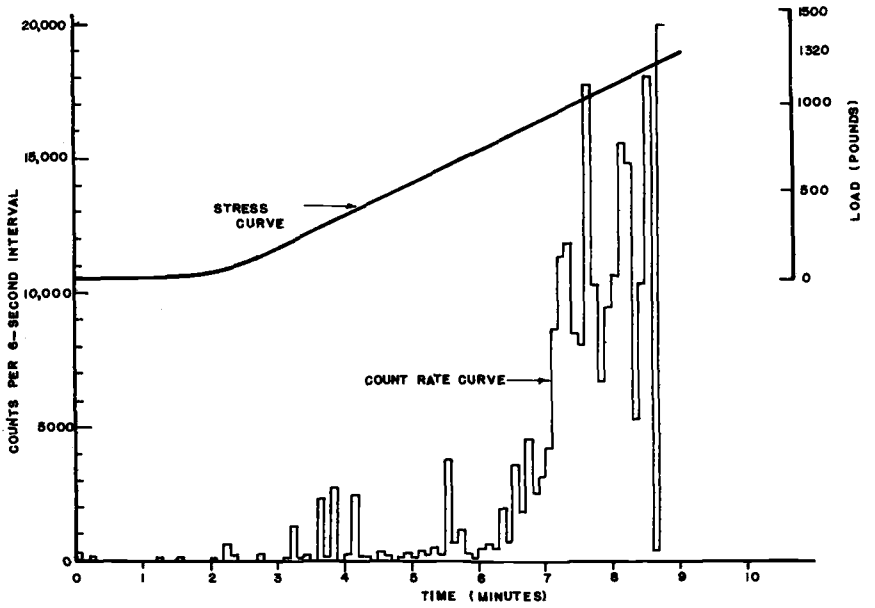

FIG. 14–*Acoustic emission–tensile loading with boron epoxy composite.*

the acoustic energy is likewise usable, and in mechanical assemblies the resonant frequency technique has been mentioned and is more fully covered in Ref *1*.

In hydraulic assemblies, the detection of cavitation, a prime destructive source, particularly when an acid radical or silica dust is present in the hydraulic fluid, has been demonstrated, and the increased leakage flow at null resulting from damage to the orifice has been shown to be a useful indicator of incipient failure as well as being useful in predicting remaining life in the component.

In pneumatic components, the detection of external leakage has been demonstrated.

In structural components, the detection of stress corrosion, particularly the initial attack, and the subsequent surface and subsurface cracking which occurs, are also detectable. Failures due to fatigue, tensile stress, and compressive stress are detectable. (See Ref *4*.)

The noisy characteristics of the composite materials were mentioned. Although carbon filament fiber composites and fiberglass were not covered, work has been performed on all types of composites. The characteristics of all these composites are similar to those of the boron filament fiber composites which were covered. These materials do not yield and the first 50 percent of the total load shows very little acoustic emission unless defects are present. Accordingly, defects existing in structural components fabricated of composites are readily detectable, and tests can be made by loading the part from 30 to 50 percent of rated load, and if significant acoustic emission occurs, the part can be discarded or reworked, as required.

In metals loaded up to 30 percent of ultimate, an inverse relationship exists between acoustic emission and fatigue life. This relationship has been observed during research. In other words, the structural component of metal which exhibits the highest acoustic emission when compared with similar components will have the shortest fatigue life, thus it should be possible to develop sorting tests which will allow receiving and inspection testing of such components. This same principle applies to rotational equipment and has been demonstrated in our research to be effective in the sorting of ball bearings, for example. Although not covered in this report, these sorting tests were quite effective [*7*].

The relationship noted, particularly in the composite materials, between total count and total life is interesting and has been observed in the metals as well. Should this relationship prove applicable to all materials, it will be very valuable during accelerated testing in determining how long a specific component, a pressure vessel for example, would last in operational employment.

The principal application envisioned for the techniques discussed herein, however, are the in-service monitoring of the various subsystems covered. Moving from specimens of materials to a complete structure is not as simple as handling small parts under a controlled environment. The structure of an aircraft in flight presents great difficulties in monitoring incipient failure because of the

presence of air flow over the structure. The monitoring of incipient failure in the hulls of submarines and tankers, for example, present equally great difficulties because of the flow of water along the hull and the interference created by this flow. Interference is particularly severe if cavitation occurs in the flow of sea water along the hull. The solution to these problems may be difficult. In some cases it is purely a matter of finding a frequency window through which to observe the acoustic emission phenomena. In other cases, the tests would have to be made at periodic intervals while the aircraft is under load though not in flight at great speeds, as during landings. In the case of the submarine, tests would have to be run while at rest, but submerged at test depths corresponding to 30 to 50 percent load on the hull.

The application of these phenomena to bridges, buildings, and large construction equipment, such as cranes, presents no important difficulties and is currently being employed to detect incipient failure. The environment in which these structures exist is not one which creates wide frequency acoustic interference.

The use of samples of material of which a structure or equipment is composed is an excellent method of determining what sort of emission can be expected under various loads and load conditions. The important difference is that in a large complex structure, for example, more transducers and channels are required, and the employment of triangulation techniques are necessary to locate the source of the defect[*2*].

To summarize, our research has shown that the application of these phenomena to hydraulic systems, mechanical rotating equipments, and static structures poses no great problems. The application to dynamic structures presents difficulties, some of which have been solved, and some which still remain.

Although experimental work on electrical and electronic systems was not covered in this report, research has been carried out which demonstrates the feasibility of detecting incipient failure in electrical/electronic components or subsystems[*6*]. The work performed indicates that very small corona emit acoustic emission and are indicative of "hot spots" in resistors, leakage in capacitors, degradation in transistors, integrated circuits, and other active devices. The problem in electronic assemblies is in the development of small, highly sensitive, and inexpensive transducers to allow the detection of incipient failure on a cost effective basis. Currently, the cost of detecting incipient failure through the use of acoustic emission is often greater than the value of the electronic assemblies involved.

In large electrical equipment, no such problems exist since they can be handled as mechanical or structural assemblies. In fact, some of the first components handled were fans, blowers, motors, and generators. Research and work performed indicate that these phenomena are useful in many other ways.

Oxidization, fire, electrolysis, galvanic action, change of state (that is, solid, liquid, or gas), radiation and irradiation, change in crystal structure, as well as the formation of chemical compounds, are all detectable.

Conclusion

The broad range detection of incipient failure through the use of the acoustic emission phenomena by a group of selected experiments and by reference to more complete papers and work performed covering the individual subsystems and materials involved. Currently a great deal of work is being done, equipment is being developed, and these techniques are actually being applied for space employment as well as for aircraft, naval vessels, bridges, buildings, and heavy construction equipment. Some work has been performed on the human body, and further application of these techniques to biological systems may well be fruitful.

References

[1] Balderston, H. L., *Materials Evaluation*, MAEVA, Vol. 27, No. 6, June 1969.

[2] Parry, D. L., *Transactions of The American Nuclear Society*, TANSA, Vol. 10, No. 1, 1967.

[3] Balderston, H. L., "Incipient Failure Detection, The Detection of Incipient Failure in Certain Hydraulic Components," Eighth Reliability and Maintainability Conference, Denver, Colo., July 1969.

[4] Balderston, H. L., "Incipient Failure Detection–The Detection of Incipient Failure in Structural Material Samples," Air Transport Association Subcommittee Meeting on Nondestructive Testing, San Antonio, Tex., Sept. 1970.

[5] Balderston, H. L., "On-Board Incipient Failure Detection Sub-system," Air Transport Association Subcommittee Meeting on Nondestructive Testing, Minneapolis, Minn., 30 Sept., 1 and 2 Oct. 1969.

[6] Balderston, H. L., "Incipient Failure Detection–The Detection of Certain Contaminating Processes," Sixth Annual Reliability and Maintainability Conference, Cocoa Beach, Fla., July 1967.

[7] "Incipient Failure Detection Feasibility Study," NASA-MSFC Contract NAS 8-5608; Boeing Document D180-10579-5, The Boeing Company, May 1971.

A. E. Brown[1] *and R. G. Liptai*[1]

Round Robin Testing of Acoustic Emission Source

REFERENCE: Brown, A. E. and Liptai, R. G., "Round Robin Testing of Acoustic Emission Source," *Acoustic Emission, ASTM STP 505,* American Society for Testing and Materials, 1972, pp. 318-331.

ABSTRACT: The use of a martensitic phase transformation in Au-47.5 atomic percent Cd alloy as a source of acoustic emissions is discussed. The use of this source as a standard provided a means of comparing acoustic emission data from several laboratories. The results of round robin testing of this alloy at various laboratories are also presented.

KEY WORDS: acoustics, acoustic detection, acoustic measurement, stress waves, phase transformations, alloy systems, cadmium containing alloys, gold containing alloys, temperature cycling tests, amplitude, interfaces

Most of the metallic elements and alloy systems exist in alternative crystalline forms, depending on temperature and pressure. This condition is called allotropy or polymorphism. For example, iron transforms from a body centered cubic lattice when heated above 1670 F (910 C) at atmospheric pressure. A second allotropic change in iron occurs on further heating at 2552 F (1400 C) at atmospheric pressure. Changes in mechanical and physical properties accompany almost all solid-solid transformations.

Work was performed under the auspices of the U. S. Atomic Energy Commission. The round robin participants are as follows: (A) H. L. Balderston-Hine, Boeing, Seattle, Wash,; (B) T. F. Drouillard, Dow Chemical Co., Boulder, Colo.; (C) H. Dunegan, Dunegan Research Corp., Livermore, Calif.; (D) T. H. Feiertag, University of California, Los Alamos Testing Laboratory, N. Mex.; (E) J. R. Frederick, University of Michigan, Ann Arbor, Mich.; (F) L. Glassman, Georgia Institute of Technology, Atlanta, Ga.; (G) R. S. Jenkins and R. Muenow, Law Engineering Testing Co., Atlanta, Ga.; (H) F. C. Keledy, Trodyne Corp, Teterboro, N. J.; (I) D. A. Tiede, McDonnell-Douglas Astronautics, Santa Monica, Calif.; (J) G. L. Veach and V. Nakamura, General Dynamics, Ft. Worth, Tex.; (K) A. E. Brown and R. G. Liptai, U. C., Lawrence Radiation Laboratory, Livermore, Calif. In the text these participants will be referred to by the letters in parentheses.

[1] Technical associate, Acoustic Emission Laboratory, Mechanical Engineering Support Division and head of the Mechanical Engineering Structural Test and Evaluation Section, respectively, University of California, Lawrence Radiation Laboratory, Livermore, Calif. 94550.

It is a customary practice to group phase transformations in metals and alloys into either of two general categories: (1) nucleations and growth, or (2) martensitic transformations. The category depends on the atomic mechanism involved in the transformation process. In the former, thermal activation and diffusion play an important role and transformation is based on the atom-by-atom transfer across the interface. In contrast, martensitic transformations are diffusionless, shearlike reactions carried out by cooperative movement of atoms. In many cases, transformations, once started, continue at sonic speed and very low temperature until halted or retarded by interface boundaries, strain energy barriers, or loss of coherence between interfaces. Martensitic transformations do not involve a compositional change and are accompanied by a shape deformation.

Although not an absolute criteria very high transformation rates usually characterize martensitic reactions. The formation of martensitic crystallites (plates) in the transforming matrix usually occurs very rapidly (10^{-5} to 10^{-8} s). Also, autocatalytic effects are produced where the formation of crystallites triggers a burst of new crystallites, thus accelerating the transformation. The high rate of formation in the imposing restrictions of the surrounding matrix causes acoustic emissions, or stress waves to be generated during martensitic transformations. Audible sounds and "clicks" have been reported in the literature for many years.

The martensitic transformation in Au-47.5 atomic percent Cd has been studied by acoustic emission techniques.[3] The cubic-to-orthorhombic transformation in this alloy occurs at about 71 C on heating and at about 60 C on cooling. Studies of the interface motion in single crystals have shown that the interface "jumping" characteristics are more pronounced on heating than on cooling. This phenomena was observed by noting that the energy of acoustic emissions was almost two orders of magnitude larger on heating than on cooling. It was conjectured that emission activity is proportional to the fraction of material transformed, however, experiments have not been conducted to verify this.

The formation of a plate in the source alloy has been reported to be 3×10^{-7} s, the rate of propagation has been reported to be 3300 ft/s. Low energy emissions from 0 to 10 C have been noted before the start of transformation suggesting the pretransformation operation on nucleation mechanism. Preliminary experiments[3] showed that the acoustic emission response from the transformation in Au-47.5 atomic percent Cd was repeatable during heating and

[2] With the exception of participant J (Fig. 7, top), this pattern may have been cause by the signal conditioning equipment or by the alloy "memory" interrupting the thermal cycles.

[3] Liptai, R. G., Dunegan, H. L., and Tatro, C. A., *International Journal of Nondestructive Testing*, IJNTA, Vol. 1, No. 3, Aug. 1969, pp. 213-222.

cooling cycles. This characteristic suggested its use as a well defined and repeatable source of real acoustic emissions.

Acoustic Emission Source Design

Specimen Preparation

Crystals of Au-47.5 atomic percent Cd were grown by Bridgman techniques.[4] The specimen used for the acoustic emission source was cylindrical, 0.25 in. in diameter by 0.20 in. long. Experiments showed the high temperature phase of this alloy to be single crystal and the low temperature phase to be polycrystalline.

Source Design

The Au-47.5 atomic percent Cd crystal designed into the acoustic emission source transducer is shown in Figs. 1 and 2. The source transducer consists of a brass outer case, a 110-V heater, and the crystal, which is held in place by epoxy potting compound. It generally requires 1 to 2 min of heating and cooling for each to go through the transformation.

Experimental Procedure

A block diagram of the general experimental system for acoustic emission monitoring is shown in Fig. 3.

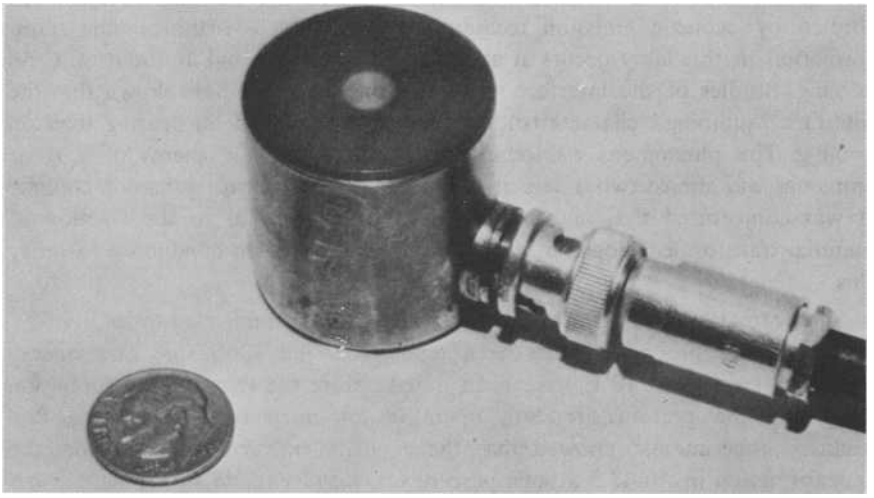

FIG. 1—*Au-47.5 at. percent Cd acoustic emission source.*

[4] Chang, L. C. and Read, T. A., *Transactions,* American Institute of Mining Engineers, TAIEA, Vol. 189, 1951, pp. 47-52.

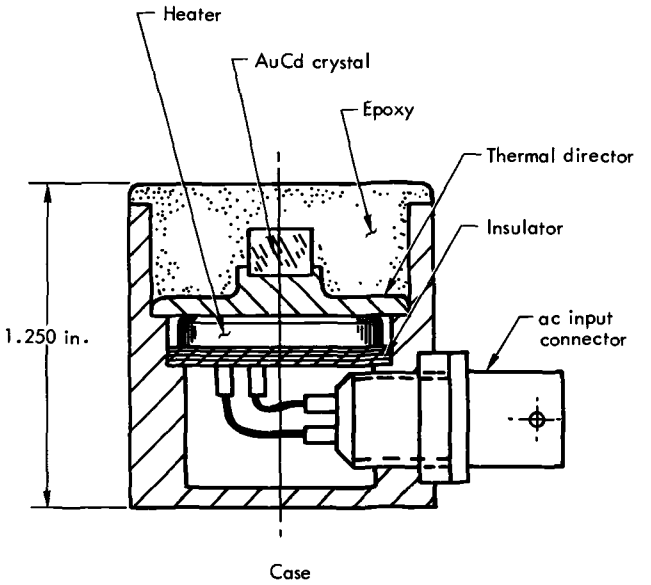

FIG. 2—*Diagram of Au-47.5 at. percent Cd acoustic emission source.*

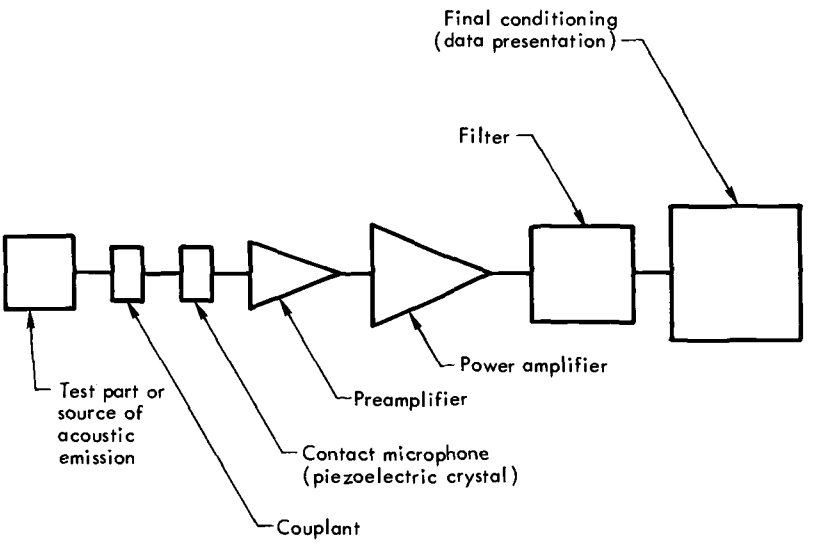

FIG. 3—*Block diagram of experimental acoustic emission monitoring system.*

Couplant

A couplant fluid is used to expel any air or voids, which may restrict full surface contact between the specimen and transducer. The coupling agents fall into two broad categories:

(1) The highly viscous sticky, materials that may couple transverse or torsional waves as well as bulk and extensional waves emanating from the source, and

(2) The less viscious materials that sustain only the bulk and extensional waves.

Couplants in the first category may, on heating, fall into the second category. While investigation has disclosed that most, if not all, solid specimens exhibit some shear wave radiation, all solid specimens exhibit bulk and extensional wave radiation under external stress levels, depending on the history of the specimen. Therefore, to detect the maximum amount of acoustic emission from a specimen, a couplant that remains highly viscous after heating is desirable.

Transducers

All contact piezoelectric sensors are useful in detecting acoustic emission patterns or characteristics. This is evidenced by the widespread use of polarized ceramics and accelerometers with individual damping factors and resonances. Three types of transducers are often used for acoustic emission detection: single ended, differential, and balanced output.

The single ended transducer has two faces, therefore two electrodes for contacts.

In a correctly constructed differential transducer the magnitude and polarity of each element should be equal and opposite. If joined together electrically but separated within the case, the magnitudes would cancel each other. Therefore, a differential input preamplifier is essential for correct operation of this transducer. External radiated noise sensitivity is minimal with the differentially connected transducer while there is essentially little change in detected emission amplitudes. The differential transducer has three electrical faces (contacts). The first face is applied closest to the specimen to be monitored and has an electrical potential closest to ground potential. With reference to the first face, the remaining two are alternately positive and negative polarity.

The differential transducer has basic differences from the balanced output transducer. The balanced output transducer uses a single ended, two contact, piezoelectric element. Output voltage is applied to a phase splitter circuit, which may be a solid state device in the transducer housing. The transducer case would have to be larger than cases for differential transducers, if the phase splitter must share the same case. When the phase splitter shares the transducer case, the

reduction in the effective output impedance can result in a reduced sensitivity to radiated noise. High radiated noise immunity is not easily achieved.

Preamplification

The acoustic emission signals are a composite of extensional, bulk, and transverse waveforms. A transducer that has cross coupling is desirable to ensure maximum sensitivity to these signals.

A piezoelectric device is primarily a charge generator highly sensitive to capacitive loading from cables and amplifiers. Therefore, it is common practice to connect the transducer output to a cable as short as practical with very little total capacitance, then to a preamplifier capable of a voltage gain of 100 to 1000 with a subsequent low output impedance for transmission to another amplifier. The latter amplifier may be at some distance from the test site.

The state of the art in cutting piezoelectric wafers with accuracy and in obtaining wafers with sufficient electromechanical uniformity through the volume may not require better than a 60 dB common mode rejection ration for differential input preamplifiers.

Consideration has been given to logarithmic amplification to handle the large dynamic ranges encountered in acoustic emission detection. However, because of noise in the preamplifier, the signal-to-noise ratio from the logarithmic amplifier may render the amplifier unusable.

Power Amplifier

The power amplifier fills the requirement of additional amplification as well as increased current output to drive conditioning equipment such as tape recorders, counters, and pulse height analyzers. Over the frequency range of interest, the frequency-to-amplitude response is generally within 3 dB.

Filter

Filtering for bandpass and high pass or low pass or both, is generally required. The filters may be located either in the preamplifier, between the preamplifier and power amplifier, in the power amplifier, or following the power amplifier but ahead of any analog or digital processors. Because most transducers have multiple sensitivity peaks (aside from the natural resonance), at least one of these peaks is utilized and accentuated through the use of filters. The high pass filter is used to avoid extraneous low frequency noise, such as power line frequency.

Final Conditioning

The basic data presentation consists of counting the events above a set threshold and presenting the counts as either a linear function of time (rate count) or a linear summation of such events for some portion of the test. (A -

K). Events as a function of time are, at times, processed by a logarithmic tachometer, thereby presenting the data on 3 or 4-cycle semilog paper(K). The output of a summation counter also may be presented logarithmically.

Amplitude (A,B,F) is frequently used and has some of the appearance of a count rate plot. The most common means of plotting amplitudes is through an rms voltmeter with a plotter output jack. A 3 or more, cycle semilog plot of amplitude will be the result. A plot thus constructed has some of the appearance of a log tachometer plot. The primary differences between amplitude and rate plots become apparent when, (1) a change in the system gain results in a much exaggerated displacement of the amplitude base, but little, if any, change in count rate, and, (2) very narrow bursts of emission occurring at a very high repetition frequency produce a disproportionately greater amplitude change than rate change. Isolated bursts of tens of milliseconds duration may not show much amplitude change but become very apparent on a rate counter.

Another data processing method assumes that each acoustic burst is unique and isolated in time and that there is no useful information in the background "noise." This method uses an integrator rectifier system (H, J), which looks at the acoustic burst and provides the start of a pulse. At the end of some integration time, sometimes selectable, the pulse terminates and stands by for the next acoustic burst. These pulses are then counted.

Another technique that can be used is self biasing(J), which takes the average value of background noise to establish a threshold value from which any burst exceeding this average level is detected. This method negates data retrieval from the increase in uniform background noise. When the emission is of uniform amplitude and high repetition frequency the selfbiasing increases, thus eliminating detection of continuous emission. A growth in background noise has been associated with dislocation motion and fine grain materials, while burst data is more common from large grain materials, composite structures, phase changes, and mechanical slippages within or without the test specimen. Occasionally the bursts of emission are well formed and isolated, but more frequently they are composed of several bursts occurring within the same time interval and can cause the resulting emission to last up to 2 or 3 s. Multiple bursts may cause an increase in the apparent frequency and count, while the integrator concept must ignore some of these events. The final result seems to change only the absolute values not the shape of the acoustic patterns as plotted, if only burst information is desired.

Another approach to the display of acoustic data is by means of a pulse height analyzer and computer combination (D). Pulse height data are taken for a predetermined period of time and dumped into a memory bank. Again, the pulse height data are collected and dumped into another memory file. This continues until the run is completed. The computer then displays the data as a pseudo three-dimensional plot composed of a dotted raster.

Discussion

The Au-47.5 atomic percent Cd has been useful in adjusting system amplification factors to match one system to another. However the matching is limited to an identical data presentation technique, that is, a comparison of summation of counts or count rates, or a comparison of conditioned sums or rates.

One of the more interesting features in the several reports was the variety of system gains reported. The data[2] all had the same geometrical patterns for a given display technique. Many had recorded similar counts, within a factor of 10, while the stated system gains varied by more than 1000. Analysis indicated that such differences in gain were not real because of different reference points or thresholds of count amplitudes. Thresholds, for the start of counting, ranged from 10 mV to 1.4 V. When all thresholds had been normalized, the system gains for many of the tests were within 3 dB.

During the course of testing the Au-47.5 atomic percent Cd source in the various laboratories, the reported acoustic emissions became progressively less from one investigator to the next. One particularly abrupt attenuation of emission occurred after the crystal heater had been on for an extended period of time and the epoxy face had been degraded. It was discovered that irreversible crystal damage had occurred (the cooling transformation could not be detected), therefore a new unit was built as a replacement. While the emissions diminish as a function of either temperature cycling, or overheating, or both, the amount of attenuation would not seem to be rapid. Emissions are uniform after cycling through the phase change several times and remain uniform for more than 30 additional cycles. The number of cycles required to attenuate the emissions was not determined.

Attenuation could be caused by (1) the diffusion process (segregation) in the Au-47.5 atomic percent Cd crystal, because small compositional changes appear to change the emissions behavior; (2) an increase in the acoustic mismatch between the crystal and the epoxy; or (3) changes in the attenuation of the epoxy with time.

The most common electronic system used to monitor acoustic emission is shown in Fig. 3. The most popular display technique is either a strip chart or x-y plot of linear count rate and summation of count as a function of time (Fig. 4). The count rate plotted from a logarithmic tachometer is shown in Fig. 5. The logarithmic tachometer (K) has no reset time as the digital count rate systems do, but it does have an averaging time constant that may be set to either 0, 0.25, 0.5, 1, 2, or 5 s. In Fig. 5, a 1 s averaging time constant is provided at the tachometer output. Acoustic emission data from the rms voltmeter are shown as linear and logarithmic amplitude plots in Fig. 6. The similarity of amplitude to count rate may be seen in Figs. 5 and 6.

The "conditioned" (H, J) count rate and summation of count (Fig. 7) are

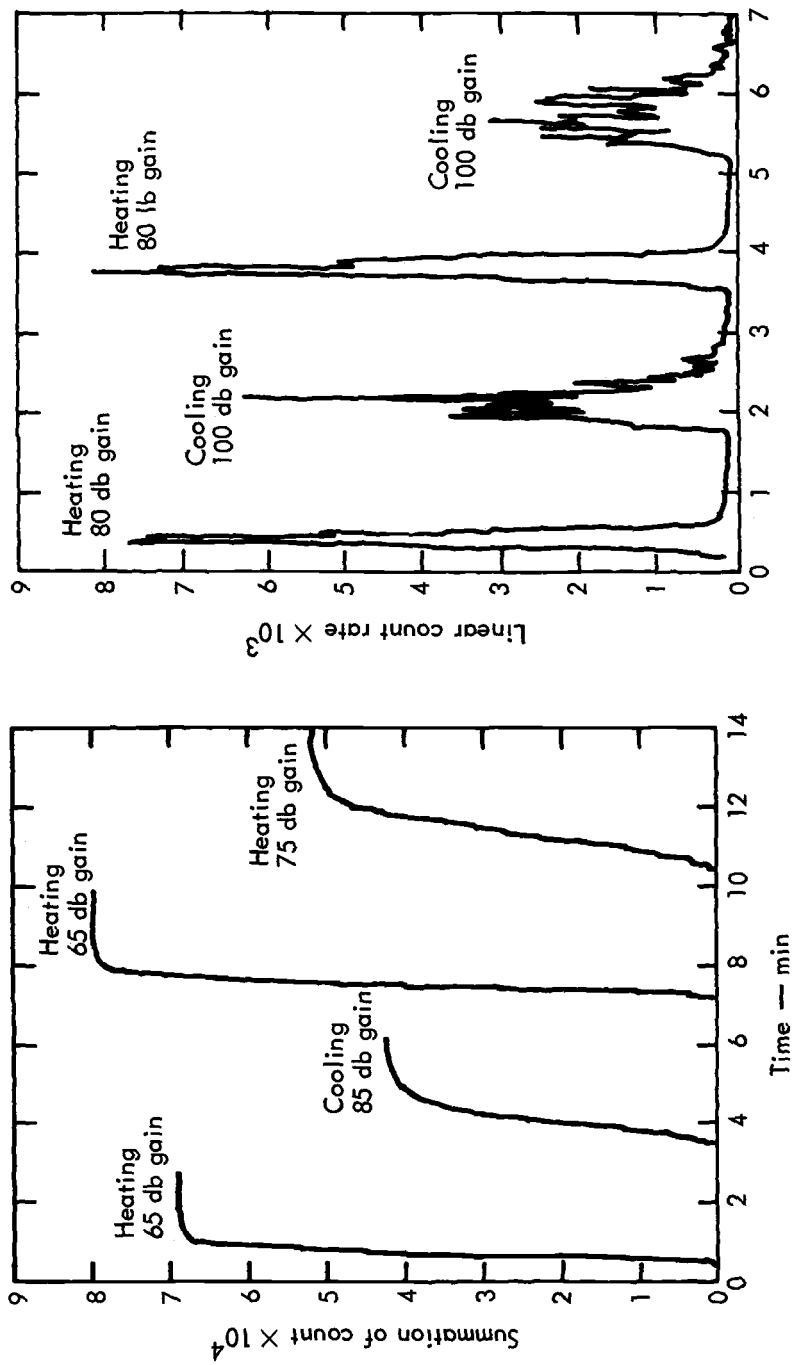

FIG. 4—*Acoustic emission as a function of time for Au-47.5 at. percent Cd source.*

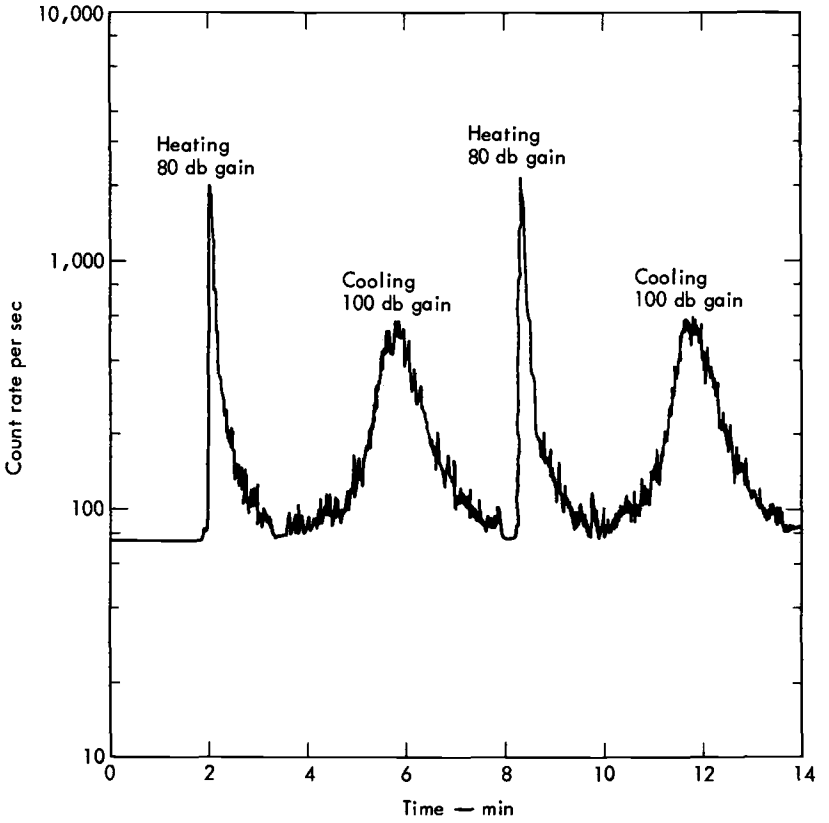

FIG. 5—*Acoustic emission data from logarithmic tachometer. Count rate with 1 s averaging time constant(K).*

based on counting each event of emission as 1. This differs from the more popular method of determining the weighted cyclic event by counting the number of times the damped waveform exceeds a predetermined threshold (Fig. 8).

A technique which has been seldom used, (D) is shown in Fig. 9. A pulse height analyzer in combination with a computer displays a pseudo three-dimensional plot of time, amplitude, and number of events as a function of amplitude. With very little effort the axis displaying time could be modified to indicate either strain, temperature, or stress.

Conclusions

This study showed that the use of the martensitic phase transformation in Au-47.5 atomic percent Cd provided an excellent source for comparing acoustic

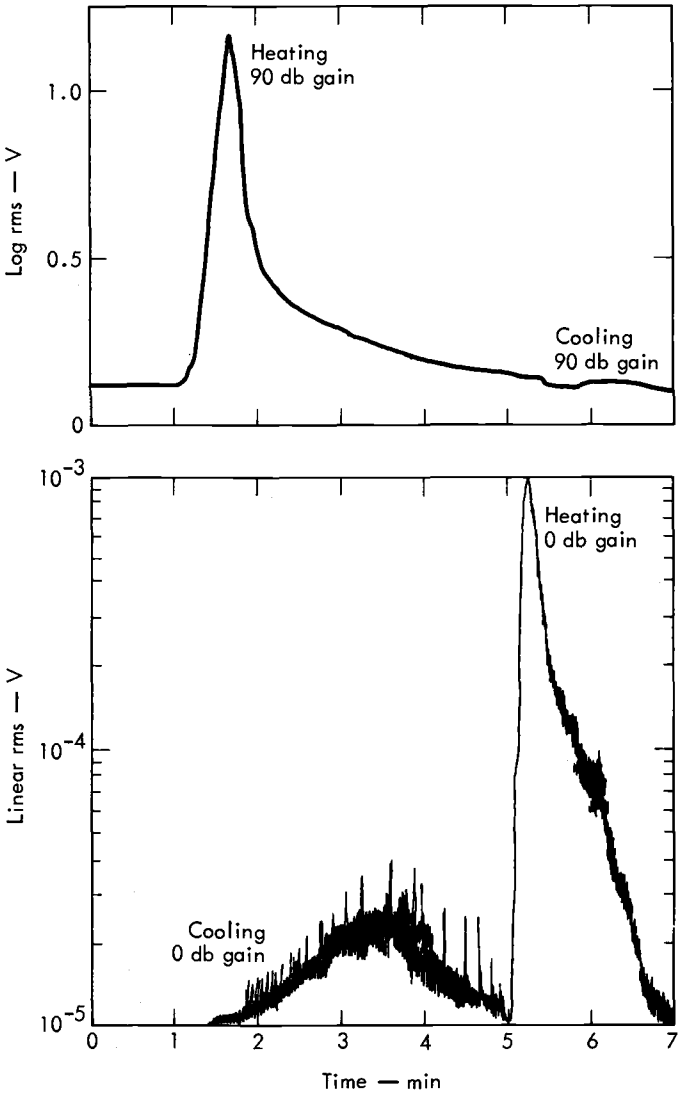

FIG. 6—*Acoustic emission data from rms voltmeter.*

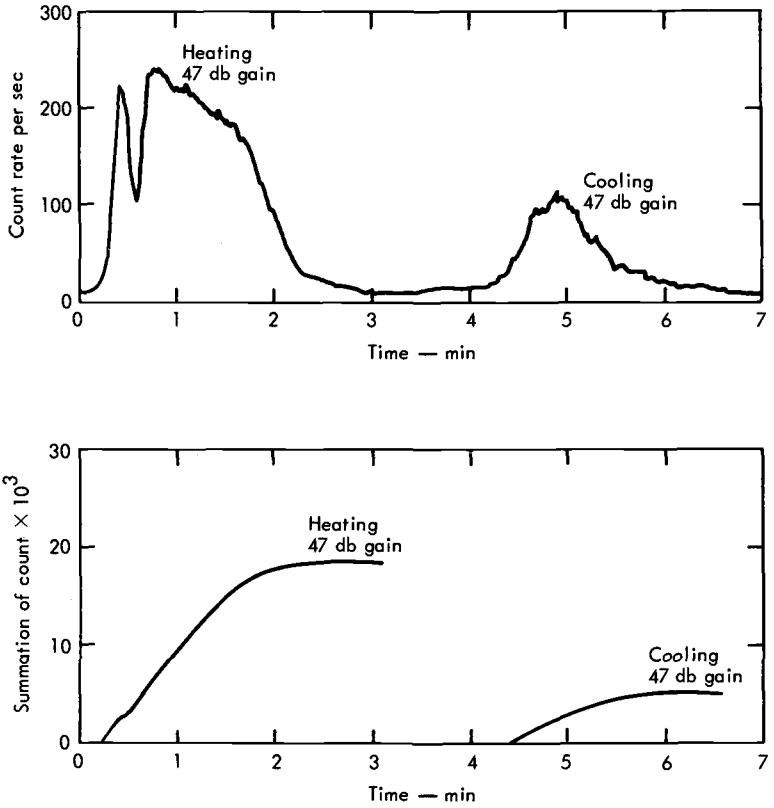

FIG. 7—*Conditioned acoustic emission count of burst emissions(J).*

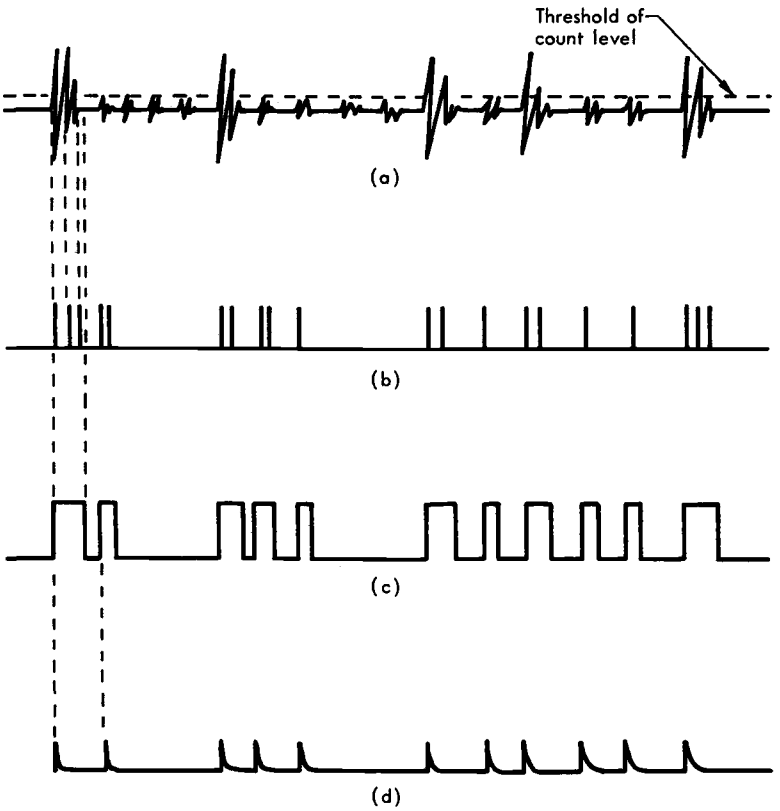

FIG. 8—*Acoustic emission counting.* (a) *Acoustic emission as amplified(A,D),* (b) *result of passing acoustic emission through a frequency counter prior to digitizing;* (c) *result of integrating the acoustic bursts; and* (d) *result of passing integrated acoustic bursts through a frequency counter prior to digitizing.*

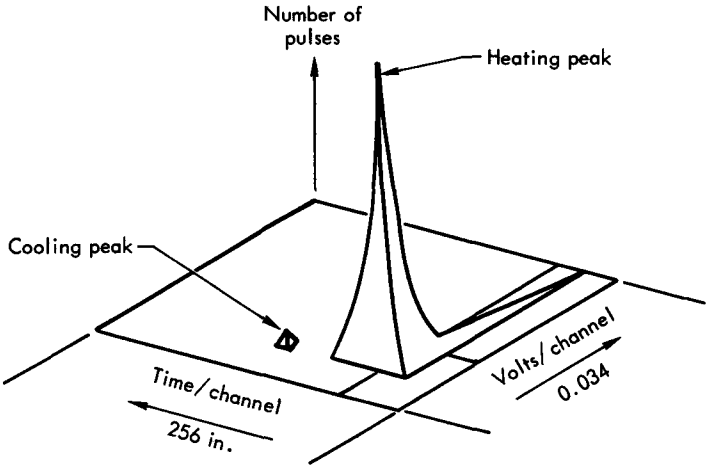

FIG. 9–*Pulse height analysis of acoustic emission data(D).*

emission data from various laboratories. The results indicated that although many counting and display techniques were used to characterize the acoustic emissions from the martensitic phase transformation during heating and cooling, all of the methods produced equivalent information. No significant differences were noted in characterizing the transformation. Also, because repeated cycling (heating and cooling) apparently changed or lowered the acoustic emission activity as a function of the number of cycles, the Au-47.5 atomic percent Cd alloy is inappropriate for use as a standard source of acoustic emissions.

Acknowledgments

We wish to express our appreciation to the laboratories that participated in the round robin testing. We wish to acknowledge our thanks to D. R. Green who designed the acoustic emission source and to B. A. Kuhn who provided experimental assistance. Also, we wish to thank C. A. Tatro and R. B. Engle for their continued interest and encouragement.

DISCUSSION

B. W. Maxfield [1] (discussion summary)

Electromagnetic Detection of Acoustic Emission Signals

The relatively large acoustic emission (AE) signals that result from the martensitic phase transformation in a gold-47.5 atomic percent cadmium alloy[2,3] have been detected for the first time using an inductive means which we refer to as electromagnetic detection (ED). This is the reverse process of electromagnetic generation of acoustic waves and has been discussed elsewhere.[4] The detection efficiency is directly proportional to the applied steady magnetic field; useful signals are obtained with applied magnetic fields above about 4 kG. All measurements were done on a cylindrical specimen 6 mm in diameter and 5 mm long placed inside a 300-turn coil of copper wire. At a field of 10 kG and a system gain of 106 dB (bandwidth of 1 MHz) about 50,000 counts were observed upon heating through the martensitic phase transformation and about 1/20 that number on cooling. This is the same general behavior as observed previously.[3] Using a high speed recorder and spectrum analyzer, the temporal and frequency characteristics of many typical AE signals were determined. A large response was observed to occur at only a few frequencies. The relative strength of each frequency component varied from one event to the next. The characteristic frequencies evident in these measurements correspond reasonably well to those expected for the various acoustic normal modes of the specimen. This acoustic cavity effect may explain the relatively large signal levels. The location of the AE event within the specimen could determine which modes get excited during each event. Hence a large event-to-event variation in the

Work supported by the Alfred P. Sloan Foundation. Use of facilities supplied by the Materials Science Center, Cornell University are also acknowledged.

[1] Alfred P. Sloan Research Fellow, Laboratory of Atomic and Solid State Physics, Cornell Univeristy, Ithaca, N. Y. 14850.

[2] Liptai, R. G., Dunegan, H. L., and Tatro, C. A., *International Journal of Nondestructive Testing*, IJNTA, Vol. 1, 1969, p. 213.

[3] Brown, A. E. and Liptai, R. G., "Round-Robin Testing of Acoustic Emission Source," *Acoustic Emission, ASTM STP 505*, American Society for Testing and Matierals, 1972, pp. 318-331.

[4] Gaerttner, M. R., Wallace, W. D., and Maxfield, B. W., *Physical Review*, PRVAA, Vol. 184, 1969, p. 702.

amplitude of each frequency component would be expected. The advantage of ED is that no mechanical contact need be made to the material under study. This freedom from bonding problems makes ED readily adaptable to a variety of environmental conditions. The coils may be used in either a resonant or nonresonant mode. When used in a nonresonant mode (as was done for the experiments reported here) the detection efficiency is proportional to frequency and transducer ringing can be eliminated completely. In a resonant mode, the frequency response is determined primarily by that of the coil but the detection efficiency is increased by the Q of the coil. A small permanent, pulsed field or electromagnet must be used to produce a steady magnetic field. For magnetic materials, the detection efficiency sometimes peaks between 1 and 5 kG. Also, a knowledge of the acoustical and electrical properties of the material under study is necessary in order to determine the detection efficiency, because the material acts as its own transducer. Therefore, each material must be assessed individually. This new method of detecting AE signals might be useful in studying the frequency spectrum from various AE sources and other applications where transducer resonance or bonding problems must be overcome.

GENERAL DISCUSSION

Alan Beattie
Sandia Laboratory
Alburquerque, N. M.

Discussed the processing of acoustic emission signals which would permit a convenient method for energy analysis. With the scheme, the sorting of signals into energy bands was possible.

T. E. Long
Montana State University
Missoula, Montana

Reported on some preliminary investigations of acoustic emissions from snow. A method for detecting impending avalanches is being sought.

Marc Hoff
Grumman Aircraft Corp.
Bethpage, N. Y.

Described an experiment in which computer assisted triangulation techniques were used to follow crack propagation in a scored flat diaphram.

Acoustic Emission Working Group Subcommittee Report: Recommended Acoustic Terminology

At the 8th meeting of the Acoustic Emission Working Group (AEWG) on 9 December 1971 in Bal Harbour, Florida, the Terminology Subcommittee presented its first report on a recommended acoustic emission terminology. The members of the AEWG Terminology Subcommittee are:

T. T. Anderson – Chairman	Argonne National Laboratory
R. B. Engle	Lawrence Livermore Laboratory
J. R. Frederick	University of Michigan
D. R. Hay	Drexel University
E. L. McCabe	The Boeing Company
G. A. Spiering	Teledyne Material Research

The AEWG passed a motion stating that an amended version of this first report be presented to the ASTM for inclusion in its Special Technical Publication (*STP 505*) on Acoustic Emission. While many of the terms listed are still under discussion it was the AEWG's belief that it would be better to make this report widely available at this time in order to assist in the early adoption of standard terms throughout the technical community. The papers published in the STP for example were in no way standardized to the recommended terms in this report.

The AEWG in the past five years has greatly increased the ease of communicating results of acoustic emission programs. We believe that publication of this first report on a recommended acoustic emission terminology will substantially aid our efforts.

Respectfully submitted,

Allen Green
Dunegan Research Corporation
Chairman

T. T. Anderson
Argonne National Laboratory
Chairman, Terminology Subcommittee

Acoustic Emission Terminology

Acoustic Emission

Acoustic emission is a transient elastic wave generated by the rapid release of energy within a material.

Discussion – Acoustic emission is the recommended term for general use. Alternate terms in the literature include (1) stress wave emission, (2) microseism, and (3) prefix modifiers of emission or of acoustic emission.

Emission Event

An emission event is a rapid physical change in a material, that releases energy appearing as acoustic emission.

Emission Signal

An emission signal is an observed signal obtained by detection of acoustic emission.

Burst Emission

Burst emission is the qualitative description of emission signals, related to individual emission events within the material.

Discussion – Use of burst emission is recommended only for describing qualitative appearance of emission signals. Ambiguity of the term has occasioned recommendations that its use be limited.

Continuous Emission

Continuous emission is the qualitative description of an apparent sustained signal level from rapidly occurring acoustic emission events.

Discussion – Use of continuous emission is recommended only for describing qualitative appearance of emission signals. Ambiguity of the term has occasioned recommendations that its use be limited.

Emission Count

Emission count is a weighted measure of acoustic emission events which have occurred in a given time period. The method of measurement and the weighting procedure should be described.

Discussion – The weighting procedure affects the value and parameter dependency of emission count. A typical method of weighting is to count the number of times the emission signal exceeds a predetermined signal-amplitude threshold. By this method a single event may be counted several times, and large signals are weighted more heavily than small signals. Other methods include dead time gating to eliminate counts from ring down, measuring the time the signal is

above the threshold level, and counting the emission signal weighted by its peak amplitude.

Kaiser Effect

The Kaiser effect is the immediately irreversible characteristic of acoustic emission phenomenon resulting from an applied stress. If the effect is present there is little or no acoustic emission until previously applied stress levels are exceeded.

Signature

A signature is a set of identifiable characteristics of acoustic emission signals attributable to a particular type of source.